# Plan B for particle physics: finding long lived particles at CERN

Proefschrift

ter verkrijging van
de graad van Doctor aan de Universiteit Leiden,
op gezag van Rector Magnificus prof. mr. C.J.J.M. Stolker,
volgens besluit van het College voor Promoties
te verdedigen op donderdag 15 November 2018
klokke 11:15 uur

door

Kyrylo Bondarenko

geboren te Kiev (Oekraïne) in 1990

| | |
|---|---|
| Promotores: | Dr. Alexey Boyarsky |
| | Prof. dr. Ana Achúcarro |
| Promotiecommissie: | Prof. dr. N. Serra (University of Zurich, Switzerland) |
| | Prof. dr. S.I. Vilchynskyy (Shevchenko University of Kyiv, Ukraine) |
| | Dr. O. Ruchayskiy (University of Copenhagen, Denmark) |
| | Prof. dr. E.R. Eliel |
| | Prof. dr. K.E. Schalm |
| | Dr. D.F.E. Samtleben |

The cover shows the scheme of the SHiP experiment, that is planned to be performed at CERN. The sensitivity of this facility to the light feebly interacting particles is one of the main topics of this thesis.

Casimir PhD series Delft-Leiden 2018-38

ISBN 978-90-8593-368-7

An electronic version of this thesis can be found at https://openaccess.leidenuniv.nl

# Contents

# Chapter 1

# Introduction: Physics beyond the Standard Model

## 1.1 Standard Model of particle physics

Our current understanding of elementary particles and interactions between them is summarized in the so called *Standard Model of elementary particle physics* (SM). This is a renormalizable quantum field theory, based on the gauge group $SU(3) \times SU(2) \times U(1)$ and includes spin-$\frac{1}{2}$ particles (matter), spin-1 particles (mediators of interaction) and a spin-0 Higgs boson, see Fig. 1.1. It contains three fermionic families (or *flavors*) of matter and one Higgs $SU(2)$ doublet (see e.g. [1, 2] for reviews). The Standard Model has been developed during most of the XXth century, and its predictions have been tested and confirmed by numerous experiments. The Large Hadron Collider's runs at 7 and 8 TeV culminated in the discovery of a Higgs boson-like particle with a mass of about 126 GeV – the last critical Standard Model component [3–7]. Thus, for the first time, we are in the situation when all the particles needed to explain the results of all previous accelerator experiments, have been found. At the same time, no significant deviations from the Standard Model were found in direct or in indirect searches for new physics (see e.g. the summary of the recent search results in [8–27] and most up-to-date information at [28–31]). For this particular value of the Higgs mass the Standard Model remains mathematically consistent and valid as an effective field theory up to a very high energy scale, possibly all the way to the scale of quantum gravity, the Planck scale [32–36].

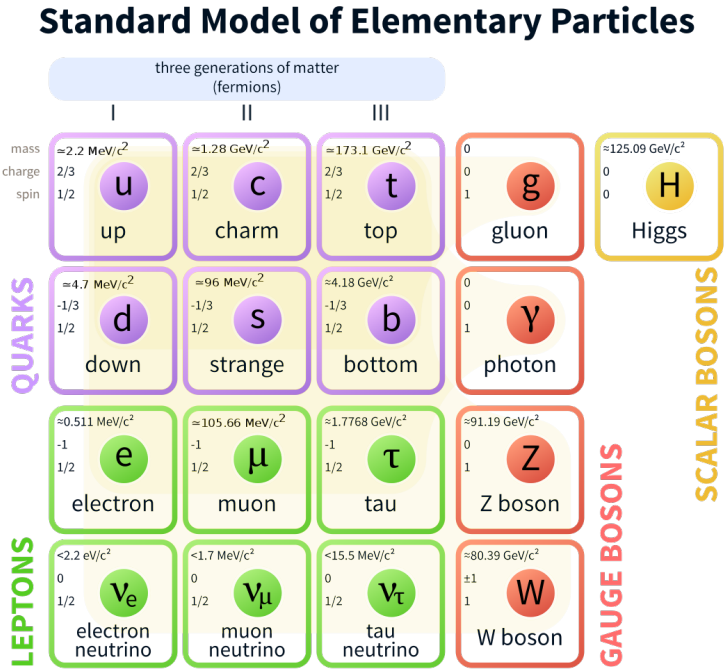


**Figure 1.1**: The Standard Model of particle physics. Matter particles (left 3 columns) are organised in three *generations* (or *flavors*). Gauge bosons are mediators of the strong (gluons), weak ($W$ and $Z$ bosons) and electromagnetic (photons) interactions. The Higgs mechanism is responsible for providing masses to fermions, and to $W$ and $Z$ bosons. The Higgs boson is the manifestation of this mechanism. Credits: Wikipedia

## 1.2 Beyond the Standard Model

However, it is clear that the SM is not a complete theory. It fails to explain a number of *observed phenomena* in particle physics, astrophysics and cosmology. These major unsolved challenges are commonly known as "beyond the Standard Model" problems:

**Beyond-the-Standard-Model (=BSM) problems**

- ▷ **Neutrino masses and oscillations**: what makes neutrinos disappear and then re-appear in a different form? Why do neutrinos have mass?
- ▷ **Baryon asymmetry of the Universe** (BAU): what mechanism has created the (tiny) matter-antimatter disbalance in the early Universe?
- ▷ **Dark Matter** (DM) : what is the nature of the most prevalent kind of matter in our Universe?
- ▷ **Initial conditions problem**: What is the origin of the initial state to which we trace back the evolution of the Universe? In particular, if the initial state was created during a stage of accelerated expansion (**cosmological inflation**), what was driving it?

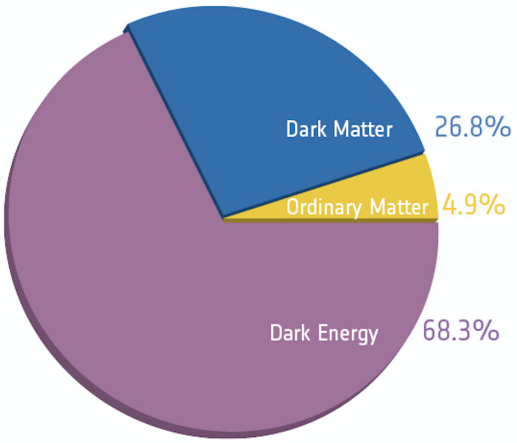


**Figure 1.2**: Composition of the Universe based on the precise measuremsnts of the Cosmic Microwave Background anisotropies by the Planck collaboration [37]. Credits: European Space Agency and Planck collaboration.

Some yet unknown particles or interactions would be needed to explain these puzzles and to answer these questions. But in that case, why haven't they yet been observed?

### 1.2.1 Dark matter

Using the laws of particle physics, combined with Einstein's gravity we can model the evolution of the Universe and see in much detail how its current state has emerged from very simple initial conditions. In the modern era of *precision cosmology* detailed predictions of this picture are confirmed with high accuracy using astronomical observations of various types [37]. Ironically, this success revealed one of the greatest mysteries of modern science: 95% of the total energy density of our Universe is composed of entities of unknown nature, see Fig. 1.2. In particular, we see that most of the matter in the Universe does not emit any light – **dark matter**. Indeed, numerous independent tracers of the gravitational potential (observations of the motion of stars in galaxies and galaxies in clusters; emissions from hot ionized gas in galaxy groups and clusters; 21 cm line in galaxies; both weak and strong gravitational lensing measurements) demonstrate that the dynamics of galaxies and galaxy clusters cannot be explained by the Newtonian potential created by visible matter only. Moreover, cosmological data (analysis of the cosmic microwave background anisotropies and of the statistics of galaxy number counts) show that the large scale structure of the Universe started to develop much before the decoupling of photons at the time of recombination of hydrogen and, therefore, much before ordinary matter could start clustering (for reviews see e.g. [38–40]). This body of evidence points at the existence

of a new substance, distributed in objects of all scales and providing a contribution to the total energy density of the Universe at the level of about 25%. Various attempts to explain this phenomenon by the presence of macroscopic compact objects (such as, for example, old stars) or by modifications of the laws of gravity (or of dynamics) failed to provide a consistent description of all the above phenomena [41]. Therefore, a microscopic origin of the dark matter phenomenon (i.e., a new particle or particles) remains the most plausible hypothesis.

Neutrinos are the only electrically neutral and long-lived particles in the Standard Model. As the experiments show that neutrinos have mass, they could play the role of dark matter particles. Neutrinos are involved in weak interactions that keep these particles in the early Universe in thermal equilibrium down to temperatures of a few MeV. At lower temperatures, the interaction rate of weak reactions drops below the expansion rate of the Universe and neutrinos "freeze out" from the equilibrium. Therefore, a background of relic neutrinos was created just before primordial nucleosynthesis took off. As the interaction strength and, therefore, the decoupling temperature and concentration of these particles are known, their present day density is fully defined by the sum of the masses for all neutrino flavors. To constitute all of dark matter (DM), this mass should be about 11.5 eV (see e.g. [42]). Clearly, this mass is in conflict with the existing experimental bounds for neutrino mass: measurements of the electron spectrum of $\beta$-decay put the combination of neutrino masses below 2 eV [43], while from the cosmological data one can infer an upper bound of the sum of neutrino masses to be 0.58 eV at 95% confidence level [37]. The fact that SM neutrinos could not constitute 100% of DM follows also from the study of the phase space density of DM dominated objects that should not exceed the density of a degenerate Fermi gas: Fermionic particles could play the role of DM in dwarf galaxies only if their mass is above a few hundred eV (the so-called 'Tremaine-Gunn bound' [44], for review see [45] and references therein) and in galaxies, if their mass is tens of eV. Moreover, as the mass of neutrinos is much smaller than their decoupling temperature, they decouple relativistically and become non-relativistic only deeply in the matter-dominated epoch ("*hot dark matter*"). For such type of dark matter the history of structure formation would be very different and the Universe would look rather differently nowadays [46]. All these strong arguments prove convincingly that *the dominant fraction of dark matter* can not be made of the Standard Model neutrinos and therefore *the Standard Model of elementary particles does not contain a viable DM candidate.*

### 1.2.2 Matter-antimatter asymmetry of the Universe

One of the most important arguments for the existence of physics beyond the Standard Model is the baryon asymmetry of the Universe (BAU).

Historically, the first antimatter particle – positron – was observed in the cosmic rays [47]. Nevertheless, a wide range of observations: $\gamma$-ray spectra [48], mea-

surements of the Cosmic Microwave Background(CMB) [49] and of the primordial abundances of light elements [50–52] indicate that there is only primordial (baryonic) matter in the Universe, see e.g. [53–55]. The best current determination of the baryon minus anti-baryon number density $n_B$, normalised to the entropy density $s$, is from the CMB (PLANCK [49]):

$$\frac{n_B}{s} = (8.59 \pm 0.13) \times 10^{-11}. \tag{1.2.1}$$

At the same time, all observed antimatter around us is consistent with being produced in the interaction of cosmic rays with the interstellar medium [56, 57]. So we clearly observe asymmetry between matter and antimatter.

It is unlikely that the Universe was born into an asymmetric state (in particular, because inflation – the period of exponentially fast acceleration – would dilute any primordial charge, including baryon charge, into an exponentially small quantity). One can think of a mechanism that would separate baryons from antibaryons in a baryon-symmetric Universe on scales of the order of the observable Universe today, but to invent such mechanism is at least as difficult as generating an asymmetry in the early Universe. Therefore, we will concentrate on the latter possibility.

In order to generate an asymmetry between baryons and anti-baryons in the early Universe, one needs to fulfill three conditions, refered to as "Sakharov conditions" [58]:

1. **A process that violates baryon number**

   Clearly, to evolve from a state with zero baryonic number $B = 0$, to a state with $B \neq 0$, requires non-conservation of the baryon number. It is simple to add a baryon-number-violating process to the Standard Model. However, such a process would lead to the decay of the proton (through a process such as $p \to \pi^0 + e^+$). The current limit on the proton lifetime [59], $\tau_p > 8.2 \times 10^{33}$ years for the process $p \to \pi_0 e^+$, puts severe constraints on such models.

   As it turns out, there is a non-perturbative process in the Standard Model that enables this violation at high temperature. Indeed, as it has been pointed out in [60], both baryon and lepton number symmetries are *anomalous* (as a consequence of chiral anomaly in the presence of $SU(2)$ gauge fields). At zero temperature with $W$-bosons being massive particles, the probability of such a process is exponentially suppressed. However, this rate is relatively fast before [61] and during the Electroweak Phase Transition [62].

   Thus, *the first Sakharov condition is fulfilled in the Standard Model*

2. $C$ **and** $CP$ **violation** (and violation of any other discrete symmetry that commutes with the Hamiltonian, but anti-commutes with the baryon number).

Particles and anti-particles must behave differently — otherwise, although there were processes that violate baryon number, particles and antiparticles could simultaneously use the $B$ violation with equal rate and opposite total amount to make cancelling $B$ and anti-$B$ asymmetries. Since baryon number anticommutes with $C$ and $CP$, the violation of both is required.

Charge symmetry $C$ is broken in the Standard Model as a consequence of maximal parity breaking by the weak interactions [63]. Therefore, in any process that preserves $CP$, the charge symmetry would be broken. Moreover, $CP$ violations have also been observed in the Standard Model, for example in the systems of kaons [64–66], $B$-mesons [67, 68], see [69] for review. However, the resulting $CP$-violation is too small to account for baryogenesis [70–72].

Thus, *although the necessary ingredients of the second Sakharov condition are present in the Standard Model, their values are, probably, too small to account for the observed baryon asymmetry.*

3. **Departure from thermal equilibrium**

The above processes should be out of thermal equilibrium. Indeed, in thermal equilibrium, there are no asymmetries in unconserved quantum numbers, and $B$ is not conserved by the first Sakharov condition. The only conserved global charges of the Standard Model are $B/3 - L_\alpha$ (where $L_\alpha$ is lepton number for generation $\alpha \in (e, \mu, \tau)$). If the corresponding chemical potentials are zero (as they should be in the absence of initial asymmetry), they will remain zero in thermal equilibrium. So generating the BAU is a dynamical process; phase transitions and the expansion of the Universe are sources of non-equilibrium.

It has been shown that the non-equilibrium first order electroweak phase transition, necessary for baryogenesis in the Standard Model can only occur if the Higgs mass is smaller than $M_H \simeq 72$ GeV [73, 74] (see also [75]). Therefore, *the third Sakharov condition is not satisfied in the Standard Model given the mass of the Higgs particle. This suggests that generation of baryon-antibaryon asymmetry in the SM can not arise.*

Many extensions of the Standard Model are capable of incorporating the baryon asymmetry of the Universe (see e.g. [76–79]). In particular, BAU can be generated in classes of models with heavy neutral leptons. The idea of this scenario, called *leptogenesis* [80], has developed since 1980s (see reviews [81–85] and refs. therein). In particular, it was found that the Majorana mass scale of right-handed neutrinos can be as low as a TeV [86, 87] or even a GeV [88–90] (reaching all the way down to hundreds of MeV [91, 92]) and thus providing hope to probe the leptogenesis scenario directly at particle physics laboratories. Another possibility is to generate Baryon Asymmetry of the Universe using so-called hidden-sector particles, connected to the

SM through scalar portal. There are many other mechanisms for generating a baryon asymmetry of the Universe unrelated to the heavy neutral leptons or scalar portal (for reviews see, e.g. [77, 78, 93–97]). We will not discuss them here further.

### 1.2.3 Neutrino masses and oscillations

All massive fermions have left and right polarizations ("chiralities"). Neutrinos are the only exception to this rule. In the Standard Model neutrinos are massless and only left-chiral neutrino states participate in the weak interaction [98] – manifestation of the parity violation in the Standard Model [63]. However, starting from the famous "Solar neutrino problem" [99] numerous experiments have convincingly established that the SM neutrinos are massive and can experience transition between flavors (see [100] for the historical account or [101] for the most up-to-date status), unlike charged leptons – a quantum phenomenon, known as *neutrino oscillations*, first predicted in [102]. Neutrinos are produced and detected via weak processes; therefore, by definition, they are produced or detected as *flavor* (or *charge*) states $\nu_\alpha$ (i.e. the states that couple to the $e$, $\mu$ and $\tau$ leptons, respectively). However, such states turn out to be a linear combination of the states $\nu_i$, $(i = 1, 2, \dots)$ that obey the Klein-Gordon equation $(\Box + m_i^2)\nu_i = 0$ with the observed mass splittings [101]

$$\Delta m^2_\odot \equiv \Delta m^2_{21} = 7.55^{+0.20}_{-0.16}\cdot 10^{-5}\ \text{eV}^2,\ \ \Delta m^2_{\text{atm}} \equiv \Delta m^2_{31} = \begin{cases} 2.50^{+0.03}_{-0.03}\cdot 10^{-3}\ \text{eV}^2 & \text{(NO)} \\ 2.42^{+0.03}_{-0.04}\cdot 10^{-3}\ \text{eV}^2 & \text{(IO)} \end{cases}, \tag{1.2.2}$$

where $\Delta m^2_{ij} \equiv |m_i^2 - m_j^2|$ and NO and IO mean normal and inverted neutrino mass ordering correspondingly. The transformation to this *propagation* or *mass basis* is given by the famous Pontecorvo-Maki-Nakagawa-Sakata matrix [103] that generically depends on three Euler angles, $(\theta_{12}, \theta_{13}, \theta_{23})$, a Dirac CP violating phase, $\delta$, and two more Majorana phases $(\alpha_1, \alpha_2)$, in case neutrinos are Majorana particles:

$$\begin{pmatrix} \nu_e \\ \nu_\mu \\ \nu_\tau \end{pmatrix} = U_{\text{PMNS}}(\theta_{12}, \theta_{13}, \theta_{23}, \delta, \alpha_1, \alpha_2) \begin{pmatrix} \nu_1 \\ \nu_2 \\ \nu_3 \end{pmatrix}. \tag{1.2.3}$$

where

$$U_{\text{PMNS}} = \begin{pmatrix} c_{12}c_{13} & s_{12}c_{13} & s_{13}e^{-i\delta} \\ -c_{23}s_{12} - s_{23}c_{12}s_{13}e^{i\delta} & c_{23}c_{12} - s_{23}s_{12}s_{13}e^{i\delta} & s_{23}c_{13} \\ s_{23}s_{12} - c_{23}c_{12}s_{13}e^{i\delta} & -s_{23}c_{12} - c_{23}s_{12}s_{13}e^{i\delta} & c_{23}c_{13} \end{pmatrix} \times \begin{pmatrix} 1 & 0 & 0 \\ & e^{i\alpha_1} & 0 \\ 0 & 0 & e^{i\alpha_2} \end{pmatrix}$$

with $s_{ij} = \sin\theta_{ij}$, $c_{ij} = \cos\theta_{ij}$.

At first sight the phenomenology of neutrino masses and mixing can be realised purely within the Standard Model. Indeed, one can write a Majorana mass term by

making a Dirac spinor $\chi_\alpha$ out of two (chiral) neutrino fields

$$\chi_\alpha = \frac{\nu_\alpha + \nu_\alpha^c}{\sqrt{2}},$$

where $\nu_\alpha^c$ is a charged conjugated neutrino field $\nu_\alpha$. The mass term then is simply $m\bar{\chi}_\alpha\chi_\alpha$. Similarly, all the mass/mixing phenomenology can be described by the $3\times3$ matrix

$$\text{Neutrino mass term} = \sum_{\alpha,\beta} c_{\alpha\beta}\frac{v^2}{\Lambda}\bar{\chi}_\alpha\chi_\beta \tag{1.2.4}$$

Here $v$ is the vacuum expectation value of the Higgs field and $\Lambda$ is a parameter having the dimension of mass; $c_{\alpha\beta}$ is a dimensionless $3\times3$ matrix that encodes phenomenology of mixing and the hierarchy of neutrino masses. However, expression (1.2.4) is valid only in the broken (Higgs) phase of the Standard Model. Gauge invariant definition of the neutrino field $\nu_\alpha = (\tilde{H}\cdot L_\alpha)$ where $L_\alpha$ is the left lepton doublet ($\alpha$ is the flavor index $\alpha = \{e,\mu,\tau\}$); $H$ is the Higgs doublet and $\tilde{H}_a = \epsilon_{ab}H_b$. As a result neutrino mass and mixing term can be written in the gauge invariant way only by introducing the so-called "Weinberg operator" [104]:

$$\Delta\mathcal{L}_{\text{osc}} = c_{\alpha\beta}\frac{(\bar{L}_\alpha^c\cdot\tilde{H})(\tilde{H}\cdot L_\beta)}{\Lambda} \tag{1.2.5}$$

where $L_\alpha^c$ is a charge-conjugation of the left lepton doublet, $L_\alpha$. $\Delta\mathcal{L}_{\text{osc}}$ is a non-renormalizable dimension-5 operator. Generation of such operator clearly requires adding new particles to SM (for a review see e.g. [105]).

## 1.3 Portals to new physics

New particles that interact with SM particles may be directly responsible for some of the BSM phenomena or can serve as mediators (or "*portals*"), coupling to states in the "hidden sectors" and at the same time interacting with the Standard Model particles. Such portals can be renormalizable (mass dimension $\leq 4$) or be realized as higher-dimensional operators suppressed by the dimensionful couplings $\Lambda^{-n}$, with $\Lambda$ being the energy scale of the hidden sector. In the latter case the most promising are the dimension 5 operators that are not suppressed too much by the energy scale $\Lambda$.

In the Standard Model there can be only three *renormalizable* portals:

– the scalar portal that couples the gauge singlet scalar $S$ to the $H^\dagger H$ term constructed of the Higgs doublet field $H_a$, $a = 1,2$ with the portal Lagrangian

$$\mathcal{L}_{\text{scalar portal}} = \alpha_1 S H^\dagger H + \alpha S^2 H^\dagger H; \tag{1.3.1}$$

– the neutrino portal that couples the new gauge singlet fermion $N$ to the $\epsilon_{ab}\bar{L}_a H_b$ term, where $L_a$ is the SU(2) lepton doublet and $\epsilon_{ab}$ is absolutely antisymmetric tensor in 2 dimensions,

$$\mathcal{L}_{\text{neutrino portal}} = F_\ell(\epsilon_{ab}\bar{L}_{\ell,a}H_b)N, \tag{1.3.2}$$

with $\ell = e, \mu, \tau$;

– the vector portal that couples the field strength of a new U(1) field $A'_\mu$ to the U(1) hyperfield field strength $B_\mu$,

$$\mathcal{L}_{\text{vector portal}} = \frac{\epsilon}{2}F'_{\mu\nu}F^{\mu\nu}, \tag{1.3.3}$$

where $F'_{\mu\nu} = \partial_\mu A'_\nu - \partial_\nu A'_\mu$ and $F_{\mu\nu} = \partial_\mu B_\nu - \partial_\nu B_\mu$;

Among the higher dimension portals it is worth to mention the very popular axion portal that is coupled to the Standard Model through interaction with gauge fields,

$$\mathcal{L}_{\text{axion portal}} = \frac{g_i}{\Lambda}aF_{i,\mu\nu}\tilde{F}^{i,\mu\nu}, \tag{1.3.4}$$

where $a$ is a new pseudo Nambu-Goldstone boson, $F_{i,\mu\nu}$ is a field strength tensor of the SM gauge bosons, $\tilde{F}_{\mu\nu} = \frac{1}{2}\varepsilon_{\mu\nu\alpha\beta}F^{\alpha\beta}$ and $g_i$ is a corresponding coupling constant.

These portals have different physical motivation and different phenomenology. To illustrate this, below we will concentrate on the scalar and neutrino portals.

## 1.4 Intensity and energy frontiers in searches for new physics

The development of the Standard Model has come to an end with the confirmation of one of its most important predictions – the discovery of the Higgs boson. The quest for new particles has not ended, however. The observed but unexplained phenomena in particle physics and cosmology that we discussed in previous section indicate that other particles exist in the Universe. It is possible that these particles evaded detection so far because they are too heavy to be created at accelerators. Alternatively, some of the hypothetical particles can be sufficiently light (lighter than the Higgs or $W$-boson), but interact very weakly with the Standard Model sector (we will use the term *feeble interaction* to distinguish this from the weak interactions of the Standard Model). In order to explore this latter possibility, the particle physics community is turning its attention to so-called *Intensity Frontier experiments*, rather than *Energy Frontier experiments* like at the LHC or Tevatron (Figure 1.3). Such experiments aim to create high-intensity particle beams and use large detectors to search for the rare interactions of feebly interacting hypothetical particles. Several Intensity Frontiers experiments have been proposed in recent years: DUNE [106], NA62 [107–109], SHiP [110, 111], etc.

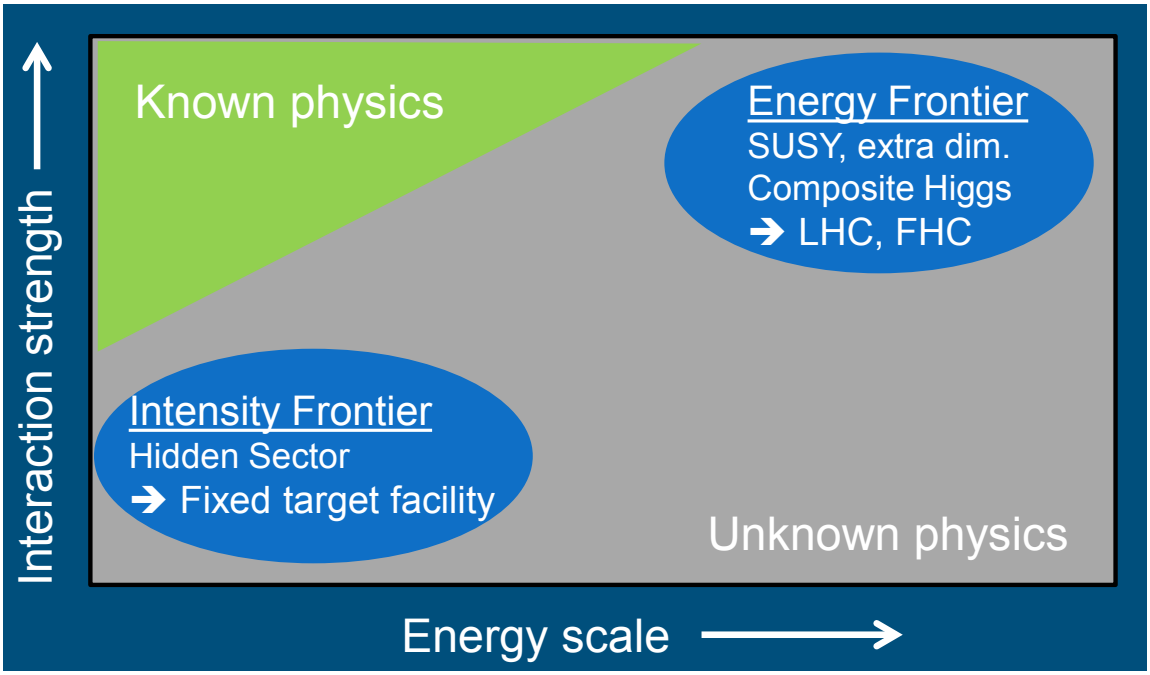


**Figure 1.3**: New physics that can be explored in intensity frontier experiments and its complimentarity with the energy frontier. Figure from [110].

Although LHC is the flagship of the Energy Frontier exploration, its high luminosity (especially in Run 3 and beyond) means that huge numbers of heavy, flavored mesons and vector bosons are created. This opens the possibility to supplement the High Luminosity phase of the LHC with companion experiments directed at the Intensity Frontier. Several such experiments have been proposed: CODEX-b [112], MATHUSLA [113, 114] and FASER [115, 116]. Therefore, it is important to compare LHC companion experiments to the proposed and specialized Intensity Frontier experiments. In Sec. 5 we will study and compare sensitivities of a specialized Intensity Frontier experiment (SHiP) and one of the most promising LHC companion experiments (MATHUSLA).

## 1.5 Neutrino portal

Heavy neutral leptons or sterile neutrinos $N_I$, $I = 1, \ldots, \mathcal{N}$ are singlets with respect to the SM gauge group and couple to the gauge-invariant combination $(\bar{L}^c_\alpha \cdot \tilde{H})$ (where $L_\alpha$, $\alpha = 1, \ldots, 3$, are SM lepton doublets and $\tilde{H}_i = \varepsilon_{ij} H^*_j$ is the conjugated SM Higgs doublet) as follows

$$\mathcal{L}^c_{\text{neutrino portal}} = F_{\alpha I}(\bar{L}_\alpha \cdot \tilde{H}) N_I + h.c. \,, \tag{1.5.1}$$

with $F_{\alpha I}$ denoting dimensionless Yukawa couplings. The name "sterile neutrino" stems from the fact that the interaction (1.5.1) fixes the SM gauge charges of $N_I$

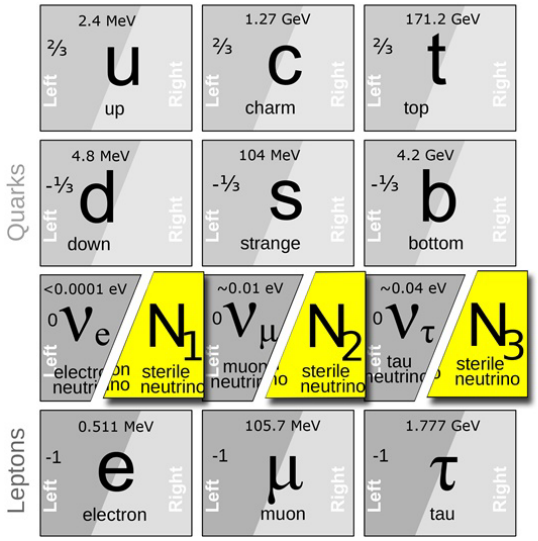


**Figure 1.4**: Three generations of Standard Model fermions with the three right-chiral sterile neutrinos $N_1$, $N_2$, $N_3$. Figure from [110].

to be zero. Also, as only the right-chiral part of the $N$ field interacts with the active neutrino field the sterile neutrinos are often called *right-handed neutrinos*. Due to electroweak symmetry breaking, the SM Higgs field has a nonzero vacuum expectation value $v$ and the interaction (1.5.1) provides heavy neutral leptons and SM (or *active*) neutrinos — with the mixing mass term ($v = 246\,\text{GeV}$)

$$M^D_{\alpha I} \equiv F_{\alpha I} v/\sqrt{2}\,.$$

The neutrino portal could be a connection between the SM and some hidden sector. But in the minimal realization of the hidden sector, the truly neutral nature of $N$ allows one to introduce for it a Majorana mass term, consistent with the SM gauge invariance

$$\mathcal{L}_{\text{HNL}} = i\bar{N}_I \partial\!\!\!/ N_I + \left( M^D_{\alpha I} \bar{\nu}_\alpha N_I - \frac{M_{N,I}}{2} \bar{N}^c_I N_I + h.c. \right). \tag{1.5.2}$$

In this case the only parameters of the "hidden sector" are the masses of the sterile neutrinos $M_{N,I}$, $I = 1 \ldots \mathcal{N}$. If $\mathcal{N} = 3$ the number of sterile neutrinos coincides with the number of active neutrinos and every active neutrino gets its right-handed partner as all other fermions of the Standard Model. This case seems the most attractive possibility as the structure of the SM with three generations is restored, see Fig. 1.4.

The mass eigenstates of the active-plus-sterile sector are mixtures of $\nu$ and $N$, with small mixing angles and large splitting between mass scales of sterile and active neutrinos. The heavy mass eigenstates are "almost sterile neutrinos" while light mass eigenstates are "almost active neutrinos". In what follows we keep the same

terminology for the mass states as for the gauge states. As a result of mixing, HNL couples to the SM fields in the same way as active neutrinos,

$$\mathcal{L}_{int} = \frac{g}{2\sqrt{2}} W^+_\mu \overline{N^c_I} \sum_\alpha U^*_{\alpha I} \gamma^\mu (1-\gamma_5) \ell^-_\alpha + \frac{g}{4\cos\theta_W} Z_\mu \overline{N^c_I} \sum_\alpha U^*_{\alpha I} \gamma^\mu (1-\gamma_5) \nu_\alpha + \text{h.c.}\,, \tag{1.5.3}$$

except the coupling is strongly suppressed by the small *mixing angles*

$$U_{\alpha I} = M^D_{\alpha I} M^{-1}_{N,I}. \tag{1.5.4}$$

Although, the neutrino portal could be a mediator to the large hidden sector, it is interesting to note that even the minimal realization discussed above is sufficient to solve the BSM problems. We will discuss this point in the next sections.

### 1.5.1 HNLs and neutrino masses, seesaw formula

If neutrinos are Majorana particles, the phenomenology of their oscillations can be described via the Weinberg operator (1.2.5). This operator of mass dimension 5 can be resolved in many different ways (for a review see e.g. [105]), but the simplest way is by the introducing a neutral fermion, i.e., sterile neutrino. In the Higgs phase, the combination of the neutrino portal interactions (1.5.2) lead to the mixing between sterile and active neutrinos. As a result *flavor eigenstates* do not coincide with the *mass eigenstates*. The latter are obtained by diagonalizing the matrix

$$\mathcal{M}_{\nu,N} \;=\; \left(\begin{array}{c|c} 0 & m_D \\ \hline m_D^T & M_I \end{array}\right), \tag{1.5.5}$$

where $m_D$ is $3 \times \mathcal{N}$ Dirac mass matrix, $(m_D)_{\alpha I} = F_{\alpha I} v$, $v = \sqrt{2}\langle H \rangle$ and $M_I$ is $\mathcal{N} \times \mathcal{N}$ matrix of Majorana masses. In the limit $m_D \ll M_I$, one can easily see that the Lagrangian (1.5.2), indeed, leads to the Weinberg operator (1.2.5) for neutrinos with

$$\frac{c_{\alpha\beta} v^2}{\Lambda} \equiv (\mathcal{M}_\nu)_{\alpha\beta} = -\sum_I (m_D)_{\alpha I} \frac{1}{M_I} (m_D)_{\beta I}. \tag{1.5.6}$$

The smallness of the Dirac mass term as compared to the Majorana masses $M_I$ means that the active neutrino masses (3 eigenvalues of the matrix $(\mathcal{M}_\nu)_{\alpha\beta}$) become much smaller than the scale $M_I$ and the electroweak scale. This mechanism is therefore known as the *seesaw mechanism* [117–120], see also [121] and refs. therein.[1]

[1] This mechanism is often called *Type-I seesaw mechanism* because there are other ways to "resolve" the Weinberg operator (see e.g. [105, 122]). For example, in the *Type-II seesaw mechanism* an extra SU(2) triplet scalar is introduced [123–126], in the *type-III seesaw mechanism* an extra fermion in the adjoint of SU(2) is added to the model [127].

Adding $\mathcal{N}$ new particles $N_I$ to the Lagrangian $\mathcal{L}_{\rm SM}$ adds

$$N_{\rm parameters} = 7 \times \mathcal{N} - 3 \tag{1.5.7}$$

new parameters to the Lagrangian. These parameters can be chosen as follows: $\mathcal{N}$ real Majorana masses $M_I$ *plus* $3 \times \mathcal{N}$ complex Yukawa couplings $F_{\alpha\, I}$ *minus* 3 phases absorbed in redefinitions of $\nu_e, \nu_\mu, \nu_\tau$. The Pontecorvo–Maki–Nakagawa–Sakata matrix (1.2.3) plus three mass eigenstates $m_1, m_2, m_3$ of the active neutrino sector provide 9 parameters that can be determined experimentally. This shows that one needs $\mathcal{N} \geq 2$ to explain the neutrino oscillations by means of heavy neutral leptons.

To see how neutrino oscillation data limit the HNL parameters, let us first look at the *simplest (unrealistic) toy model with just one HNL*, $N_1$. In this case only one combination of neutrino flavors becomes massive, and its mass, $m_\nu$, allows us to limit the sum of the Yukawa couplings, $|F_1|$:

$$|F_1|^2 \equiv \sum_\alpha |F_{\alpha 1}|^2 = \left(4.1 \times 10^{-8}\right)^2 \left(\frac{m_\nu}{m_{\rm atm}}\right) \left(\frac{M_1}{1\ {\rm GeV}}\right) \qquad \text{(single HNL case)}, \tag{1.5.8}$$

where $m_{\rm atm} = \sqrt{\Delta m^2_{\rm atm}}$, see Eq. (1.2.2). We see that $|F_1|$ becomes smaller as $M_1$ becomes lighter. On the other hand, the mixing element of HNL in the weak interaction is given by

$$U^2 = 5.0 \times 10^{-11} \left(\frac{m_\nu}{m_{\rm atm}}\right) \left(\frac{1\ {\rm GeV}}{M_1}\right) \qquad \text{(single HNL case)} \tag{1.5.9}$$

which is also very small and the dependence on the HNL mass, $M_1$ is opposite to Eq. (1.5.8).

In order to explain two mass differences $\Delta m^2_{\rm atm}$ and $\Delta m^2_\odot$ (see Eq. (1.2.2)), one needs $\mathcal{N} \geq 2$. As it turns out, in this case, much larger values of $|F|$ and $U^2$ are possible. Even in the simplest case of *two HNLs having the same mass* $M_N$, the mixing angle is expressed via one free parameter $X_\omega \geq 1$ (in the notations of [128]) that gives the following equation for $U^2 \equiv \sum_{\alpha,I} U^2_{\alpha I}$ [128–130]

$$U^2 = \frac{\sum_\nu m_\nu}{2M_N}(X^2_\omega + X^{-2}_\omega) \simeq 5 \times 10^{-10} \kappa \left(\frac{1\ {\rm GeV}}{M_N}\right) \left(\frac{X_\omega}{100}\right)^2, \tag{1.5.10}$$

where $\sum_\nu m_\nu = \kappa \times m_{\rm atm}$, i.e. $\kappa \simeq 1$ for normal hierarchy and $\kappa \simeq 2$ for inverted hierarchy. One sees that $U^2$ can be much larger that the naive estimate given by (1.5.9).

The Lagrangian (1.5.2) remains perturbative with Yukawa coupling $|F_{\alpha I}| \lesssim 1$ which corresponds to the scale $\Lambda \sim 10^{15}$ GeV in the Weinberg operator (1.5.6). Actually, the analysis shows that the theory stays perturbative up to $M_{N,I} \lesssim 10^{16}$ GeV [131]. In the opposite limit $M_{N,I} \to 0$ the neutrinos become massive Dirac fermions

and the smallness of their masses is explained by small Yukawa coupling: $F_{\alpha I} \sim 10^{-11}$. The Lagrangian has in this case an exact, global, non-anomalous $U(1)_{B-L}$ symmetry.[2] This symmetry is broken when both the $F_{\alpha I}$ and the $M_{N,I}$ are nonvanishing, a fact that teaches us that any value of $M_{N,I}$ is technically natural [132], as defined by 'tHooft [133].

### 1.5.2 HNL and baryon asymmetry of the Universe. Leptogenesis

Leptogenesis [80] describes a class of mechanisms, which make use of the $L$ violation that is present in Majorana neutrino mass models. Leptogenesis is defined here to include all scenarios which produce a lepton (anti-)asymmetry via CP-violating out-of-equilibrium processes, and rely on the equilibrium SM non-perturbative B+L violation, to partially transform the lepton deficit into a baryon excess. Leptogenesis therefore occurs before/at the electroweak phase transition. A small advantage is that there are no $\Delta B = 1$ interactions, so no concerns with proton decay. More importantly, a natural way to understand why neutrinos are much lighter than other SM fermions, is to suppose that their masses are Majorana, that is, $L$-violating. So in such extensions of the SM, the first Sakharov condition comes for free.

Baryon asymmetry of the Universe (BAU) can be generated through leptogenesis using HNLs of different mass scales, from sub-GeV to $10^{15}$ GeV (see [110] and references therein). In the case of GeV-scale HNLs, the masses of active neutrinos can also generate the Baryon Asymmetry of the Universe via HNL oscillations [88, 89]. Since HNLs at the GeV-scale possess only the Yukawa interaction at the unbroken phase in the Early Universe and its couplings are very suppressed as mentioned above, they can be out of equilibrium state. Then, the CP violation in the production and evolution of HNLs with oscillation effects generates the asymmetry of left-handed leptons which is partially converted into the baryon asymmetry of the Universe.

The successful baryogenesis requires an upper bound on the Yukawa couplings (to avoid fast washout of the baryon asymmetry due to the rapid scatterings of HNLs). This upper bound is more strong for $\mathcal{N} = 2$ case [134] and gets relaxed if more HNLs contribute to the neutrino masses.

### 1.5.3 HNL and dark matter

The only electrically neutral and long-lived particle in the Standard Model are neutrinos. To constitute all of the DM in the Universe the total mass of the neutrino of all flavors ($m_{\nu_e} + m_{\nu_\mu} + m_{\nu_\tau}$) should be about 11.5 eV (see e.g. [42]). But, if the DM particle is a fermion, the phase-space number density of DM in the faintest galaxies should not exceed the density of a degenerate Fermi gas. As the DM mass density is bounded from below observationally, this puts a lower bound on the mass

[2] This is the only global symmetry, exact at both classical and quantum levels, admitted by the Standard Model Lagrangian $\mathcal{L}_{\rm SM}$.

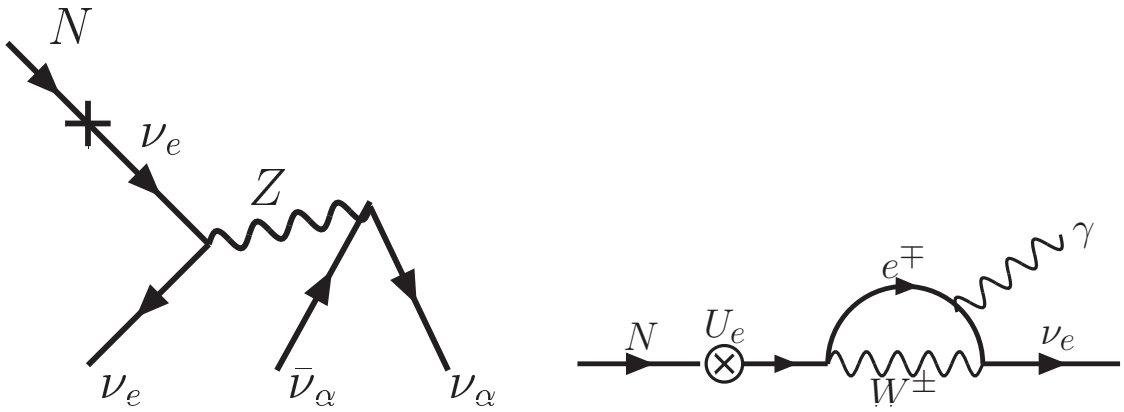


**Figure 1.5**: Decay channels of the sterile neutrino with the mass below twice the electron mass. Right panel shows radiative decay channel that allows to look for the signal of sterile neutrino dark matter in the spectra of dark matter dominated objects. Figure from [110].

of fermionic DM particles to be a few hundreds of eV (the so-called "Tremaine-Gunn bound" [44]). Therefore, cosmological and astrophysical requirements to neutrino dark matter contradict each other.

The *sterile neutrino* allows to resolve this contradiction. Its interaction with the Standard Model particles is similar to that of the active neutrino, but suppressed by the mixing angles $U_{\alpha,I}$ (see Eq. (1.5.3)). Therefore, the number density of the sterile neutrinos created in the early Universe can be much lower and account for the correct DM abundance with a much larger range of masses of the particle, easily satisfying the Tremaine-Gunn bound. The production through mixing with active neutrinos always contributes to the relic sterile neutrino abundance [135–138]. If a large lepton asymmetry or new particles and fields are present in the model then additional production mechanism are possible [139–143] (see [144–146] for review).

The sterile neutrino has a finite lifetime. It can decay to 3 active (anti)neutrinos and has also subdominant decay channel into a neutrino and a photon (Figure 1.5). To be a dark matter candidate its lifetime should be greater than the lifetime of the Universe. In view of the huge amount of dark matter particles in galaxies it will give rise to a strong signal that would be immediately observed, so the lifetime of sterile neutrino DM has to be at least $3 \cdot 10^6$ larger than the age of the Universe [147, 148].

Taking into account constraints from X-rays and cosmology, the allowed parameter space for the sterile neutrino DM candidate is shown in Fig. 1.6. The black line corresponds to the recently observed unidentified spectral line at the energy $E \sim 3.5$ keV in the stacked X-ray spectra of Andromeda galaxy, Perseus galaxy clusters, stacked galaxy clusters and the Galactic Center of the Milky Way [149–151], which is consistent with predictions for decaying dark matter with a mass $M_N \approx 7.1 \pm 0.1$ keV.

Importantly, the sterile neutrino DM candidate does not contribute to neutrino oscillations and cannot be searched in direct detection experiments [148].

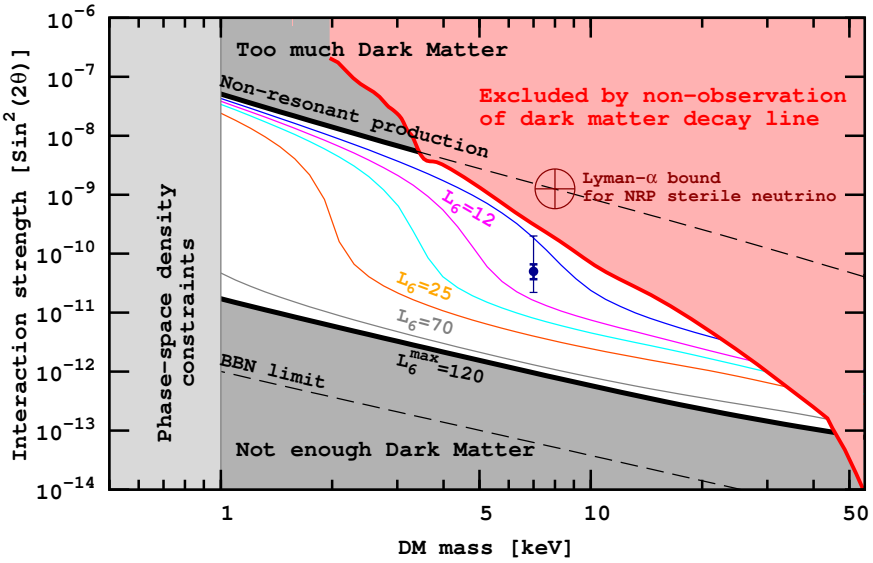


**Figure 1.6**: The parameter space of sterile neutrino dark matter produced via mixing with the active neutrinos (*unshaded region*). The two thick black lines bounding this region are production curves for non-resonant production [138] (*upper line*, "NRP") and for resonant production (RP) with the maximal lepton asymmetry, attainable in the $\nu$MSM (*lower line*, marked "$L_6^{max} = 120$") [90, 134, 140] ($L_6$ is defined as the ratio of the lepton density to the entropy density times $10^6$ ). The thin coloured curves between these lines represent production curves for different values of lepton asymmetry. The red shaded upper right corner represents X-ray constraints [152–156] (rescaled by a factor of two to account for possible systematic uncertainties in the determination of DM content). The region below 1 keV is ruled out according to the phase-space density arguments [157] (see text for details). The point at $\sim 7.1$ keV corresponds to the unidentified spectral detected in stacked X-ray spectra of galaxies and galaxy clusters [149, 150]. Thick errorbars are $\pm 1\sigma$ limits on the flux as determine from data. Thin errorbars correspond to the uncertainty in the DM distribution. Figure from [110].

### 1.5.4 $\nu$MSM

Let us discuss here the framework of the so-called $\nu$MSM (neutrino Minimal Standard Model). This is a simple extension of the SM by introducing $\mathcal{N}$ right-handed neutrinos $N_I$ ($I = 1, 2, \cdots, \mathcal{N}$) in order to explain the three observational phenomena which cannot be explained by the SM, *i.e.*, the non-zero masses of active neutrinos, the cosmic dark matter, and the baryon asymmetry of the universe. These right-handed neutrinos are introduced with Majorana masses $M_I$

$$|m_D|_{\alpha I} \ll M_I < \mathcal{O}(10^2)\ \text{GeV}\,, \tag{1.5.11}$$

where the Dirac mass is given by $|m_D|_{\alpha I} = |F_{\alpha I}|\langle H\rangle$. The first inequality, between Dirac and Majorana masses, is imposed by the seesaw mechanism. The scale of Majorana mass for the seesaw mechanism cannot be determined from active neutrino masses and can vary over a wide range (see Section 1.5.1). The possibility, discussed here, is to choose Majorana masses that are comparable to or smaller than the electroweak scale $\mathcal{O}(10^2)$ GeV, so that the masses of HNLs are comparable to, or smaller than, masses of quarks and charged leptons. Interestingly, even when HNLs are lighter than the electroweak scale, sufficient baryon asymmetry can be generated via oscillations, as was mentioned in Section 1.5.2. Even in the minimal option required for explaining two mass differences $\Delta m^2_{\rm atm}$ and $\Delta m^2_{\odot}$ (see Eq. (1.2.2)), say the two HNLs case, the sufficient baryon asymmetry can be generated as demonstrated in Ref. [89].

The two mass scales, $\Delta m^2_{\rm atm}$ and $\Delta m^2_{\odot}$, confirmed by various oscillation experiments, require that there must be at least two massive states of active neutrinos with different mass eigenvalues. This implies that the number of right-handed neutrinos must be equal or larger than two ($\mathcal{N} \geq 2$). Notice that the lightest active neutrino becomes exactly massless for the minimal choice $\mathcal{N} = 2$.

Our DM candidate is a HNL with $\mathcal{O}(10)$ keV mass (see the discussions in Sec. 1.5.3) We might expect that HNLs needed to explain $\Delta m^2_{\rm atm}$ and $\Delta m^2_{\odot}$ also may play the role of dark matter. However, that is impossible for the following reasons. First, it is shown [158] that HNLs that are responsible for the masses of active neutrinos must has sizable Yukawa couplings which would produce too much dark matter particles by the Dodelson-Widrow mechanism [135], so the present abundance would exceed the observed value. In addition, such HNLs cannot be dark matter since they give too much $X$-rays from their radiative decays [148]. Therefore, we must introduce right-handed neutrino(s) for dark matter, in addition to at least two right-handed neutrinos for active neutrino masses. In this case the number of right-handed neutrino must be $\mathcal{N} \geq 3$.

As a result, the minimal number of right-handed neutrinos explaining the neutrino masses, dark matter, and the baryon asymmetry at the same time equals $\mathcal{N} = 3$. In this case, the HNL $N_1$ plays a role of dark matter (see Section 1.5.3) and the heavier HNLs $N_2$ and $N_3$ are responsible for the seesaw mechanism and baryogenesis. The model with $\mathcal{N} = 3$ introduces 18 new parameters in addition to the parameters of the SM (see Eq. (1.5.7)), which are three Majorana masses $M_I$ and 15 (physical) parameters in the neutrino Yukawa couplings $F_{\alpha I}$. The number of parameters associated with the heavier HNLs $N_2$ and $N_3$ is 11. Seven of these are parameters of the active neutrinos (two mass-squared-differences and three mixing angles of the active neutrinos and one Dirac-type phase and one Majorana-type phase in the PMNS matrix), and 4 are parameters of HNLs (their masses $M_{2,3} = M_N \pm \Delta M/2$ and one complex parameter). The residual 7 parameters are for dark matter $N_1$ (mass of $N_1$, three mixing elements $|U_{\alpha 1}|$ and three CP violating phases).

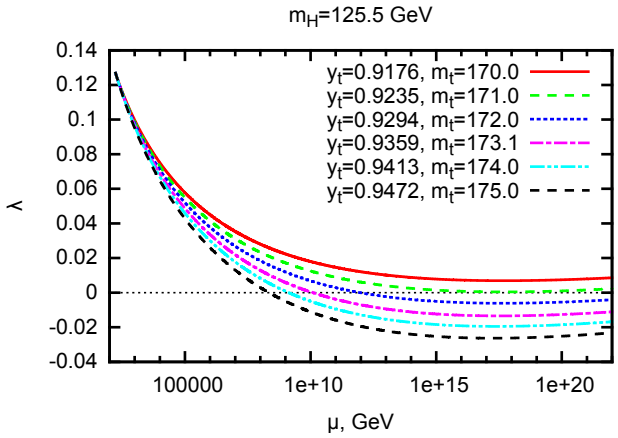


**Figure 1.7**: Renormalization group running of the Higgs coupling constant $\lambda$ for the Higgs mass $M_h = 125.7$ GeV and several values of the top quark Yukawa $y_t(\mu = 173.2\text{GeV})$. Figure from [110].

One important consequence of this model is that the lightest active neutrino is lighter than $\mathcal{O}(10^{-5})$ eV [148, 158]. This comes from the fact that the dark matter HNL is allowed to give a tiny contribution to the seesaw. Therefore, the mass eigenvalues of heavier active neutrinos can be identified from $\Delta m^2_{\text{atm}}$ and $\Delta m^2_{\odot}$ (the ordering of masses is still unknown).

It is important to note that the SM plus $\nu$MSM which introduces new feebly interacting particles below electroweak scale can be consistent up to the Planck scale. The *inflation* can be incorporated to $\nu$MSM (and in the Standard Model) through the non-minimal coupling of the SM Higgs field to the gravitational Ricci scalar $R$ [159], $\frac{\xi h^2}{2} R$. The predictions of this inflation model are consistent with the recent Planck data [160].

The most minimal way to describe *the accelerated expansion of the Universe* at the present epoch in any theory, including the $\nu$MSM, is simply to add the cosmological constant $\Lambda$. The extremely small value of $\Lambda$ remains without explanation (this is exactly the cosmological constant problem), but this "solution" fits all the cosmological data.

Finally, let us discuss the *vacuum stability* and the $\nu$MSM. The experimentally measured values of the Higgs mass and of the top quark's Yukawa coupling lead to quite a peculiar behaviour of the scalar self-coupling $\lambda$ in the SM (and also in the $\nu$MSM, since HNLs couplings are small and can be safely neglected), see Fig. 1.7. This constant decreases with energy, reaches its minimum at energies close to the Planck scale, and then increases [161]. Depending on the values of the Higgs mass and top quark Yukawa coupling allowed by experiments, $\lambda$ can cross zero at energies as small as $10^{10}$ GeV and remain negative around the Planck scale, or be positive at any energy, or just touch zero at an energy scale close to the Planck one [32–34, 162–

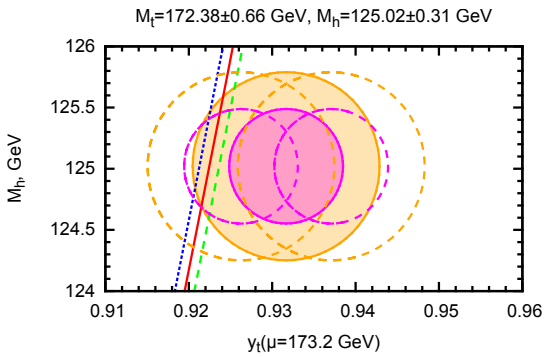


**Figure 1.8**: The figure shows the borderline between the regions of absolute stability and metastability of the SM vacuum on the plane of the Higgs boson mass and top quark Yukawa coupling in the $\overline{\text{MS}}$ scheme taken at $\mu = 173.2\,\text{GeV}$. The diagonal line stands for the critical value of the top Yukawa coupling $y_t^{\text{crit}}$ as a function of the Higgs mass and the dashed lines account for the uncertainty associated to the error in the strong coupling constant $\alpha_s$. The SM vacuum is absolutely stable to the left of these lines and metastable to the right. The filled ellipses correspond to experimental values of $y_t$ extracted from the latest CMS determination [165] of the Monte-Carlo top quark mass $M_t = 172.38 \pm 0.10\,(\text{stat}) \pm 0.65\,(\text{syst})\,\text{GeV}$, if this is identified with the pole mass. The Higgs mass $M_h = 125.02 \pm 0.27\,(\text{stat}) \pm 0.15\,(\text{syst})\,\text{GeV}$ is taken from CMS measurements [166]. Dashed ellipses encode the shifts associated to the ambiguous relation between pole and Monte Carlo masses. See [36] and references therein for more discussion. Figure from [110].

164]. The behaviour of the Higgs self-coupling is closely related to the problem of stability of the SM vacuum: if $\lambda$ is negative in some domain of energies, the effective potential of the scalar field without gravity develops a second, deeper minimum at the scalar field values of the order of Planck scale. In this case the SM vacuum becomes metastable. The situation is uncertain: the SM vacuum can be absolutely stable or metastable within experimental and theoretical error-bars, see Fig. 1.8.

If the SM vacuum is indeed metastable, there is a danger of transition from our vacuum to another, unwanted one, with Planck scale physics. Though the life-time of the SM vacuum exceeds the age of the Universe is by many orders of magnitude [167], it may happen that the Universe evolution during or after inflation could drive the system out of our vacuum. To prevent this, some kind of new physics should intervene to save the Universe from collapse in the Planck vacuum. In [35] has been demonstrated that the specific threshold effects in the SM (and in the $\nu$MSM) with non-minimal coupling to gravity at the energy scale $M_P/\xi$ may lead to relaxation of the system in the SM metastable vacuum. No new heavy particles are needed for this to happen.

### 1.5.5 Summary

The motivation for the existence of a neutrino portal steams from both experiment and theory and points to the existence of heavy neutral leptons. These particles may play an essential role in cosmology, providing a dark matter candidate and producing baryon asymmetry of the Universe. In neutrino physics they provide the source of neutrino masses and mixings. If the masses of HNLs are smaller than $\sim 5$ GeV, it will be possible to search for them in decays of heavy mesons carrying strangeness, charm or beauty, created in high-intensity fixed-target experiments such as SHiP. Heavier HNL's can be searched for in collider experiments at the LHC and in future experimental facilities like FCC-ee [168]. Virtual HNLs lead to lepton flavor number violation that can potentially be seen in the processes like $\mu \to 3e, \mu \to e\gamma$ or $\tau \to 3\mu$. They also generically imply the lepton number violation that can manifest itself in neutrino-less double beta decays. It goes without saying that the discovery of such particles or indirect indication of their existence would revolutionise our understanding of particle physics and cosmology, whereas constraining their properties would help to elucidate various ideas on physics beyond of the Standard Model.

## 1.6 Scalar portal

The Higgs boson was recently found at the LHC at CERN [169–172] directly confirming the existence of the fundamental scalars in nature. Therefore, the idea of another fundamental scalar is viable and well-motivated. Such scalar particle appears in many extensions of the Standard Model. If the new particle has no SM charges it can be light and naturally obtain very suppressed couplings to other SM particles. This particle could be a portal between SM and hidden sector that is well motivated by such experimental observations as baryonic asymmetry of the Universe (see e.g. [76] for a review), dark matter [173–175] and the hierarchy problem [176–180].

If one considers a complex dark sector, many new avenues open up for new processes, such as dark baryogengesis [181], see Fig. 1.9. These processes appear naturally within the content of Asymmetric Dark Matter. The details of the baryogenesis depends on the properties of the dark sector and will not be discussed here.

Another interesting application of the additional scalar particle is to consider it to be an inflaton. In this case, the new scalar particle could be still light and, what is especially intriguing, its parameter space can be probed by high-intensity experiments [182, 183].

### 1.6.1 Scalar as a mediator between DM and the SM

Light scalars may certainly provide an interesting connection to the puzzle of dark matter (DM). It is quite conceivable that dark matter resides in the form of a SM singlet particle which is protected against decay by a (discrete) symmetry. In this case, a light scalar could mediate the interactions between DM and the SM.

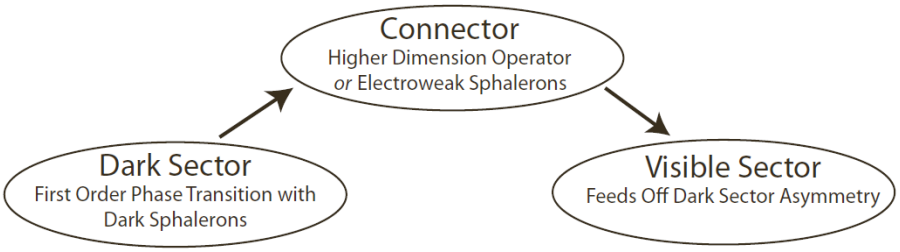


**Figure 1.9**: In a Hidden Valley with asymmetric dark matter, the dark baryon asymmetry created in a first-order phase transition in a Hidden Valley can be transferred to the Standard Model sector [181].

The Lagrangian for the minimal model reads

$$\mathcal{L} = \mathcal{L}_{\rm SM} - \theta \frac{m_f}{v} S\, \bar{f} f \;\; - \frac{1}{2} \kappa\, S \bar{\chi} \chi \;, \tag{1.6.1}$$

where $\chi$ denotes the dark matter particle which we assume to be a Majorana fermion, while $S$ stands for the scalar mediator. The coupling of the scalar to SM fermions $f$ arises from mixing with the SM Higgs particle, as we will discuss in Section 2.1.

In the hot early universe, the dark matter fermions are in thermal equilibrium due to their interactions with the SM bath. DM pairs can directly annihilate into SM particles via an intermediate scalar $S$. Alternatively, if kinematically allowed, they can annihilate into pairs of scalars, which subsequently decay to SM particles. As far as the experimental constraints on the scalar $S$ are concerned, only its interactions with the SM are relevant. Indeed, the coupling $\theta$ is subject to strong bounds and, hence, processes involving this coupling must be suppressed. Therefore, we shall assume that the second class of processes dominates. The annihilation cross section for $\chi\chi \to SS$ can be estimated as [184]

$$\sigma\, v_{\rm rel} \simeq \sigma_1\, v_{\rm rel}^2 = \frac{\kappa^4 m_\chi}{24\,\pi} \sqrt{m_\chi^2 - m_S^2}\, \frac{9 m_\chi^4 - 8 m_\chi^2 m_S^2 + 2 m_S^4}{(2 m_\chi^2 - m_S^2)^4}\, v_{\rm rel}^2 \,, \tag{1.6.2}$$

where $v_{\rm rel}$ denotes the relative velocity between two dark matter particles. Notice that this process is p-wave suppressed due to the CP properties of the initial and final state particles. Imposing that the relic density of $\chi$ matches the observed dark matter density $\Omega_\chi h^2 = 0.1199$ [49], we can determine $\kappa$. More specifically for $p$-wave suppressed annihilations and $m_\chi = 5$–$10\,\text{GeV}$ the corrent value of the current DM abundance is achieved for $\sigma_1 \simeq 1.6 \cdot 10^{-25} \text{cm}^3/\text{s}$ (see e.g. [185]).

Another consequence of the model (1.6.1) is an emergence of dark matter self-interaction, that could be relevant for cosmology. Current observations do not actually constrain the DM self-interaction cross section to be smaller than that of the strong interaction between nucleons (for a recent review, see [186]), which is many

orders of magnitude less stringent than corresponding bounds on DM interacting with standard model particles [187, 188]. Self-interacting DM (SIDM) thus remains a fascinating option which, if confirmed observationally, would significantly reduce the number of possible DM candidates from particle physics. Such observations would, furthermore, offer a window into the particle properties of DM that may be impossible to access by other means – a fact which has created significant attention in recent years (see, e.g. Refs. [189–191]).

Observations of colliding *clusters* lead to the strongest currently existing constraints on SIDM, with $\sigma/m_\chi \lesssim 0.47\,\mathrm{cm}^2/\mathrm{g}$, and it has been argued that their small cores (if any) lead to even stronger bounds [190]. While not undisputed, this has triggered much phenomenological interest in velocity-dependent self-interactions in order to evade cluster bounds and at the same time allow for $\sigma/m_\chi \sim 1\,\mathrm{cm}^2/\mathrm{g}$ at (dwarf) galaxy scales, where the typical DM velocities are up to one order of magnitude smaller [192–195] (and more recently [190, 196, 197]). However, to obtain velocity dependence of the self-interaction one need to consider a sub-GeV scale mediator [186], which is a good motivation for search of light, feebly interacting particles.

However, the situation is not so clear because of large systematic uncertainties in observations. So one needs to deal with *ensembles* of many astrophysical objects, thereby reducing the systematic uncertainties related to individual objects. Such approach was introduced in [198]. As a result no velocity dependence was observed. However, the theoretical model used for description of SIDM halo shows significant deviations from simulations, so it should be also improved [199].

## 1.7 Summary

The Standard Model of particle physics is a highly successful theory that provides a consistent description of experimentally observed particles and their interactions. Its predictions have been tested and confirmed by numerous experiments. Nevertheless, SM cannot be a complete theory of nature because of the existence of phenomena that cannot be explained by it. To incorporate these phenomena new particles should be introduced. We do not observe new particles because they are either too heavy or light but superweakly interacting. The particles of the second type could be searched in intensity frontier experiments.

In this work we consider two specific models of feebly interacting particles, Higgs-like scalar and a heavy neutral lepton. We discuss their search by means of new generation intensity frontier experiments. In Chapter 2 and Chapter 3 we discuss the phenomenology for the scalar portal and HNLs correspondingly. In Chapter 4 we overview two specific proposals of such experiments, namely SHiP and MATHUSLA. In Chapter 5 we discuss the main features of their sensitivities analytically and present results of numerical simulations. Finally, in Chapter 6 we discuss a possibility

to exploit the specialized neutrino detector iSHiP for the search of light dark matter and axion-like particles.

# Chapter 2

# Scalar portal

In this Chapter we will discuss the implications of introducing a light scalar particle $S$ into the standard model. As a first step we extend the renormalizable Lagrangian of the Standard model with a CP-even scalar particle coupled to the Higgs doublet. We calculate the (small) mixing angle of the Higgs and $S$ fields so as to be able to write a first-order approximation of the extended standard-model Lagrangian. We then apply this result to the calculation of the production mechanisms for the light scalar particle, namely through a direct channel and through the decay of hadrons. The direct channel effectively involves just a single process which has been studied in [182].

The hadronic decay channel is much richer involving many mesonic (11) and baryonic (13) paths. Here, following Refs. [182, 200], we focus on the mesonic channels and calculate branching ratios for 2-body meson decay as well as 3-body meson decay, each involving the production of one light scalar particle. The values of the branching ratios vary by 12 orders of magnitude.

In an experiment one not only wants to produce the light scalar particles but also detect them. In the final part of this Chapter I present my calculations of their decay widths. I explore the decay into leptons and into hadrons, where, again, the hadronic channel is more rich. The results are presented as a function of the, hitherto unknown, mass of the light scalar particle.

## 2.1 Scalar portal effective Lagrangian

The general renormalizable SM Lagrangian with a new (CP-even) scalar particle added to the Standard Model (SM) is given by

$$\mathcal{L} = \mathcal{L}_{SM} + \frac{1}{2}\partial_\mu S \partial^\mu S + (\alpha_1 S + \alpha S^2)(H^\dagger H) + \lambda_2 S^2 + \lambda_3 S^3 + \lambda_4 S^4, \qquad (2.1.1)$$

where $S$ is the new light scalar particle coupled to the Higgs doublet $H$ with coupling constants $\alpha_1, \alpha$, and $\lambda_2, \lambda_3, \lambda_4$ are self-interaction coupling constants of the scalar $S$.

There are two main properties of the Lagrangian (2.1.1) that make it noticeable from the point of view of connection to the hidden sector. Firstly, it contains only renormalizable terms, which means that its phenomenological relevance is not suppressed by the energy scale of the new physics. Secondly, as dark matter seems to be not charged under SM interactions, the singlet scalar gives a simple possibility to directly connect dark matter to SM trough this portal.

After the spontaneous symmetry breaking, the Higgs doublet chooses the following vacuum,

$$H = \begin{pmatrix} 0 \\ \dfrac{v+h}{\sqrt{2}} \end{pmatrix}, \tag{2.1.2}$$

where $v$ is the vacuum expectation value and $h$ is the Higgs boson field. Thus, substituting it into the initial Lagrangian (2.1.1) we get,

$$\mathcal{L} = \mathcal{L}_{SM} + \frac{1}{2}\partial_\mu S \partial^\mu S + \frac{\alpha_1}{2} S h^2 + \frac{\alpha}{2}(S^2 h^2 + 2vS^2 h) + \alpha_1 v S h + \frac{\alpha_1 v^2 S + (\alpha v^2 + 2\lambda_2) S^2}{2} + .... \tag{2.1.3}$$

The last term can be written in a form of a mass term as

$$\frac{\alpha_1 v^2 S + (\alpha v^2 + 2\lambda_2) S^2}{2} = \frac{\alpha v^2 + 2\lambda_2}{2}\tilde{S}^2 + c = -\frac{m_S^2}{2}\tilde{S}^2 + c, \tag{2.1.4}$$

where $m_S^2 = -(\alpha v^2 + 2\lambda_2)$ is the mass of $S$ field, the $\tilde{S} = S + \frac{\alpha_1 v^2}{2(\alpha v^2 + 2\lambda_2)}$ is a redefined field, and $c$ is some constant. Henceforth, we will use $S$ instead of $\tilde{S}$.

The mass Lagrangian of the Higgs field and $S$ field is

$$\mathcal{L}_{mass}^{h,S} = -\frac{M_h^2 h^2}{2} - \frac{m_S^2}{2} S^2 + \alpha_1 v S h. \tag{2.1.5}$$

If $\alpha_1 = 0$ (for example because of $Z_2$ symmetry $S \to -S$) the phenomenology is significantly different from the case when $\alpha_1$ is not equal to zero [110]. We will not discuss this special case and concentrate on the most general $\alpha_1 \neq 0$ possibility.

We need to diagonalize the Lagrangian (2.1.5) to get the proper mass for the Higgs and scalar fields as we have terms $\propto Sh$, of which we have to get rid. The standard procedure is the following: find such orthogonal matrix $O$ for which the mass matrix $M$ will be diagonal $O^T M O = \mathrm{diag}(m_1, m_2)$. The matrix $O$ could be chosen as a rotation matrix,

$$O = \begin{pmatrix} \cos\theta & \sin\theta \\ -\sin\theta & \cos\theta \end{pmatrix}. \tag{2.1.6}$$

From the Lagrangian (2.1.3) the mass matrix is,

$$M = \begin{pmatrix} -\frac{1}{2}M_h^2 & \frac{1}{2}\alpha_1 v \\ \frac{1}{2}\alpha_1 v & -\frac{1}{2}m_S^2 \end{pmatrix}. \tag{2.1.7}$$

Therefore, the mass matrix will be diagonalized if the condition

$$\tan 2\theta = \frac{2\alpha_1 v}{M_h^2 - m_S^2} \tag{2.1.8}$$

is valid. For small mixing angle $\theta \ll 1$ and assuming that the scalar particle is much lighter than the Higgs boson $m_S \ll M_h$ we obtain the condition,

$$\boxed{\theta \approx \frac{\alpha_1 v}{M_h^2}}. \tag{2.1.9}$$

Thus, the Higgs and scalar field should be transformed as,

$$h \to h + \theta S, \tag{2.1.10}$$

$$S \to S - \theta h. \tag{2.1.11}$$

Looking at the interaction Lagrangian for the Higgs field with the SM particles, one can see that after the transformations (2.1.10) and (2.1.11) we have the interaction of the scalar particle $S$ with the SM particles

$$\begin{aligned} \mathcal{L}_{SM}^{h+\theta S} = &-\sum_f \frac{m_f}{v}(h+\theta S)\bar{f}f + \frac{2M_W^2}{v}(h+\theta S)W^+W^- + \frac{M_Z^2}{v}(h+\theta S)Z^2 + \\ &+ \frac{M_W^2}{v^2}(h+\theta S)^2 W^+W^- + \frac{M_Z^2}{2v^2}(h+\theta S)^2 Z^2 - \frac{M_h^2}{2v}(h+\theta S)^3 - \frac{M_h^2}{8v^2}(h+\theta S)^4, \end{aligned} \tag{2.1.12}$$

where $f$, $W^\pm$, $Z$ are fields of the SM fermions, $W$-boson and $Z$-boson respectively and $m_f$, $M_W$, $M_Z$ are their masses. Using (2.1.12) we obtain the Lagrangian of interaction, to first order in $\theta$, of the $S$-particle with SM particles, in the unitary gauge:

$$\begin{aligned} \mathcal{L}_{SM,partial}^{S} = &\boxed{-\sum_f \theta\frac{m_f}{v}S\bar{f}f} + 2\theta\frac{M_W^2}{v}SW^+W^- + \theta\frac{M_Z^2}{v}SZ^2 + \\ &+ 2\theta\frac{M_W^2}{v^2}ShW^+W^- + \theta\frac{M_Z^2}{v^2}ShZ^2 - 3\theta\frac{M_h^2}{2v}Sh^2 - \theta\frac{M_h^2}{2v^2}Sh^3. \end{aligned} \tag{2.1.13}$$

## 2.2 Light scalar production

The scalar particle $S$ could be produced in primary $p$-$p$ collisions or in the decay of produced hadrons.

### 2.2.1 Direct production

The examples of the processes where the light scalar particle could be produced in a direct $p$-$p$ collision in the deep inelastic scattering (DIS) are given in Fig. 2.1. This production channel for the case of proton fixed-target experiment was studied in [182]. It was found that the main contribution to this type of production comes from gluon fusion with a top quark in the loop because of the large Yukawa coupling of the top quark. The production probability of this channel is shown in Fig. 2.2. The production probability is small because it competes with QCD processes.

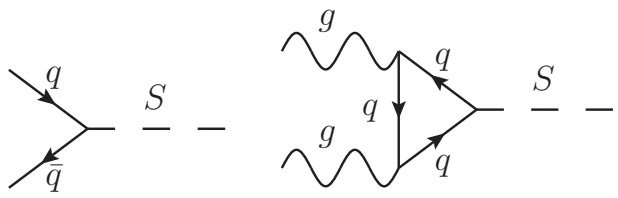


**Figure 2.1**: Deep inelastic scattering production channels of scalar particle: quark-antiquark fusion (left) and gluon fusion (right).

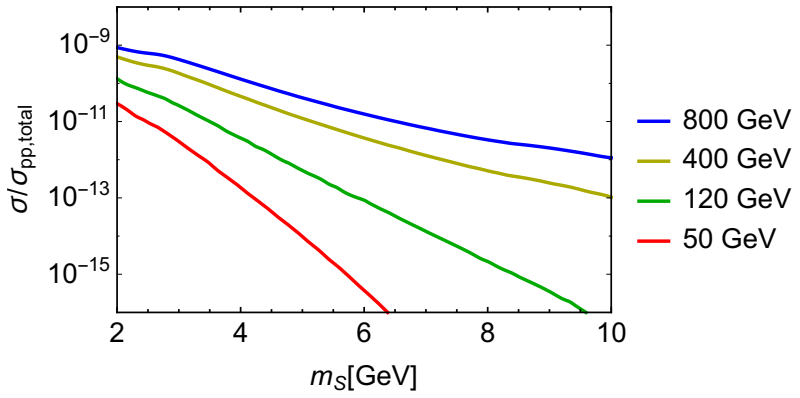


**Figure 2.2**: Production probability of $S$ particle from gluon fusion at proton fixed-target experiments for different energies of proton beam.

### 2.2.2 Production from hadrons

In light scalar production from hadron decays, the main contribution comes from the lightest hadrons in each flavor.[1] The list of the main hadron candidates is as

[1]Indeed, if $X$ is the lightest hadron in the family, it can decay *only* through weak interaction, so it has a small decay width $\Gamma_X$ (in comparison to hadrons that could decay through electromagnetic or

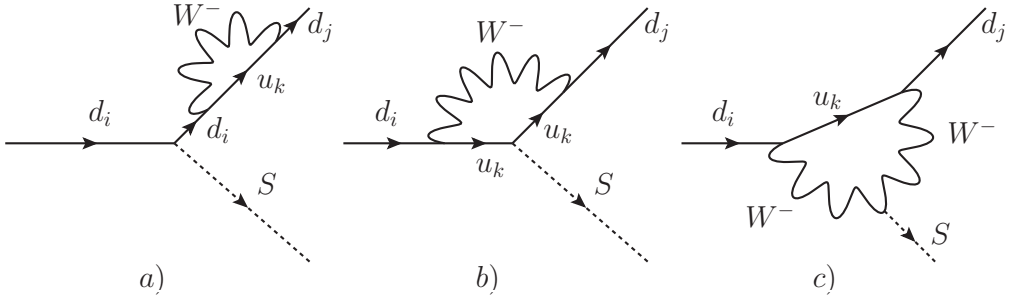


**Figure 2.3**: Diagrams of $S$ particle production: flavor changing quarks transitions in unitary gauge.

follows (the information is given in the format "Hadron name(quark contents, mass in MeV)")

**Mesons**

- s-mesons $K^-(s\bar{u}, 494)$, $K^0_{S,L}(s\bar{d}, 498)$;
- c-mesons $D^0(c\bar{u}, 1865)$, $D^+(c\bar{d}, 1870)$, $D_s(c\bar{s}, 1968)$, $J/\psi(c\bar{c}, 3097)$;
- b-mesons $B^-(b\bar{u}, 5279)$, $B^0(b\bar{d}, 5280)$, $B_s(b\bar{s}, 5367)$, $B_c(b\bar{c}, 6276)$, $\Upsilon(b\bar{b}, 9460)$;

**Baryons**

- light baryons $\Lambda^0(uds, 1116)$, $\Sigma^+(uus, 1189)$, $\Sigma^-(dds, 1197)$, $\Xi^0(uss, 1315)$, $\Xi^-(dss, 1322)$, $\Omega^-(sss, 1672)$;
- c-baryons $\Lambda_c(udc, 2287)$, $\Xi^+_c(usc, 2468)$, $\Xi^0_c(dsc, 2480)$;
- b-baryons $\Lambda_b(udb, 5619)$, $\Xi^0_b(usb, 5792)$, $\Xi^-_b(dsb, 5795)$, $\Omega_b(ssb, 6071)$.

The light scalar $S$ can be produced from the hadron through two-body decay via the flavor changing quark transitions (see diagrams in Fig. 2.3). In the Ref. [182] only production channels from $K$, $D$ and $B$ mesons were considered as the most effective ones. We will follow their approach.

The flavor changing amplitude was calculated using different techniques in many papers [201–204]. To be specific, the result for the amplitude $b \to s + S$ is:

$$M_{fi} = \frac{3\theta g^2}{64\pi^2 M_W^2 v} \sum_{i=u,c,t} V^*_{is} V_{ib} m^2_{u_i} \left[ m_b \bar{s}_L b_R + m_s \bar{s}_R b_L \right] \approx$$

$$\approx |m_b \gg m_s| \approx \frac{3\theta g^2}{64\pi^2 M_W^2 v} \sum_{i=u,c,t} V^*_{is} V_{ib} m^2_{u_i} m_b \bar{s}_L b_R. \quad (2.2.1)$$

strong interactions). The probability of light scalar production from hadron is inversely proportional to the hadron decay width thus the light scalar production from the lightest hadrons is the most efficient.

Generalizing this result (2.2.1) and taking into account that the mass of every next quark generation is much larger than for previous ones, one can write the effective Lagrangian of flavor changing quark interactions with $S$ particle as

$$\mathcal{L}_{eff}^{Sqq} = \theta \frac{S}{v} \sum_{\substack{i,j=1 \\ i<j}}^{3} \left( \xi_d^{ij} m_{d_j} \bar{d}_i P_R d_j + \xi_u^{ij} m_{u_j} \bar{u}_i P_R u_j + h.c. \right). \tag{2.2.2}$$

Here $m_{d_j}$ and $m_{u_j}$ are masses of up and down quarks, $P_R$ is a projector on the right chiral state, $V_{ij}$ are the elements of the CKM matrix, $G_F$ is the Fermi constant, and

$$\xi_d^{ij} = \frac{3G_F\sqrt{2}}{16\pi^2} \sum_{k=u,c,t} V_{ki}^* m_k^2 V_{kj}, \qquad \xi_u^{ij} = \frac{3G_F\sqrt{2}}{16\pi^2} \sum_{k=d,s,b} V_{ik}^* m_k^2 V_{jk}. \tag{2.2.3}$$

Numerical values of some of the constants $\xi$ are given in the Table 2.1.

| $\xi$ | Value |
|---|---|
| $\xi_d^{ds}$ | $3.3 \cdot 10^{-6}$ |
| $\xi_u^{uc}$ | $1.4 \cdot 10^{-9}$ |
| $\xi_d^{db}$ | $7.9 \cdot 10^{-5}$ |
| $\xi_d^{sb}$ | $3.6 \cdot 10^{-4}$ |

**Table 2.1**: Values of some useful $\xi$ constants.

The matrix element for the $h \to Sh'$ decay is [204]

$$\mathcal{M}(h \to Sh') \approx \theta \frac{M_h^2}{2v} \xi_{u/d}^{\alpha\beta}, \tag{2.2.4}$$

where $h$ and $h'$ are mesons, which differ from each other by replacing $\beta$ with $\alpha$ quark.

In particular, estimates for $s$, $c$ and $b$ mesons are:

$$\mathcal{M}(K \to S\pi) \approx \theta \frac{M_K^2}{v} \frac{1}{2} \frac{3G_F\sqrt{2}}{16\pi^2} \sum_{i=u,c,t} V_{is}^* m_i^2 V_{id} \approx 1.7 \cdot 10^{-9} \cdot \theta \text{ GeV}; \tag{2.2.5}$$

$$\mathcal{M}(D \to S\pi) \approx \theta \frac{M_D^2}{v} \frac{1}{2} \frac{3G_F\sqrt{2}}{16\pi^2} \sum_{i=d,s,b} V_{ic}^* m_i^2 V_{iu} \approx 1.0 \cdot 10^{-11} \cdot \theta \text{ GeV}; \tag{2.2.6}$$

$$\mathcal{M}(B \to S\pi) \approx \theta \frac{M_B^2}{v} \frac{1}{2} \frac{3G_F\sqrt{2}}{16\pi^2} \sum_{i=u,c,t} V_{ib}^* m_i^2 V_{id} \approx 4.5 \cdot 10^{-6} \cdot \theta \text{ GeV}; \tag{2.2.7}$$

$$\mathcal{M}(B \to SK) \approx \theta \frac{M_B^2}{v} \frac{1}{2} \frac{3G_F\sqrt{2}}{16\pi^2} \sum_{i=u,c,t} V_{ib}^* m_i^2 V_{is} \approx 2.0 \cdot 10^{-5} \cdot \theta \text{ GeV}. \tag{2.2.8}$$

The matrix element for the $D$ meson decay is suppressed compared to $K$ or $B$ for two reasons:

- The heaviest quark in the intermediate state for the $D$ decay is the $b$ quark, that is much lighter than the $t$ quark in $K$ and $B$ mesons.

- CKM elements for the $D$ decay are much smaller than for $K$ and $B$ mesons.

Using this information, we estimate the branching ratio for mesons into the scalar $S$ and some other meson $h'$ as

$$\mathrm{BR}(h \to Sh') = \frac{1}{\Gamma_{tot}(h)} \frac{|\mathcal{M}(h \to Sh')|^2}{16\pi M_h} \frac{2|p_S|}{M_h}, \tag{2.2.9}$$

where $p_S$ is the momentum of the scalar $S$,

$$|p_S| = \frac{\sqrt{(M_h^2 - (m_S + m_h')^2)(M_h^2 - (m_S - m_h')^2)}}{2M_h}. \tag{2.2.10}$$

The results for different reactions are given in the Table 2.2.

| Meson | $\mathrm{BR}(h \to SX) / \left(\frac{2\lvert p_S\rvert}{M_h}\theta^2\right)$ |
|---|---|
| $K^\pm \to S\pi^\pm$ | $1.8 \cdot 10^{-3}$ |
| $K_L^0 \to S\pi^0$ | $7.4 \cdot 10^{-3}$ |
| $K_s^0 \to S\pi^0$ | $1.3 \cdot 10^{-5}$ |
| $D^\pm \to S\pi^\pm$ | $3.0 \cdot 10^{-12}$ |
| $B^\pm \to SK^\pm$ | 4.5 |
| $B^0 \to SK^0$ | 4.2 |
| $B^\pm \to S\pi^\pm$ | 0.22 |
| $B^0 \to S\pi^0$ | 0.20 |

**Table 2.2**: Branching ratios of the 2-body meson decay.

The branching ratio of the $D \to S\pi$ decay is very small and it turns out that three-body decay is more probable [205, 206],

$$\mathrm{BR}(h \to Se\nu) = \frac{\sqrt{2} G_F M_h^4}{96\pi^2 m_\mu^2 (1 - m_\mu^2/M_h^2)^2} \times \mathrm{BR}(h \to \mu\nu) \left(\frac{7}{9}\right)^2 f\left(\frac{m_S^2}{M_h^2}\right), \tag{2.2.11}$$

where $f(x) = (1 - 8x + x^2)(1 - x^2) - 12x^2 \ln x$. The numerical values of the $h \to Se\nu$ decay for $D, K$ and $B$ mesons are given in the Table 2.3.

For kaons, we need to take into account that a large number of them will be scattered in the hadron absorber before decay. The scattered kaons are effectively lost to the light scalar production process. In Appendix 4.1.2, a simple estimate is made of the probability of the kaon decay $P_{decay}$ before scattering using the lifetime and the cross section for the kaon in the material of the hadron absorber. The results are given in the Table 2.4.

| Meson | $\mathrm{BR}(h \to Se\nu)/f\,(x)\,\theta^2$ |
|---|---|
| $D \to Se\nu$ | $5.2 \cdot 10^{-9}$ |
| $K \to Se\nu$ | $4.1 \cdot 10^{-8}$ |
| $B \to Se\nu$ | $< 7.4 \cdot 10^{-10}$ |

**Table 2.3**: Branching ratios of the 3-body meson decay. From the experimental data, we have only the upper bound on the $\mathrm{BR}(B \to \mu\nu)$, thus we put an upper bound on the $B \to Se\nu$ decay.

| Meson | $P_{decay}$ | $\mathrm{BR}(K \to S\pi) \times P_{decay} / \left(\theta^2 \frac{2\lvert p_S \rvert}{M_K}\right)$ |
|---|---|---|
| $K^{\pm}$ | $1.7 \cdot 10^{-3}$ | $3.1 \cdot 10^{-6}$ |
| $K_L^0$ | $4 \cdot 10^{-4}$ | $3.0 \cdot 10^{-6}$ |
| $K_s^0$ | 0.2 | $2.6 \cdot 10^{-6}$ |

**Table 2.4**: The decay probability for kaons in the SHiP absorber and the effective branching ratios.

We expect to produce the following number of mesons at SHiP for the 5 years of experiment: $N_K = 5.7 \cdot 10^{19}$ of kaons, $N_D = 6.8 \cdot 10^{17}$ of $D$ mesons and $N_B = 6.4 \cdot 10^{13}$ of $B$ mesons (see Sec. 4.1.1 for more details). Production from $B$ mesons is $10^4$ times more efficient than from $D$ mesons. The expected number of light scalars is given in Fig. 2.4.

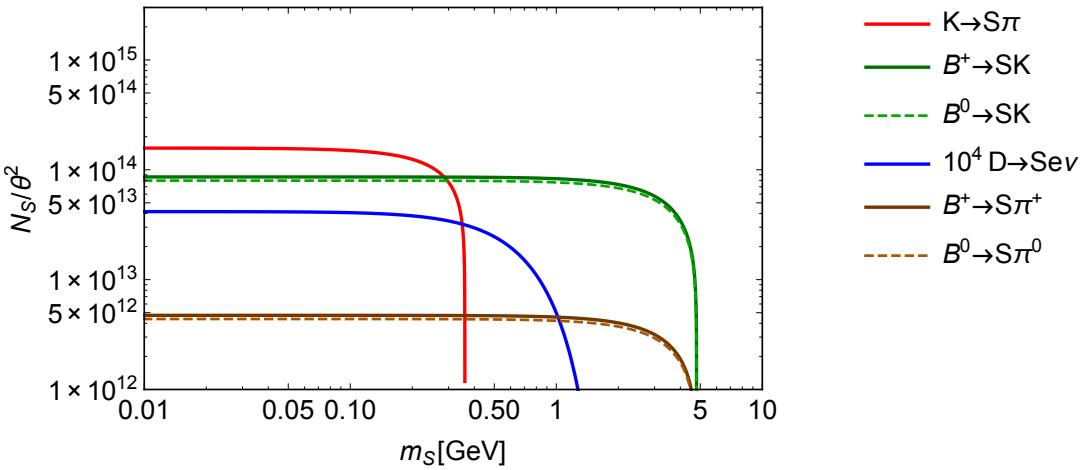


**Figure 2.4**: The expected number of produced light scalars at SHiP as a function of the mass of the scalar particle.

## 2.3 Decay widths of a scalar particle

The light scalar particle $S$ interacts with the SM particles due to mixing with the Higgs boson, and its branching ratios coincide with the light Higgs branching ratios.

The main decay channels are decays into leptons and hadrons, see the paper [182]. Following this paper, we discuss separately two mass regions of the scalar $S$ for decay into hadrons: below 1 GeV, where it is calculated using chiral perturbation theory and above 2 GeV, where it is estimated using perturbative QCD. The decay into photons is suppressed and is not be considered here.

### 2.3.1 Decay into leptons

The decay width for $S$ particle into lepton is given by

$$\boxed{\Gamma(S \to l^+ l^-) = \frac{\theta^2 m_l^2 m_S}{8\pi v^2}\left(1 - \frac{4m_l^2}{m_S^2}\right)^{3/2}}, \tag{2.3.1}$$

where $\theta$ is the mixing angle. This formula is valid for any mass of the scalar $m_S$.

### 2.3.2 Decay into hadrons

**The scalar mass below 1 GeV** If the mass of the scalar particle $S$ is above the hadronic threshold, i.e. $m_S > 2m_\pi$, then the decay into pions is possible. The best (known to us) description of this decay is given in the paper [207], which combines chiral perturbation theory next to leading order with the method of dispersion relations. Using data on pion-pion scattering, the authors produced a prediction for the light Higgs decay width into 2 pions, see Fig. 2.5.

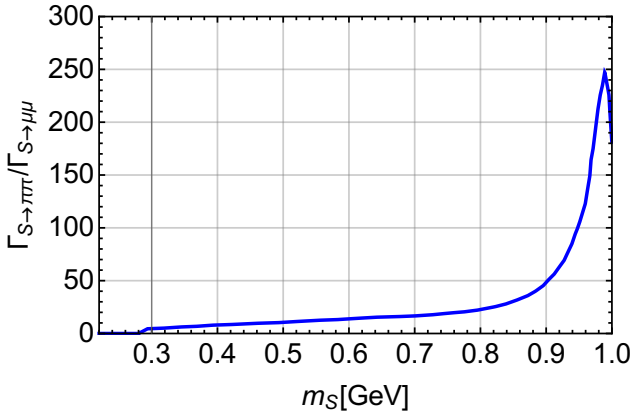


**Figure 2.5**: The ratio of the decay widths of the Higgs boson into pions and muons as a function of the scalar mass. Adapted from work [207].

**The scalar mass above 2 GeV** For this mass region, the decay width into hadrons can be estimated as the decay width into gluons and quarks. The decay width into gluons (with QCD corrections) [182, 208] is,

$$\boxed{\Gamma(S \to gg) = |F|^2 \left(\frac{\alpha_s}{4\pi}\right)^2 \frac{\theta^2 m_S^3}{8\pi v^2}\left(1 + \frac{m_t^2}{8v^2\pi^2}\right)}. \tag{2.3.2}$$

Here $m_t$ is the mass of the top quark and $F = \sum_q F_q$ is a sum of the loop contributions from quarks, which is defined as,

$$F_q = -2y_q(1 + (1 - y_q)x_q^2), \tag{2.3.3}$$

with $y_q = 4m_q^2/m_S^2$ and

$$x_q = \begin{cases} \text{Arctan}\dfrac{1}{\sqrt{y_q - 1}}, & \text{for } \; y_q > 1, \\ \dfrac{1}{2}\left(\pi + i\log\dfrac{1 + \sqrt{y_q - 1}}{1 - \sqrt{y_q - 1}}\right), & \text{for } \; y_q \leq 1. \end{cases} \tag{2.3.4}$$

We use the following quark masses (in GeV):

$m_u = 2.3 \cdot 10^{-3}$, $m_d = 4.8 \cdot 10^{-3}$, $m_s = 0.0924$, $m_c = 1.23$, $m_b = 4.2$, and $m_t = 173$.

Decay into quarks with the QCD corrections is calculated in the paper [208]. The decay width into quarks is basically the same as into leptons (2.3.1), multiplied by the color factor 3, and taking into account running masses for quarks and QCD corrections, namely

$$\boxed{\Gamma(S \to \bar{q}q) = 3\frac{\theta^2 m_S \overline{m}_q^2(m_S)}{8\pi v^2}\beta^3\big(1 + \Delta_{\text{QCD}} + \Delta_t\big)}, \tag{2.3.5}$$

where

$$\beta = \left(1 - \frac{4\overline{m}_q^2(m_S)}{m_S^2}\right)^{1/2}, \tag{2.3.6}$$

$$\begin{aligned} \Delta_{\text{QCD}} = {} & 5.67\frac{\alpha_s(m_S)}{\pi} + (35.94 - 1.36N_f)\left(\frac{\alpha_s(m_S)}{\pi}\right)^2 \\ & + (164.14 - 25.77N_f + 0.259N_f^2)\left(\frac{\alpha_s(m_S)}{\pi}\right)^3, \end{aligned} \tag{2.3.7}$$

$$\Delta_t = \left(\frac{\alpha_s(m_S)}{\pi}\right)^2\left(1.57 - \frac{2}{3}\log\frac{m_S^2}{m_t^2} + \frac{1}{9}\log^2\frac{\overline{m}_q^2(m_S)}{m_S^2}\right), \tag{2.3.8}$$

and the running mass [208] $\overline{m}_q(m_S)$ is given by

$$\overline{m}_q(m_S) = \overline{m}_q(Q)\frac{c(\alpha_s(m_S)/\pi)}{c(\alpha_s(Q)/\pi)}, \tag{2.3.9}$$

with the coefficient $c$, which is equal to,

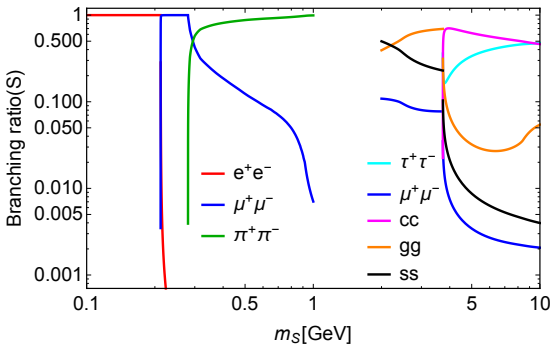


**Figure 2.6**: Branching ratios of the scalar $S$ as a function of its mass.

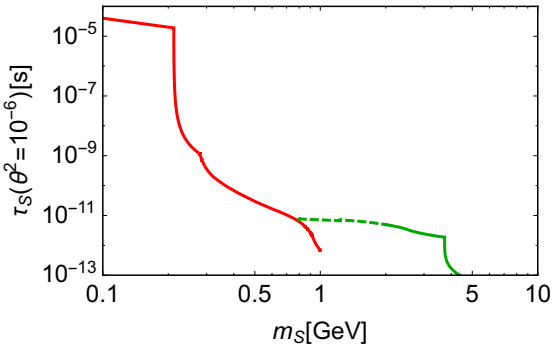


**Figure 2.7**: Lifetime of the scalar $S$ as a function of its mass with the mixing angle $\theta^2 = 10^{-6}$, where the green dashed line in the middle region is calculated using perturbative QCD formulas.

$$c(x) = \left(\frac{9}{2}x\right)^{4/9}(1 + 0.895x + 1.371x^2 + 1.952x^3), \qquad \text{for } M_s < m_S < M_c, \tag{2.3.10}$$

$$c(x) = \left(\frac{25}{6}x\right)^{12/25}(1 + 1.014x + 1.389x^2 + 1.091x^3), \qquad \text{for } M_c < m_S < M_b, \tag{2.3.11}$$

$$c(x) = \left(\frac{23}{6}x\right)^{12/23}(1 + 1.175x + 1.501x^2 + 0.1725x^3), \qquad \text{for } M_b < m_S < M_t. \tag{2.3.12}$$

We use the quark masses in MS-bar scheme at $Q = 2$ TeV scale [209]: $\overline{m}_c = 1.23$ and $\overline{m}_s = 0.0924$.
The resulting branching ratios for the scalar $S$ and its lifetime are presented in Figs. 2.6 and 2.7.

# Chapter 3

# Neutrino portal

In general, the number of model parameters in the neutrino portal increases with the number of HNLs (see e.g. reviews [144, 210]). For example, the model containing two sterile neutrinos has a total of eleven free parameters, whereas the model with three has a total of eighteen free parameters [144]. Despite this, not all of them play an important role, since phenomenology is sensitive to only the mass of the HNL(s) and the absolute values of mixing angles, $|U_{\alpha I}|$.

In contrast to the behavior of active neutrinos, sterile neutrinos that are no degenerate in mass are produced and decay independently – i.e., without oscillations between themselves. Thus, from a phenomenological point of view it is sufficient to describe one sterile neutrino with only four parameters: the sterile neutrino mass $M_N$ plus the mixing angles with the three known active neutrinos $U_\alpha$, see Eq. (1.5.2) for fixed $I$ value. Such *Heavy Neutral Leptons* can be searched for in different high-energy experiments. In this section, we will discuss their phenomenology.

## 3.1 HNL production in proton fixed-target experiments

In fixed-target experiments, such as NA62, SHiP or DUNE, the initial interaction is a proton-nuclei collision. In such collisions, HNLs can be produced in a number of ways:

*a)* Production from hadron decays;
*b)* Production from Deep Inelastic Scattering (DIS) p-nucleon interaction;
*c)* Production from the coherent proton-nucleus scattering.

Below we provide an overview of each of the channels summarizing previous results and emphasizing novel points.

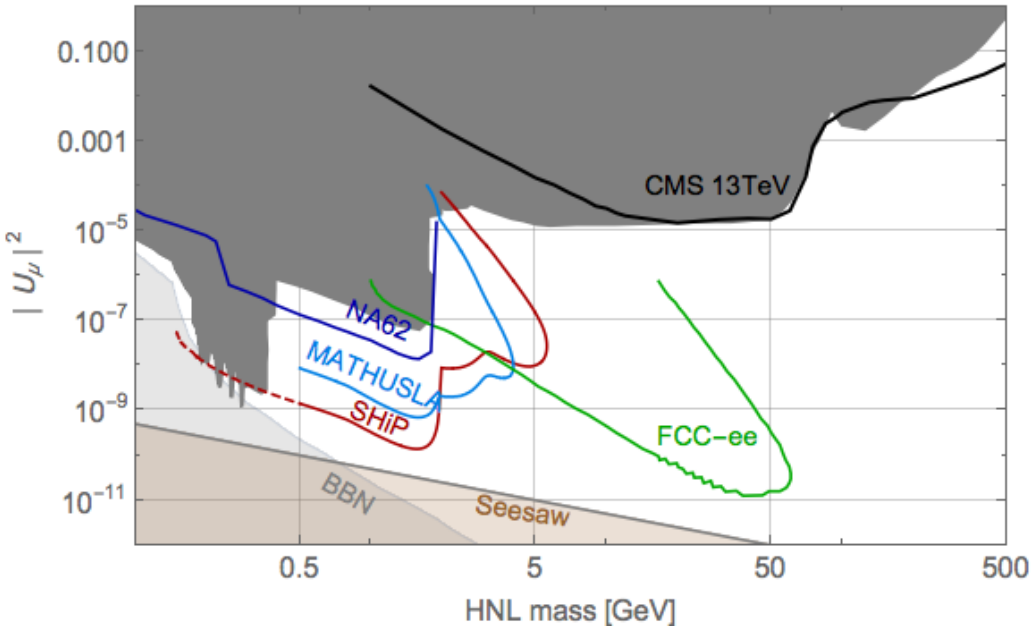


**Figure 3.1**: Existing limits and future prospects for searches for HNLs. Only mixing with muon flavor is shown. For the list of previous experiments (gray area) see [110]. The black solid line is a recent bound from the CMS 13 TeV run [211]. The sensitivity estimates from prospective experiments are based on [168] (FCC-ee), [109] (NA62), [212] (SHiP) and [213] (MATHUSLA). The sensitivity of SHiP below kaon mass (dashed line) is based on the number of HNLs produced in the decay of $D$-mesons only and does not take into account contributions from kaon decays, see [212] for details. The primordial nucleosynthesis bounds on HNL lifetime are from [214]. The Seesaw line indicates the parameters obeying the seesaw relation $|U_\mu|^2 \sim m_\nu/M_N$, where for active neutrino mass we substitute $m_\nu = \sqrt{\Delta m^2_{\rm atm}} \approx 0.05\,\text{eV}$ [110].

### 3.1.1 Production from hadrons

The main channels of HNL production from hadrons are via decays of sufficiently long-lived hadrons, i.e. the lightest hadrons of each flavor[1]. In the framework of the Fermi theory, the decays are inferred by the weak charged currents. One can also investigate the production through neutral current from the hidden flavored mesons $J/\psi(c\bar{c}, 3097)$, $\Upsilon(b\bar{b}, 9460)$ as sources of HNLs. These mesons are short-lived, but 1.5–2 times heavier than the corresponding open flavored mesons, giving a chance to produce heavier HNLs.

Since the region of HNL masses below that of the kaon is strongly constrained by previous experiments (see [110] for details, reproduced in Fig. 3.1), we concentrate on the production channels for HNL masses $M_N > 0.5$GeV.

[1]Such hadrons decay *only* through weak interactions with relatively small decay width (as compared to electromagnetic or strong interaction). As the probability of HNL production from the hadron's decay is inversely proportional to the hadron's decay width, the HNL production from the lightest hadrons is significantly more efficient.

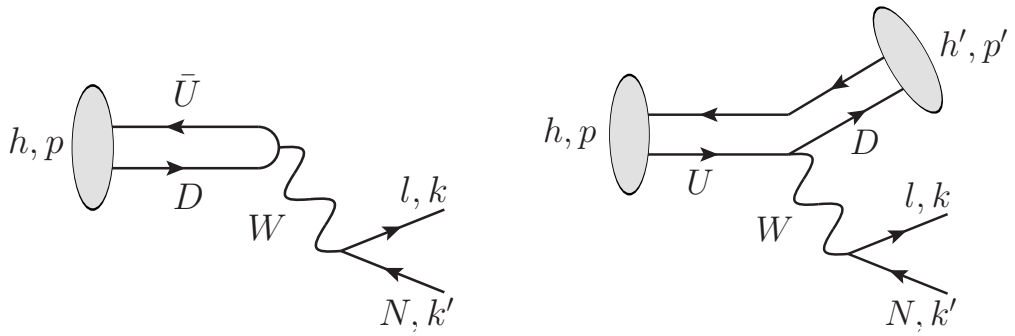


**Figure 3.2**: *Left:* The diagram of leptonic decay of the meson $h$ with 4-momentum $p$. *Right:* The diagram of semileptonic decay of the meson $h$ with 4-momentum $p$ into meson $h'$ with 4-momentum $p'$. In both diagrams the 4-momentum transferred to the lepton pair is $q = k + k'$.

HNLs are produced in meson decay either via a 2-body purely leptonic decay (left panel of Fig. 3.2) or semileptonic decay (right panel of Fig. 3.2) [215, 216]. The branching fractions of the leptonic decay have already been determined e.g. in [217, 218]. However, in the case of semileptonic decays, only the processes with a single pseudo-scalar or vector meson in the final state have been considered so far [218] (see also [219] and [220])

$$h \to h'_P \ell N \tag{3.1.1}$$

$$h \to h'_V \ell N \tag{3.1.2}$$

(where $h'_P$ is a *pseudo-scalar* and $h'_V$ is a *vector* meson). We reproduce computations of the branching ratios for these production channels in the Appendix A paying special attention to the treatment of form factors.

Finally, to calculate the number of produced HNLs one should ultimately know the *production fraction*, $f(\bar{q}q \to h)$ i.e. the probability a given hadron being produced from the corresponding heavy quark. It can either be determined experimentally or computed from Pythia simulations (as e.g. in [221]).

#### 3.1.1.1 Production from light unflavored and strange mesons

Among the light unflavored and strange mesons the relevant mesons for the HNL production are:[2] $\pi^+(u\bar{d}, 139.6)$, $K^+(u\bar{s}, 494)$, $K^0_S(d\bar{s}, 498)$ and $K^0_L(d\bar{s}, 498)$.

The only possible production channel from the $\pi^+$ is the 2-body decay $\pi^+ \to \ell^+_\alpha N$ with $\ell = e, \mu$. The production from $K^+$ is possible through the 2-body decay of the same type. There are also 3-body decays $K^+ \to \pi^0 \ell^+_\alpha N$ and $K^0_{L/S} \to \pi^- \ell^+_\alpha N$.

[2]The particle lists here and below are given in the format 'Meson name(quark contents, mass in MeV)').

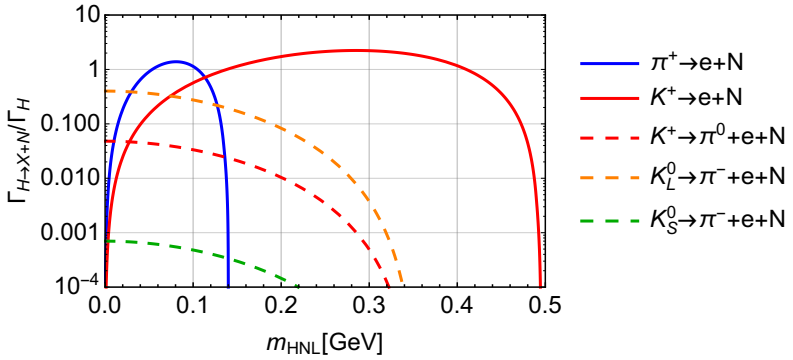


**Figure 3.3**: Decay width to HNLs divided by the measured total decay width for pions and kaons correspondingly. In this Figure we take $U_e = 1$, $U_\mu = U_\tau = 0$.

The resulting branching ratios for corresponding mesons are shown in Fig. 3.3. For small HNL masses, the largest branching ratio is that of $K_L^0 \to \pi^- \ell_\alpha^+ N$ due to the helicity suppression in the 2-body decays and small decay width of $K_L^0$.

#### 3.1.1.2 Production from charmed mesons

The following charmed mesons are most relevant for the HNL production: $D^0(c\bar{u}, 1865)$, $D^+(c\bar{d}, 1870)$, $D_s(c\bar{s}, 1968)$.

$D^0$ is a neutral meson and therefore its decay through the charged current interaction necessarily involves a meson in a final state. The largest branching is to $K$ meson, owing to the CKM suppression $|V_{cd}|/|V_{cs}| \approx 0.22$. Then the mass of the resulting HNL is limited to $M_N < M_D - M_K \approx 1.4$GeV. For the charmed *baryons* the same argument is applicable: they should decay into baryons and the most probable is strange baryon, hence $M_N < M_{\Lambda_c} - M_\Lambda \approx 1.2$GeV. Therefore these channels are open only for HNL mass *below* $\sim 1.4$GeV.

Charged charmed mesons $D^\pm$ and $D_s$ would exhibit 2-body decays into an HNL and a charged lepton, so they can produce HNLs almost as heavy as themselves. The branching ratio of $D_s \to N + X$ is more than 10 times larger than any ratio of other $D$-mesons. The number of $D_s$ mesons is, of course, suppressed as compared to $D^\pm$ and $D^0$ mesons, however only by a factor of few[3]. Indeed, at energies relevant for $\bar{c}c$ production, the fraction of strange quarks is already sizeable, $\chi_{\bar{s}s} \sim 1/7$ [222]. *As a result, the two-body decays of $D_s$ mesons dominate in the HNL production from charmed mesons*, see Fig. 3.4.

#### 3.1.1.3 Production from beauty mesons

The lightest beauty mesons are $B^-(b\bar{u}, 5279)$, $B^0(b\bar{d}, 5280)$, $B_s(b\bar{s}, 5367)$, $B_c(b\bar{c}, 6276)$. Similarly to the $D^0$ case, neutral $B$-mesons ($B^0$ and $B_s$) decay through a charged

[3]For example at SPS energy (400 GeV) the production fractions of the charmed mesons are given by $f(D^+) = 0.204$, $f(D^0) = 0.622$, $f(D_s) = 0.104$ [221].

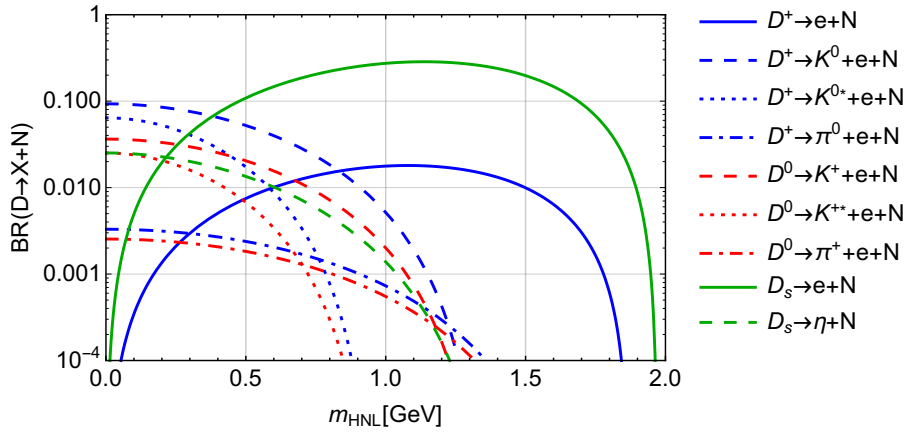


**Figure 3.4**: Dominant branching ratios of HNL production from different charmed and beauty mesons. For charged mesons 2-body leptonic decays are shown, while for the neutral mesons decays are necessarily semileptonic. For these plots we take $U_e = 1$, $U_\mu = U_\tau = 0$.

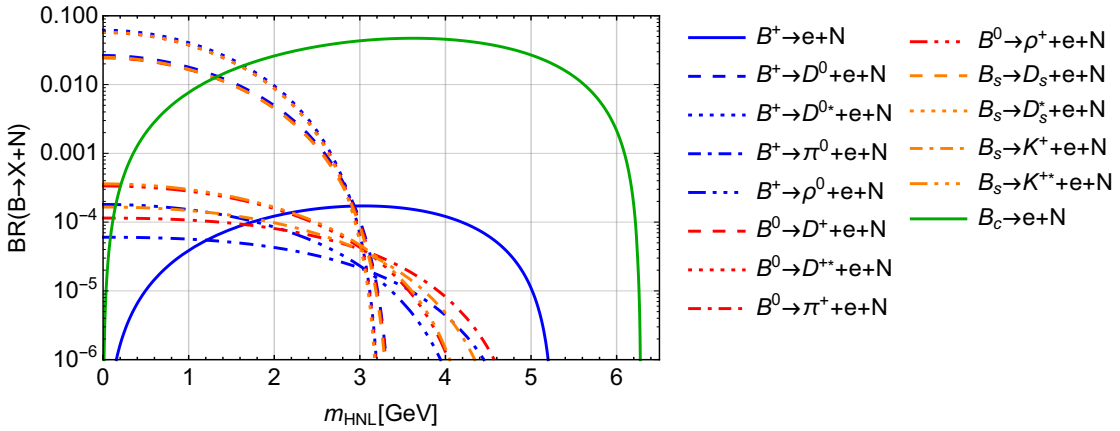


**Figure 3.5**: Dominant branching ratios of HNL production from different beauty mesons. For charged mesons 2-body leptonic decays are shown, while for the neutral mesons decays are necessarily semileptonic. For these plots we take $U_e = 1$, $U_\mu = U_\tau = 0$.

current with a meson in the final state. The largest branching is to the $D$ meson because of the values of the CKM matrix elements ($|V_{cb}|/|V_{ub}| \approx 0.1$). Thus the mass of the resulting HNL is limited: $M_N < M_B - M_D \approx 3.4$ GeV.

Charged beauty mesons $B^\pm$ and $B_c^\pm$ have 2-body decays into HNL and charged lepton, so they can produce HNLs almost as heavy as themselves. Branching ratios of $B$-mesons into HNL for different decay channels and pure electron mixing are shown in Fig. 3.5.

The production fraction of $f(b \to B_c)$ has only been measured at LHC energies, where it is reaching a few $\times\, 10^{-3}$ [223]. At lower energies, it is not known. Nevertheless, production from $B_c$ meson is an important production channel in the mass

| Decay $B^+ \to \ell^+ \nu_\ell X$ | | BR [%] |
|---|---|---|
| Inclusive branching: $l = e,\, \mu$ | | $11.0 \pm 0.3$ |
| Dominant 1-meson channels: pseudo-scalar meson | $\overline{D}^0 \ell^+ \nu_\ell$ | $2.27 \pm 0.11$ |
| vector meson | $\overline{D}^*(2007)^0 \ell^+ \nu_\ell$ | $5.7 \pm 0.19$ |
| Two above channels together: | | $8.0 \pm 0.2$ |
| Channels with 2 mesons: | $D^- \pi^+ \ell^+ \nu_\ell$ | $0.42 \pm 0.05$ |
| | $D^{*-} \pi^+ \ell^+ \nu_\ell$ | $0.61 \pm 0.06$ |
| $D^- \pi^+ \ell^+ \nu_\ell$ above is saturated by 1-meson modes | $\overline{D}_0^*(2420)^0 \ell^+ \nu_\ell$ | $0.25 \pm 0.05$ |
| | $\overline{D}_2^*(2460)^0 \ell^+ \nu_\ell$ | $0.15 \pm 0.02$ |
| $D^{*-} \pi^+ \ell^+ \nu_\ell$ is augmented with 1-meson modes | $\overline{D}_1(2420)^0 \ell^+ \nu_\ell$ | $0.30 \pm 0.02$ |
| | $\overline{D}_1'(2430)^0 \ell^+ \nu_\ell$ | $0.27 \pm 0.06$ |
| | $\overline{D}_2^*(2460)^0 \ell^+ \nu_\ell$ | $0.1 \pm 0.02$ |
| Hence 1-meson modes contribute additionally | | $1.09 \pm 0.12$ |
| Sum of other multi-meson channels, $n > 1$: | $\overline{D}^{(*)} n\pi \ell^+ \nu_\ell$ | $0.84 \pm 0.27$ |
| Inclusive branching: $l = \tau$ | | not known |
| Dominant 1-meson channels: pseudo-scalar meson | $\overline{D}^0 \tau^+ \nu_\tau$ | $0.77 \pm 0.25$ |
| vector meson | $\overline{D}^*(2007)^0 \tau^+ \nu_\tau$ | $1.88 \pm 0.20$ |

**Table 3.1**: Experimentally measured branching ratios for the main semileptonic decay modes of the $B^+$ and $B^0$ meson [222]. Decays to pseudoscalar ($D$) and vector ($D^*$) mesons together constitute 73% (for $B^+$) and 69% (for $B^0$). Charmless channels are not shown because of their low contribution

range $m_N \gtrsim 3.4$ GeV.

To understand this result let us compare HNL production from $B_c$ with production from 2-body $B^+$ decay. Decay widths for both cases are given by (see Eq. (A.1.4))

$$\mathrm{Br}(h \to \ell_\alpha N) \approx \frac{G_F^2 f_h^2 m_h m_N^2}{8\pi \Gamma_h} |V_h^{\mathrm{CKM}}|^2 |U_\alpha|^2 K(m_N/m_h), \tag{3.1.3}$$

where we take $m_N \gg m_\ell$ and $K$ is a kinematic suppression. Neglecting kinematic factor, the ratio for the numbers of HNLs is

$$\frac{N_{\mathrm{HNL}}(B_c \to \ell N)}{N_{\mathrm{HNL}}(B^+ \to \ell N)} \approx \underbrace{\frac{f_{b\to B_c}}{f_{b\to B^+}}}_{\approx 0.008} \times \underbrace{\frac{\Gamma_{B^+}}{\Gamma_{B_c}}}_{\approx 0.3} \times \underbrace{\left(\frac{f_{B_c}}{f_{B^+}}\right)^2}_{\approx 5} \times \underbrace{\frac{m_{B_c}}{m_{B^+}}}_{\approx 1.2} \times \underbrace{\left(\frac{V_{cb}^{\mathrm{CKM}}}{V_{ub}^{\mathrm{CKM}}}\right)^2}_{\approx 100} \approx 1.44. \tag{3.1.4}$$

We see that small fragmentation fraction of $B_c$ meson is compensated by the ratio of CKM elements and meson decay constants.

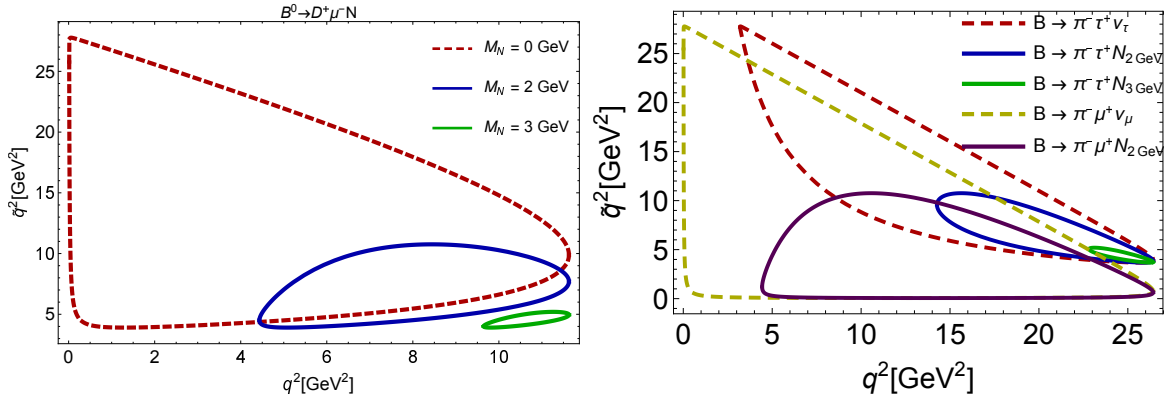


**Figure 3.6**: Dalitz plot for the semileptonic decay $B^0 \to D^+\mu^- N$. Available phase-space shrinks drastically when the HNL mass is large. $q^2$ is the invariant mass of the lepton pair, $\tilde{q}^2$ is the invariant mass of final meson and charged lepton.

#### 3.1.1.4 Multi-hadron final states

$D$ and especially $B$ mesons are heavy enough to decay into HNL and multi-meson final states. While any single multi-meson channel would be clearly phase-space suppressed as compared to 2-body or 3-body decays considered above, one should check that the "inclusive" multi-hadron decay width does not give a sizeable contribution.

To estimate the relative relevance of single and multi-meson decay channels, we first consider the branching ratios of the semileptonic decays of $B^+$ and $B^0$ (with ordinary massless neutrino $\nu_\ell$ in the final state)

$$B \to \ell^+ \nu_\ell X \quad , \quad l = e,\, \mu\,, \tag{3.1.5}$$

where $X$ stands for one or many hadrons. The results are summarized in Table 3.1. Clearly, by taking into account *only* the single meson states we would *underestimate* the total inclusive width of the process (3.1.5) by about 20%.

In case of semileptonic decays with the HNL in the final state, the available phase-space shrinks considerably, see Fig. 3.6. The effect of the mass can also be estimated by comparing the decays involving light leptons ($e/\mu$) to those with the $\tau$-lepton in the final state. Comparison with SM decay rates into $\tau$-lepton shows that 3-body decays into heavy sterile neutrinos are suppressed with respect to decays into light neutrinos. *Thus inclusive semileptonic decay of flavored mesons to HNLs are dominated by single-meson final states with the contributions from other states introducing a small correction.*

#### 3.1.1.5 Quarkonia decays

Next we investigate the hidden flavored mesons $J/\psi(c\bar{c}, 3097)$ and $\Upsilon(b\bar{b}, 9460)$ as sources of HNLs. These mesons are short-lived, but 1.5-2 times heavier than the

| | |
|---|---|
| Strange baryons | $\Lambda^0(uds, 1116)$, $\Sigma^+(uus, 1189)$, $\Sigma^-(dds, 1197)$, $\Xi^0(uss, 1315)$, $\Xi^-(dss, 1322)$, $\Omega^-(sss, 1672)$ |
| Charmed baryons | $\Lambda_c(udc, 2287)$, $\Sigma_c^{++}(uuc, 2453)$, $\Sigma_c^0(ddc, 2453)$, $\Xi_c^+(usc, 2468)$, $\Xi_c^0(dsc, 2480)$, $\Omega_c^-(ssc, 2695)$, $\Xi_{cc}^+(dcc, 3519)$ |
| Beauty baryons | $\Lambda_b(udb, 5619)$, $\Sigma_b^+(uub, 5811)$, $\Sigma_b^-(ddb, 5815)$, $\Xi_b^0(usb, 5792)$, $\Xi_b^-(dsb, 5795)$, $\Omega_b^-(ssb, 6071)$ |

**Table 3.2**: Long-lived flavored baryons. For each quark content (indicated in parentheses) only the lightest baryon of given quark content (ground state, masses are in MeV) is shown, see footnote 1 on page 42. The baryons considered in [221] have blue background. The baryons unobserved so far (such as $\Omega_{cc}^+(scc)$, $\Omega_{cb}(scb)$, etc.) are not listed.

corresponding open flavored mesons, giving a chance to produce heavier HNLs. We have studied these mesons in Appendix D, here we provide the summary of the results.

The number of HNLs produced from $J/\psi$ decays is always subdominant to the number of HNLs produced in $D$-meson decays (for $M_N < m_D$). Therefore, the range of interest is $2\text{GeV} \leq M_N \leq m_{J/\psi}$ where this number should be compared with the number of HNLs produced via $B$-meson decays. The resulting ratio is given by

$$\frac{\text{HNLs from } J/\psi}{\text{HNLs from } B} = \frac{X_{c\bar{c}} \times f(J/\psi) \times \text{BR}_{J/\psi \to N\bar{\nu}}}{X_{b\bar{b}} \times f(B) \times \text{BR}_{B \to NX}} = \\ = 3 \times 10^{-4} \left(\frac{X_{c\bar{c}}}{10^{-3}}\right) \left(\frac{10^{-7}}{X_{b\bar{b}}}\right) \quad (3.1.6)$$

where we have adopted $f(B) \times BR(B \to N + X) \sim 10^{-2}$ (c.f. Fig. 3.5) and used $f(J/\psi) \sim 10^{-2}$. The numbers in (3.1.6) are normalized to the 400 GeV SPS proton beam. One sees that $J/\psi$ can play a role only below $b\bar{b}$ production threshold (as $X_{b\bar{b}}$ tends to zero).

For experiments where a sizeable number of $b\bar{b}$ pairs is produced, one can use the $\Upsilon$ decays to produce HNLs with $M_N \gtrsim 5\text{GeV}$. The number of thus produced HNLs is given by

$$N_{\Upsilon \to N\bar{\nu}} \simeq 10^{-10} N_\Upsilon \times \left(\frac{U^2}{10^{-5}}\right) \quad (3.1.7)$$

where $N_\Upsilon$ is the total number of $\Upsilon$ mesons produced and we have normalized $U^2$ to the current experimental limit for $M_N > 5$ GeV (c.f. Fig. 3.1). It should be noted that HNLs with the mass of 5 GeV and $U^2 \sim 10^{-5}$ have the decay length $c\tau \sim$ cm.

#### 3.1.1.6 Production from baryons

Semileptonic decays of heavy flavored baryons (Table 3.2) produce HNLs. Baryon number conservation implies that either proton or neutron (or other heavier baryons) must be produced in the heavy baryon decay. This shrinks the kinematic window for the sterile neutrino by about 1 GeV. The corresponding heavy meson decays have an obvious advantage in this respect. Moreover, since both baryons and sterile neutrinos are fermions, only the baryon decays into three and more particles in the final state can yield sterile neutrinos, which further shrinks the sterile neutrino kinematic window with respect to the meson case, where 2-body, purely leptonic decays can produce sterile neutrinos.

Furthermore, lightly-flavored baryons and strange baryons (see Table 3.2) can only produce HNLs in the mass range where the bounds are very strong already (roughly below kaon mass, see FIG. 3.1). Indeed, as weak decays change the strangeness by 1 unit, there the double-strange $\Xi$-baryons can only decay to $\Lambda$ or $\Sigma$ baryons (plus electron or muon and HNL). The maximal mass of the HNL that can be produced in this process is *smaller* than $(M_{\Xi^-} - M_{\Lambda^0}) \simeq 200\,\text{MeV}$. Then, $\Omega^-$ baryon decays to $\Xi^0 \ell^- N$ with the maximal HNL mass not exceeding $M_{\Omega^-} - M_{\Xi^0} \simeq 350\,\text{MeV}$. Finally, weak decays of $\Lambda$ or $\Sigma$ baryons to $(p, n)$ can produce only HNLs lighter than $\sim 250\,\text{MeV}$.

The production of HNL in the decays of charmed and beauty hyperons has been investigated in Ref. [224]; these results have been recently checked in [225]. The number of such baryons is of course strongly suppressed as compared to the number of mesons with the same flavor. At the same time, the masses of HNLs produced in the decay of charmed (beauty) baryons are *below* the threshold of HNL production of the corresponding charmed (beauty) mesons due to the presence of a baryon in the final state. This makes such a production channel strongly subdominant. Dedicated studies for SHiP [221] and at the LHC [225] confirm this conclusion. It should be noted that Refs. [221, 224] use form factors from Ref. [226] which are about 20 years old. A lot of progress has been made since then (see e.g. [227, 228], where some of these form factors were re-estimated and a factor of $\sim 2$ differences with older estimates were established).

### 3.1.2 HNL production from tau leptons

At the center-of-mass energies well above the $\bar{c}c$ threshold $\tau$-leptons are copiously produced mostly via $D_s \to \tau + X$ decays. Then HNLs can be produced in $\tau$ decays that are important in the case of dominant mixing with $\tau$ flavor (which is the one least constrained, see [110, Chapter 4]). The main decay channels of $\tau$ are $\tau \to N + h_{P/V}$, $\tau \to N \ell_\alpha \bar{\nu}_\alpha$ and $\tau \to \nu_\tau \ell_\alpha N$, where $\alpha = e, \mu$. Computations of the corresponding decays widths are similar to the processes $N \to \ell_\alpha h_{P/V}$ (c.f. Appendix B.2) and

purely leptonic decays of HNL (see Section 3.2.1.1). The results are

$$\Gamma(\tau \to N h_P) = \frac{G_F^2 f_h^2 m_\tau^3}{16\pi} |V_{UD}|^2 |U_\tau|^2 \left[ \left(1 - y_N^2\right)^2 - y_h^2 (1 + y_N^2) \right] \sqrt{\lambda(1, y_N^2, y_h^2)} \tag{3.1.8}$$

$$\Gamma(\tau \to N h_V) = \frac{G_F^2 g_h^2 m_\tau^3}{16\pi m_h^2} |V_{UD}|^2 |U_\tau|^2 \left[ \left(1 - y_N^2\right)^2 + y_h^2 (1 + y_N^2 - 2y_h^2) \right] \sqrt{\lambda(1, y_N^2, y_h^2)} \tag{3.1.9}$$

$$\begin{aligned}
\Gamma(\tau \to N \ell_\alpha \bar{\nu}_\alpha) = {} & \frac{G_F^2 m_\tau^5}{96\pi^3} |U_\tau|^2 \int_{y_\ell^2}^{(1-y_N)^2} \frac{d\xi}{\xi^3} \left(\xi - y_\ell^2\right)^2 \sqrt{\lambda(1, \xi, y_N^2)} \times \\
& \times \left( \left(\xi + 2y_\ell^2\right) \left[1 - y_N^2\right]^2 + \xi \left(\xi - y_\ell^2\right) \left[1 + y_N^2 - y_\ell^2\right] - \xi y_\ell^4 - 2\xi^3 \right) \\
\approx {} & \frac{G_F^2 m_\tau^5}{192\pi^3} |U_\tau|^2 \left[1 - 8y_N^2 + 8y_N^6 - y_N^8 - 12 y_N^4 \log(y_N^2)\right], \quad \text{for } y_l \to 0
\end{aligned} \tag{3.1.10}$$

$$\begin{aligned}
\Gamma(\tau \to \nu_\tau \ell_\alpha N) = {} & \frac{G_F^2 m_\tau^5}{96\pi^3} |U_\alpha|^2 \int_{(y_\ell + y_N)^2}^{1} \frac{d\xi}{\xi^3} (1 - \xi)^2 \sqrt{\lambda(\xi, y_N^2, y_\ell^2)} \times \\
& \times \left( 2\xi^3 + \xi - \xi(1 - \xi) \left[1 - y_N^2 - y_\ell^2\right] - (2 + \xi) \left[y_N^2 - y_\ell^2\right]^2 \right) \approx \\
\approx {} & \frac{G_F^2 m_\tau^5}{192\pi^3} |U_\alpha|^2 \left[1 - 8y_N^2 + 8y_N^6 - y_N^8 - 12 y_N^4 \log(y_N^2)\right], \quad \text{for } y_l \to 0
\end{aligned} \tag{3.1.11}$$

where $y_i = m_i/m_\tau$, $V_{UD}$ is an element of the CKM matrix which corresponds to quark content of the meson $h_P$; $f_h$ and $g_h$ are pseudoscalar and vector meson decay constants (see Tables C.2 and C.3) and $\lambda$ is the Källén function [229]:

$$\lambda(a, b, c) = a^2 + b^2 + c^2 - 2ab - 2ac - 2bc \tag{3.1.12}$$

The results of this section fully agree with the literature [218].

### 3.1.3 HNL production via Drell-Yan and other parton-parton scatterings

The different matrix elements for HNL production in the proton-proton collisions are shown in Fig. 3.7. Here we are limited by the beam energy being not high enough to produce real weak bosons on the target protons. There are three types of processes: Drell-Yan-type process (a), gluon fusion (b) and $W\gamma/g$ fusion (c). Process (b) starts to play an important role for much higher center-of-mass energies [230, 231], processes (a) and (c) should be studied more accurately.

Let us start with the Drell-Yan process (a) in Fig. 3.7. The cross section at the

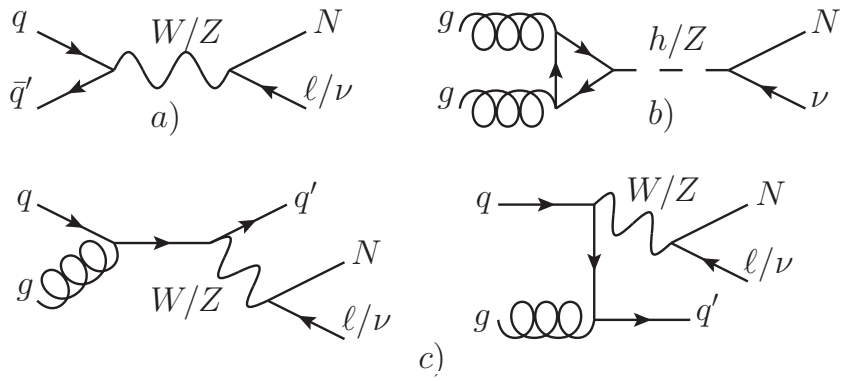


**Figure 3.7**: HNL production channels: a) Drell-Yan-type process; b) gluon fusion; c) quark-gluon fusion.

parton level is [232, 233]

$$\sigma(\bar{q}q' \to N\ell) = \frac{G_F^2 |V_{qq'}|^2 |U_\ell|^2 s_{\bar{q}q'}}{6N_c\pi} \left(1 - \frac{3M_N^2}{2s_{\bar{q}q'}} + \frac{M_N^6}{2s_{\bar{q}q'}^3}\right), \quad s_{\bar{q}q'} > M_N^2 \tag{3.1.13}$$

where $V_{qq'}$ is an element of the CKM matrix, $N_c = 3$ is a number of colors and the centre-of-mass energy of the system $\bar{q}q'$ is given by

$$s_{\bar{q}q'} = sx_1x_2 \tag{3.1.14}$$

where $x_1$ and $x_2$ are fractions of the total proton's momentum carried by the quark $q'$ and anti-quark $\bar{q}$ respectively. The total cross-section, therefore, is written as

$$\begin{aligned}\sigma(\bar{q}q' \to N\ell) = 2\sum_{\bar{q},q'} &\frac{G_F^2 |V_{qq'}|^2 |U_\ell|^2 s}{6N_c\pi} \\ &\times \int \frac{dx_1}{x_1} x_1^2 f_{\bar{q}}(x_1, s_{\bar{q}q'}) \int \frac{dx_2}{x_2} x_2^2 f_{q'}(x_2, s_{\bar{q}q'}) \left(1 - \frac{3M_N^2}{2sx_1x_2} + \frac{M_N^6}{2s^3x_1^3x_2^3}\right) \\ &\equiv \frac{G_F^2 |V_{qq'}|^2 |U_\ell|^2 s}{6N_c\pi} S(\sqrt{s}, M_N)\end{aligned} \tag{3.1.15}$$

where $f_q(x, Q^2)$ is the parton distribution function (PDF). The corresponding integral $S(\sqrt{s}, M_N)$ as a function of $M_N$ and the production probability for this channel are shown in Fig. 3.8. For numerical estimates we have used the LHAPDF package [234] with the CT10NLO PDF set [235].

This can be roughly understood as follows: PDFs peak at $x \ll 1$ (see Fig. 3.9) and therefore the probability that the center-of-mass energy of a parton pair exceeds the HNL mass, $\sqrt{s_{parton}} \gg M_N$, is small. On the other hand, the probability of a flavored meson to decay into an HNL (for $|U|^2 \sim 1$) is of the order of few % and

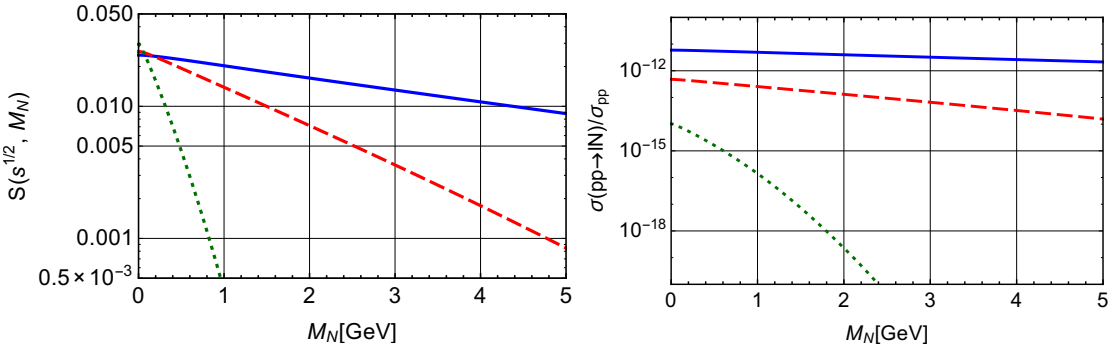


**Figure 3.8**: Integral (3.1.15) as a function of HNL's mass, neglecting lepton mass (left panel) and probability of HNL production in $p$-$p$ collision for $|U_\ell| = 1$ (right panel) for $\sqrt{s} = 100$ GeV (blue line), $\sqrt{s} = 28$ GeV (red dashed line) and $\sqrt{s} = 4$ GeV (green dotted line). The suppression of the integral as compared to $M_N = 0$ case is due to PDFs being small at $x \sim 1$ and condition $x_1 x_2 s > M_N^2$. Total $p$-$p$ cross-section is taken from [222].

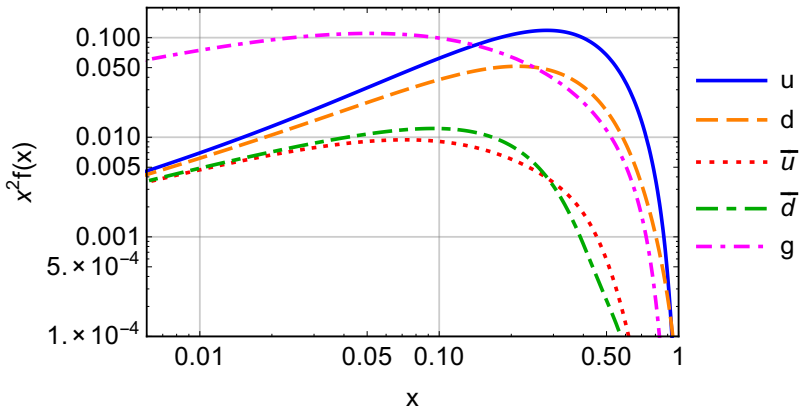


**Figure 3.9**: Combination $x^2 f(x)$ used in Eq. (3.1.15) for quark and gluon PDFs (for $\sqrt{s} \sim 30$ GeV). The functions peak at small values of $x$ and therefore the probability of the center-of-mass energy of the parton pair close to $\sqrt{s}$ is small.

therefore "wins" over the direct production, especially at the fixed-target experiments where the beam energies do not exceed hundreds of GeV. In case of the quark-gluon initial state (process (c) in Fig. 3.7) similar considerations also work and the resulting cross-section is also small, with an additional suppression due to the 3-body final state. *We see that the direct production channel is strongly suppressed in comparison with the production from mesons for HNLs with masses* $M_N \lesssim 5\,\text{GeV}$.

### 3.1.4 Coherent proton-nucleus scattering

The coherent scattering of a proton on the nuclei as a whole could be an effective way of producing new particles in fixed-target experiments. There are two reasons for this. Firstly, parton scattering in the electromagnetic field of the nuclei is proportional to

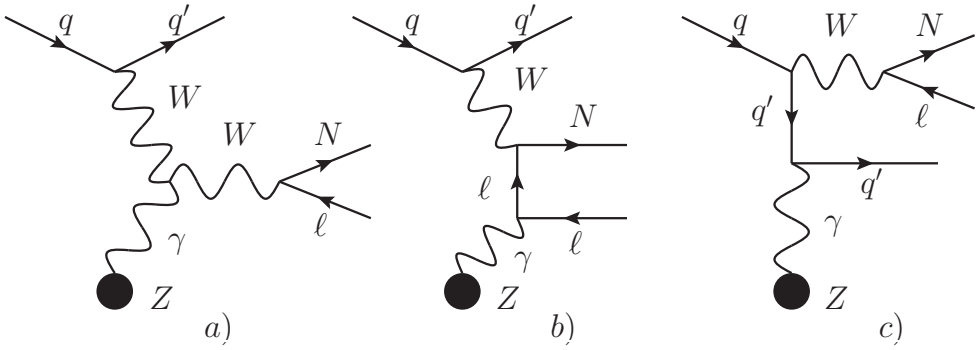


**Figure 3.10**: Possible Feynman diagrams for the HNL production in the proton coherent scattering off the nuclei.

$Z^2$ (where $Z$ is the nuclei charge) which can reach a factor $10^3$ enhancement for heavy nuclei. Secondly, the center of mass energy of the proton-nucleus system is higher than for the proton-proton scattering. The coherent production of the HNLs will be discussed in the forthcoming paper [236]. Here we announce the main result: the coherent HNL production channel is subdominant to the meson decay for all HNL masses and mixing angles (for HNL masses below 5 GeV). In case of SHiP one expects less than 1 HNL *produced* via coherent scattering for $10^{20}$ PoT.

### 3.1.5 Summary

In summary, production of HNL in proton fixed-target experiments occurs predominantly via (semi)leptonic decays of the lightest $c$- and $b$- mesons (Figs. 3.4, 3.5). The production from heavier mesons is suppressed by the strong force-mediated SM decays, while production from baryons is kinematically suppressed. Other production channels are subdominant for all masses $0.5\,\text{GeV} \leq M_N \leq 5\,\text{GeV}$ as discussed in Sections 3.1.3–3.1.4.

## 3.2 HNL decay modes

All HNL decays are mediated by the charged or the neutral current interactions. In this Section, we systematically revisit the most relevant decay channels. Most of the results for sufficiently light HNLs exist in the literature [217, 218, 220, 237–239]. For a few modes, there are discrepancies by factors of few between different works, we comment on these discrepancies in due course.

All the results presented below *do not take into account charge conjugated channels* which are possible for the Majorana HNL; to account for the Majorana nature one should multiply all the decay widths by 2. The branching ratios are the same for Majorana case and for the case considered here.

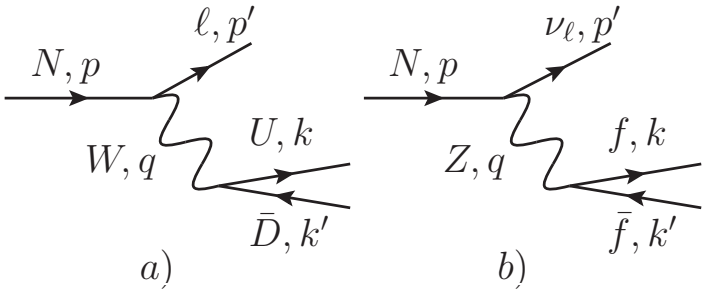


**Figure 3.11**: Diagram for the HNL decays mediated by charged (a) and neutral (b) currents.

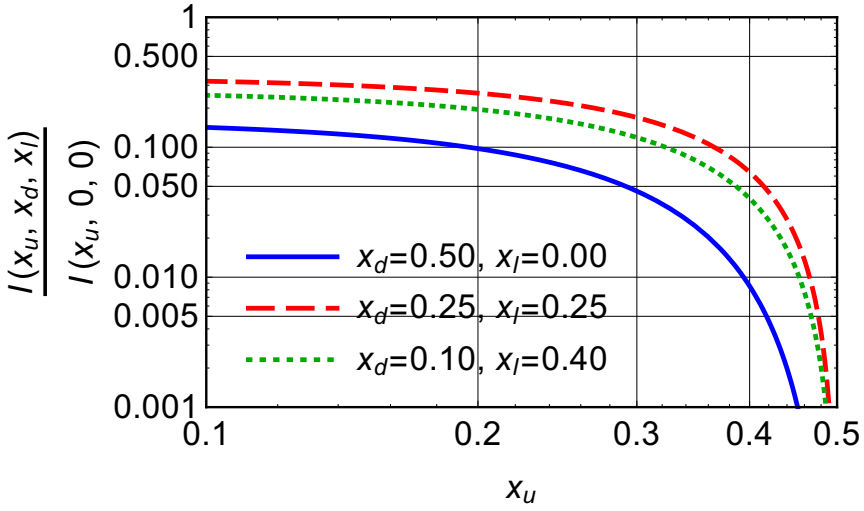


**Figure 3.12**: Function $I(x_u, x_d, x_l)/I(x_u, 0, 0)$ for several choices of $x_d$ and $x_l$ (see Eq. (3.2.2) for $I(x_u, x_d, x_l)$ definition).

### 3.2.1 3-body basic channels

Two basic diagrams, presented in the Fig. 3.11, contribute to all decays. For the charged current-mediated decay (Fig. 3.11(a)) the final particles $(U, D)$ could be either a lepton pair $(\nu_\alpha, \ell_\alpha)$ or a pair of up and down quarks $(u_i, d_j)$. For the neutral current-mediated decay $f$ stands for any fermion. The tree-level decay width into free quarks, while unphysical by itself for the interesting mass range, is important in estimates of the full hadronic width at $M_N \gg \Lambda_{\rm QCD}$, see Section 3.2.2.2 below.

For the decays $N \to \nu_\alpha \ell_\alpha^- \ell_\alpha^+$ and $N \to \nu_\alpha \nu_\alpha \bar{\nu}_\alpha$ both diagrams contribute, which leads to the interference (see Section 3.2.1.2).

#### 3.2.1.1 Charged current-mediated decays

The general formula for the charged current-mediated processes $N \to \ell_\alpha^- \nu_\beta \ell_\beta^+$, $\alpha \neq \beta$, and $N \to \ell_\alpha u_i \bar{d}_j$ is [237–240]

$$\Gamma(N \to \ell_\alpha^- U \bar{D}) = N_W \frac{G_F^2 M_N^5}{192\pi^3} |U_\alpha|^2 I(x_u, x_d, x_l) \tag{3.2.1}$$

where $x_l = \frac{m_{\ell_\alpha}}{M_N}$, $x_u = \frac{m_U}{M_N}$, $x_d = \frac{m_D}{M_N}$. The factor $N_W = 1$ for the case of the final leptons and $N_W = N_c |V_{ij}|^2$ in the case of the final quarks, where $N_c = 3$ is the number of colors, and $V_{ij}$ is the corresponding matrix element of the CKM matrix. The function $I(x_u, x_d, x_l)$ that describes corrections due to finite masses of final state fermions is given by

$$I(x_u, x_d, x_l) \equiv 12 \int\limits_{(x_d+x_l)^2}^{(1-x_u)^2} \frac{dx}{x} \left(x - x_l^2 - x_d^2\right) \left(1 + x_u^2 - x\right) \sqrt{\lambda(x, x_l^2, x_d^2)\lambda(1, x, x_u^2)}, \tag{3.2.2}$$

where $\lambda(a, b, c)$ is given by Eq. (3.1.12).

Several properties of the function (3.2.2):

1. $I(0, 0, 0) = 1$

2. Function $I(a, b, c)$ is symmetric under *any* permutation of its arguments $a, b, c$.[4]

3. In the case of mass hierarchy $m_a, m_b \ll m_c$ (where $a, b, c$ are leptons and/or quarks in some order) one can use an approximate result

$$I(x, 0, 0) = (1 - 8x^2 + 8x^6 - x^8 - 12x^4 \log x^2) \tag{3.2.3}$$

   where $x = \frac{m_c}{M_N}$.

4. The ratio $I(x_u, x_d, x_l)/I(x_u, 0, 0)$ for several choices of $x_d, x_l$ is plotted in Fig. 3.12. It decreases with each argument.

#### 3.2.1.2 Decays mediated by neutral current interaction and the interference case

Decay width for neutral current-mediated decay $N \to \nu_\alpha f \bar{f}$ depends on the type of the final fermion. For charged lepton pair $l_\beta \bar{l}_\beta$ the results are different for the case $\alpha \neq \beta$ and $\alpha = \beta$, because of the existence of the charge current mediated diagrams

[4] This property is non-obvious but can be verified by the direct computation.

in the latter case. Nevertheless, the decay width can be written in a unified way,

$$\Gamma(N \to \nu_\alpha f \bar{f}) = N_Z \frac{G_F^2 M_N^5}{192\pi^3} \cdot |U_\alpha|^2 \cdot \Bigg[ C_1^f \Bigg( (1 - 14x^2 - 2x^4 - 12x^6)\sqrt{1-4x^2} + \\ + 12x^4(x^4-1)L(x) \Bigg) + 4C_2^f \Bigg( x^2(2 + 10x^2 - 12x^4)\sqrt{1-4x^2} + \\ + 6x^4(1 - 2x^2 + 2x^4)L(x) \Bigg) \Bigg], \tag{3.2.4}$$

where $x = \dfrac{m_f}{M_N}$, $L(x) = \log\left[\dfrac{1 - 3x^2 - (1-x^2)\sqrt{1-4x^2}}{x^2(1+\sqrt{1-4x^2})}\right]$ and $N_Z = 1$ for the case of leptons in the final state or $N_Z = N_c$ for the case of quarks. The values of $C_1^f$ and $C_2^f$ are given in the Table 3.3. This result agrees with [218, 238, 239].

| $f$ | $C_1^f$ | $C_2^f$ |
|---|---|---|
| $u,\ c,\ t$ | $\frac{1}{4}\left(1 - \frac{8}{3}\sin^2\theta_W + \frac{32}{9}\sin^4\theta_W\right)$ | $\frac{1}{3}\sin^2\theta_W\left(\frac{4}{3}\sin^2\theta_W - 1\right)$ |
| $d,\ s,\ b$ | $\frac{1}{4}\left(1 - \frac{4}{3}\sin^2\theta_W + \frac{8}{9}\sin^4\theta_W\right)$ | $\frac{1}{6}\sin^2\theta_W\left(\frac{2}{3}\sin^2\theta_W - 1\right)$ |
| $\ell_\beta,\ \beta \neq \alpha$ | $\frac{1}{4}\left(1 - 4\sin^2\theta_W + 8\sin^4\theta_W\right)$ | $\frac{1}{2}\sin^2\theta_W\left(2\sin^2\theta_W - 1\right)$ |
| $\ell_\beta,\ \beta = \alpha$ | $\frac{1}{4}\left(1 + 4\sin^2\theta_W + 8\sin^4\theta_W\right)$ | $\frac{1}{2}\sin^2\theta_W\left(2\sin^2\theta_W + 1\right)$ |

**Table 3.3**: Coefficients $C_1$ and $C_2$ for the neutral current-mediated decay width.

In the case of pure neutrino final state only neutral currents contribute and the decays width reads

$$\Gamma(N \to \nu_\alpha \nu_\beta \bar{\nu}_\beta) = (1 + \delta_{\alpha\beta})\frac{G_F^2 M_N^5}{768\pi^3}|U_\alpha|^2. \tag{3.2.5}$$

### 3.2.2 Decay into hadrons

In this Section, we consider hadronic final states for $M_N$ both below and above $\Lambda_{\rm QCD}$ scale and discuss the range of validity of our results.

#### 3.2.2.1 A single meson in the final state

At $M_N \lesssim \Lambda_{\rm QCD}$ the quark pair predominantly binds into a single meson. There are both charged and neutral current-mediated processes with a meson in the final state: $N \to \ell_\alpha h^+_{P/V}$ and $N \to \nu_\alpha h^0_{P/V}$, where $h^+_P$ ($h^0_P$) are charged (neutral) pseudoscalar mesons and $h^+_V$ ($h^0_V$) are charged (neutral) vector mesons. In formulas below $x_h \equiv m_h/M_N$, $x_\ell = m_\ell/M_N$, $f_h$ and $g_h$ are the corresponding meson decay constants (see Appendix C.1), $\theta_W$ is a Weinberg angle and the function $\lambda$ is given by eq. (3.1.12). The details of the calculations are given in the Appendix B.2.

The decay width to the charged pseudo-scalar mesons ($\pi^\pm, K^\pm, D^\pm, D_s, B^\pm, B_c$) is given by

$$\Gamma(N \to \ell_\alpha^- h_P^+) = \frac{G_F^2 f_h^2 |V_{UD}|^2 |U_\alpha|^2 M_N^3}{16\pi} \left[ \left(1 - x_\ell^2\right)^2 - x_h^2 (1 + x_\ell^2) \right] \sqrt{\lambda(1, x_h^2, x_\ell^2)}, \tag{3.2.6}$$

in full agreement with the literature [218, 238, 239].

The decay width to the pseudo-scalar neutral meson ($\pi^0, \eta, \eta', \eta_c$) is given by

$$\Gamma(N \to \nu_\alpha h_P^0) = \frac{G_F^2 f_h^2 M_N^3}{32\pi} |U_\alpha|^2 \left(1 - x_h^2\right)^2 \tag{3.2.7}$$

Our answer agrees with [218], but is twice larger than [238, 239]. The source of the difference is unknown.[5]

The HNL decay width into charged vector mesons ($\rho^\pm$, $a_1^\pm$, $D^{\pm *}$, $D_s^{\pm *}$) is given by

$$\Gamma(N \to \ell_\alpha^- h_V^+) = \frac{G_F^2 g_h^2 |V_{UD}|^2 |U_\alpha|^2 M_N^3}{16\pi m_h^2} \left( \left(1 - x_\ell^2\right)^2 + x_h^2 \left(1 + x_\ell^2\right) - 2x_h^4 \right) \sqrt{\lambda(1, x_h^2, x_\ell^2)} \tag{3.2.8}$$

that agrees with the literature [218, 238, 239].

*However*, there is a disagreement regarding the numerical value of the meson constant $g_\rho$ between [218] and [238, 239]. We extract the value of this constant from the decay $\tau \to \nu_\tau \rho$ and obtain the result that numerically agrees with the latter works, see discussion in Appendix C.1.3.

For the decay into neutral vector meson ($\rho^0$, $a_1^0$, $\omega$, $\phi$, $J/\psi$) we found that the result depends on the quark content of meson. To take it into account we introduce dimensionless $\kappa_h$ factor to the meson decay constant (B.2.6). The decay width is given by

$$\Gamma(N \to \nu_\alpha h_V^0) = \frac{G_F^2 \kappa_h^2 g_\rho^2 |U_\alpha|^2 M_N^3}{32\pi m_h^2} \left(1 + 2x_h^2\right) \left(1 - x_h^2\right)^2. \tag{3.2.9}$$

Our result for $\rho^0$ and results in [218] and [238] are all different. The source of the difference is unknown. For decays into $\omega$, $\phi$ and $J/\psi$ mesons we agree with [238]. The result for the $a_1^0$ meson appears for the first time.[6]

The branching ratios for the one-meson and lepton channels below 1 GeV are given on the left panel of Fig. 3.13.

[5] This cannot be due to the Majorana or Dirac nature of HNL, because the same discrepancy would then appear in Eq. (3.2.6).

[6] Refs. [238, 239] quote also 2-body decays $N \to \nu_\alpha h_V^0$, $h_V^0 = K^{*0}, \bar{K}^{*0}, D^{*0}, \bar{D}^{*0}$, with the rate given by (3.2.9) (with a different $\kappa$). This is not justified since the weak neutral current does not couple to the corresponding vector meson $h_V^0$ at tree level.

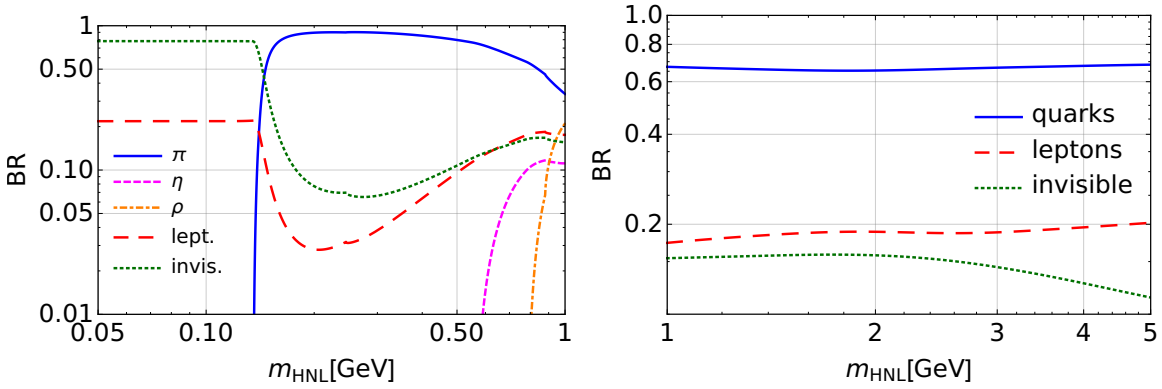


**Figure 3.13**: The branching ratios of the HNL for the mixing ratio $U_e : U_\mu : U_\tau = 1 : 1 : 1$. *Left panel:* region of masses below 1 GeV; *Right panel:* region of masses above 1 GeV, for quarks the QCD corrections (3.2.10), (3.2.11) are taken into account.

#### 3.2.2.2 Full hadronic width vs. decay into single meson final state

Decays into multi-hadron final states become kinematically accessible as soon as $M_N > 2m_\pi$. To estimate their branching fractions and their contribution to the total decay width, we can compute the total hadronic decay width of HNLs, $\Gamma_{\rm had}$ and compare it with the combined width of all single-meson states, $\Gamma_{1\,\rm meson}$. The total hadronic decay width can be estimated via decay width into quarks (Sections 3.2.1.1–3.2.1.2) times the additional loop corrections.

The QCD loop corrections to the tree-level decay into quarks have been estimated in the case of $\tau$ lepton hadronic decays. In this case, the tree-level computation of the $\tau$ decay to two quarks plus neutrino underestimates the full hadronic decay width by 20% [241–243]. The loop corrections, $\Delta_{\rm QCD}$, defined via

$$1 + \Delta_{\rm QCD} \equiv \frac{\Gamma(\tau \to \nu_\tau + \text{hadrons})}{\Gamma_{\rm tree}(\tau \to \nu_\tau \bar{u} q)} \tag{3.2.10}$$

have been computed up to three loops [243] and is given by:

$$\Delta_{\rm QCD} = \frac{\alpha_s}{\pi} + 5.2\frac{\alpha_s^2}{\pi^2} + 26.4\frac{\alpha_s^3}{\pi^3}, \tag{3.2.11}$$

where $\alpha_s = \alpha_s(m_\tau)$.[7] We use (3.2.11) with $\alpha_s = \alpha_s(M_N)$ as an estimation for the QCD correction for the HNL decay, for both charged and neutral current processes. We expect therefore that QCD correction to the HNL decay width into quarks is smaller than 30% for $M_N \gtrsim 1$ GeV (Fig. 3.14).

Full hadronic decay width dominates the HNL lifetime for masses $M_N \gtrsim 1$ GeV (see Fig. 3.13). The latter is important to define the upper bound of sensitivity

[7] Numerically this gives for the $\tau$-lepton $\Delta_{\rm QCD} \approx 0.18$, which is within a few % of the experimental value $\Delta_{\rm Exp} = 0.21$. The extra difference comes from the QED corrections.

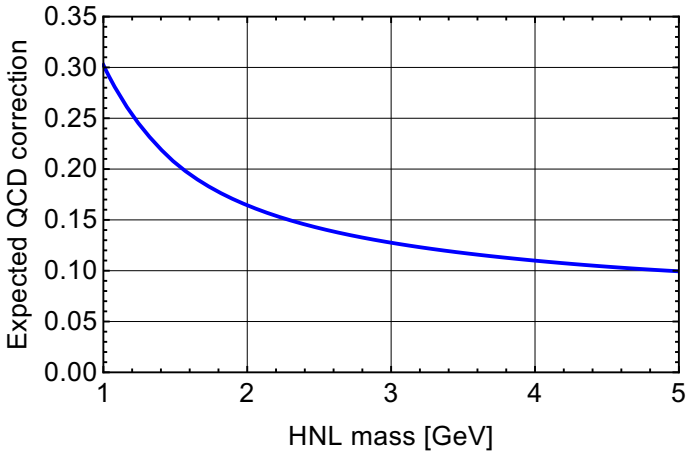


**Figure 3.14**: The estimate of the QCD corrections for the HNL decay into quark pairs, using the three-loop formula (3.2.11) for $\tau$-lepton.

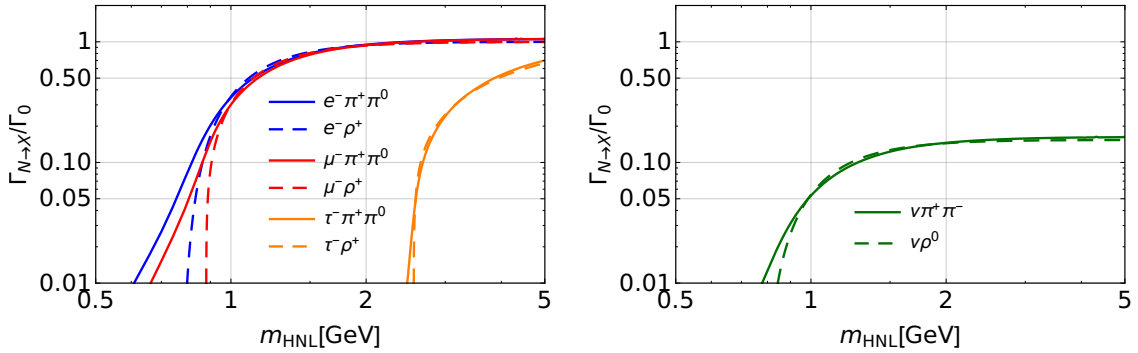


**Figure 3.15**: *Left panel:* Decay widths of charged current channels with $\rho$ or $2\pi$ divided by $\Gamma_0 = \frac{1}{16\pi} G_F^2 \frac{g_\rho^2}{m_\rho^2} |V_{ud}|^2 |U_\alpha|^2 M_N^3$, which is the prefactor in Eq. (3.2.8). *Right panel:* The same for neutral current channels.

for the experiments like SHiP or MATHUSLA (see Fig. 3.1). This upper bound is defined by the requirements that HNLs can reach the detector.

#### 3.2.2.3 Multi-meson final states

When discussing "single-meson channels" above, we have also included there decays with the $\rho$-meson. By doing so, we have essentially incorporated all the two-pion decays $N \to \pi^+\pi^0\ell^-$ for $M_N > m_\rho$. Indeed, we have verified by direct computation of $N \to \pi^+\pi^0\ell^-$ that they coincide with $N \to \rho^+\ell^-$ for all relevant masses (Fig. 3.15). Of course, the decay channel to two pions is also open for $2m_\pi < M_N < m_\rho$, but its contribution there is completely negligible and we ignore it in what follows.

Figs. 3.13 and 3.16 demonstrate that one-meson channels are definitely enough for all the hadronic modes if sterile neutrino mass does not exceed 1 GeV. The ratio between the combined decay width into single-meson final states ($\pi^\pm$, $\pi^0$, $\eta$, $\eta'$, $\rho^\pm$,

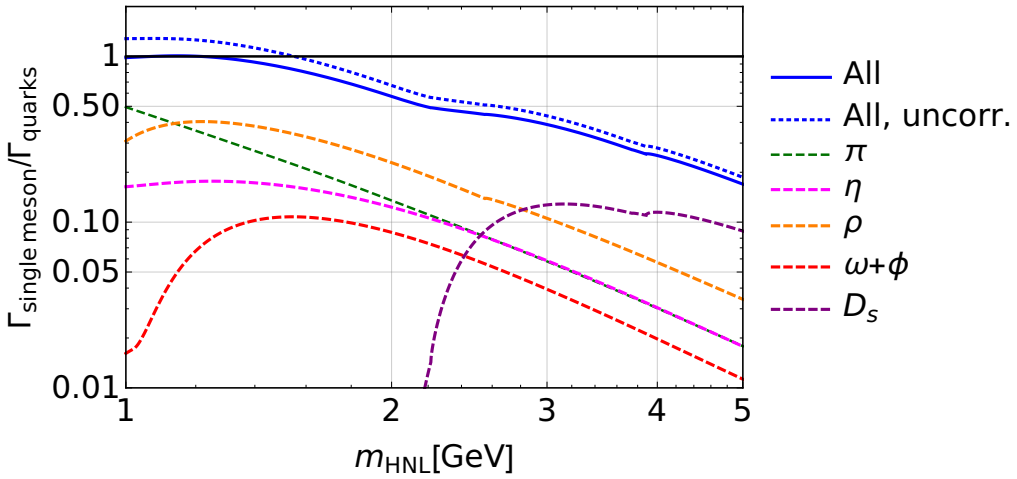


**Figure 3.16**: HNL decay widths into all relevant single meson channels, divided by the total decay width into quarks with QCD corrections, estimated as in (3.2.11) (all dashed lines). The blue solid line is the sum of all mesons divided by decay width into quarks with QCD corrections, the blue dotted line is the same but without QCD corrections.

| 3-body decays |
|---|
| $N \to \ell_\alpha^- \pi^+ \pi^0$ |
| $N \to \nu_\alpha \pi^+ \pi^-$ |
| $N \to \nu_\alpha \pi^0 \pi^0$ |
| $N \to \ell_\alpha^- K^+ \bar{K}^0$ |
| $N \to \nu_\alpha K^+ K^-$ |
| $N \to \nu_\alpha K^0 \bar{K}^0$ |
| $N \to \ell_\alpha^- K^+ \pi^0$ |
| $N \to \ell_\alpha^- K^0 \pi^+$ |

| 4-body decays |
|---|
| $N \to \nu_\alpha (3\pi)^0$ |
| $N \to \ell_\alpha^- (3\pi)^+$ |
| $N \to \nu_\alpha (2\pi K)^0$ |
| $N \to \ell_\alpha^- (2\pi K)^+$ |
| $N \to \nu_\alpha (2K\pi)^0$ |
| $N \to \ell_\alpha^- (2K\pi)^+$ |
| $N \to \ell_\alpha^- (3K)^+$ |
| $N \to \nu_\alpha (3K)^0$ |

| Branching ratios $\tau^- \to \nu_\tau + X^-$ | [%] |
|---|---|
| $\tau \to \nu_\tau + \pi^-$ | 10.8 |
| $\tau \to \nu_\tau + \pi^- \pi^0$ | 25.5 |
| $\tau \to \nu_\tau + \pi^0 \pi^- \pi^0$ | 9.2 |
| $\tau \to \nu_\tau + \pi^- \pi^+ \pi^-$ | 9.0 |
| $\tau \to \nu_\tau + \pi^- \pi^+ \pi^- \pi^0$ | 4.64 |
| $\tau \to \nu_\tau + \pi^- \pi^0 \pi^0 \pi^0$ | 1.04 |
| $\tau \to \nu_\tau + 5\pi$ | $\mathcal{O}(1)$ |
| $\tau \to \nu_\tau + K^-$ or $K^- \pi^0$ | $\mathcal{O}(1)$ |
| $\tau \to \nu_\tau + K^- K^0$ | $\mathcal{O}(0.1)$ |
| $\tau \to \nu_\tau + K^- K^0 \pi^0$ | $\mathcal{O}(0.1)$ |

**Table 3.4**: Possible multi-meson decay channels of HNLs with $M_N > 2m_\pi$ threshold. Right panel shows branching ratios of hadronic decays of the $\tau$-lepton and demonstrates the relative importance of various hadronic 2-, 3-, 4- and 5-body channels.

$\rho^0$, $\omega$+$\phi$, $D_s$) and into quarks is shown in Fig. 3.16.[8] One sees that the decay width into quarks is larger for $M_N \gtrsim 2$ GeV, which means that multi-meson final states are important in this region.

The main expected 3- and 4-body decay channels of HNLs are presented in Table 3.4. We also add information about multi-meson decays of $\tau$ because they give us information about decay through charged current of the HNL of the same mass as

[8] We ignore CKM-suppressed decays into kaons as well as decays to heavy flavor meson ($D$,$B$).

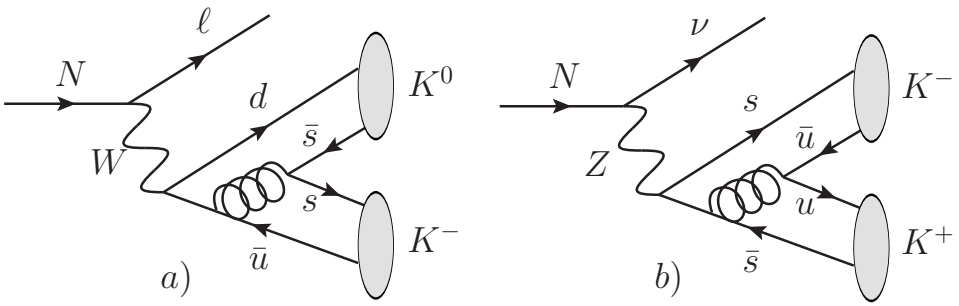


**Figure 3.17**: HNL decays into 2 kaons through charged (a) and neutral (b) currents.

$\tau$-lepton. The main difference between HNL and $\tau$-lepton comes from the possibility of the HNL decay through the neutral current, which we discuss below.

The main hadronic channels of the $\tau$ are $n$-pions channels. Decay channel into 2 pions is the most probable, but there is a large contribution from the 3-pion channels and still appreciable contribution from the 4-pion ones. For bigger masses the contribution from the channels with higher multiplicity become more important as the Fig. 3.16 demonstrates.

The decay into kaons is suppressed for the $\tau$-lepton. For some channels like $\tau \to \nu_\tau K$ or $\tau \to \nu_\tau K\pi$ this suppression comes from the Cabibbo angle between $s$ and $u$ quarks. The same argument holds for HNL decays into a lepton and $D$ meson, but not in $D_s$. The decays like $\tau \to \nu_\tau K^- K^0$ are not suppressed by the CKM matrix and still are small. We think that this is because for such decays the probability of the QCD string fragmentation into strange quarks is much smaller than into $u$ and $d$ quarks for the given $\tau$-lepton mass (see diagram (a) in Fig. 3.17). At higher masses, the probability of such fragmentation should be higher, but still too small to take it into account. On the other hand, the HNL decay into two kaons can give a noticeable contribution, because of the existence of the neutral current decay (see diagram (b) in Fig. 3.17), for which the previous arguments do not apply.

# Chapter 4

# Description of experiments

## 4.1 SHiP

SHiP is a dedicated beam-line experiment extracted from the super proton synchrotron (SPS) based at CERN [110] (see FIG. 4.2). It will fire a 400 GeV proton beam at a Molybdenum and Tungsten target, with a center-of-mass energy $E_{\mathrm{CM}} \approx 27$ GeV. There will be approximately a total of $2{\cdot}10^{20}$ proton-target collisions (PoT) in 5 years of operation.

The target is followed by a 5 m long hadron stopper, intended to stop all $\pi^{\pm}$ and $K$ mesons before they decay. After the hadron absorber there is a so-called active muon shield, a system of magnets constructed to sweep muons away from the fiducial decay volume. For sweeping of 350 GeV muons active muon shield contains a 18 m long magnet with a magnetic field $B \approx 1.8$ T [244]. The entire active muon shield system has a length of 34 m.

After the muon shield, there is the SHiP neutrino detector, called iSHiP. This is schematically shown in Fig. 4.1. The iSHiP consists of a magnetized target with

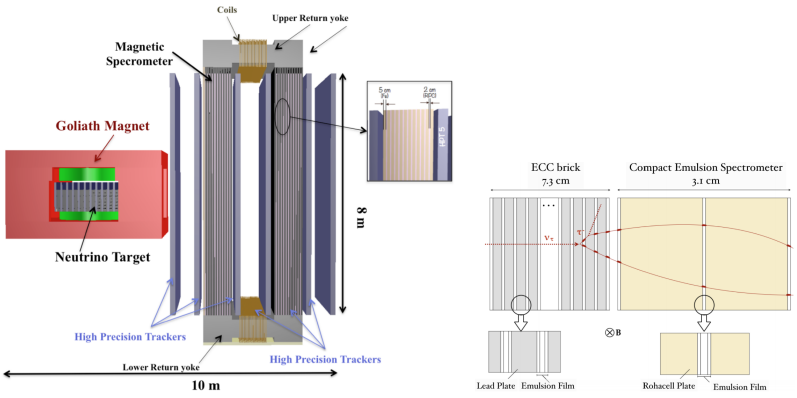


**Figure 4.1**: Construction of the the iSHiP detector [245]

the length of $l_{\text{iSHiP}} \simeq 5$ m with a modular structure. Each module consists of walls of emulsion cloud chambers (ECC) and a compact emulsion spectrometer (CES).

ECC bricks are plates of high atomic number passive material (e.g. lead) interleaved with thin nuclear emulsion foils. Electronic trackers provide time stamping for each event and are located between the target walls. They allow the reconstructed tracks to be connected between the emulsion target and those measured in the spectrometer downstream. This layout has already proven to be effective in detecting all $\nu$ flavors. For example it is possible to separate the $\nu_\tau$ via the decay of the $\tau$ lepton in the muon channel by measuring the electric charge of the muon in the spectrometer. This can be further optimized by adopting a magnetized target which would allow the separation of $\nu_\tau$ through the decay of the $\tau$ lepton in the hadronic channel. The emulsion spectrometer (CES ) is made of a sequence of very low-density layers and emulsion foils that measures the electric charge and momentum of particles.

There is an upstream tagger, that together with the muon spectrometer of the neutrino detector, will detect and veto charged particles produced outside of the main decay volume. The fiducial decay volume begins approximately 63.8 m downstream from the primary target and is contained within a cylindrical vacuum tank 50 m long with an elliptical cross-section of 12.5 $m^2$.

A straw tagger is placed in a vacuum 5 m downstream from the entrance lid of the vacuum tank to help reduce the background arising from interactions in the material upstream of the decay volume. An additional background tagger surrounds the fiducial decay volume, the walls of which enclose 30 cm of liquid scintillator.

The tracking system aimed to measure the decay products of hidden particles is located at the end of the decay volume. It consists of 5 m long straw tubes organized in to 4 stations, with a magnetic field of 1 T between the second and third station. The high-accuracy timing information provided by a dedicated detector following the straw tracker will be used to discriminate the combinatorial background.

The particle identification system is placed outside the vacuum tank, and features an electromagnetic and a hadronic calorimeter, followed by a muon system made of four active layers interlaced with iron.

### 4.1.1 Production of heavy flavor at the SHiP

The number of mesons produced at the SHiP target can be estimated as

$$N_h = 2 \times fh \times X_{q\bar{q}} \times N_{PoT}, \tag{4.1.1}$$

where $X_{q\bar{q}}$ represents the $q\bar{q}$ production rate, $fh$ is the meson $h$ production fraction[1] and expected number of protons on target $N_{PoT} = 2 \cdot 10^{20}$. The following cross sections have been used for the estimates:

[1] $fh$ is equal to the number of $h$ mesons divided by the number of corresponding quarks.

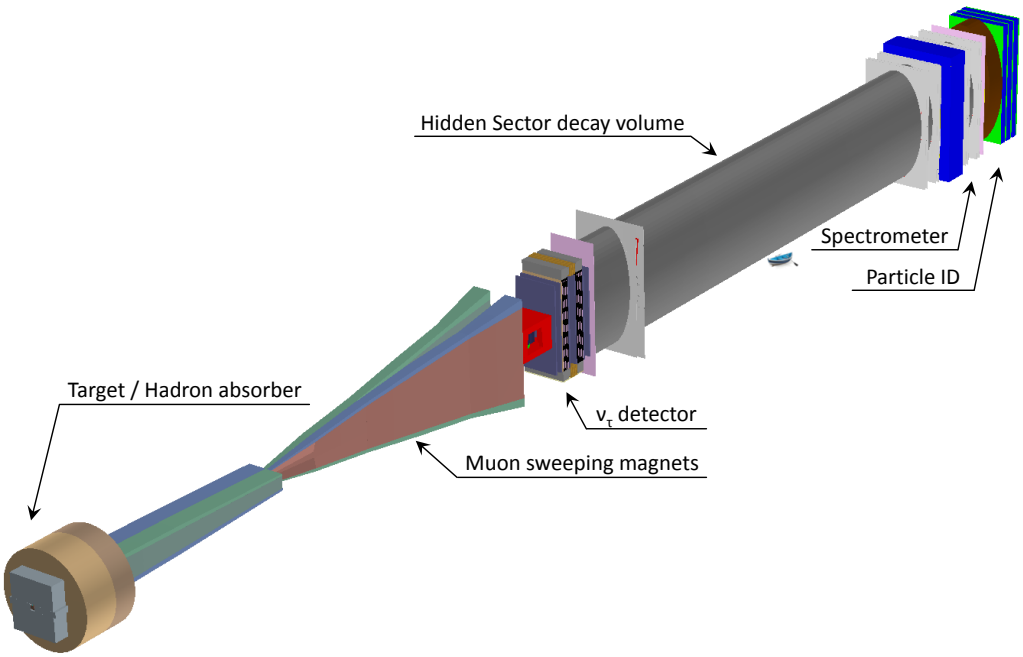


**Figure 4.2**: Scheme of the SHiP experimental setup with indication of its main parts.

- The proton-nucleon cross section is $\sigma(pN) \simeq 10.7$ mbarn;
- $X_{ss} \approx 1/7$ [218];
- $\sigma(cc) \approx 41.4$ $\mu$barn [246] and the fraction $X_{cc} = 9 \times 10^{-3}$;
- $\sigma(bb) = 2.9$ nbarn [246] and the fraction $X_{bb} = 2.7 \times 10^{-7}$.

Simulation is needed to calculate the meson production fraction. It should take into account the properties of the target (e.g. materials, geometry) and the cascade processes (e.g. birth of the excited meson states like $D^*$ and its decay into $D$). The values of $fh$ for the case of the SHiP experiment were calculated in the paper [221]. These values with the number of different mesons are given in the Table 4.1. For kaons, we do not divide them into species.

The expected number of $\tau$ leptons for $N_{PoT} = 2 \times 10^{20}$ is $N_\tau = 3 \times 10^{15}$.

### 4.1.2 Kaon decay fraction at the SHiP

In this section, we calculate the fraction of kaons that decay before scattering on the absorber material. We assume that scattered kaons fly in a random direction and their products do not hit the detector.

| Meson | $fh$ | $N_h$ |
|---|---|---|
| $K$ | – | $5.7 \cdot 10^{19}$ |
| $D^{\pm}$ | 0.207 | $3.2 \cdot 10^{17}$ |
| $D^0$ | 0.632 | $9.9 \cdot 10^{17}$ |
| $D_s$ | 0.088 | $1.4 \cdot 10^{17}$ |
| $J/\psi$ | 0.01 | $6.8 \cdot 10^{15}$ |
| $B^{\pm}$ | 0.417 | $4.6 \cdot 10^{13}$ |
| $B^0$ | 0.418 | $4.6 \cdot 10^{13}$ |
| $B_s$ | 0.113 | $1.2 \cdot 10^{13}$ |

**Table 4.1**: Production fraction and expected number of different mesons at the SHiP.

The cross section for kaon-nucleon scattering is (see "Plots of cross sections and related quantities" review in Particle Data Group [222])

$$\sigma_{KN} = 20 \text{ mb} = 2 \cdot 10^{-26} \text{ cm}^2. \tag{4.1.2}$$

The number density for nucleons in the SHiP absorber (iron)

$$n_N = 4.8 \cdot 10^{24} \text{ cm}^{-3}. \tag{4.1.3}$$

Therefore, the mean free path of the kaon in the absorber is

$$l = \frac{1}{\sigma_{KN} n_N} = 10 \text{ cm}. \tag{4.1.4}$$

The mean distance before the kaon decay is

$$d = \gamma c \tau, \tag{4.1.5}$$

where $\gamma$ is the gamma factor and $\tau$ is the lifetime. In our estimation, we take $\gamma \sim 15$, which is corresponds to the gamma factor between center-of-mass and laboratory frame of the colliding protons.

For the small distance $dx$, the probability of scattering is equal to $P_{\text{scat}} = \frac{dx}{l}$, and the probability of the decay is $P_{\text{decay}} = \frac{dx}{d}$. Thus, the ratio between the number of scattered and decayed kaons is equal to

$$\frac{N_{\text{scat}}}{N_{\text{decay}}} = \frac{d}{l}, \tag{4.1.6}$$

and the full number of the decayed kaons is

$$N_{\text{decay}} = N_0 \frac{l}{l+d}, \tag{4.1.7}$$

where $N_0$ is the initial number of kaons. So, the probability of the kaon decay $P_{decay}$ before scattering is

$$P_{decay} = \frac{N_{decay}}{N_0} = \frac{l}{l+d}. \tag{4.1.8}$$

| Meson | $P_{decay}$ |
|---|---|
| $K_L^0$ | $4 \cdot 10^{-4}$ |
| $K^{\pm}$ | $1.7 \cdot 10^{-3}$ |
| $K_s^0$ | $2 \cdot 10^{-1}$ |

**Table 4.2**: The decay probability for kaons in the SHiP absorber.

## 4.2 MATHUSLA

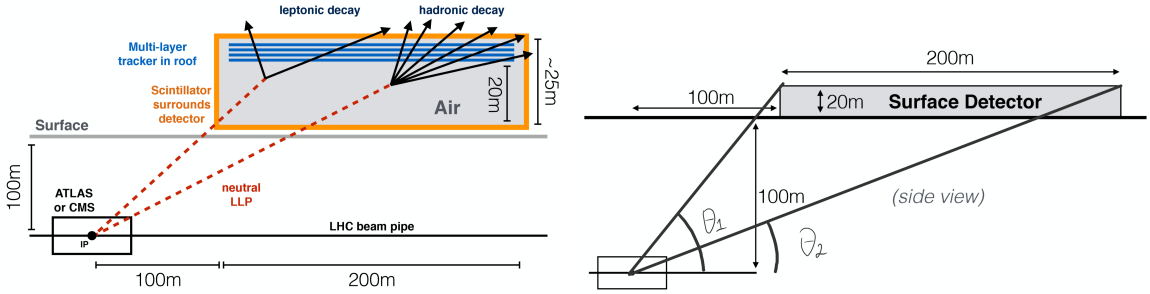


**Figure 4.3**: The proposed design for the MATHUSLA experiment (left) [113] and the main experimental dimensions, adapted from [247].

The MATHUSLA (MAssive Timing Hodoscope for Ultra Stable neutraL pArticles) is a proposed experiment [113, 114] that consists of 20 m×200 m×200 m surface detector, installed above the ATLAS or CMS detectors (see Fig. 4.3). The long-lived particles, created during the LHC collisions, travel 100+ meters of rock and decay within a large decay volume ($8 \times 10^5$ m$^3$) of the detector. A multi-layer tracker on the detector's roof will catch the charged tracks, originating from the particle decays. The ground between the ATLAS/CMS and the MATHUSLA detector would serve as a passive shield, significantly reducing the Standard Model background (with the exception of neutrinos, muons, and $K_L^0$ created near the surface). Assuming the isotropic angular distribution of a given particle traveling to the MATHUSLA, the

average distance that it should travel to reach the MATHUSLA detector is equal to

$$\bar{l}_{\text{tar-det}} \equiv \left\langle \frac{L_{ground}}{\sin\theta} \right\rangle = 192.5 \text{ m}, \tag{4.2.1}$$

where $L_{\text{ground}} = 100$ m. The average distance where a particle travels inside the detector, $\bar{L}_{\text{det}}$, is given by

$$\bar{l}_{\text{det}} \equiv \left\langle \frac{20 \text{ m}}{\sin\theta} \right\rangle = 38.5 \text{ m}. \tag{4.2.2}$$

Geometrical parameters of the MATHUSLA experiment are summarized in Table 4.3. Relevant parameters of mesons at the experiment are provided by FONLL pro-

| Parameter | $\theta_1$ | $\theta_2$ | $\eta_1$ | $\eta_2$ | $\bar{l}_{\text{tar-det}}$, m | $\bar{l}_{\text{det}}$, m | $\Delta\phi$ |
|---|---|---|---|---|---|---|---|
| Value | 44.3° | 22.9° | 0.9 | 1.6 | 192.5 | 38.5 | $\pi/2$ |

**Table 4.3**: Parameters of the MATHUSLA experiment [247]. For the definition of angles $\theta_{1,2}$ see Fig. 4.3, and $\Delta\phi$ is the azimuthal size of the MATHUSLA.

gram [248, 249]. They are summarized in Table 4.4.

| Parameter | $N_{c\bar{c}}$ | $\langle p_D \rangle$ | $N_{b\bar{b}}$ | $\langle p_B \rangle$, GeV |
|---|---|---|---|---|
| Value | $3.6 \times 10^{14}$ | 5.1 | $3.6 \times 10^{13}$ | 12.2 |

**Table 4.4**: Parameters of mesons production at the MATHUSLA experiment.

# Chapter 5

# Sensitivity of the SHiP and MATHUSLA experiments

## 5.1 Analytical estimates

A number of experiments have been proposed in recent years in order to probe for light, long-lived particles [110–116, 250]. The searches for such particles are also included in the scientific programs of existing experiments [106, 107, 251].

Although the LHC experiment is the flagship of the *Energy Frontier* exploration, its increased luminosity in the current and future runs mean that huge numbers of heavy flavored mesons and vector bosons are being created. This opens up the possibility to supplement the High Luminosity phase of the LHC with companion experiments. Several such experiments have been proposed: CODEX-b [112], MATHUSLA [113, 114] and FASER [115, 116].

Given that all these experiments can probe similar parameter spaces it is important to be able to assess their scientific reach uniformly, with clearly specified and identical assumptions. While Monte-Carlo simulations of both production and decay, complemented with background studies, will eventually offer the ultimate sensitivity curve for each of these experiments, it is crucial to have a sufficiently simple and fully controlled analytical estimate first. Such an estimate uncovers the main factors that influence the sensitivity. This permits us to scan over different models and experiment designs in a quick and efficient manner.

As it turns out, the ratios between the sensitivities of the experiments to a great extent do not depend on the specific model of the particle candidate, and are determined mainly by the geometry and the collision energies of the experiments, which allow for a comparison in a largely model-independent way. To illustrate this point we compare the potential of two proposed experiments: SHiP and MATHUSLA (see Sections 4.1, 4.2) [213]. We analyze their sensitivity to the scalar and neutrino portals, described in Chapters 2 and 3. In both models, for particle masses $M_X \lesssim$

$m_{B_c}$ the main production channel is the decay of heavy flavored mesons.[1] This explains why both of them can be studied at the same time. We concentrate on the mass range $M_X \gtrsim m_K$ since the domain of lower masses for the HNL and Higgs-like scalar is expected to be probed by the currently running NA62 experiment [109, 251].

The sensitivity of the experiment is determined by the number of events one expects in the detector for a given value of each of the parameters. In realistic experiments such events need to be disentangled from the "background" signals.

For the SHiP experiment, detailed simulations have shown that one expects the number of background events to be very low, so that the experiment is "background free" [111, 244, 252, 253]. For the MATHUSLA experiment the background is also expected to be low [247] although no detailed studies have been performed yet. Even assuming the most favorable case of $N_{\rm bg} \ll 1$ one needs *on average* $\bar{N}_{\rm events} = 2.3$ expected signal events to observe at least one event with the probability higher than 90%.[2]

For both experiments considered here, the point of production is separated from the decay volume by some macroscopic distance $l_{\text{target-det}}$. For such experiments, the sensitivity curve has a typical "cigar-like shape" in the plane "mass vs. interaction strength". The *upper boundary* is determined by the condition that the decay length of a produced particle becomes comparable to the distance to the detector, $l_{\rm decay} \sim l_{\text{target-detector}}$. The *lower boundary* of the sensitivity region is determined by the parameters at which decays become too rare (i.e. $l_{\rm decay} \gg l_{\rm det}$). The intersection of these bounds defines the *maximal mass* which can be probed at the experiment.

The number of decay events in the detector factorizes into

$$N_{\rm events} = N_{\rm prod} \times P_{\rm decay} \tag{5.1.1}$$

where $N_{\rm prod}$ is the number of produced particles $X$. In the mass range $m_K \lesssim M_X \lesssim m_B$ the main production channels in proton-proton collisions for both HNLs and Higgs portal scalars are decays of heavy flavor mesons, see Sections 2.2 and 3.1 for discussion.[3] Therefore the number of produced feebly interacting particles $N_{\rm prod}$ is given by

$$N_{\rm prod} \approx \sum_{q,\text{meson}} \overbrace{2N_{q\bar{q}} \times f_{q\to\text{meson}}}^{N_{\rm meson}} \underset{\text{meson}\to X}{\rm BR} \times \epsilon_{\rm decay} \tag{5.1.2}$$

Here $N_{\bar{q}q}$ is the number of quark pairs produced; $f_{q\to\text{meson}}$ is the fraction of quark pairs that hadronise into a meson of a given type (such that the product of the two gives the number of mesons of a given type); $\text{BR}_{\text{meson}\to X}$ is the branching of

[1] A significant part of the analysis is the same for neutrino and scalar models, so we denote the new particle by $X$.

[2] To obtain the 95% confidence limit one should assume $\bar{N}_{\rm events} = 3$, as the Poisson probability to see *at least one* event, while expecting 3 "on average" is $0.899\ldots$.

[3] We denote by $m_{...}$ masses of lightest flavor mesons: kaons ($m_K$), $D^+$ ($m_D$) and $B^+$ ($m_B$).

the meson decay into $X$. Finally, $\epsilon_{\text{decay}}$ is the *decay acceptance* – the fraction of particles $X$ whose trajectory intersects the decay volume (i.e. particles that could decay inside).

The probability of decay into a state that can be detected is given by

$$P_{\text{decay}} = \left[\exp\left(-\frac{l_{\text{target-det}}}{l_{\text{decay}}}\right) - \exp\left(-\frac{l_{\text{target-det}} + l_{\text{det}}}{l_{\text{decay}}}\right)\right] \times \epsilon_{\text{det}} \times \text{BR}_{\text{vis}} \tag{5.1.3}$$

Here $l_{\text{target-det}}$ is the distance between the target and the entrance into the detector (see Sections 4.1, 4.2). For the purpose of presentation, in (5.1.3) we ignored the fact that particles travel slightly different distances, depending on their off-axis angle. The decay length $l_{\text{decay}}$ in Eq. (5.1.3) is defined as

$$l_{\text{decay}} = c\tau_X \beta\gamma \tag{5.1.4}$$

where $\tau_X$ is the particle $X$'s lifetime, $c\beta$ is its speed and $\gamma$ is the Lorentz gamma-factor. Larger values of the $\gamma$-factor suppress the decay probability. This affects the upper and lower regions of the cigar-like sensitivity plots in the opposite fashions. For the lower limit, an experiment with the lower $\gamma$-factor is sensitive to the small coupling constants as we will see from Eq. (5.1.5). For sufficiently large couplings, having a larger $\gamma$-factor ensures that particles do not decay before reaching the detector, thus increasing the sensitivity to the upper range of the sensitivity curve.

The branching ratio $\text{BR}_{\text{vis}}$ is the fraction of all decays that produce final states that can be detected. Finally, $\epsilon_{\text{det}} \leq 1$ is the *detection acceptance* – the fraction of all decays inside the decay volume for which the decay products could be registered.

### 5.1.1 Sensitivity comparison: main factors

For both neutrino and scalar portal, a single production channel dominates for each particular $M_X$. In this case, one can compare the sensitivity of two experiments without using specific branching ratio of particle production.

Let us first compare the lower boundary of the sensitivity region, where $l_{\text{decay}} \gg l_{\text{det}}$ and the decays are rare:

$$\frac{N^{SHiP}_{\text{decay}}}{N^{\text{MAT}}_{\text{decay}}} \simeq \frac{N^{SHiP}_{\text{meson}}}{N^{\text{MAT}}_{\text{meson}}} \times \frac{l^{SHiP}_{\text{det}}}{l^{\text{MAT}}_{\text{det}}} \times \frac{\langle\gamma^{\text{MAT}}_{\text{meson}}\rangle}{\langle\gamma^{SHiP}_{\text{meson}}\rangle} \times \frac{\epsilon_{SHiP}}{\epsilon_{\text{MAT}}} \tag{5.1.5}$$

The particles are assumed relativistic (we will see below when this assumption is justified) and the Lorentz-factor $\gamma_X \gg 1$ is estimated as

$$\langle\gamma_X\rangle \approx \frac{\langle E_{X,\text{meson frame}}\rangle}{M_X}\langle\gamma_{\text{meson}}\rangle, \tag{5.1.6}$$

where $\langle E_{X,\text{meson frame}}\rangle$ is the average energy of the particle $X$ in the meson rest frame.

| **Experiment** | $N_D$ | $\langle\gamma\rangle_D$ | $N_B$ | $\langle\gamma\rangle_B$ | $\langle l_{\rm det}\rangle$, m |
|---|---|---|---|---|---|
| MATHUSLA | $3.6 \times 10^{14}$ | 2.6 | $2.6 \times 10^{13}$ | 2.3 | 38 |
| SHiP | $7.8 \times 10^{17}$ | 19.2 | $5.4 \times 10^{13}$ | 16.6 | 50 |

**Table 5.1**: Main numbers for the SHiP and MATHUSLA experiments. The total number of all $D$ and $B$ mesons (*not including antiparticles*) is reported for both experiments. For SHiP the numbers of mesons and $\gamma$-factors are based on Monte Carlo simulations [111], including enhancement due to the cascade production [246], for MATHUSLA the numbers are based on the FONLL simulations in order to include low $p_T$ mesons (see text for details). The estimates assume $T_{SHiP} = 5$ years of running for SHiP and the integrated luminosity of $\mathcal{L}_h = 3000$ fb$^{-1}$ for HL-LHC, relevant for MATHUSLA.

The relevant parameters for the MATHUSLA and SHiP experiments are summarized in Table 5.1 (see next Section for details).

### 5.1.2 Number and momentum distributions of mesons

In this Section, we estimate the number of mesons of a given type and their average $\gamma$-factor. For HNLs with masses $M_N \lesssim m_{D_s}$ 2-body decays of $D_s$ provide dominant contribution (see e.g. Sec. 3.1), while for scalars the production from $D$ mesons is negligible as compared to $B$-meson decays even for masses $m_K \lesssim M_S \lesssim m_D$ (see Sec. 2.2).

For the SHiP experiment, the production of charmed and beauty mesons were studied in detailed Pythia simulations, and the corresponding numbers can be found in the SHiP Technical proposal [111] and reproduced in Table 5.1. At the LHC production of heavy flavor mesons has been studied in both Run I and Run II (c.f. [254, 255]). However, in order to estimate the number of mesons for the MATHUSLA experiment, $N^{\rm MAT}_{\rm meson}$, one needs to know the meson $p_T$ distribution in the MATHUSLA angular range, Table 4.3. The relevant distributions were measured for $B^+$ mesons by the CMS collaboration [255] (13 TeV) with the $p_T$ cut $p_T^B \geqslant 10$ GeV, and for $D^+/D_0$ mesons by the ATLAS collaboration [254] (7 TeV) for$p_T^D \geqslant 3.5$ GeV (measurements performed by the LHCb collaboration [256–258] are performed in the forward rapidity range and therefore are not directly relevant for the MATHUSLA experiment). The low-$p_T$ mesons, unaccounted in these studies, are the most relevant for the MATHUSLA sensitivity estimate for two reasons. Firstly, the spectrum of mesons produced in $pp$ collisions has the form $d\sigma/dp_T \propto p_T^{-n}$ [259] for $p_T$ above few GeV. This increases the number of $D$ or $B$ mesons as compared to those that passed the LHC cuts. Secondly, low-$p_T$ mesons have the smallest $\gamma$-factor and therefore the shortest decay length (5.1.4) and the largest probability to decay inside the detector.

In order to evaluate the number of heavy flavor mesons at low $p_T$ (and to estimate the $D$-meson production for $\sqrt{s} = 13$ TeV) we use the FONLL program [248, 249, 260, 261]. The FONLL predictions have been calibrated against the accelerator

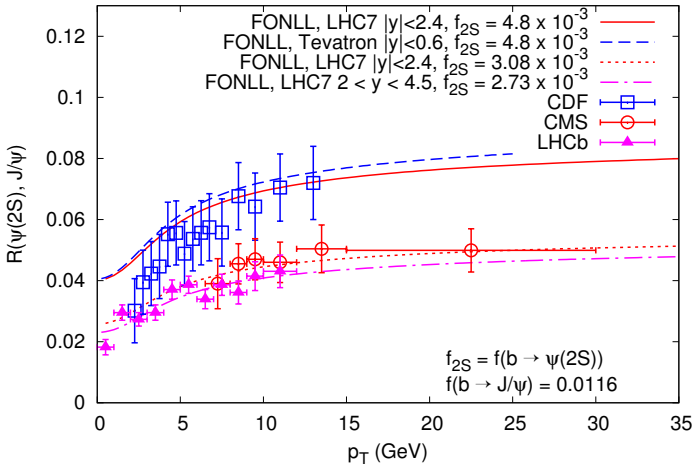


**Figure 5.1**: FONLL prediction of the ratio of the cross-section for non-prompt (i.e. from $b$-hadrons) production of $\psi(2S)$ and $J/\psi$ as a function of their transverse momentum, compared to the experimental data from CDF at the Tevatron and CMS and LHCb at the LHC (the figure is reproduced from [260]).

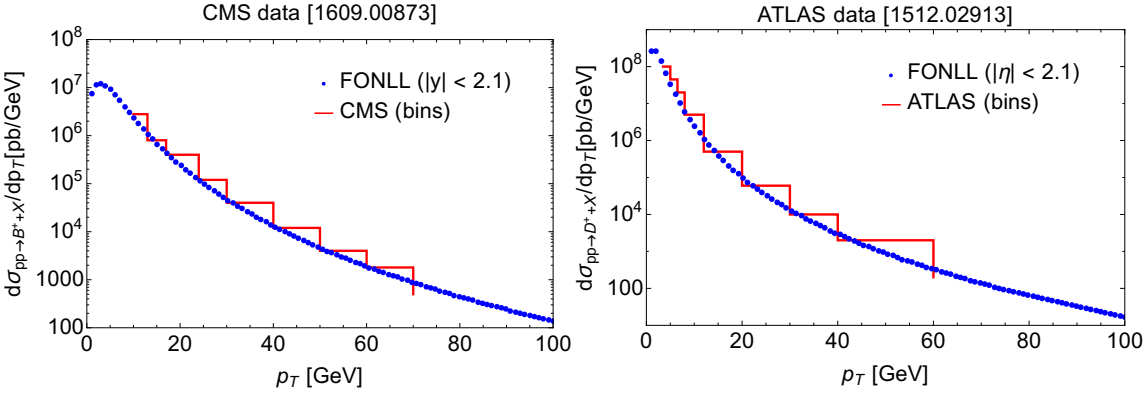


**Figure 5.2**: Comparison of the $p_T|$ spectrum of $B^+, D^+$ mesons as simulated by FONLL with the measurements by ATLAS and CMS experiments. Only the central values of the FONLL predictions are shown. See text for details.

data and were found to be in very good agreement, see e.g.[13, 254, 255, 257, 262]. In particular, by comparing the FONLL predictions with the Tevatron and LHC measurements of $B^+$ production, we see that FONLL predicts low-$p_T$ distribution accurately, see Fig. 5.1. We provide the central value of the FONLL predictions down to $p_T = 0$, confronted with the measurements of the CMS [255] and ATLAS [254] collaborations in Fig. 5.2. As expected, the distributions have maxima, after which they fall down. The position of the maximum affects the total number of produced mesons $N_{\text{meson}}$ and the average meson momentum $\langle|\mathbf{p}|\rangle_M$. Decreasing the position of the maximum by $x$ changes the estimate of the decay events by $x^2$ which makes the accurate prediction of this number very important.

Using the results of FONLL simulations we find the number of low $p_T$ mesons travelling in the MATHUSLA direction

$$\frac{N_D|_{p_T<3.5\text{ GeV}}}{N_D|_{p_T>3.5\text{ GeV}}} = 3.8, \quad \frac{N_B|_{p_T<10\text{ GeV}}}{N_B|_{p_T>10\text{ GeV}}} = 5.7 \tag{5.1.7}$$

At masses $M_X \gtrsim 3$ GeV the contribution of $B_c$ meson decays may become important, depending on the production fraction $f(b \to B_c)$ (see Sec. 3.1.1.3). The production fraction of $B_c$ mesons have been measured at the LHCb [223], and found to be in the range $f(b \to B_c) \simeq 2.6 \times 10^{-3}$. Earlier measurements at Tevatron have found a similar value $f(b \to B_c) \simeq 2 \times 10^{-3}$ [263–265]. For SHiP the corresponding production fraction at $\sqrt{s} \sim 30\,\text{GeV}$ is not known and therefore we perform our analysis for two extreme cases: *(i)* $f(b \to B_c)$ at SHiP the same as at the LHC and *(ii)* "no $B_c$ mesons".

To evaluate the pseudo-rapidity and $p_T$ distributions of $B_c$ mesons we compared the results of BCVEGPY 2.0 package [266] (that simulates the distribution of $B_c$ mesons and was tested at the LHC energies) with that of FONLL for $B^+$ mesons. We conclude that $p_T$ and $\eta$ distributions of $B_c$ and $B^+$ have similar shapes. Therefore we used the appropriately rescaled distributions of $B^+$ mesons in order to estimate the $B_c$ contribution for the SHiP experiment.

The numbers for both experiments are summarized in Table 5.1. One sees that the number of charmed mesons is much larger at SHiP, the numbers of $B$ mesons are comparable between the experiments and the average mesons momenta (and therefore $\gamma$-factors) are lower at MATHUSLA. This is caused by their different geometric orientation relative to the proton beams directions: SHiP is located in the forward direction, while MATHUSLA is about 20° off-axis.

### 5.1.3 Shape of the sensitivity curve

#### 5.1.3.1 Upper bound of the sensitivity curve

Let us now discuss the upper bound of the sensitivity curve, the value of $U^2$ that we call $U^2_{\text{top}}$. For simplicity, we will concentrate on the HNL case and later will comment on small differences that arise in the scalar case.

The dependence of the decay probability (5.1.3) on the mixing angle is such that for a fixed mass $M_N$ the number of decay events increases as $U^4$, then reaches the maximum and falls exponentially (see Fig. 5.3, left). The mixing angle for which the amount of detected HNLs is maximal $U_{\max}(M_N)$ could be estimated from the condition that the HNL decay width is equal to the distance from the target to the detector

$$l_{\text{decay}}(M_N, U^2_{\max}(M_N)) \simeq l_{\text{target-det}} \tag{5.1.8}$$

The HNL mass dependence of $U_{\max}$ is shown on Fig. 5.3, right.

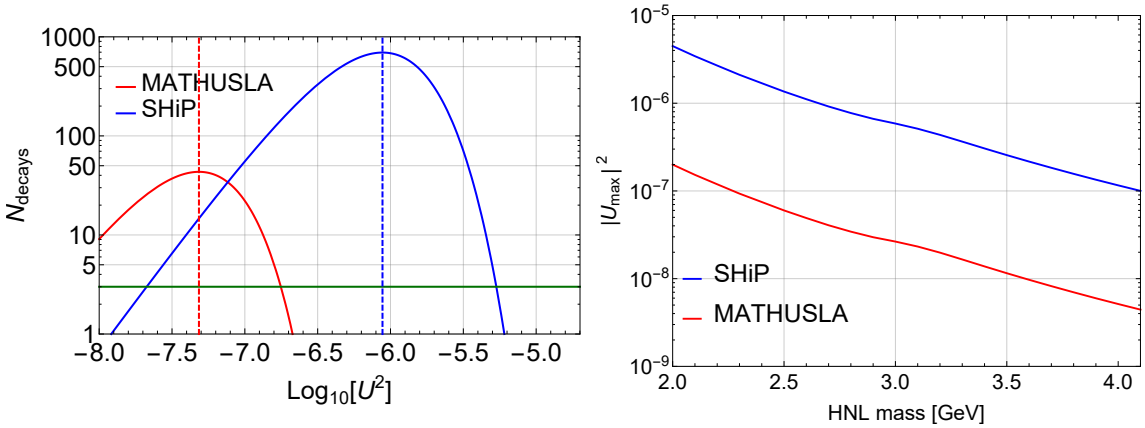


**Figure 5.3**: Left: the number of HNL decays events as a function of coupling $|U|^2$ for $M_N = 3$ GeV at SHiP and MATHUSLA experiments; green horizontal line denotes 3 decay events, while dashed vertical line corresponds to $U_{\max}$. Right: values of $|U_{\max}|^2$ for the MATHUSLA and SHiP experiments. Note that $U_{\max}$ is not equal to the upper boundary of the sensitivity curve!

The upper bound of sensitivity, $U_{\text{top}}$, appears when the exponential suppression due to the increasing probability to decay before reaching the detector outweighs the amount of produced HNLs. If all HNLs had the same energy, $\langle E_N \rangle$, then the upper bound of sensitivity would be given by $U^2_{\text{top}}(M_N) \simeq U^2_{\max}(M_N) \times \log\left(N_{\text{prod}}(M_N, U^2_{\max}(M_N))\right)$. The ratio $R$ between $U^2_{\text{top}}$ and $U^2_{\max}$ in this case is presented in Fig. 5.4 as dashed lines for two experiments.

However, for the correct estimation of $U_{\text{top}}$ it is important to take into account the distribution of the HNLs by energy $dN/dE_N$. The upper bound will be determined by the high-energy tail of the distribution, as the decrease of $c\tau$ with the growth of $U^2$ can be compensated by the increase of $\gamma$-factor of the HNL that occur in decays of most energetic mesons. The resulting decay probability (5.1.3) is modified as

$$P_{\text{decay}} \approx \int dE_N \, \frac{dN}{dE_N} e^{-l_{\text{target-det}} \Gamma_N M_N / E_N}. \tag{5.1.9}$$

The HNLs in question are produced from decays of $B$-mesons. The high-energy tail of $B$ mesons distribution function at SHiP is well described by the exponential distribution, see the left Fig. 5.5.

$$\frac{dN}{dE_B} = f_0 e^{-E_B \delta}, \quad \delta \approx 2.5 \cdot 10^{-2} \text{ GeV}^{-1} \quad \text{and} \quad f_0 \approx 0.1 \text{ GeV}^{-1} \tag{5.1.10}$$

The distribution of $B$-mesons in MATHUSLA experiment for $E_B \lesssim 300$ GeV can be approximated by the power law function, see the right Fig. 5.5:

$$\frac{dN}{dE_B} \approx \tilde{f}_0 E_B^{-\alpha}, \quad \tilde{f}_0 \approx 1.6 \cdot 10^4 \text{ GeV}^{\alpha - 1}, \quad \alpha \simeq 4.6 \tag{5.1.11}$$

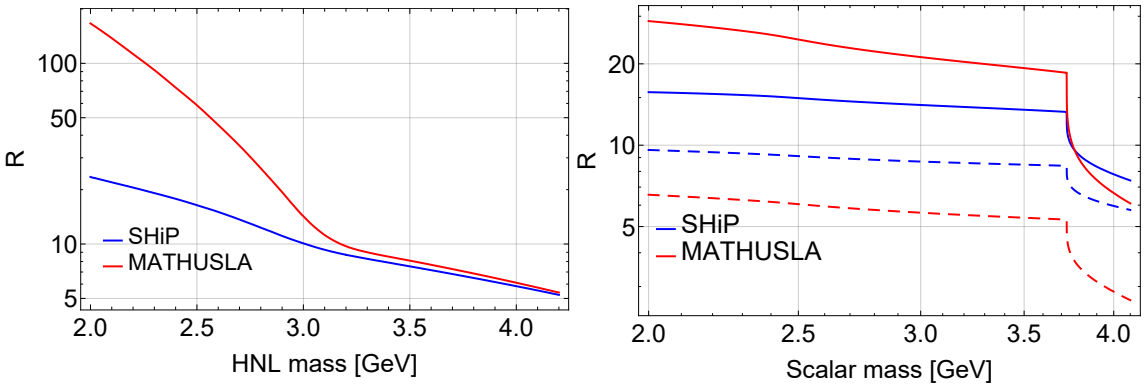


**Figure 5.4**: Ratios $R = U^2_{\rm top}/U^2_{\rm max}$ for HNLs mixing with $\nu_e$ (left) and for scalars (right) at SHiP and MATHUSLA experiments. Dashed lines are obtained under the assumption that all particles have the same average energy and neglecting the energy distribution tails.

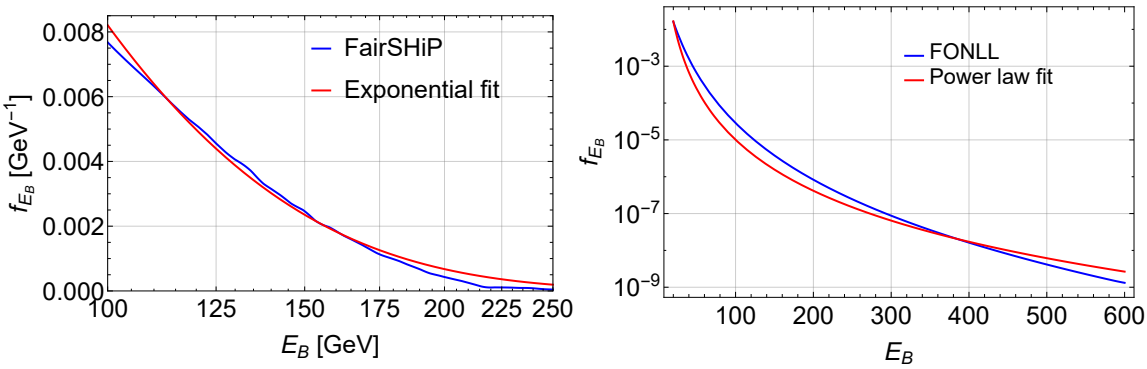


**Figure 5.5**: Fits of the high energy $B$ mesons distribution function at SHiP (data taken from [246]), left, and at MATHUSLA (provided by FONLL), right

Using the distributions (5.1.10)–(5.1.11) and relation between the energy of the parent $B$-meson and daughter HNL, we can improve the estimates of the upper sensitivity bound (see details in the Appendix F). The corresponding ratios $R = U^2_{\rm top}/U^2_{\rm max}$ for SHiP and MATHUSLA are given in Fig. 5.4. For SHiP the dependence of $R$ on the HNL mass is logarithmic, while for MATHUSLA it is a power law.

Finally, we comment on the difference between the HNL and scalar cases. The decay width $\Gamma_S$ changes with mass slower than $\Gamma_N$, see the discussion in Sec. 5.1.3.2. In addition, ${\rm Br}_{B\to S+X}$ behaves with mass monotonically, while for HNLs new production channels appear at different masses. Therefore the upper bound width for scalars changes with mass less than for HNLs.

### 5.1.3.2 Maximal probed mass

The maximal mass probed by the experiment is defined as the mass at which the lower sensitivity bound (decays are very rare) meets the upper sensitivity bound

(particles decay before reaching the detector). It can be roughly estimated from the relation

$$l_{\text{target-det}} \lesssim l_{\text{decay}} \tag{5.1.12}$$

where for the models in question

$$l_{\text{decay}} \simeq \frac{\langle E \rangle}{M_X} \times \begin{cases} 170\,\text{cm} \left(\dfrac{10^{-5}}{U^2}\right) \left(\dfrac{2\,\text{GeV}}{M_X}\right)^5, & \text{HNL. Mixing with } U_{e/\mu} \text{ only} \\ 454\,\text{cm} \left(\dfrac{10^{-5}}{U_\tau^2}\right) \left(\dfrac{2\,\text{GeV}}{M_X}\right)^5, & \text{HNL. Mixing with } U_\tau \text{ only} \\ 0.015\,\text{cm} \left(\dfrac{10^{-5}}{\sin^2\theta}\right) \left(\dfrac{2\,\text{GeV}}{M_X}\right)^2, & \text{scalar} \end{cases} \tag{5.1.13}$$

where $\langle E \rangle$ is the average energy of a particle $X$, $M_X$ is the particle's mass and $U^2$ (correspondingly, $\sin^2\theta$) are dimensionless parameters that specify how much weaker is the parameter controlling the interaction of the particle $X$ than the interaction of neutrino (correspondingly, Higgs boson), see Sections 2.3 and 3.2 for details.

The maximal mass can be found from Eq. (5.1.12) via

$$M_{X,\text{max}} \propto \left(\frac{\langle E \rangle}{|\phi|^2_{\text{min}} l_{\text{target-det}}}\right)^{1/(\alpha+1)} \tag{5.1.14}$$

where $\alpha = 2$ (correspondingly $\alpha = 5$) for the case of scalar (correspondingly, HNL) and $|\phi|^2 = |\phi|^2_{\text{min}}$, is the value of parameter $U^2$ (or $\sin^2\theta$) that corresponds to $\bar{N}_{\text{events}}$ detected events for $M_X < M_{X,\text{max}}$.

For the ratio of the maximally probed masses at SHiP and MATHUSLA, we obtain

$$\frac{M^{SHiP}_{X,\text{max}}}{M^{\text{MAT}}_{X,\text{max}}} \approx \left(\frac{\langle E \rangle^{SHiP}}{\langle E \rangle^{\text{MAT}}} \times \frac{|\phi|^{2,\text{MAT}}_{\text{min}}}{|\phi|^{2,SHiP}_{\text{min}}} \times \frac{l^{\text{MAT}}_{\text{tar-det}}}{l^{SHiP}_{\text{tar-det}}}\right)^{1/(\alpha+1)} \tag{5.1.15}$$

This estimation is valid for the masses $M_X$ not too close to the production threshold, which corresponds to masses $M_X = m_B - m_K$ for scalars and $M_X = m_B$ for HNLs.

### 5.1.4 Results

Our results are summarized in Fig. 5.6 for HNLs mixed with light (electron) and heavy ($\tau$) flavors. In Fig. 5.7 we show the sensitivity of both experiments to the scalar.

Qualitatively, for particles produced in $B$-meson decays (HNLs with masses $M_N > m_D$ and scalars with masses $M_S > m_K$) MATHUSLA can probe factor $\sim 2-3$ smaller mixing angles ($U^2$ or $\sin^2\theta$) than SHiP. This conclusion holds *assuming* no background events for both experiments and *similar detection efficiency*. For the HNLs in the mass range $m_K \lesssim M_N \lesssim m_D$ the smaller $\gamma$-factor of MATHUSLA

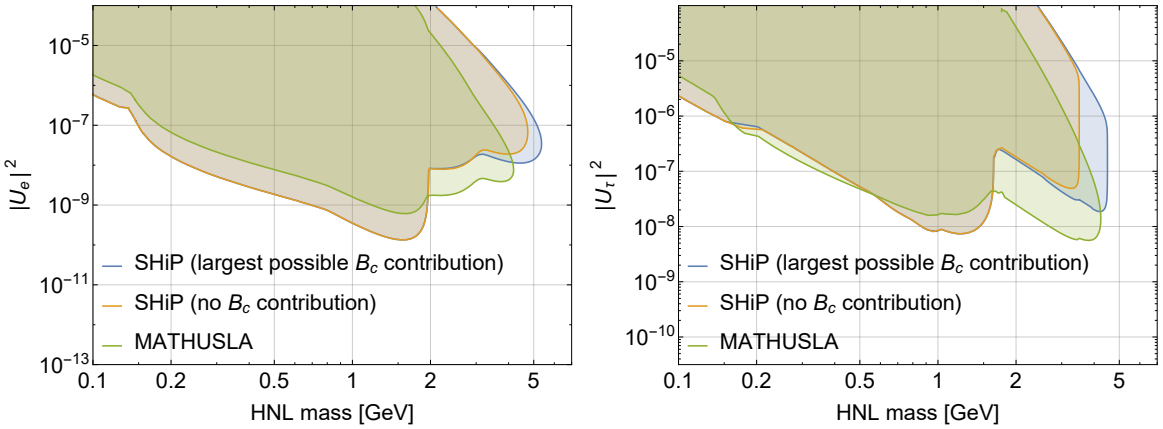


**Figure 5.6**: Comparison of sensitivity for SHiP and MATHUSLA for HNL models. The production fraction of $B_c$ mesons at SHiP is not known, so we take the largest possible contribution of $B_c$ based on the production fraction measured at the LHC, $f(b \to B_c) = 2.6 \times 10^{-3}$. In case of the SHiP experiment we take into account proper geometrical acceptance (calibrated against the Monte-Carlo simulations [212] and select only those channels where at least two charged tracks from the HNL decay appear. In the case of the MATHUSLA experiment we optimistically used both decay and detection acceptances equal to 100%.

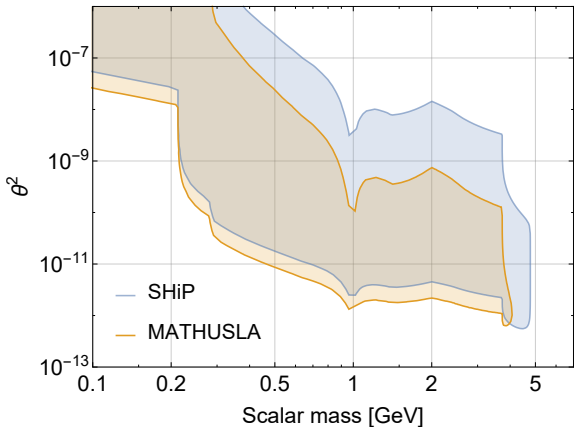


**Figure 5.7**: Comparison of sensitivities of SHiP and MATHUSLA experiments for the scalar portal model. In case of the SHiP experiment, we took into account proper geometrical acceptance (calibrated against the Monte-Carlo simulations [267] and also selected only those channels where at least two charged tracks from the HNL decay appear. In case of MATHUSLA experiment we optimistically used both decay and detection acceptances equal to 100%.

does not compensate 3 orders of magnitude difference in the number of $D$ mesons (see Table 5.1) and therefore the SHiP reaches about 1 order of magnitude lower in

sensitivity for $U^2$. The comparison between the number of events is

$$\left.\frac{N^{N,SHiP}_{\rm decay}}{N^{N,\rm MAT}_{\rm decay}}\right|_{M_N\lesssim m_D} \simeq 127, \quad \left.\frac{N^{N,SHiP}_{\rm decay}}{N^{N,\rm MAT}_{\rm decay}}\right|_{M_N\gtrsim m_D} \simeq \left.\frac{N^{S,SHiP}_{\rm decay}}{N^{S,\rm MAT}_{\rm decay}}\right|_{M_S\gtrsim m_K} \simeq \frac{1}{7.6} \tag{5.1.16}$$

The smaller $\gamma$-factor of MATHUSLA adversely affects the maximal mass that can be probed (as well as the upper bound of the sensitivity curves). The maximally probed masses ratios (5.1.15) are

$$\text{HNL:} \quad \frac{M^{N,SHiP}_{\rm max}}{M^{N,\rm MAT}_{\rm max}} \approx 1.7, \qquad \text{Scalar:} \quad \frac{M^{S,SHiP}_{\rm max}}{M^{S,\rm MAT}_{\rm max}} \approx 2.2 \tag{5.1.17}$$

## 5.2 Monte Carlo-based sensitivity estimates

The sensitivity estimates depend on the geometric acceptance. The latter is a function of particle's mass and in the case of the HNL, also the function of the mixing type. In order to evaluate the acceptance we compared our results with the `FairSHiP` simulations [212, 267]. `FairSHiP` is a `FairRoot`-based [268] Monte Carlo software framework developed by the SHiP collaboration. In the simulation, fixed-target collisions of protons are generated by `Pythia 8` [269], neutrino interactions by `GENIE` [270] and inelastic muon interactions by `Pythia 6` [271]. Secondary heavy flavor production in cascade interactions of hadrons originated by the initial proton collision [246] is also taken into account, which leads to the increase of the overall production fraction, taken into account in Table 5.1. The SHiP detector response is simulated with the `GEANT4` [272]; the SHiP spectrometer tracking stations are described in [273] and the particle identification tools are presented in [274].

### 5.2.1 FairSHiP: simulation framework for the SHiP experiment

The experimental sensitivity to HNLs was previously explored for several benchmark models [111, 252] assuming particular ratio between the three HNL mixing angles [129, 218]. The current study updates the previous results in a number of important ways. Recent work [275] revised branching ratios of HNL production and decay channels and evaluated several new channels not considered before. In addition, the estimates of the number of $D$- and $B$-mesons now include cascade production [246]. We further add an evaluation of the SHiP sensitivity limit for large values of the mixing angles $U^2$. In addition, our current sensitivity estimates are not limited to a set of benchmark models. Instead, we provide a model-independent way to compute the sensitivity for *any* model ratio of mixing angles.

A single `FairShip` simulation takes the HNL mass, $M_N$, and its couplings to the Standard Model flavors $U_e, U_\mu, U_\tau$ as input parameters. The mass dependent branching ratios (based on [275], see Sec. 3.1) for leptonic and semileptonic decays of charm and beauty mesons, $\tau$ leptons, etc to HNL, are made available to `Pythia`

| $pp$ cross-section $\sigma_{pp}$ | $\bar{c}c$ fraction $X_{\bar{c}c}$ [276] | $b\bar{b}$ fraction $X_{\bar{b}b}$ [277] | Cascade enhancement $f_{\text{cascade}}$ | |
|---|---|---|---|---|
| | | | charm [246] | beauty [246] |
| 10.7 mb | $1.7 \times 10^{-3}$ | $1.6 \times 10^{-7}$ | 2.3 | 1.7 |

**Table 5.2**: Charm and beauty production values. Total number of mesons of a given flavor is defined by $N_q = 2 \times X_{\bar{q}q} \times f_{\text{cascade}} \times N_{\text{PoT}}$. The number of protons on target over 5 years of the experiment's run is $N_{\text{PoT}} = 2 \times 10^{20}$.

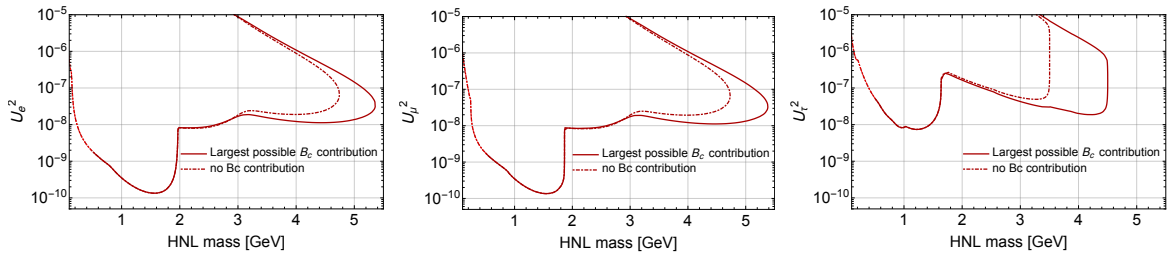


**Figure 5.8**: SHiP sensitivity curves (90%CL) for mixing with a single flavor: $U_e$ (left), $U_\mu$ (middle), $U_\tau$ (right). Dashed-dotted line: contribution from $B_c$ mesons not included; solid line: contribution of $B_c$ mesons is included with the production fraction equal to that at the LHC energies: $f(b \to B_c) = 2.6 \times 10^{-3}$. The region between two curves shows a range of potential contribution from $B_c$ depending on its actual production fraction. Below $m_K$ only contributions from $D$-mesons have been included (dashed lines).

8. A registered "decay event" in the detector requires two charged tracks that also satisfy a number of selection criteria as described in [274].

For HNLs with masses $M_N \lesssim 500$ MeV, kaon decays provide the dominant production channel. While $\mathcal{O}(10^{20})$ kaons are expected at SHiP, most of them scatter in the target and/or hadron stopper before decaying. A proper estimate of the number of kaons decaying into HNLs is not currently included in the `FairSHiP`. It is expected that NA62 experiment [107, 109, 251] will cover the region below kaon mass.

Detailed background studies have been performed for the SHiP experiment [111, 244, 252, 253]. They demonstrate that there is a negligible amount of background events after selection and veto cuts over the lifetime of the experiment. The experiment is essentially "background free" which greatly simplifies the analysis – it is sufficient to count the number of events for a given value of mixings. One therefore defines the *90% confidence region* as a region in the parameter space where one expect $\bar{N}_{\text{events}} = 2.3$ signal events *on average*.

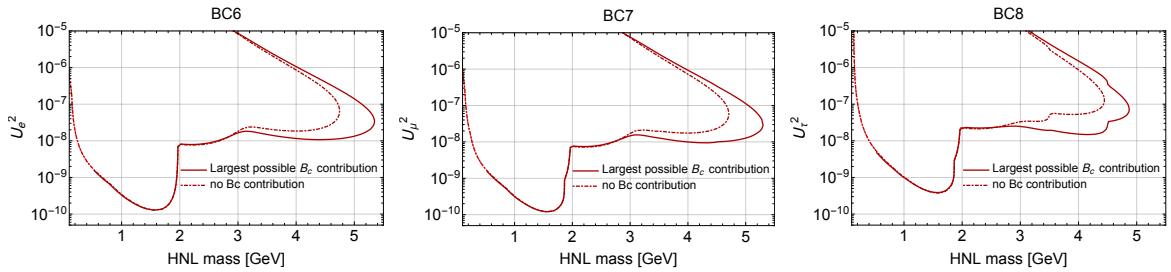


**Figure 5.9**: Sensitivity curves for 3 benchmark models, 90%CL (see text for details)

### 5.2.2 Sensitivity towards HNLs

#### 5.2.2.1 Sensitivity for mixing with individual flavors and benchmark models

We present our results in several forms. Firstly, we present sensitivity curves (90% CL) for mixing with each individual flavor (Fig. 5.8). For masses above $\sim$ 3 GeV, the contribution of $B_c$ mesons to the HNL production can have an important (even dominant) role for the production fractions $f(b \to B_c)$ as low as $10^{-3}$ (see Sec. 3.1.1.3 for details). As the yield of $B_c$ mesons at SHiP energies is not known, we provide two estimates. For the optimistic estimate $f(b \to B_c)$ is assumed at the LHC level $2.6 \times 10^{-3}$ [223] while for the pessimistic estimate we do not include $B_c$ mesons at all.

We also provide sensitivity estimates of three "benchmark models" used in the Technical proposal [111]. These models allow to explain the data of neutrino flavor oscillations while at the same time maximizing the mixing to a one particular flavor [129, 218]. They are

– **BC6:** $U_e^2 : U_\mu^2 : U_\tau^2 = 52 : 1 : 1$
– **BC7:** $U_e^2 : U_\mu^2 : U_\tau^2 = 1 : 16 : 3.8$
– **BC8:** $U_e^2 : U_\mu^2 : U_\tau^2 = 0.061 : 1 : 4.3$

The sensitivity curves for these models are shown in Fig. 5.9.

#### 5.2.2.2 Full sensitivity matrix for HNLs at SHiP

We will demonstrate below that the lower limit of the sensitivity curve has a simple analytical dependence on the set of mixing angles $\overrightarrow{U^2} \equiv \{U_e^2, U_\mu^2, U_\tau^2\}$. This allows to extract all the relevant information about the lower limit of sensitivity for any model with just a handful of simulations.

Production of HNLs at SHiP proceeds via leptonic or semileptonic heavy flavor decays with other channels being irrelevant (c.f. [275]). The dependence on $U_\alpha^2$ factors out and therefore the total number of produced HNLs is given by

$$N_{\text{prod}}(M_N|\overrightarrow{U^2}) = \sum_\alpha U_\alpha^2 N_\alpha \tag{5.2.1}$$

where $N_\alpha$ is the number of HNLs that would be produced through *all possible channels* with the mixings $U_\alpha = 1; U_{\beta\neq\alpha=0}$:

$$N_\alpha \equiv \sum_{\text{hadrons } h} N_h \left( \sum_{\text{channels}} \text{BR}_{h\to N+X_\alpha} \Big|_{U_\alpha=1;U_{\beta\neq\alpha=0}} \right) \tag{5.2.2}$$

Here $N_h$ is the number of hadrons of a given type $h$; $\text{BR}_{h\to N+X_\alpha}$ is a branching ratio for their decay into an HNL plus any number of other particles (whose total flavor lepton number $L_\alpha = 1$). By its definition $N_\alpha$ depends on the HNL mass and flavor *type* only. To make notations compact we will sometimes rewrite Eq. (5.2.1) as

$$N_{\text{prod}} = \overrightarrow{U^2} \cdot \overrightarrow{N} \tag{5.2.3}$$

In the limit when the decay length is much larger than the distance to the detector (and of the detector size), the $U_\alpha^2$ dependence also factorizes similarly to Eq. (5.2.1):

$$P_{\text{decay}}(M_N|\overrightarrow{U^2}) = \sum_\alpha U_\alpha^2 P_\alpha \tag{5.2.4}$$

The corresponding $P_\alpha$ is given by:

$$P_\alpha = \frac{l_{\text{det}}}{l_{\text{decay}}} \sum_X \text{BR}(N \to X_{\text{detectable}}) \Big|_{U_\alpha=1;U_{\beta\neq\alpha=0}} \tag{5.2.5}$$

Here $l_{\text{decay}} = c\tau_N\gamma$ is the decay length of an HNL, $l_{\text{det}}$ is the detector length (we assume that $l_{\text{decay}} \gg l_{\text{det}}$) and all quantities in the right hand side, including $l_{\text{decay}}$, are evaluated for $U_\alpha = 1; U_{\beta\neq\alpha} = 0$.

As a result, the number of detected events will be given by

$$N_{\text{decay}}\left[M_N|\overrightarrow{U^2}\right] = \sum_{\alpha,\beta} U_\alpha^2 \mathcal{M}_{\alpha\beta}(M_N) U_\beta^2 \tag{5.2.6}$$

where the matrix $M_{\alpha\beta}(M_N)$ is defined as

$$\mathcal{M}_{\alpha\beta} \equiv N_\alpha P_\beta \tag{5.2.7}$$

where $N_\alpha$ and $P_\alpha$ are defined via Eqs. (5.2.2) and (5.2.5) correspondingly. The matrix $M_{\alpha\beta}$ depends *only* on HNL's mass and *does not* depend on the mixing angles.

#### 5.2.2.3 Procedure to determine the sensitivity matrix

To determine $M_{\alpha\beta}$ one needs to run 9 Monte Carlo simulations for each mass. Namely, one runs 3 simulations with vectors $\overrightarrow{U^2} = (x, 0, 0)$, $\overrightarrow{U^2} = (0, x, 0)$, $\overrightarrow{U^2} = (0, 0, x)$, where $x$ is any sufficiently small number such that $l_{\text{decay}} \gg l_{\text{det}}$. Next one runs a

set of 6 non-physical simulations, where a particle is produced solely via channel $\alpha$ and decays solely through the channel $\beta \neq \alpha$, thus providing non-diagonal matrix elements.

The resulting matrix has the form

$$\mathcal{M}_{\alpha\beta}\Big[M_N{=}1.5\,\text{GeV}\Big] = 10^{20} \begin{pmatrix} 1.33 & 1.14 & 0.35 \\ 1.46 & 1.46 & 0.38 \\ 7.46 \cdot 10^{-4} & 6.79 \cdot 10^{-4} & 1.75 \cdot 10^{-4} \end{pmatrix} \tag{5.2.8}$$

Knowing this matrix one can compute the sensitivity curve $U_\alpha(M)$ by solving the equation

$$\sum_{\alpha\beta} U_\alpha^2 \mathcal{M}_{\alpha\beta}(M_N) U_\beta^2 = N_{\text{events}} \tag{5.2.9}$$

By choosing different values of $N_{\text{events}}$ one can obtain 90%, 95%, etc. confidence intervals or simply predict how many events one expects for a given vector of mixing angles $\overrightarrow{U^2}$. It should be stressed that only the *lower* limit of sensitivity can be assessed with such method (which is important for $M_N \gtrsim 2$ GeV).

For each mass we provide the results in the form

| HNL Mass | $\mathcal{M}_{ee}$ | $\mathcal{M}_{e\mu}$ | $\mathcal{M}_{e\tau}$ | $\mathcal{M}_{\mu e}$ | $\mathcal{M}_{\mu\mu}$ | $\mathcal{M}_{\mu\tau}$ | $\mathcal{M}_{\tau e}$ | $\mathcal{M}_{\tau\mu}$ | $\mathcal{M}_{\tau\tau}$ |
|---|---|---|---|---|---|---|---|---|---|

The results are available at https://ship.web.cern.ch/ship/Sensitivity_Matrix/README that provides instructions for reading the file and generating sensitivity curves at different confidence levels.

### 5.2.3 Sensitivity towards dark scalars

SHiP sensitivity to the scalar portal discussed in the Sec. 5.1 was validated by FairShip simulation tool, see Fig. 5.10. We see that simulations are in good agreement with the analytical estimate.

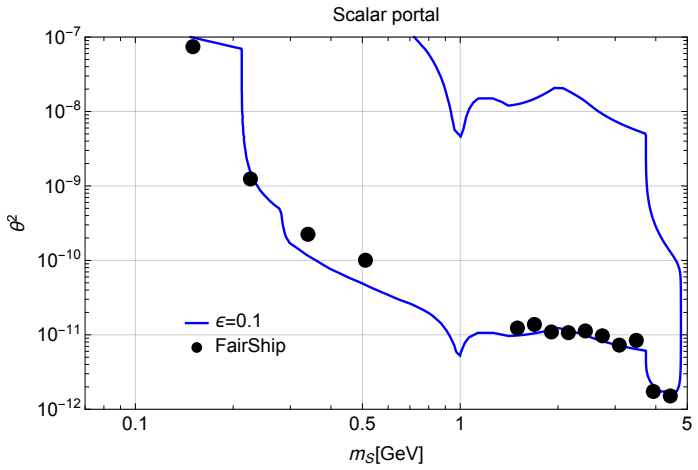


**Figure 5.10**: Comparison between analytical estimation of the SHiP sensitivity for acceptance $\epsilon = 0.1$ (blue line) with the results of the FairShip simulation (black points).

# Chapter 6

# Searching for new physics with the SHiP neutrino detector (iSHiP)

## 6.1 Light dark matter at the iSHiP

### 6.1.1 Production of DM particles

Light dark matter (LDM) is a weakly interacting massive particle (WIMP) with the mass below the Lee-Weinberg bound. The original idea for WIMPs was first proposed in the paper [278]. In this paper, it was assumed that a new weakly interacting stable particle $\chi$ interacting with the SM particles through neutral weak interactions (so-called "heavy neutrino"), which can play the role of DM. These particles were in thermal equilibrium in the early Universe. They keep the equilibrium number density via annihilation $\chi + \bar{\chi} \leftrightarrow \text{SM} + \text{SM}$. During the Universe expansion, the density of DM drops and hence the annihilation rate decreases.

At some moment, the annihilation rate is insufficient to maintain the equilibrium number density and therefore $\chi$ degree of freedom freezes out. WIMP "remembers" the density of the Universe at the time of freeze-out. It is given by

$$\Omega_\chi h^2 \sim \frac{[3 \cdot 10^{-27}]\text{cm}^3/\text{sec}}{\langle \sigma_{ann} v \rangle}, \tag{6.1.1}$$

where $\langle \sigma_{ann} v \rangle \sim G_F^2 m_\chi^2 N_{\text{channels}}$ is the anihilation rate at the time of freeze-out. For a "heavy neutrino" mass $m_\chi \sim \mathcal{O}(1)$ GeV, annihilation into the SM channels leads to a too small cross-section, which leads to too large DM abundance. Requiring that (6.1.1) does not exceed the present number density of the Universe, it was obtained in [278] that the lower bound $m_\chi > 5$ GeV.

To increase the annihilation rate we need a new light mediator $m_{\text{mediator}} \ll m_W$ with a sizeable coupling to the SM sector,

$$G_F \to G_F^{\text{mediator}} = \frac{4\pi\tilde{\alpha}}{m^2_{\text{mediator}}}. \tag{6.1.2}$$

One of possible mediators is a scalar mediator. The Lagrangian of the interaction of DM with a scalar is (1.6.1).

There are three $\chi$ particles production mechanisms which are relevant to proton beam dump experiments [279]:

- Production in deep inelastic proton-proton scattering (DIS).
- Coherent proton-nucleus and proton-proton collisions.
- Decays of secondary particles — kaons, $D$ and $B$ mesons.

The first two channels remain opened for very wide range of $\chi$ masses, while the third channel closes for $m_\chi \gtrsim m_B/2 \simeq 2.5$ GeV.

#### 6.1.1.1 DIS production

DIS channel is a production of $\chi\bar{\chi}$ pairs through scattering of partons inside the protons, namely gluons and $u-$, $d-$, $s-$ quarks. This is relevant because of the high proton-proton CM energy, $\sqrt{s_{pp}} = 28.4$ GeV. Using the couplings to quarks and gluons, one can draw the diagrams of DIS productions, see Fig. 6.1.

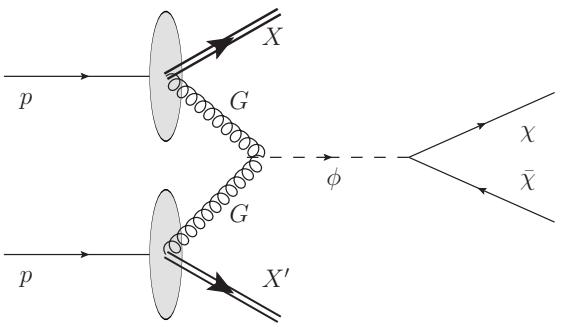


**Figure 6.1**: The production of the $\chi\bar{\chi}$ pairs in DIS.

The "hard" cross-sections for the parton (which can be either $G$ or $q$) in region of parameters $m_\phi < 2m_\chi$ are:

$$\sigma_{GG\to\chi\bar{\chi}}(s_{GG}) = \alpha_{\phi\chi\chi}\frac{\alpha_s^2(s_{GG})F_G^2\sin^2(\theta)\left(1-\frac{4m_\chi^2}{s_{GG}}\right)^{\frac{3}{2}}}{256\pi^3 v_H^2\left(1-\frac{m_\phi^2}{s_{GG}}\right)^2}, \tag{6.1.3}$$

$$\sigma_{q\bar{q}\to\chi\bar{\chi}}(s_{qq}) = \frac{\alpha_{\phi\chi\chi}y_q^2(1-\frac{4m_\chi^2}{s_{qq}})^{3/2}}{4s_{qq}\left(1-\frac{m_\phi^2}{s_{qq}}\right)^2}, \tag{6.1.4}$$

where $s_{PP} = x_1x_2s_{pp}$ is an invariant mass of two partons, and $x$ is the momentum fraction of one of the partons defined as $p_{P_i}^\mu \approx x_i p_{p_i}^\mu$, $F_G$ is effective coupling constant

to gluons, $y_q$ is Yukawa coupling of the quark $q$ and $v_H$ is the vacuum expectation value of the Higgs field.

The total cross section is obtained by integrating the "hard" cross-section with two parton distribution functions of two gluons $f_{p/G}(x, Q^2)$, where $Q^2 = s_{GG}$ is the "soft"/"hard" fragmentation scale. Namely, one has

$$\sigma_{\rm DIS} = \int_0^1 dx_1 \int_0^1 dx_2 f_{p/P}(x_1, s_{PP}) f_{p/P}(x_2, s_{PP}) \sigma_{PP\to\chi\bar{\chi}}(s_{PP}). \tag{6.1.5}$$

The corresponding DIS branching fractions

$$\mathrm{Br}^{\rm DIS}_{\chi\bar{\chi}} = \frac{\sigma_{\rm DIS}}{\sigma_{p+p\to\rm all}}, \tag{6.1.6}$$

where $\sigma_{p+p\to\rm all} \approx 100$ GeV$^{-2}$ for the SHiP center-of-mass energy [222]. Examples of DIS production of $\chi$ particles for different proton beam energies are shown in Fig. 6.2.

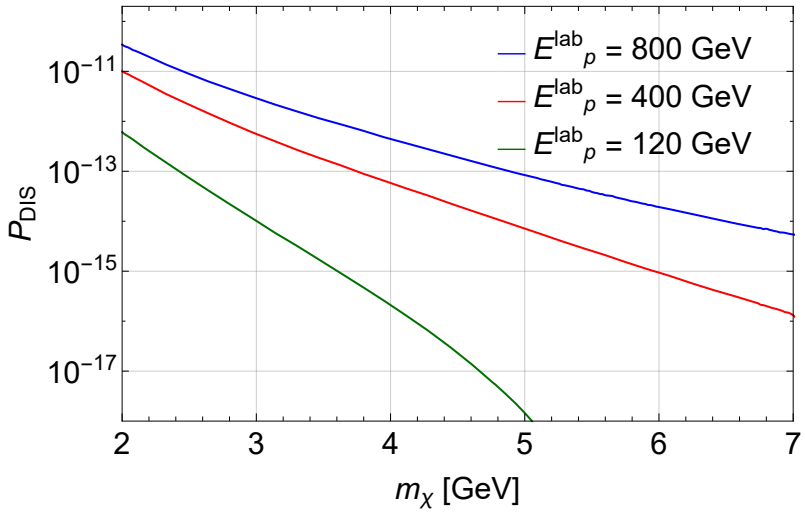


**Figure 6.2**: Production probability of $\chi$ particles in DIS for different proton beam energies.

#### 6.1.1.2 Coherent production

Other direct production channels are coherent proton-nucleus scattering $p + Z \to p + Z + \chi + \bar{\chi}$. Scattering goes through $Spp$ and $S\gamma\gamma$ vertices. The leading order diagrams for direct production are shown in Fig. 6.3.

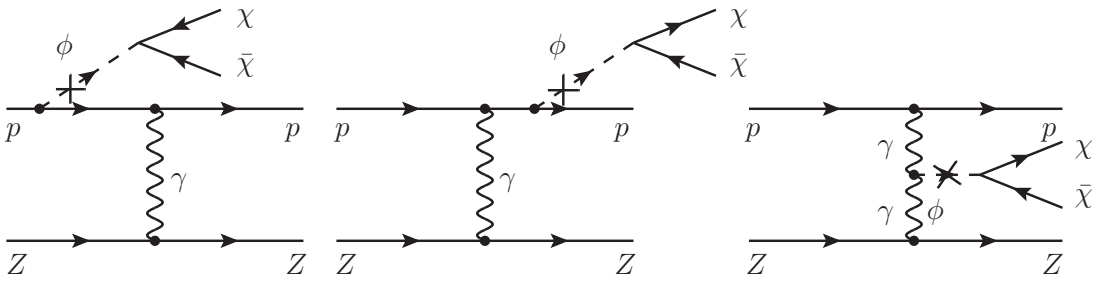


**Figure 6.3**: Diagrams of production of the $\chi\bar{\chi}$ pairs in coherent $pZ$ scattering.

The corresponding branching ratios are

$$\mathrm{Br}_{p+Z\to p+Z+\chi+\bar{\chi}} = \frac{\sigma_{p+Z\to p+Z+\chi+\bar{\chi}}}{\sigma_{p+Z\to \mathrm{all}}}, \quad \mathrm{Br}_{p+p\to p+p+\chi+\bar{\chi}} = \frac{\sigma_{p+p\to p+p+\chi+\bar{\chi}}}{\sigma_{p+p\to \mathrm{all}}}, \tag{6.1.7}$$

where $\sigma_{p+p\to \mathrm{all}} \approx 100\ \mathrm{GeV}^{-2}$ and $\sigma_{p+Z\to \mathrm{all}} \approx 53A^{0.77}\ \mathrm{mb} \approx 4400\ \mathrm{GeV}^{-2}$ [222] (for Molybdenum) are calculated in the forthcoming paper [236]. Here we will give only the main results. The upper bounds on the cross-sections valid for light DM pairs are

$$\sigma_{p+Z\to p+Z+\chi+\bar{\chi}} \lesssim \frac{\alpha_{\mathrm{EM}}^2 Z^2 y_N^2}{4\pi m_p^2} \ln\left(\frac{E_{p.o.t.}^2}{4m_\chi^2}\right) \alpha_{\phi\chi\chi} \sin^2(\theta) \simeq 10^{-3} \alpha_{\phi\chi\chi} \sin^2(\theta)\ \mathrm{GeV}^{-2}. \tag{6.1.8}$$

For light $\chi$ particles, the proton coherent production branching ratio is in $Z$ times suppressed in comparison with the nucleus coherent production. However, heavy $\chi$ particles require a large transferred momenta, which strongly suppress coherent production from nucleus, and thus the proton production becomes the dominant one.

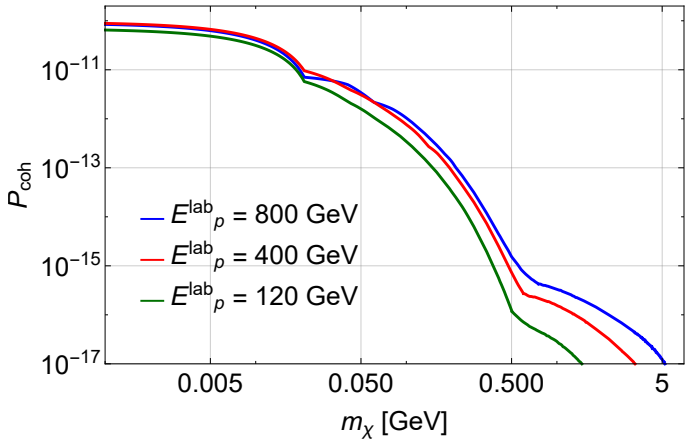


**Figure 6.4**: The production probability of $\chi\bar{\chi}$ pairs in coherent scattering for different proton beam energies.

#### 6.1.1.3 Production from mesons

Let us discuss $\chi\bar{\chi}$ pairs production from heavy flavored mesons. The relevant processes, mediated by the Lagrangian 2.1.12, are $M \to M' + \chi + \bar{\chi}$, where $M, M'$ are different mesons. We'll calculate the production fractions for the processes

$$K \to \pi + \chi + \bar{\chi}, \quad D \to K + \chi + \bar{\chi}, \quad B \to K + \chi + \bar{\chi} \tag{6.1.9}$$

The diagram for production of $\chi\bar{\chi}$ pairs from mesons is shown on Fig. 6.4.

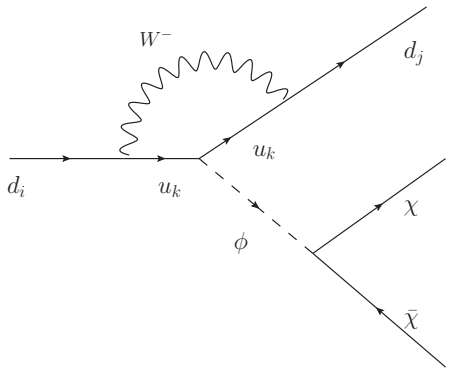


**Figure 6.5**: Diagrams of production of the $\chi\bar{\chi}$ pairs from mesons decays

At SHiP experiment there will be produced $N_{K^+} \approx 3.4 \cdot 10^{16}$, $N_{B^+} \approx N_{B^0} \approx 5.6 \cdot 10^{13}$ mesons[1] see discussion in Sec. 2.2.2. D production channel is suppressed in comparison with $B$ production channel and is not relevant. The reasons are following:

– for $D$ meson decay loop the heaviest quark running in the loop is $b$ quark, while for $B$ meson it is $t$ quark

– for $D$ meson decay loop the CKM matrix elements are much smaller than the CKM matrix elements for $B$ meson decay

#### 6.1.1.4 Summary

Amounts of DM pairs produced by each of these channels are given on Fig. 6.6.

[1]The number of kaons include $\sim 10^{-3}$ suppression due to their absorption inside the wall because of scatterings

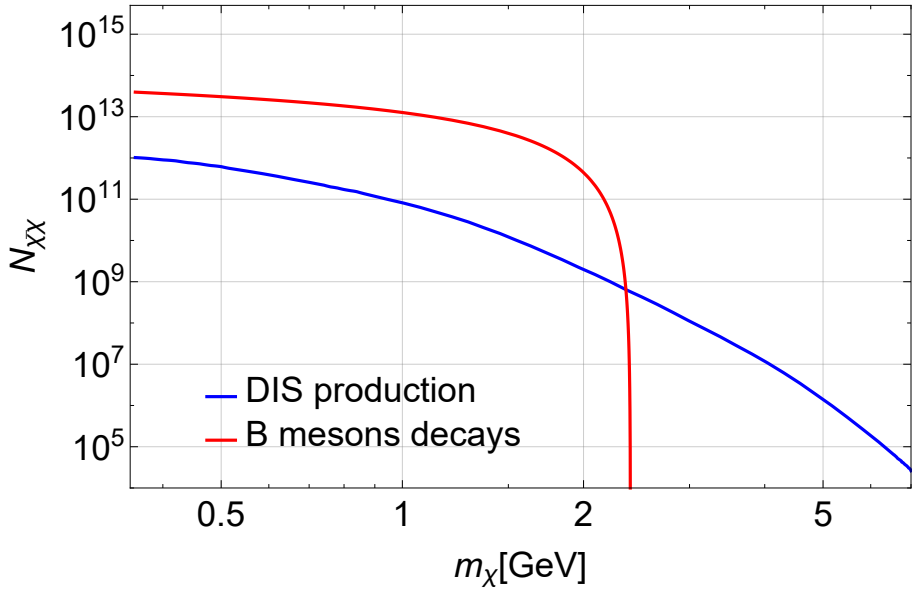


**Figure 6.6**: Number of produced $\chi\bar{\chi}$ pairs for different channels: DIS of quarks and gluons, mesons decays $B^{+/0} \to K + \chi + \bar{\chi}$, $K \to \pi + \chi + \bar{\chi}$, and coherent scattering on nuclei and protons, $p + Z/p \to p + Z/p + \chi + \bar{\chi}$. Amounts are evaluated for $m_S = m_\chi/3$

For masses $2m_\chi \lesssim m_B$ the dominant production channels are mesons decays: kaons decays for $2m_\chi \lesssim m_K - m_\pi$, and $B^+, B^0$ mesons decays for masses $m_K - m_\pi \lesssim 2m_\chi < m_B - m_K$, while for larger masses the dominant channel is DIS. Coherent production channel is always sub-dominant and doesn't present on Fig. 6.6.

The reason for this is the following. $\chi\bar{\chi}$ pairs production channels compete with SM production channels. For the direct production, the main SM production channels are mediated by strong and EM interactions, while for the mesons decays the main channels are mediated by weak interactions. Therefore direct production channels are strongly suppressed in comparison with mesons channel (even taking into account that one needs to produce mesons first).

### 6.1.2 Number of scattering events

#### 6.1.2.1 Effective interaction with nucleons

Effective low-energy coupling $g_{SNN}$ to the nucleons $N$, which is defined by the Lagrangian

$$\mathcal{L}_{SNN} = g_{SNN} \sin(\theta) S\bar{N}N, \tag{6.1.10}$$

can be related to the interaction $\mathcal{L}_{Sff}$ by the expression

$$g_{SNN} \equiv \frac{1}{v_H} \lim_{p \to p'} \langle N(p)| \sum_q m_q \bar{q}q |N(p')\rangle \equiv \frac{1}{v_H} \langle N| \sum_q m_q \bar{q}q |N\rangle, \tag{6.1.11}$$

where the shorthand notation $\langle N|..|N\rangle \equiv \lim_{p\to p'}\langle N(p)|..|N(p')\rangle$ was used. Numerical result for the coupling is [280]

$$g_{SNN} = \frac{2}{9}\frac{m_N}{v_H}\sin(\phi)\left(1+\frac{7}{2}\sum_{q=u,d,s}\frac{m_q}{m_N}\langle N|\bar{q}q|N\rangle\right) \approx 1.2\cdot 10^{-3} \tag{6.1.12}$$

#### 6.1.2.2 Scattering

$\chi$ particles are stable and therefore can't be detected by their decay. They can be, however, detected by their scattering on the target. We'll consider two scattering channels:

- elastic $\chi N$ scattering;
- deep inelastic scattering (DIS) on gluons

The diagrams corresponding to these channels are given on Fig. 6.7.

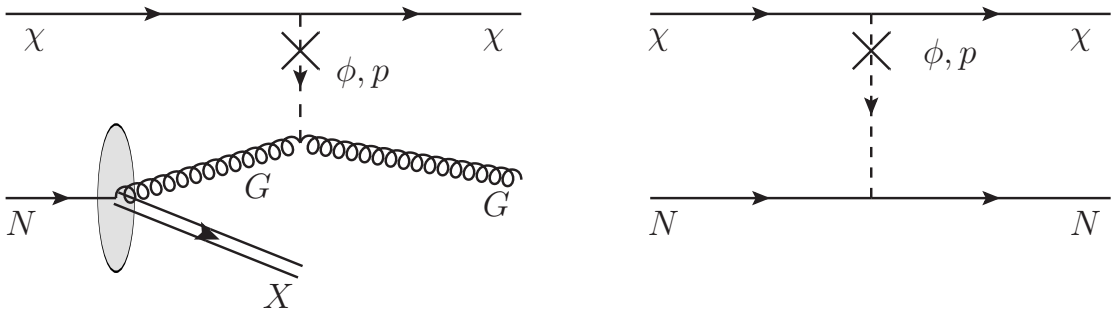


**Figure 6.7**: Scattering of the $\chi$ particle inside the detector. Left: DIS on gluons. Right: elastic scattering on nucleons

*Elastic scattering on the nucleons*, i.e. the process $\chi+N\to\chi+N$, occurs due to $SNN$ coupling (6.1.11). Because of the scalar mediator propagator the cross-section crucially depends on the minimal detectable transferred momentum $p_{\min}$. Namely, for $m_\chi \simeq 1$ GeV one has approximate formula

$$\sigma_{\chi N\to\chi N} \simeq \frac{m_N^2 m_\chi^2}{4\left(E_{\chi N}^{\rm CM}\right)^2 p^2 \max(p_{\min}^2, m_S^2)} g_{\phi NN}^2 \alpha_{\phi\chi\chi}\sin^2(\theta), \tag{6.1.13}$$

where $E_{\chi N}^{\rm CM}$ is $\chi N$ CM frame energy and $p$ is $\chi$ CM frame momentum.

The cross-section increases with increasing the ratio $m_\chi/m_\phi$, being maximal for $m_\chi \gg p_{\min} > m_\phi$. Taking the energy of $\chi$ particle at nucleon's lab frame to be $E_\chi = 12$ GeV, one obtains

$$\sigma_{\chi N\to\chi N} \approx 10^{-5}\left(\frac{m_\chi}{1\text{ GeV}}\right)^2\left(\frac{50\text{ MeV}}{p_{\min}}\right)^2 \alpha_{S\chi\chi}\sin^2(\theta)\text{ GeV}^{-2} \tag{6.1.14}$$

Another contribution in the scattering is the *deep inelastic scattering* of the $\chi$ particles on gluons inside the nucleons. Using the Lagrangian 2.1.1 and introducing the modulus of the Mandelstam invariant $Q^2 = -t$, for the differential cross-section of the process one has

$$\frac{d\sigma_{\text{DIS}}}{dQ^2} = \frac{\alpha_s(Q^2)}{128\pi^4 v_H^2} \frac{|F_G(Q^2)|^2 Q^4 (2m_\chi^2 + Q^2)}{(m_S^2 + Q^2)^2 s_{\chi G}(x)}, \tag{6.1.15}$$

where $s_{\chi G}$ is $\chi G$ invariant mass expressed in terms of $\chi p$ invariant mass $s_{\chi p}$ and amount $x$ of the proton energy carried by gluon as $s_{\chi G}(x) = m_\chi^2(1-x) + x s_{\chi p}$.

The total cross-section is

$$\sigma_{\text{DIS}} = \int_0^1 dx \int^{s_{\chi G} - 2m_\chi^2} dQ^2 \frac{d\sigma_{\text{DIS}}}{dQ^2} f_{N/G}(x, Q^2) \theta(s_{pG}(x) - Q^2), \tag{6.1.16}$$

where $f_{N/G}$ is the DIS of the gluon inside the nucleon. Unlike the case of elastic scattering (6.1.14), for the DIS cross-section there is no $p_{\min}$ dependence, since it occurs only for kinematic range

$$Q^2 \gtrsim r_N^{-2} \simeq 1 \text{ GeV}^2, \tag{6.1.17}$$

for which the scattering probes the internal structure of the nucleon. Due to this reason the cross-section is almost independent on the nucleon mass and has the form

$$\sigma_{\text{DIS}} \approx \eta \cdot \left( \frac{\alpha_s(1 \text{ GeV}^2)}{4\pi v_H} \right)^2 \sin^2(\theta) \alpha_{S\chi\chi} \simeq 5 \cdot 10^{-8} \sin^2(\theta) \alpha_{S\chi\chi} \text{ GeV}^{-2}, \tag{6.1.18}$$

where $\eta \simeq 10^{-1}$ is the additional suppression coming from the kinematic range (6.1.17). One sees that for $m_\chi > m_S$ the elastic cross-section (6.1.14) dominates.

The mass dependence of total scattering cross-section given by the sum of cross-sections (6.1.14), (6.1.16) is presented on Fig. 6.8.

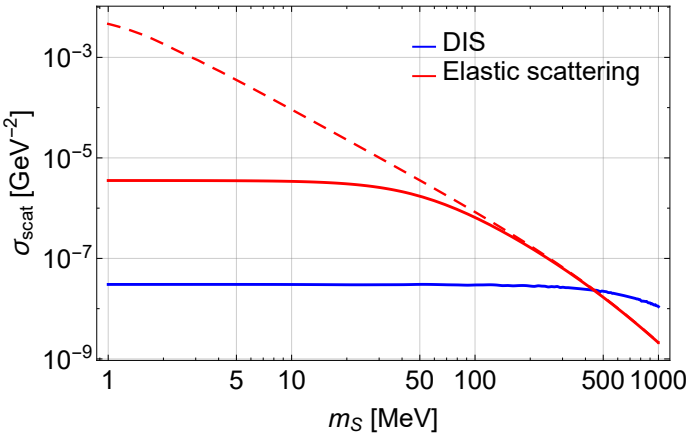


**Figure 6.8**: Dependence of scattering cross-sections of DM in iSHiP on scalar mediator mass for fixed DM mass $m_\chi = 1$GeV. For elastic scattering it is assumed that $p_{\min} = 50$ MeV (solid line) and $p_{\min} = 1$ MeV (dashed line)

For the given scattering events detector of length $l_{\text{detector}}$, with target of nuclear number density $n$ and mass number $A$, the scattering probability is

$$P_{\text{scat}} \approx l_{\text{detector}} \cdot A \cdot n \ \sigma_{\text{scat}} \tag{6.1.19}$$

Normalizing $A$ and $n$ on lead[2], for the domain $m_\chi > m_S$ we have

$$P_{\text{scat}} \approx 1.4 \cdot 10^{-8} \frac{l_{\text{detector}}}{5 \text{ m}} \cdot \frac{A \cdot n}{7 \cdot 10^{24} \text{ cm}^{-3}} \left( \frac{m_\chi}{\max[m_S, p_{\min}]} \right)^2 \tag{6.1.20}$$

### 6.1.2.3 Summary

From Fig. 6.6 we see that in the region $m_\chi \lesssim 2$ GeV the main production channel of $\chi$ particles is the decay $B^\pm \to K^\pm + \chi + \bar{\chi}$. For $m_\chi \simeq$ GeV the number of $\chi\bar{\chi}$ pairs is

$$N_{\chi\bar{\chi}} \approx 2 \cdot N_{B^+ \to \chi\bar{\chi}} \approx 2 \cdot 10^{12} \alpha_{S\chi\chi} \sin^2(\theta) \tag{6.1.21}$$

Using (6.1.20) one finds that the total number of scatterings is

$$N_{\text{scat}} = 2 N_{\chi\bar{\chi}} \cdot P_{\text{scat}} \approx 6 \cdot 10^4 \left( \frac{m_\chi}{\max[m_S, p_{\min}]} \right)^2 \alpha_{S\chi\chi}^2 \sin^4(\theta) \tag{6.1.22}$$

In dependence on the ratio $m_\chi / \max[m_\phi, p_{\min}]$ the number of scattering events varies from $6{\cdot}10^4 \alpha_{S\chi\chi}^2 \sin^4(\theta)$ (for $m_\chi \simeq m_S$) to $6{\cdot}10^{10} \alpha_{S\chi\chi}^2 \sin^4(\theta)$ (for $m_S < p_{\min} \simeq 1$ MeV). However, using the LHC constraint $\sin^2(\theta)\alpha_{S\chi\chi} \lesssim 10^{-5}$ and CHARM constraint

[2]The number density for lead can be estimated as $n = \rho N_A / M$, where $\rho = 11.34$ g/cm$^3$ is mass density, $\approx M = 207$ g/mol is molar mass and $N_A = 6.02 \cdot 10^{23}$ is Avogadro's number

$\sin^2(\theta) \lesssim 10^{-6}$ for $m_S \lesssim m_K - m_\pi$, one obtains the upper bound

$$N_{\text{scat}} \lesssim 10^{-2} \tag{6.1.23}$$

One sees that the SHiP experiment doesn't have the sensitivity to $\chi$ scatterings.

### 6.1.3 Other experiments

Apart from SHiP there are other proton beam dump experiments which could provide compatible sensitivity to DM. Examples of such experiments are MiniBooNE [281], DUNE (previously known as LBNE) [106] and T2K [282]. Their parameters are given in Table 6.1.

| Experiment | $N_{p.o.t.}$ | $E_{p.o.t.}$, GeV | $E_{pp}^{\text{CM}}$, GeV | Detector length, m |
|---|---|---|---|---|
| SHiP | $2 \cdot 10^{20}$ | 400 | 28.3 | 5 |
| MiniBooNE | $2 \cdot 10^{20}$ | 8 | 4.2 | 12 |
| T2K-Super K | $10^{22}$ | 30 | 7.9 | $\simeq 40$ |
| DUNE | $\simeq 10^{22}$ | 60-120 | 11.04-15.5 | 7 |

**Table 6.1**: Parameters of different experiments

Let's briefly estimate their sensitivity to heavy DM with the mass $2m_\chi \gtrsim m_K - m_\pi$. For this region, the DM pairs are produced mainly by $B$ mesons decay. The number of $B$ mesons can be calculated as[3]

$$N_{B^+} \approx N_{p.o.t.} \times \frac{\sigma_{pp\to b\bar{b}}(E_{\text{CM}})}{\sigma_{p+p\to\text{all}}(E_{\text{CM}})} \times f_{b\to B^+}, \tag{6.1.24}$$

where $f_{b\to B^+} \simeq 0.4$ is fragmentation fraction of $b$ quark into $B^+$ meson. The total $pp$ cross-section $\sigma_{p+p\to\text{all}}$ is widely independent on beam energy and is approximately $\sigma_{pp\to\text{all}} \approx 40$ mb [222]. The $b\bar{b}$ pair production cross-section, however, strongly depends on energy $E_{pp}^{\text{CM}}$. For $E_{p.o.t.} = 28.3$ GeV (SHiP) and $E_{p.o.t.} = 15.5$ GeV (DUNE) we compared the simulated cross-sections with [110] and [218]. It was found that the predictions agrees well. The values of cross-section for the energies from Table 6.1 are given in Table 6.2.

[3]Within this estimation, it was neglected the number of $B$ mesons produced by scatterings of secondary particles. For SHiP experiment the number of such $B$ mesons is 74 percents of the number of primary particles (see report), while for experiments with lower beam energy this amount is expected to be suppressed

| $E_{pp}^{\rm CM}$, GeV | 28.3 (SHiP) | 15.5 (DUNE) | 11 (DUNE) | 7.9 (T2K) | 4.2 (MiniBooNE) |
|---|---|---|---|---|---|
| $\sigma_{pp\to b\bar{b}+X}$, pb | $1.6\cdot 10^3$ | 2.4 | $8\cdot 10^{-4}$ | 0 | 0 |
| $\sigma_{pp\to b\bar{b}+X}/\sigma_{pp\to \rm all}$ | $4\cdot 10^{-8}$ | $6\cdot 10^{-11}$ | $2\cdot 10^{-14}$ | 0 | 0 |

**Table 6.2**: Average values of $b\bar{b}$ production cross-section in dependence on the proton pair CM energy

Using these results, one finds that T2K and MiniBooNE experiments won't produce $B$ mesons, while for SHiP and DUNE one has

$$\frac{N_{b\bar{b}}^{\rm SHiP}}{N_{b\bar{b}}^{\rm DUNE}} \simeq \frac{N_{p.o.t.}^{\rm SHiP}}{N_{p.o.t.}^{\rm DUNE}} \times \frac{\sigma_{pp\to b\bar{b}+X}^{\rm SHiP}}{\sigma_{pp\to b\bar{b}+X}^{\rm DUNE}} \simeq 7 \tag{6.1.25}$$

Since the lengths of near detector at DUNE and iSHiP detector are comparable (see Table 6.1), we conclude that the sensitivity of DUNE experiment will not be better than that of SHiP.

## 6.2 Axions at the iSHiP

### 6.2.1 Axion portal

Axion-like particle (ALP) portal introduces a pseudo-scalar particle $a$ interacting with the density of Chern-Simons charge of the electromagnetic field:

$$\mathcal{L}_a = \frac{1}{2}(\partial_\mu a)^2 - \frac{m_a^2 a^2}{2} - \frac{g_\gamma}{4} a F_{\mu\nu}\tilde{F}^{\mu\nu}, \quad \tilde{F}_{\mu\nu} = \frac{1}{2}\epsilon_{\mu\nu\alpha\beta}F^{\alpha\beta}, \tag{6.2.1}$$

where $g_\gamma$ is a coupling constant with the dimension $\text{GeV}^{-1}$. There is a wide class of models for which ALPs emerge as a Goldstone boson of some underlying spontaneously broken global symmetry [283–286]. Then, the mass of $a$ is generated if there is some symmetry breaking interactions. If the underlying symmetry scale is very large, while symmetry breaking effects occur at small scales, the mass of the ALP is naturally small. One of the example of such a model is a QCD axion, for which $U(1)$ symmetry first becomes spontaneously broken at some large scale $\Lambda$, and then becomes broken explicitly by QCD effects at the scale $\Lambda_{\rm QCD}$. The axion mass is then $m_a \simeq \Lambda_{\rm QCD}^2/\Lambda_{\rm PQ} \ll \Lambda_{\rm QCD}$.

Therefore, ALPs are good candidates for searching at intensity frontier experiments and in particular at the SHiP.

### 6.2.2 Probing ALPs at the iSHiP

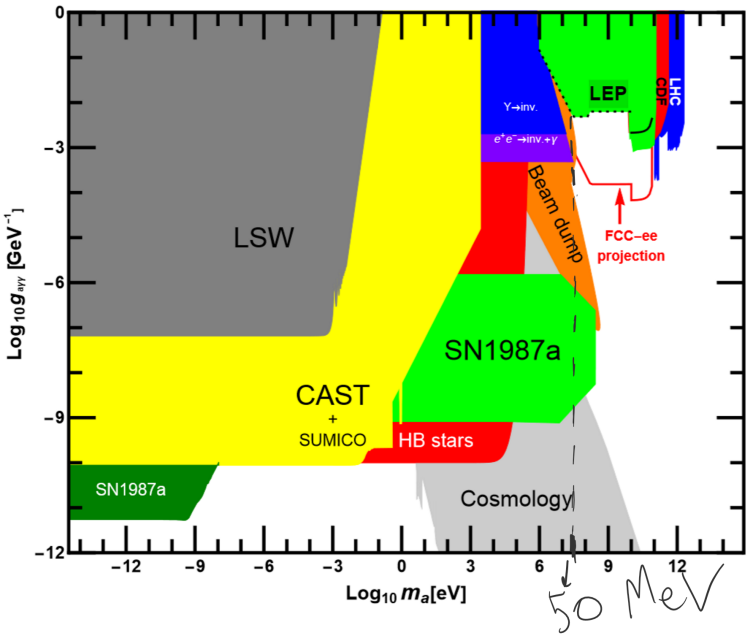


**Figure 6.9**: Bounds on an ALP model provided by laboratory experiments and cosmology [287].

Using the current bounds on ALP models, see Fig. 6.9, we can divide ALP models that are not excluded on two classes: light ALPs, with $m_a \lesssim 1$ eV, $g_\gamma \lesssim 10^{-10}$ GeV$^{-1}$ and heavy ALPs $m_a \gtrsim 50$ MeV, $g_\gamma \lesssim 10^{-1}$ GeV$^{-1}$. Before discussing the probing of ALPs at the iSHiP, let us talk about production at the SHiP experiment.

#### 6.2.2.1 Production

At the SHiP experiment, ALPs can be produced in the following processes:

- Conversion of secondary produced photons to ALPs $\gamma \to a$ in the magnetic field of the active muon shield.
- Primakov conversion $\gamma + e \to a + e$ inside the muon active shield magnetic field.
- Coherent proton-nucleus scattering.

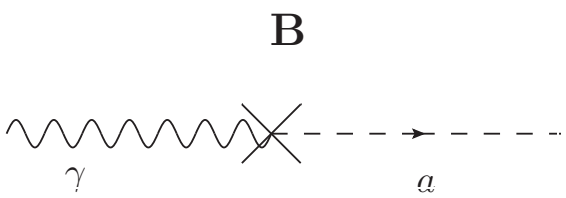


**Figure 6.10**: ALP production from conversion in the magnetic field.

**Magnetic field conversion** Consider $\gamma \to a$ conversion of secondary produced photons in the magnetic field $B$ of the muon shield. Conversion probability is [288]

$$P_{\text{conv.}}^{\text{magn}} = \frac{4B^2 E_\gamma^2 g_\gamma^2}{m_a^4} \sin^2\left(\frac{m_a^2 l}{4E_\gamma}\right), \tag{6.2.2}$$

where $l$ is a radiation length in the iron medium of the shield and $E_\gamma$ is the energy of converted photon. It is almost energy-independent for $E_\gamma > 1$ MeV and equal to $l_{\text{rad}} \simeq \mathcal{O}(1\text{ cm})$, see [222].

There are two different production regimes through the magnetic field conversion. The first regime is for small masses $m_a \ll 10\text{ eV}\left(\frac{E_\gamma}{1\text{ MeV}}\frac{1\text{ cm}}{l_{\text{rad}}}\right)^{1/2}$ and the production probability is

$$P_{\text{conv.}}^{\text{magn}} \approx (Blg_\gamma)^2/4 \simeq 10^{-22}\left(\frac{B}{1\text{ T}}\frac{l_{\text{rad}}}{1\text{ cm}}\frac{g_\gamma}{10^{-10}\text{ GeV}^{-1}}\right)^2. \tag{6.2.3}$$

The second regime is for masses $m_a \gg 10\text{ eV}\left(\frac{E_\gamma}{1\text{ MeV}}\frac{1\text{ cm}}{l_{\text{rad}}}\right)^{1/2}$. The production probability is

$$P_{\text{conv.}}^{\text{magn}} \approx \frac{2B^2 E_\gamma^2 g_\gamma^2}{m_a^4} \simeq 10^{-30}\left(\frac{B}{1\text{ T}}\frac{E_\gamma}{1\text{ MeV}}\frac{g_\gamma}{10^{-10}\text{ GeV}^{-1}}\right)^2\left(\frac{100\text{ eV}}{m_a}\right)^4. \tag{6.2.4}$$

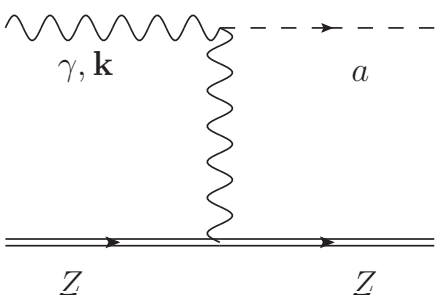


**Figure 6.11**: ALP production from the Primakov conversion.

**Primakov conversion** Other production mechanism is the Primakov conversion $\gamma + Z \to a + Z$ of secondary photons on the Coulomb potential of nuclei inside the wall. For the Coulomb screening radius $r_0 \simeq 20$ keV, and photons with energy in the range of MeV, and nuclei at rest frame, the cross-section is

$$\sigma_{\gamma e\to ae} \approx Z^2 g_\gamma^2 \alpha_{\rm EM} \ln\left(1+4|\mathbf{k}|^2 r_0^2\right) \approx 10^{-19} \left(\frac{g_\gamma}{10^{-10}\ {\rm GeV}^{-1}}\right)^2\ {\rm GeV}^{-2}, \tag{6.2.5}$$

and the conversion probability is

$$P_{\rm conv.}^{\rm Prim} \approx l_{\rm rad}\sigma_{\gamma e\to ae} n_Z \approx 10^{-24} \left(\frac{g_\gamma}{10^{-10}\ {\rm GeV}^{-1}}\right)^2 \frac{l_{\rm abs}}{\rm cm}. \tag{6.2.6}$$

There is another Primakov conversion $\gamma e \to ae$ of secondary photons on electrons inside the wall (and is the main Primakov conversion when $|\mathbf{k}| \lesssim r_0^{-1}$). For keV photons the cross-section is

$$\sigma_{\gamma e\to ae} \approx g_\gamma^2 \alpha_{\rm EM} \ln\left(|\mathbf{k}|/m_a\right) \approx 10^{-22} \left(\frac{g_\gamma}{10^{-10}\ {\rm GeV}^{-1}}\right)^2\ {\rm GeV}^{-2}, \tag{6.2.7}$$

and the conversion probability is

$$P_{\rm conv.}^{\rm Prim} \approx l_{\rm rad}\sigma_{\gamma e\to ae} n_e \approx 10^{-26} \left(\frac{g_\gamma}{10^{-10}\ {\rm GeV}^{-1}}\right)^2 \frac{l_{\rm abs}}{\rm cm}. \tag{6.2.8}$$

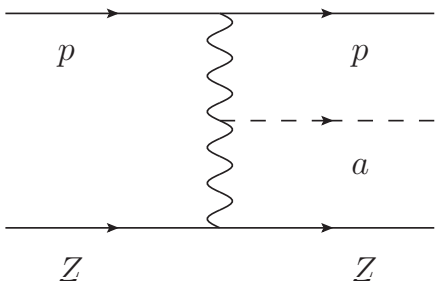


**Figure 6.12**: ALP coherent production.

**Coherent production** Consider ALP production in initial proton-nuclei interaction $p + Z \to p + Z + a$. The production probability can be estimated as

$$P_{\rm coh} \simeq \frac{\sigma_{pZ\to pZa}}{\sigma_{pZ\to \rm all}} \simeq 5{\cdot}10^{-10} Z^2 \alpha_{\rm EM} \left(\frac{g_\gamma}{10^{-3}\ {\rm GeV}^{-1}}\right)^2 \frac{4500\ {\rm GeV}^{-2}}{\sigma_{pZ\to \rm all}} \approx 10^{-22} \left(\frac{g_\gamma}{10^{-10}\ {\rm GeV}^{-1}}\right)^2, \tag{6.2.9}$$

where the rough estimation in the second line is in agreement with the exact calculations [289].

**Summary** Comparing the probabilities (6.2.4), (6.2.8), (6.2.9), we conclude that for the region with masses $m_a \ll 10 \text{ eV} \left(\frac{E_\gamma}{1 \text{ MeV}} \frac{1 \text{ cm}}{l_{\text{rad}}}\right)^{1/2}$ the conversion in the magnetic field is the main production channel. For higher masses, Primakov conversion and coherent production compete with each other. The number of conversion is proportional to the number of photons that is limited by the quantity

$$N_\gamma \lesssim N_{\text{p.o.t}} \cdot \frac{E_{p.o.t.}}{E_\gamma} \simeq 10^{25} \frac{1 \text{ MeV}}{E_\gamma}. \tag{6.2.10}$$

Therefore, the coherent production is dominated for $E_\gamma > 10$ MeV.

Using (6.2.4), the number of light ALPs produced at the SHiP can be estimated as

$$N_{\text{prod}} \leq N_{\text{magn}} \lesssim 10^3 \left(\frac{g_\gamma}{10^{-10} \text{ GeV}^{-1}}\right)^2 \frac{l}{\text{cm}} \frac{\text{MeV}}{E_\gamma}. \tag{6.2.11}$$

The number of heavy ALPs can be estimated using (6.2.9):

$$N_{\text{prod}} = P_{\text{coh}} N_{\text{p.o.t.}} \simeq 10^{14} \left(\frac{g_\gamma}{10^{-2} \text{ GeV}^{-1}}\right)^2. \tag{6.2.12}$$

We see that the number of light ALPs produced at the SHiP is strongly suppressed by the tiny coupling.

#### 6.2.2.2 Detection

At the SHiP experiment ALPs can be detected in the following ways:

- Primakov inverse conversion $a + e \to \gamma + e$ at the iSHiP.
- Conversion to photons in the magnetic field, $a \to \gamma$, inside the iSHiP magnetic field.
- ALPs decay inside the vacuum camera.

Light ALPs are excluded at the stage of production, hence here we will consider only heavy ALPs. For such particles, the magnetic conversion is suppressed and the main detection channel at the iSHiP is the Primakov conversion process.

The ratio of detection probabilities per unit length for the Primakov conversion (scattering) and decay is

$$\frac{dP_{\text{scattering}}/dl}{dP_{\text{decay}}/dl} \sim \alpha_{\text{EM}} Z^2 \lambda^3_{\text{Compton}} n^{\text{iSHiP}}_{\text{target}} \sim 10 \left(\frac{\lambda_{\text{Compton}}}{d^{\text{iSHiP}}_{\text{target}}}\right)^3, \tag{6.2.13}$$

where $\lambda_{\text{Compton}} = \frac{\hbar}{m_a c}$ is the Compton wave-length and the inter-atomic length $d^{\text{iSHiP}}_{\text{target}} \simeq 10^{-8}$ cm is defined as $n^{\text{iSHiP}}_{\text{target}} \simeq \left(d^{\text{iSHiP}}_{\text{target}}\right)^{-3}$. The decay detection efficiency starts to dominate for $m_a \gtrsim 30$ eV.

Therefore, the iSHiP is not effective for the detection of ALPs.

# Appendix A

# HNL production from hadrons

The calculation of the weak decays involving hadrons is summarized in [290]. In the absence of QED and QCD corrections the effective weak interaction Lagrangian at low energies can be written as

$$\mathcal{L}_{\text{weak}} = \mathcal{L}_{\text{cc}} + \mathcal{L}_{\text{nc}} \tag{A.0.1}$$

where the *charged current* terms have the form

$$\mathcal{L}_{\text{cc}} = \frac{G_F}{\sqrt{2}} \left| \sum_{U,D} V_{UD} J^{\mu,+}_{UD} + \sum_{\ell} J^{\mu,+}_{\ell} \right|^2 , \tag{A.0.2}$$

where

$$J^{\mu,+}_{UD} = \bar{D}\gamma^{\mu}(1-\gamma^5)U, \tag{A.0.3}$$
$$J^{\mu,+}_{\ell} = \bar{\ell}\gamma^{\mu}(1-\gamma^5)\nu_{\ell}, \tag{A.0.4}$$

and $V_{UD}$ is the CKM element which corresponds to the quark flavor transition in the hadronic current. For the *neutral current*, the interaction has the same form

$$\mathcal{L}_{\text{nc}} = \frac{G_F}{\sqrt{2}} \left( \sum_{f} J^{\mu,0}_{f} \right)^2 , \tag{A.0.5}$$

where summation goes over all fermions,

$$J^{\mu,0}_{f} = \bar{f}\gamma^{\mu}(v_f - a_f\gamma^5)f, \tag{A.0.6}$$
$$v_f = I_{3f} - 2Q_f \sin^2\theta_W, \quad a_f = I_{3f} \tag{A.0.7}$$

and $I_{3f}$ is the fermion isospin projection and $Q_f$ is its electric charge ($Q_e = -1$). In the following Sections we describe different processes with HNL and hadrons.

## A.1 Leptonic decay of a pseudoscalar meson

Consider a decay of pseudoscalar meson $h$ into charged lepton $\ell$ and HNL:

$$h \to \ell + N, \tag{A.1.1}$$

see left diagram in Fig. 3.2. The corresponding matrix element is given by

$$\mathcal{M} = \frac{G_F}{\sqrt{2}} V_{UD} \langle 0| J^{\mu}_{UD} |h\rangle \langle \ell, N| J_{\ell,\mu} |0\rangle , \tag{A.1.2}$$

where the corresponding quark contents of meson $h$ is $|h\rangle = \left|\bar{U}D\right\rangle$. In order to fix the notations we remind that the charged meson coupling constant, $f_h$, for a pseudoscalar meson constructed from up ($U$) and down ($D$) type quarks is defined as

$$\langle 0| J^{\mu}_{UD} |h\rangle = \langle 0| \bar{U}\gamma^{\mu}\gamma_5 D |h\rangle \equiv i f_h p^{\mu} \tag{A.1.3}$$

where $p_\mu$ is 4-momentum of the pseudo-scalar meson $h$. The numerical values of the decay constants for different mesons are summarized in Table C.2.

After standard calculation one finds the decay width of this reaction

$$\Gamma(h \to \ell_\alpha N) = \frac{G_F^2 f_h^2 m_h^3}{8\pi} |V_{UD}|^2 |U_\alpha|^2 \left[ y_N^2 + y_\ell^2 - \left(y_N^2 - y_\ell^2\right)^2 \right] \sqrt{\lambda(1, y_N^2, y_\ell^2)}, \tag{A.1.4}$$

where $y_\ell = m_\ell/m_h$, $y_N = M_N/m_h$ and $\lambda$ is given by (3.1.12).

## A.2 Semileptonic decay of a pseudoscalar meson

The process with pseudoscalar or vector meson $h'_{P/V}$ in the final state

$$h \to h'_{P/V} + \ell + N, \tag{A.2.1}$$

is mediated by the current that has $V - A$ form (see right diagram in Fig. 3.2). Properties of the hadronic matrix element $\left\langle h'_{P/V}\right| J^{\mu}_{\text{hadron}} \left|h\right\rangle$ depend on the type of final meson $h'$ [291]. In the case of a pseudoscalar meson only the vector part of the current plays a role:

$$\begin{aligned} \langle h'_P(p')| V_\mu |h(p)\rangle &= f_+(q^2)(p+p')_\mu + f_-(q^2) q_\mu = \\ &= f_+(q^2)\left(p_\mu + p'_\mu - \frac{m_h^2 - m_{h'}^2}{q^2} q_\mu\right) + f_0(q^2)\frac{m_h^2 - m_{h'}^2}{q^2} q_\mu \end{aligned} \tag{A.2.2}$$

where $q_\mu = (p - p')_\mu$ is the transferred momentum and

$$f_0(q^2) \equiv f_+(q^2) + \frac{q^2}{m_h^2 - m_{h'}^2} f_-(q^2). \tag{A.2.3}$$

For the case of a vector meson $h'_V$ in the final state both vector and axial part of the current contribute. The standard parametrization with form factors is

$$\langle h'_V(\epsilon, p'_\nu)|\, V^\mu\, |h(p_\nu)\rangle = ig(q^2)\varepsilon^{\mu\nu\sigma\rho}\epsilon^*_\nu(p+p')_\sigma(p-p')_\rho, \tag{A.2.4}$$

$$\langle h'_V(\epsilon, p'_\nu)|\, A_\mu\, |h(p_\nu)\rangle = f(q^2)\epsilon^*_\mu + a_+(q^2)(\epsilon^*\cdot p)(p+p')_\mu + a_-(q^2)(\epsilon^*\cdot p)(p-p')_\mu, \tag{A.2.5}$$

where $\epsilon_\mu$ is the polarization vector of the vector meson $h'_V$.

Using matrix elements (A.2.2–A.2.5) it is straightforward to calculate decay widths of the reactions. In the case of pseudoscalar meson $h'_P$ we follow Ref. [219] and decompose the full decay width into 4 parts,

$$\Gamma(h \to h'_P \ell_\alpha N) = \frac{G_F^2 m_h^5}{64\pi^3} C_K^2 |V_{UD}|^2 |U_\alpha|^2 \left(I_{P,1} + I_{P,2} + I_{P,3} + I_{P,4}\right), \tag{A.2.6}$$

where $I_{P,1}, I_{P,2}$ depend on $|f_+(q^2)|^2$, $I_{P,3}$ on $|f_0(q^2)|^2$ and $I_{P,4}$ on $\mathrm{Re}\left(f_0(q^2)f_+^*(q^2)\right)$. It turns out that $I_{P,4} = 0$ and explicit expressions for others are

$$I_{P,1} = \int\limits_{(y_\ell+y_N)^2}^{(1-y_{h'})^2} \frac{d\xi}{3\xi^3} |f_+(q^2)|^2 \Lambda^3(\xi), \tag{A.2.7}$$

$$I_{P,2} = \int\limits_{(y_\ell+y_N)^2}^{(1-y_{h'})^2} \frac{d\xi}{2\xi^3} |f_+(q^2)|^2 \Lambda(\xi) G_-(\xi) \lambda(1, y_{h'}^2, \xi), \tag{A.2.8}$$

$$I_{P,3} = \int\limits_{(y_\ell+y_N)^2}^{(1-y_{h'})^2} \frac{d\xi}{2\xi^3} |f_0(q^2)|^2 \Lambda(\xi) G_-(\xi) (1-y_{h'}^2)^2, \tag{A.2.9}$$

where

$$\Lambda(\xi) = \lambda^{1/2}(1, y_{h'}^2, \xi)\lambda^{1/2}(\xi, y_N^2, y_\ell^2), \tag{A.2.10}$$

$$G_-(\xi) = \xi\left(y_N^2 + y_\ell^2\right) - \left(y_N^2 - y_\ell^2\right)^2, \tag{A.2.11}$$

$y_i = \dfrac{m_i}{m_h}$, $\xi = \dfrac{q^2}{m_h^2}$ and function $\lambda(a,b,c)$ is given by (3.1.12). $C_K$ is the Clebsh-Gordan coefficient, see for example [292, (14)] and [293, (2.1)], $C_K = 1/\sqrt{2}$ for decays into $\pi^0$ and $C_K = 1$ for all other cases.

For the decay into vector meson the expression is more bulky,

$$\Gamma(h \to h'_V \ell_\alpha N) = \frac{G_F^2 m_h^7}{64\pi^3 m_{h'}^2} C_K^2 |V_{UD}|^2 |U_\alpha|^2 \Big( I_{V,g^2} + I_{V,f^2} + I_{V,a_+^2} + I_{V,a_-^2} + \\ + I_{V,gf} + I_{V,ga_+} + I_{V,ga_-} + I_{V,fa_+} + I_{V,fa_-} + I_{V,a_+a_-} \Big), \qquad \text{(A.2.12)}$$

where $I_{V,FG}$ are parts of the decay width that depend on the $FG$ form factors combination[1] and $C_K$ is the Clebsh-Gordan coefficient, $C_K = 1/\sqrt{2}$ for decays into $\rho^0$ and $C_K = 1$ for all other cases in this paper. It turns out that $I_{V,gf} = I_{V,ga_+} = I_{V,ga_-} = 0$, the other terms are given by

$$I_{V,g^2} = \frac{m_h^2 y_{h'}^2}{3} \int\limits_{(y_\ell + y_N)^2}^{(1-y_{h'})^2} \frac{d\xi}{\xi^2} g^2(q^2) \Lambda(\xi) F(\xi) \left( 2\xi^2 - G_+(\xi) \right), \qquad \text{(A.2.13)}$$

$$I_{V,f^2} = \frac{1}{24 m_h^2} \int\limits_{(y_\ell + y_N)^2}^{(1-y_{h'})^2} \frac{d\xi}{\xi^3} f^2(q^2) \Lambda(\xi) \times \\ \times \left( 3F(\xi) \left[ \xi^2 - \left( y_\ell^2 - y_N^2 \right)^2 \right] - \Lambda^2(\xi) + 12 y_{h'}^2 \xi \left[ 2\xi^2 - G_+(\xi) \right] \right), \qquad \text{(A.2.14)}$$

$$I_{V,a_+^2} = \frac{m_h^2}{24} \int\limits_{(y_\ell + y_N)^2}^{(1-y_{h'})^2} \frac{d\xi}{\xi^3} a_+^2(q^2) \Lambda(\xi) F(\xi) \left( F(\xi) \left[ 2\xi^2 - G_+(\xi) \right] + 3G_-(\xi) \left[ 1 - y_{h'}^2 \right]^2 \right), \qquad \text{(A.2.15)}$$

[1] In this computation we take all form factors as real-valued functions.

$$I_{V,a_-^2} = \frac{m_h^2}{8} \int\limits_{(y_\ell+y_N)^2}^{(1-y_{h'})^2} \frac{d\xi}{\xi} a_-^2(q^2)\Lambda(\xi)F(\xi)G_-(\xi), \tag{A.2.16}$$

$$\begin{aligned} I_{V,fa_+} = \frac{1}{12} \int\limits_{(y_\ell+y_N)^2}^{(1-y_{h'})^2} \frac{d\xi}{\xi^3} f(q^2)a_+(q^2)\Lambda(\xi)\times \\ \times \left(3\xi F(\xi)G_-(\xi) + \left(1-\xi-y_{h'}^2\right)\left[3F(\xi)\left(\xi^2 - \left(y_l^2 - y_N^2\right)^2\right) - \Lambda^2(\xi)\right]\right), \end{aligned} \tag{A.2.17}$$

$$I_{V,fa_-} = \frac{1}{4} \int\limits_{(y_\ell+y_N)^2}^{(1-y_{h'})^2} \frac{d\xi}{\xi^2} f(q^2)a_-(q^2)\Lambda(\xi)F(\xi)G_-(\xi), \tag{A.2.18}$$

$$I_{V,a_+a_-} = \frac{m_h^2}{4} \int\limits_{(y_\ell+y_N)^2}^{(1-y_{h'})^2} \frac{d\xi}{\xi^2} a_+(q^2)a_-(q^2)\Lambda(\xi)F(\xi)G_-(\xi)\left(1-y_{h'}^2\right), \tag{A.2.19}$$

where the notation is the same as in Eqs. (A.2.7-A.2.9) and

$$F(\xi) = (1-\xi)^2 - 2y_{h'}^2(1+\xi) + y_{h'}^4, \tag{A.2.20}$$

$$G_+(\xi) = \xi\left(y_N^2 + y_\ell^2\right) + \left(y_N^2 - y_\ell^2\right)^2. \tag{A.2.21}$$

# Appendix B

# HNL decays into hadronic states

## B.1 Connection between matrix elements of the unflavored mesons

### B.1.1 G-symmetry

An important symmetry of the low-energy theory of strong interactions is the so-called *G-symmetry* which is a combination of the charge conjugation $\hat{C}$ and rotation of 180° around the $y$ axis in the isotopic space $\hat{R}_y$.[1] The operation of charge conjugation acts on bilinear combinations of fermions $f_1$, $f_2$ as follows:

$$\hat{C}\bar{f}_1 f_2 = \bar{f}_2 f_1, \tag{B.1.1}$$

$$\hat{C}\bar{f}_1\gamma_5 f_2 = \bar{f}_2\gamma_5 f_1, \tag{B.1.2}$$

$$\hat{C}\bar{f}_1\gamma_\mu f_2 = -\bar{f}_2\gamma_\mu f_1, \tag{B.1.3}$$

$$\hat{C}\bar{f}_1\gamma_\mu\gamma_5 f_2 = \bar{f}_2\gamma_\mu\gamma_5 f_1. \tag{B.1.4}$$

$\hat{R}_y$ acts on the isospin doublet as

$$\hat{R}_y \begin{pmatrix} u \\ d \end{pmatrix} = \begin{pmatrix} d \\ -u \end{pmatrix}. \tag{B.1.5}$$

Acting on pion states, which are pseudoscalar isovectors, one gets

$$\hat{G}\left|\pi^+\right\rangle = \hat{R}_y\hat{C}\left|\bar{d}\gamma_5 u\right\rangle = \hat{R}_y\left|\bar{u}\gamma_5 d\right\rangle = -\left|\bar{d}\gamma_5 u\right\rangle = -\left|\pi^+\right\rangle, \tag{B.1.6}$$

$$\hat{G}\left|\pi^0\right\rangle = \hat{R}_y\hat{C}\frac{1}{\sqrt{2}}\left|\bar{u}\gamma_5 u - \bar{d}\gamma_5 d\right\rangle = \hat{R}_y\frac{1}{\sqrt{2}}\left|\bar{u}\gamma_5 u - \bar{d}\gamma_5 d\right\rangle = \\ = -\frac{1}{\sqrt{2}}\left|\bar{u}\gamma_5 u - \bar{d}\gamma_5 d\right\rangle = -\left|\pi^0\right\rangle, \tag{B.1.7}$$

[1] The latter corresponds to the interchange of $u$ and $d$ quarks with an additional phase, see Eq. (B.1.5) below.

| Current | $j_\mu^{V,s}$ | $j_\mu^{V,+/0/-}$ | $j_\mu^{A,s}$ | $j_\mu^{A,+/0/-}$ |
|---|---|---|---|---|
| $G$-parity | $-$ | $+$ | $+$ | $-$ |

**Table B.1**: Properties of axial and vector currents under $G$-symmetry.

so any pion is an odd state under $G$-symmetry. As a consequence, for the system of $n$ pions

$$\hat{G}\left|n\pi\right\rangle = (-1)^n \left|n\pi\right\rangle . \tag{B.1.8}$$

For $\rho$ mesons, which are vector isovectors, $G$-parity is positive,

$$\hat{G}\left|\rho^+\right\rangle = \hat{R}_y\hat{C}\left|\bar{d}\gamma_\mu u\right\rangle = -\hat{R}_y\left|\bar{u}\gamma_\mu d\right\rangle = \left|\bar{d}\gamma_\mu u\right\rangle = \left|\rho^+\right\rangle , \tag{B.1.9}$$

$$\begin{aligned}\hat{G}\left|\rho^0\right\rangle &= \hat{R}_y\hat{C}\frac{1}{\sqrt{2}}\left|\bar{u}\gamma_\mu u - \bar{d}\gamma_\mu d\right\rangle = -\hat{R}_y\frac{1}{\sqrt{2}}\left|\bar{u}\gamma_\mu u - \bar{d}\gamma_\mu d\right\rangle = \\ &= \frac{1}{\sqrt{2}}\left|\bar{u}\gamma_\mu u - \bar{d}\gamma_\mu d\right\rangle = \left|\rho^0\right\rangle ,\end{aligned} \tag{B.1.10}$$

while for $a_1$ mesons, which are pseudovector isovectors, $G$-parity is negative,

$$\hat{G}\left|a_1^+\right\rangle = \hat{R}_y\hat{C}\left|\bar{d}\gamma_\mu\gamma_5 u\right\rangle = \hat{R}_y\left|\bar{u}\gamma_\mu\gamma_5 d\right\rangle = -\left|\bar{d}\gamma_\mu\gamma_5 u\right\rangle = -\left|a_1^+\right\rangle , \tag{B.1.11}$$

$$\begin{aligned}\hat{G}\left|a_1^0\right\rangle &= \hat{R}_y\hat{C}\frac{1}{\sqrt{2}}\left|\bar{u}\gamma_\mu\gamma_5 u - \bar{d}\gamma_\mu\gamma_5 d\right\rangle = \hat{R}_y\frac{1}{\sqrt{2}}\left|\bar{u}\gamma_\mu\gamma_5 u - \bar{d}\gamma_\mu\gamma_5 d\right\rangle = \\ &= -\frac{1}{\sqrt{2}}\left|\bar{u}\gamma_\mu\gamma_5 u - \bar{d}\gamma_\mu\gamma_5 d\right\rangle = -\left|a_1^0\right\rangle ,\end{aligned} \tag{B.1.12}$$

### B.1.2 Classification of currents

Unflavored quarks system interacts with electromagnetic field, $W$- and $Z$-bosons through currents

$$J_\mu^{\mathrm{EM}} = \frac{2}{3}\bar{u}\gamma_\mu u - \frac{1}{3}\bar{d}\gamma_\mu d, \tag{B.1.13}$$

$$J_\mu^W = \bar{u}\gamma_\mu(1-\gamma_5)d, \tag{B.1.14}$$

$$J_\mu^Z = \bar{u}\gamma_\mu(v_u - a_u\gamma_5)u + \bar{d}\gamma_\mu(v_d - a_d\gamma_5)d, \tag{B.1.15}$$

where

$$v_u = \frac{1}{2} - \frac{4}{3}\sin^2\theta_W, \qquad a_u = \frac{1}{2}, \tag{B.1.16}$$

$$v_d = -\frac{1}{2} + \frac{2}{3}\sin^2\theta_W, \qquad a_d = -\frac{1}{2}. \tag{B.1.17}$$

To divide the currents (B.1.13)-(B.1.15) into G-odd and G-even parts let us

introduce isoscalar and isovector vector currents

$$j_\mu^{V,s} = \frac{1}{\sqrt{2}}(\bar{u}\gamma_\mu u + \bar{d}\gamma_\mu d), \tag{B.1.18}$$

$$j_\mu^{V,0} = \frac{1}{\sqrt{2}}(\bar{u}\gamma_\mu u - \bar{d}\gamma_\mu d), \tag{B.1.19}$$

$$j_\mu^{V,+} = \bar{d}\gamma_\mu u\,, \qquad j_\mu^{V,-} = \bar{u}\gamma_\mu d\,, \tag{B.1.20}$$

and isoscalar and isovector axial currents

$$j_\mu^{A,s} = \frac{1}{\sqrt{2}}(\bar{u}\gamma_\mu\gamma_5 u + \bar{d}\gamma_\mu\gamma_5 d), \tag{B.1.21}$$

$$j_\mu^{A,0} = \frac{1}{\sqrt{2}}(\bar{u}\gamma_\mu\gamma_5 u - \bar{d}\gamma_\mu\gamma_5 d), \tag{B.1.22}$$

$$j_\mu^{A,+} = \bar{d}\gamma_\mu\gamma_5 u\,, \qquad j_\mu^{A,-} = \bar{u}\gamma_\mu\gamma_5 d\,. \tag{B.1.23}$$

Currents (B.1.18)-(B.1.23) have a certain $G$-parity presented in Table B.1. Using these currents one can rewrite physical currents as

$$J_\mu^{\mathrm{EM}} = \frac{1}{\sqrt{2}} j_\mu^{V,0} + \frac{1}{3\sqrt{2}} j_\mu^{V,s}, \tag{B.1.24}$$

$$J_\mu^{W} = j_\mu^{V,-} - j_\mu^{A,-}, \tag{B.1.25}$$

$$J_\mu^{Z} = \frac{1 - 2\sin^2\theta_W}{\sqrt{2}} j_\mu^{V,0} - \frac{\sqrt{2}\sin^2\theta_W}{3} j_\mu^{V,s} - \frac{1}{\sqrt{2}} j_\mu^{A,0}. \tag{B.1.26}$$

### B.1.3 Connection between the matrix elements

$G$-even part of the currents (B.1.24)-(B.1.26) belongs to one isovector family, therefore there is an approximate connection between matrix elements for the system of even number of pions or $\rho$-meson,

$$\langle 0|\, J_\mu^{\mathrm{EM}}\, |2n\pi/\rho\rangle \approx \frac{1}{\sqrt{2}} \langle 0|\, J_\mu^{W}\, |2n\pi/\rho\rangle \approx \frac{1}{1 - 2\sin^2\theta_W} \langle 0|\, J_\mu^{Z}\, |2n\pi/\rho\rangle\,. \tag{B.1.27}$$

The special case to mention here is the $|2\pi^0\rangle$ state. In $V\pi^0\pi^0$ vertex, where $V = \gamma/Z$, system of 2 pions should have total angular momentum $J = 1$. Pions are spinless particles, so their coordinate wavefuction has negative parity which is forbidden by the Bose-Einstein statistics. Therefore

$$\langle 0|\, J_\mu^{\mathrm{EM}}\, \left|2\pi^0\right\rangle = \langle 0|\, J_\mu^{Z}\, \left|2\pi^0\right\rangle = 0. \tag{B.1.28}$$

This result is equivalent to the prohibition of the $\rho^0 \to 2\pi^0$ decay.

$G$-odd parts of the currents (B.1.24)-(B.1.26), see Table B.1, belong to one isoscalar and one isovector families, so there is only one relation between matrix

elements for the system of odd number of pions or for $a_1$-mesons,

$$\frac{1}{\sqrt{2}}\langle 0|\, J_\mu^W\, |(2n+1)\pi/a_1\rangle \approx \langle 0|\, J_\mu^Z\, |(2n+1)\pi/a_1\rangle + 2\sin^2\theta_W \langle 0|\, J_\mu^{\rm EM}\, |(2n+1)\pi/a_1\rangle\,. \tag{B.1.29}$$

The last formula can be simplified in the case of the one-pion or $a_1$ state. The direct interaction between photon and $\pi^0$ is forbidden because of the $C$ symmetry, while photon-to-$a_1$ interaction violates both $P$ and $C$ symmetry. Therefore, the matrix element $\langle 0|\, J_\mu^{\rm EM}\, |\pi/a_1\rangle = 0$ and

$$\frac{1}{\sqrt{2}}\langle 0|\, J_\mu^W\, |\pi/a_1\rangle \approx \langle 0|\, J_\mu^Z\, |\pi/a_1\rangle\,. \tag{B.1.30}$$

All the approximate relations discussed above hold up to isospin violating terms of order $(m_{\pi^+} - m_{\pi^0})/m_\pi \sim 3.4\%$.

## B.2 HNL decays to a meson and a lepton

There are 4 types of these decays: $N \to \ell_\alpha + h_{P/V}$ and $N \to \nu_\alpha + h_{P/V}$, where $h_P$ and $h_V$ are pseudoscalar and vector mesons respectively. Reaction $N \to \ell_\alpha + h_P$ is closely related to the process calculated in Section A.1. It utilizes the same matrix element and differs only by kinematics. Using the same notation, the decay width is

$$\Gamma(N \to \ell_\alpha h_P) = \frac{G_F^2 f_h^2 M_N^3}{16\pi}|V_{UD}|^2|U_\alpha|^2 \left[\left(1 - x_\ell^2\right)^2 - x_h^2(1 + x_\ell^2)\right]\sqrt{\lambda(1, x_h^2, x_\ell^2)}, \tag{B.2.1}$$

where $x_h = m_h/M_N$, $x_\ell = m_\ell/M_N$ and function $\lambda$ is given by eq. (3.1.12).

In the case of the neutral current-mediated decay $N \to \nu_\alpha + h_P$ the hadronic matrix element reads (see Section C.1.1 for details)

$$\langle 0|\, J_\mu^Z\, \left|h_P^0\right\rangle \equiv -i\frac{f_h}{\sqrt{2}}p_\mu, \tag{B.2.2}$$

where $p_\mu$ is the 4-momentum of the pseudo-scalar meson $h$, $J_\mu^Z$ current is given by Eq. (B.1.15). The decay width is

$$\Gamma(N \to \nu_\alpha h_P) = \frac{G_F^2 f_h^2 M_N^3}{32\pi}|U_\alpha|^2 \left(1 - x_h^2\right)^2, \tag{B.2.3}$$

where $x_h = m_h/M_N$ and $f_h$ are neutral meson decay constants presented in the right part of Table C.2.

Consider the process $N \to \ell_\alpha + h_V$. For the vector meson the hadronic matrix element of the charged current is defined as

$$\langle 0|\, J_{UD}^\mu\, |h_V\rangle \equiv i g_h \varepsilon^\mu(p), \tag{B.2.4}$$

where $\varepsilon^\mu(p)$ is the polarization vector of the meson and $g_h$ is the vector meson decay constant. The values of the $g_h$ are given in Table C.3. Using previous notations, the decay width of this process is

$$\Gamma(N \to \ell_\alpha^- h_V^+) = \frac{G_F^2 g_h^2 |V_{UD}|^2 |U_\alpha|^2 M_N^3}{16\pi m_h^2} \left( \left(1 - x_\ell^2\right)^2 + x_h^2 \left(1 + x_\ell^2\right) - 2x_h^4 \right) \sqrt{\lambda(1, x_h^2, x_\ell^2)}. \tag{B.2.5}$$

Finally, to calculate the HNL decay width into neutral vector meson $N \to \nu_\alpha + h_V$ we define the hadronic matrix element as

$$\langle 0 | J_\mu^Z | h_V^0 \rangle \equiv i \frac{\kappa_h g_h}{\sqrt{2}} \varepsilon^\mu(p), \tag{B.2.6}$$

where $g_h$ is the vector meson decay constant and $\kappa_h$ is the dimensionless correction factor, their values are given in Table C.3. For the decay width one obtains

$$\Gamma(N \to \nu_\alpha h_V) = \frac{G_F^2 \kappa_h^2 g_\rho^2 |U_\alpha|^2 M_N^3}{32\pi m_h^2} \left(1 + 2x_h^2\right) \left(1 - x_h^2\right)^2. \tag{B.2.7}$$

## B.3 HNL decays to a lepton and two pions

For the case of 2 pions the matrix element of the axial current is equal to zero, so the general expression for matrix element is (c.f. (A.2.2))

$$\langle \pi(p') | J_\mu | \pi(p) \rangle = f_+(q^2)(p + p')_\mu + f_-(q^2) q_\mu, \tag{B.3.1}$$

where $J_\mu$ is one of the currents (B.1.13)-(B.1.15) and $q_\mu = (p - p')_\mu$. Because of the isospin symmetry (B.1.27) ,the form factors are related as

$$f_\pm^{\text{EM}} \approx \frac{1}{\sqrt{2}} f_\pm^W \approx \frac{1}{1 - 2\sin^2\theta_W} f_\pm^Z \tag{B.3.2}$$

Electromagnetic current conservation $q_\mu J^\mu = 0$ implies $f_-^{\text{EM}}(q^2) = 0$. Therefore all the matrix elements could be expressed via a single form factor, called *pion electromagnetic form factor*,

$$\langle \pi(p') | J_\mu^{\text{EM}} | \pi(p) \rangle = F_\pi(q^2)(p + p')_\mu. \tag{B.3.3}$$

Pion electromagnetic form factor is related to the cross section of reaction $e^+e^- \to 2\pi$ as

$$\sigma(e^+e^- \to 2\pi) = \frac{\pi \alpha_{\text{EM}}^2}{3s} \beta_\pi^3(s) |F_\pi(s)|^2, \tag{B.3.4}$$

where $\beta_\pi(s) = \sqrt{1 - 4m_\pi^2/s}$, so it is well-measured experimentally. There is a lot of data on electromagnetic form factor [294–299], which agree with each other.

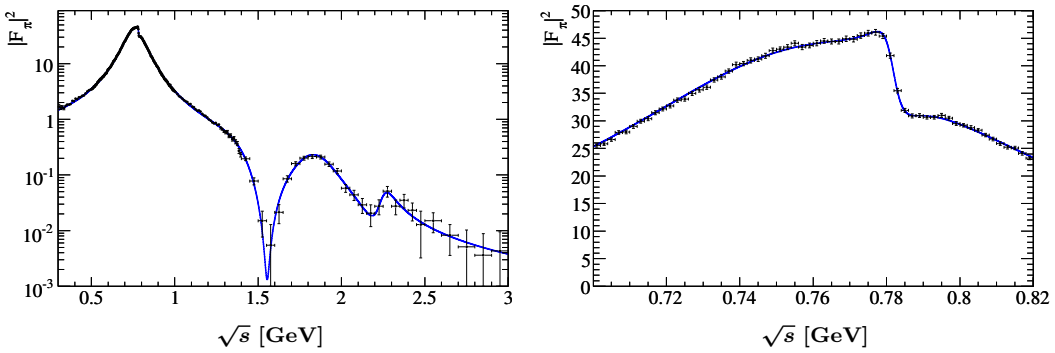


**Figure B.1**: Pion form factor squared, $|F_\pi|^2$. *Left:* Fit to the BaBaR data [294] using the vector-dominance model (blue line). *Right:* Zoom to the energies around $\sqrt{s} \simeq m_\rho$.

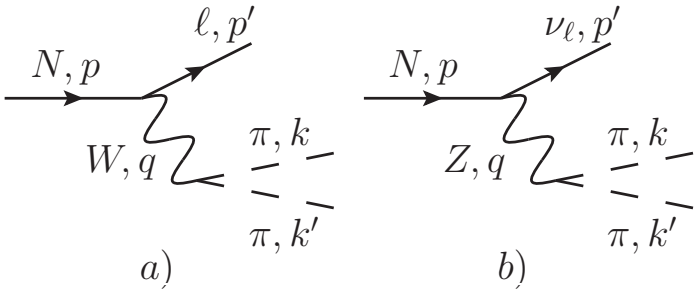


**Figure B.2**: Diagram for the HNL decay into 2 pions.

Good description of the data is given by the vector-dominance model (VDM), see Fig. B.1 [294] and Appendix E for model description.

Using matrix elements described above it is easy to find the decay widths of $N \to \ell\pi^0\pi^+$ and $N \to \nu_\ell\pi^+\pi^-$ (see Feynman diagrams in Fig. B.2),

$$\Gamma(N \to \ell_\alpha \pi^0 \pi^+) = \frac{G_F^2 M_N^3}{384\pi^3} |V_{ud}|^2 |U_\alpha|^2 \int\limits_{4m_\pi^2}^{(M_N - m_\ell)^2} \left( (1 - x_\ell^2)^2 + \frac{q^2}{M_N^2}(1 + x_\ell^2) - 2\frac{q^4}{M_N^4} \right) \times$$
$$\times \lambda^{1/2}\left(1, \frac{q^2}{M_N^2}, x_\ell^2\right) \beta_\pi^3(q^2) |F_\pi(q^2)|^2 dq^2, \qquad \text{(B.3.5)}$$

$$\Gamma(N \to \nu_\alpha \pi^+ \pi^-) = \frac{G_F^2 M_N^3}{768\pi^3} |U_\alpha|^2 (1 - 2\sin^2\theta_W)^2 \times$$
$$\times \int\limits_{4m_\pi^2}^{M_N^2} \left(1 - \frac{q^2}{M_N^2}\right)^2 \left(1 + \frac{2q^2}{M_N^2}\right) \beta_\pi^3(q^2) |F_\pi(q^2)|^2 dq^2, \qquad \text{(B.3.6)}$$

where $x_\ell = \dfrac{m_\ell}{M_N}$ and the function $\lambda$ is given by (3.1.12). The decay width $\Gamma(N \to$

$\nu_\alpha \pi^0 \pi^0) = 0$ because of Eq. (B.1.28).

Using the VDM model, formula (B.3.5) and lifetime of the $\tau$-lepton we have calculated the branching ratio $\mathrm{BR}(\tau \to \nu_\tau \pi^- \pi^0) = 25.2\%$ which is close to the experimental value 25.5%.

The decay into 2 pions is significantly enhanced by the $\rho$-resonance. It turns out, that this is the dominant channel, see Fig. 3.15 comparing the decay width of HNL into 2 pions and into $\rho$-meson. Therefore, one can replace the decay into 2 pions with 2-body decay into $\rho$-meson.

# Appendix C

# Phenomenological parameters

In this Section we summarize parameters used in this work. Values of the CKM matrix elements are given in Table C.1.

| $V_{ud}$ | $V_{us}$ | $V_{ub}$ | $V_{cd}$ | $V_{cs}$ | $V_{cb}$ |
|---|---|---|---|---|---|
| 0.974 | 0.225 | 0.00409 | 0.220 | 0.995 | 0.0405 |

**Table C.1**: CKM matrix elements [222] adopted in this work.

## C.1 Meson decay constants

The decay constants for charged pseudoscalar mesons are defined by Eq. (A.1.3), the values of $f_h$ (Table C.2) are measured experimentally and/or obtained by lattice calculations [300].

Meson decay constants for the mesons with the same-flavor quarks are defined by Eq. (B.2.2). There is a discrepancy regarding their values in the literature, therefore we have computed them directly (see Appendix C.1.1). The results of these computations are given in the right column of Table C.2. The meson decay constants for neutral mesons consisted of quarks of different flavors (such as $K^0$, $D^0$, $B^0$, $B_s$) are not needed in computing HNL production or decay, we do not provide them here.

For vector charged mesons the decay constants $g_h$ are defined by Eq. (B.2.4). In the literature they often appear as $f_h$, connected to our prescription by mass of the meson $g_h = f_h m_h$. Their values are presented in Table C.3. For vector neutral mesons the decay constants $g_h$ and dimensionless factors $\kappa_h$ are defined by Eq. (B.2.6). Their values are presented in Table C.3 as well.

| | |
|---|---|
| $f_{\pi^+}$ | 130.2 MeV [300] |
| $f_{K^+}$ | 155.6 MeV [300] |
| $f_{D^+}$ | 212 MeV [300] |
| $f_{D_s}$ | 249 MeV [300] |
| $f_{B^+}$ | 187 MeV [300] |
| $f_{B_c}$ | 434 MeV [301] |

| | |
|---|---|
| $f_{\pi^0}$ | 130.2 MeV [1] |
| $f_\eta$ | 81.7 MeV [2] |
| $f_{\eta'}$ | −94.7 MeV [2] |
| $f_{\eta_c}$ | 237 MeV [3] |

**Table C.2**: Decay constants of pseudoscalar charged mesons (left table) and pseudoscalar neutral mesons (right table).

| | |
|---|---|
| $g_{\rho^+}$ | 0.162 GeV$^2$ [302][4] |
| $g_{D^{+*}}$ | 0.535 GeV$^2$ [303] |
| $g_{D_s^{+*}}$ | 0.650 GeV$^2$ [303] |

| $h$ | $g_h$ [GeV$^2$] | $\kappa_h$ |
|---|---|---|
| $\rho^0$ | 0.162 | $1 - 2\sin^2\theta_W$[5] |
| $\omega$ | 0.153 [238] | $\frac{4}{3}\sin^2\theta_W$ |
| $\phi$ | 0.234 [302] | $\frac{4}{3}\sin^2\theta_W - 1$ |
| $J/\psi$ | 1.29 [304] | $1 - \frac{8}{3}\sin^2\theta_W$ |

**Table C.3**: Decay constants of vector charged mesons (left table) and vector neutral mesons (right table). Decay constants for $D^*_{(s)}$ mesons in [303] show large theoretical uncertainty, we quote only the average value here.

### C.1.1 Decay constants of $\eta$ and $\eta'$ mesons

To describe HNL decays into $\eta$ and $\eta'$ mesons we need to know the corresponding neutral current decay constants, that we define as (B.2.2)

$$\langle 0|\, J^Z_\mu \,|h^0_P\rangle \equiv -i\frac{f_h}{\sqrt{2}} p_\mu,$$

where $p_\mu$ is the 4-momentum of the pseudo-scalar meson $h$, $J^Z_\mu$ current is given by Eq. (B.1.15). The choice of the additional factor $(-1/\sqrt{2})$ is introduced in order to obtain $f_{\pi^0} = f_{\pi^\pm}$ and $f_{\pi^0} > 0$, see discussion below. Taking into account that for pseudoscalar mesons only axial part of the current contributes to this matrix element we can write the matrix element as

$$\langle 0|\, J^Z_\mu \,|h^0_P\rangle = \langle 0|\, \bar{q}\gamma_\mu\gamma^5\lambda^Z q \,|h^0_P\rangle\,, \tag{C.1.1}$$

where

$$q = \begin{pmatrix} u \\ d \\ s \end{pmatrix}, \qquad \lambda^Z = \frac{1}{2}\begin{pmatrix} -1 & 0 & 0 \\ 0 & 1 & 0 \\ 0 & 0 & 1 \end{pmatrix}. \tag{C.1.2}$$

[1] It should be equal to $f_{\pi^+}$, according to Eq. (B.1.30).
[2] See discussion in Section C.1.1.
[3] See discussion in Section C.1.2.
[4] See discussion in the section C.1.3.
[5] See Eq. (B.1.27).

The relevant decay constants are $f^0$ and $f^8$, they come from the set of decay constants extracted from experiments defined as [305]

$$\langle 0| J^a_\mu |h\rangle = i f^a_h p_\mu, \tag{C.1.3}$$

where $J^a_\mu = \bar{q}\gamma_\mu\gamma^5 \dfrac{\lambda^a}{\sqrt{2}} q$ with $\lambda^a$ being the Gell-Mann matrices for $a = 1 \dots 8$ and

$$\lambda^0 = \sqrt{\frac{2}{3}} \begin{pmatrix} 1 & 0 & 0 \\ 0 & 1 & 0 \\ 0 & 0 & 1 \end{pmatrix} \tag{C.1.4}$$

The overall factor in $\lambda^0$ is chosen to obey normalization condition $\mathrm{Tr}(\lambda^a\lambda^b) = 2\delta^{ab}$.

Within the chiral perturbation theory ($\chi$PT) (see [306] and references therein), the lightest mesons correspond to pseudo-Goldstone bosons $\phi^a$, that appear after the spontaneous breaking of $U_L(3) \times U_R(3)$ symmetry to group $U_V(3)$. States $\phi^a$ are orthogonal in the sense

$$\langle 0| J^a_\mu \left|\phi^b\right\rangle = i f^a_{\phi^b} p_\mu, \quad f^a_{\phi^b} = f^a_b \delta^{ab} \tag{C.1.5}$$

where and $f^a_b$ are corresponding decay constants. Using

$$\lambda^3 = \begin{pmatrix} 1 & 0 & 0 \\ 0 & -1 & 0 \\ 0 & 0 & 0 \end{pmatrix}, \qquad \lambda^8 = \sqrt{\frac{1}{3}} \begin{pmatrix} 1 & 0 & 0 \\ 0 & 1 & 0 \\ 0 & 0 & -2 \end{pmatrix}, \tag{C.1.6}$$

we can rewrite the axial part of the weak neutral current (B.2.2) as a linear combination of the $J^0_\mu$, $J^3_\mu$ and $J^8_\mu$

$$\bar{q}\gamma_\mu\gamma^5\lambda^Z q = \frac{1}{\sqrt{2}} \left( \frac{J^0_\mu}{\sqrt{6}} - \frac{J^8_\mu}{\sqrt{3}} - J^3_\mu \right) \tag{C.1.7}$$

and $f_h$ is given by

$$f_h = f^3_h + \frac{f^8_h}{\sqrt{3}} - \frac{f^0_h}{\sqrt{6}}. \tag{C.1.8}$$

For example, $\pi^0$ meson corresponds to $\phi^3$ state in $\chi$PT, so $f^0_{\pi^0} = f^8_{\pi^0} = 0$ and Eq. (C.1.8) gives $f_{\pi^0} = f^3_{\pi^0} = f_{\pi^+}$ because of the isospin symmetry, in full agreement with Eq. (B.1.30).

For $\eta$ and $\eta'$ the application of Eq. (C.1.8) is not so straightforward. These mesons are neutral unflavored mesons with zero isospin and they can oscillate between each other. So $\eta$ and $\eta'$ do not coincide with any single $\phi^a$ state. Rather they are mixtures of $\phi^0$ and $\phi^8$ states. In real world isospin is not a conserved quantum number, so $\phi^3$ state also should be taken into account, but its contribution is negli-

gible [307], so we use $f_\eta^3 = f_{\eta'}^3 = 0$. Another complication is $U(1)$ QCD anomaly for $J_\mu^0$ current that not only shifts masses of corresponding mesons but also contributes to the $f_h^0$ meson constant. To phenomenologically take into account the effect of anomaly it was proposed to use two mixing angles scheme [308],

$$\begin{pmatrix} f_\eta^8 & f_\eta^0 \\ f_{\eta'}^8 & f_{\eta'}^0 \end{pmatrix} = \begin{pmatrix} f_8 \cos\theta_8 & -f_0 \sin\theta_0 \\ f_8 \sin\theta_8 & f_0 \cos\theta_0 \end{pmatrix}. \tag{C.1.9}$$

Taking parameter values from the recent phenomenological analysis [305],

$$f_8 = 1.27(2) f_\pi, \quad f_0 = 1.14(5) f_\pi, \quad \theta_8 = -21.2(1.9)^\circ, \quad \theta_0 = -6.9(2.4)^\circ, \tag{C.1.10}$$

we find

$$f_\eta = 0.63(2) f_\pi \approx 81.7(3.1)\ \text{MeV}, \tag{C.1.11}$$

$$f_{\eta'} = -0.73(3) f_\pi \approx -94.7(4.0)\ \text{MeV}. \tag{C.1.12}$$

These numbers should be confronted with the values quoted in [218] and [238].

### C.1.2 Decay constant of $\eta_c$ meson

The decay constant of $\eta_c$ meson is defined as [309]

$$\langle 0 | \bar{c} \gamma^\mu \gamma^5 c | \eta_c \rangle \equiv i f_{\eta_c}^{\text{exp}} p^\mu, \tag{C.1.13}$$

where $f_{\eta_c}^{\text{exp}} = 335\,\text{MeV}$, as measured by CLEO collaboration [310]. Our definition (B.2.2) differs by a factor $\sqrt{2}$, so $f_{\eta_c} = f_{\eta_c}^{\text{exp}}/\sqrt{2} \approx 237\,\text{MeV}$.

### C.1.3 Decay constant of $\rho$ meson

There are 2 parametrizations of the $\rho$ charged current matrix element using $g_\rho$, defined by (B.2.4), or $f_\rho$, which is related to $g_\rho$ are $f_\rho = g_\rho/m_\rho$. The value of the decay constant can be obtained by 2 methods: from $\rho \to e^+e^-$ using the approximate symmetry (B.1.27) or from the $\tau$-lepton decay. Results obtained in Ref. [302] by these two methods differ by about 5%, $f_{\rho,ee} = 220(2)$ MeV and $f_{\rho,\tau} = 209(4)$ MeV. We calculate

$$\Gamma(\tau \to \nu\rho) = \frac{G_F^2 g_\rho^2 m_\tau^3}{16\pi m_\rho^2} |V_{ud}|^2 \left(1 + 2\frac{m_\rho^2}{m_\tau^2}\right)\left(1 - \frac{m_\rho^2}{m_\tau^2}\right)^2, \tag{C.1.14}$$

$$\Gamma(\rho \to e^+e^-) = \frac{e^4 g_\rho^2}{24\pi m_\rho^3}, \tag{C.1.15}$$

and get $g_{\rho,\tau} = 0.162\,\text{GeV}^2$ and $g_{\rho,ee} = 0.171\,\text{GeV}^2$, which corresponds to $f_{\rho,\tau} = 209\,\text{MeV}$ and $f_{\rho,ee} = 221\,\text{MeV}$ in full agreement with [302]. The difference between

these results can be explained by the relation B.1.27 being approximate. So we use $g_{\rho,\tau}$ value as more directly measured one. The results of our analysis agrees with $f_\rho$ value in [238] (within about 10%), but differ from the value adopted in [218] by $\sim 25\%$.

## C.2 Meson form factors of decay into pseudoscalar meson

To describe the semileptonic decays of the pseudoscalar meson into another pseudoscalar meson one should know the form factors $f_+(q^2)$, $f_0(q^2)$, $f_-(q^2)$ defined by Eq. (A.2.2), only two of which are independent. We use the $f_+(q^2)$, $f_0(q^2)$ pair for the decay parametrization.

In turn, there are many different parametrizations of meson form factors. One popular parametrization is the Bourrely-Caprini-Lellouch (BCL) parametrization [311] that takes into account the analytic properties of form factors (see e.g. [312, 313]),

$$f(q^2) = \frac{1}{1 - q^2/M_{\text{pole}}^2} \sum_{n=0}^{N-1} a_n \left[ \big(z(q^2)\big)^n - (-1)^{n-N} \frac{n}{N} \big(z(q^2)\big)^N \right] \tag{C.2.1}$$

where the function $z(q^2)$ is defined via

$$z(q^2) \equiv \frac{\sqrt{t_+ - q^2} - \sqrt{t_+ - t_0}}{\sqrt{t_+ - q^2} + \sqrt{t_+ - t_0}} \tag{C.2.2}$$

with

$$t_+ = \big(m_h + m_{h'}\big)^2. \tag{C.2.3}$$

The choice of $t_0$ and of the pole mass $M_{\text{pole}}$ varies from group to group that performs the analysis. In this work we follow the FLAG collaboration [313] and take

$$t_0 = \big(m_h + m_{h'}\big)\big(\sqrt{m_h} - \sqrt{m_{h'}}\big)^2. \tag{C.2.4}$$

The coefficients $a_n^+$ and $a_n^0$ are then fitted to the experimental data or lattice results.

### C.2.1 K meson form factors

Form factors of $K \to \pi$ transition are well described by the linear approximation [314, 315]

$$f_{+,0}^{K\pi}(q^2) = f_{+,0}^{K\pi}(0) \left(1 + \lambda_{+,0} \frac{q^2}{m_{\pi^+}^2}\right). \tag{C.2.5}$$

The best fit parameters are given in Table C.4.

| $h, h'$ | $f_{+,0}(0)$ | $\lambda_+$ | $\lambda_0$ |
|---|---|---|---|
| $K^0, \pi^+$ | 0.970 | 0.0267 | 0.0117 |
| $K^+, \pi^0$ | 0.970 | 0.0277 | 0.0183 |

**Table C.4**: Best fit parameters for the form factors (C.2.5) of $D \to \pi$ and $D \to K$ transitions [313–315].

### C.2.2 D meson form factors

In the recent paper [316] the form factors for $D \to K$ and $D \to \pi$ transitions are given in the form

$$f(q^2) = \frac{f(0) - c(z(q^2) - z_0)\left(1 + \frac{z(q^2)+z_0}{2}\right)}{1 - Pq^2}, \tag{C.2.6}$$

where $z_0 = z(0)$. The best fit parameter values are given in Table C.5.

| $f$ | $f(0)$ | $c$ | $P$ (GeV$^{-2}$) |
|---|---|---|---|
| $f_+^{DK}$ | 0.7647 | 0.066 | 0.224 |
| $f_0^{DK}$ | 0.7647 | 2.084 | 0 |
| $f_+^{D\pi}$ | 0.6117 | 1.985 | 0.1314 |
| $f_0^{D\pi}$ | 0.6117 | 1.188 | 0.0342 |

**Table C.5**: Best fit parameters for the form factors (C.2.6) of $D \to \pi$ and $D \to K$ transitions [316].

Form factors of $D_s \to \eta$ transition read [317]

$$f_+^{D_s\eta}(q^2) = \frac{f_+^{D_s\eta}(0)}{\left(1 - q^2/m_{D_s^*}^2\right)\left(1 - \alpha_+^{D_s\eta} q^2/m_{D_s^*}^2\right)}, \tag{C.2.7}$$

$$f_0^{D_s\eta}(q^2) = \frac{f_0^{D_s\eta}(0)}{1 - \alpha_0^{D_s\eta} q^2/m_{D_s^*}^2}, \tag{C.2.8}$$

where $f_+^{D_s\eta}(0) = 0.495$, $\alpha_+^{D_s\eta} = 0.198$ [317], $m_{D_s^*} = 2.112\,\text{GeV}$ [222]. Scalar form factor $f_0^{D_s\eta}(q^2)$ is not well constrained by experimental data, so we take $f_0^{D_s\eta}(q^2) = f_+^{D_s\eta}(q^2)$ by Eq. (A.2.3) and $\alpha_0^{D_s\eta} = 0$.

### C.2.3 B meson form factors

Most of $B$ meson form factors are available in literature in the form (C.2.1), their best fit parameter values are given in Table C.6. The form factors for $B_s \to D_s$ are almost the same as for $B \to D$ transition [318], so we use the same expressions for both cases.

| $f$ | $M_{\text{pole}}$ (GeV) | $a_0$ | $a_1$ | $a_2$ |
|---|---|---|---|---|
| $f_+^{B_{(s)}D_{(s)}}$ | $\infty$ | 0.909 | $-7.11$ | 66 |
| $f_0^{B_{(s)}D_{(s)}}$ | $\infty$ | 0.794 | $-2.45$ | 33 |
| $f_+^{B_sK}$ | $m_{B^*} = 5.325$ | 0.360 | $-0.828$ | 1.1 |
| $f_0^{B_sK}$ | $m_{B^*(0^+)} = 5.65$ | 0.233 | 0.197 | 0.18 |
| $f_+^{B\pi}$ | $m_{B^*} = 5.325$ | 0.404 | $-0.68$ | $-0.86$ |
| $f_0^{B\pi}$ | $m_{B^*(0^+)} = 5.65$ | 0.490 | $-1.61$ | 0.93 |

**Table C.6**: Best fit parameters for the form factors (C.2.1) of $B \to \pi$, $B_{(s)} \to D_{(s)}$ and $B_s \to K$ transitions [313].

## C.3 Meson form factors for decay into vector meson

One of the relevant HNL production channels is the pseudoscalar meson decay $h_P \to h'_V \ell_\alpha N$. To compute the decay width one needs to know the form factors $g(q^2)$, $f(q^2)$, $a_\pm(q^2)$, defined by Eqs. (A.2.4, A.2.5). The dimensionless linear combinations are introduced as

$$V^{hh'}(q^2) = (m_h + m_{h'})\, g^{hh'}(q^2), \tag{C.3.1}$$

$$A_0^{hh'}(q^2) = \frac{1}{2m_{h'}} \left( f^{hh'}(q^2) + q^2 a_-^{hh'}(q^2) + \left(m_h^2 - m_{h'}^2\right) a_+^{hh'}(q^2) \right), \tag{C.3.2}$$

$$A_1^{hh'}(q^2) = \frac{f^{hh'}(q^2)}{m_h + m_{h'}}, \tag{C.3.3}$$

$$A_2^{hh'}(q^2) = -(m_h + m_{h'})\, a_+^{hh'}(q^2). \tag{C.3.4}$$

For these linear combinations the following ansatz is used

$$V^{hh'}(q^2) = \frac{f_V^{hh'}}{\left(1 - q^2/(M_V^h)^2\right)\left[1 - \sigma_V^{hh'} q^2/(M_V^h)^2 - \xi_V^{hh'} q^4/(M_V^h)^4\right]}, \tag{C.3.5}$$

$$A_0^{hh'}(q^2) = \frac{f_{A_0}^{hh'}}{\left(1 - q^2/(M_P^h)^2\right)\left[1 - \sigma_{A_0}^{hh'} q^2/(M_V^h)^2 - \xi_{A_0}^{hh'} q^4/(M_V^h)^4\right]}, \tag{C.3.6}$$

$$A_{1/2}^{hh'}(q^2) = \frac{f_{A_{1/2}}^{hh'}}{1 - \sigma_{A_{1/2}}^{hh'} q^2/(M_V^h)^2 - \xi_{A_{1/2}}^{hh'} q^4/(M_V^h)^4}. \tag{C.3.7}$$

Best fit values of parameters are adopted from papers [319–321]. $f$, $\sigma$ parameters are given in Table C.7, while $\xi$ and the pole masses $M_V$ and $M_P$ are given in Table C.8.

| $h, h'$ | $f_V^{hh'}$ | $f_{A_0}^{hh'}$ | $f_{A_1}^{hh'}$ | $f_{A_2}^{hh'}$ | $\sigma_V^{hh'}$ | $\sigma_{A_0}^{hh'}$ | $\sigma_{A_1}^{hh'}$ | $\sigma_{A_2}^{hh'}$ |
|---|---|---|---|---|---|---|---|---|
| $D, K^*$ | 1.03 | 0.76 | 0.66 | 0.49 | 0.27 | 0.17 | 0.30 | 0.67 |
| $B, D^*$ | 0.76 | 0.69 | 0.66 | 0.62 | 0.57 | 0.59 | 0.78 | 1.40 |
| $B, \rho$ | 0.295 | 0.231 | 0.269 | 0.282 | 0.875 | 0.796 | 0.54 | 1.34 |
| $B_s, D_s^*$ | 0.95 | 0.67 | 0.70 | 0.75 | 0.372 | 0.350 | 0.463 | 1.04 |
| $B_s, K^*$ | 0.291 | 0.289 | 0.287 | 0.286 | $-0.516$ | $-0.383$ | 0 | 1.05 |

**Table C.7**: First part of the table with parameters of meson form factors (C.3.5-C.3.7) of decay into vector meson [319–321].

| $h, h'$ | $\xi_V^{hh'}$ | $\xi_{A_0}^{hh'}$ | $\xi_{A_1}^{hh'}$ | $\xi_{A_2}^{hh'}$ | $M_P^h$ (GeV) | $M_V^h$ (GeV) |
|---|---|---|---|---|---|---|
| $D, K^*$ | 0 | 0 | 0.20 | 0.16 | $m_{D_s} = 1.969$ | $m_{D_s^*} = 2.112$ |
| $B, D^*$ | 0 | 0 | 0 | 0.41 | $m_{B_c} = 6.275$ | $m_{B_c^*} = 6.331$ |
| $B, \rho$ | 0 | 0.055 | 0 | $-0.21$ | $m_B = 5.279$ | $m_{B^*} = 5.325$ |
| $B_s, D_s^*$ | 0.561 | 0.600 | 0.510 | 0.070 | $m_{B_c} = 6.275$ | $m_{B_c^*} = 6.331$ |
| $B_s, K^*$ | 2.10 | 1.58 | 1.06 | $-0.074$ | $m_{B_s} = 5.367$ | $m_{B_s^*} = 5.415$ |

**Table C.8**: Second part of the table with parameters of meson form factors (C.3.5-C.3.7) of decay into vector meson [319–321]. Masses of $B_c$, $D_s$ and $D_s^*$ are taken from [222], while for $B_c^*$ theoretical prediction [322] is used.

# Appendix D

# Production from $J/\psi$ and $\Upsilon$ mesons

## D.1 Production from $J/\psi$

The process $J/\psi \to N\bar{\nu}$ allows to create HNLs with masses up to $M_{J/\psi} \simeq 3.1\text{GeV}$ and therefore contribute to the production *above* the $D$-meson threshold.

To estimate $\text{BR}(J/\psi \to N\bar{\nu})$ let us first compare the processes $J/\psi \to e^+e^-$ and $J/\psi \to \nu_e\bar{\nu}_e$. The ratio of their width is given by [323]

$$\frac{\text{BR}(J/\psi \to \nu_e\bar{\nu}_e)}{\text{BR}(J/\psi \to e^+e^-)} = \frac{27G_F^2 M_{J/\psi}^4}{256\pi^2\alpha^2}\left(1 - \frac{8}{3}\sin^2\theta_W\right)^2 \sim 4.5 \times 10^{-7} \tag{D.1.1}$$

with the precision of the order of few per cent [323]. Using the measured branching ratio $\text{BR}(J/\psi \to e^+e^-) \simeq 0.06$ [222], one can estimate decay into *one flavor of neutrinos*, $\text{BR}(J/\psi \to \nu_e\bar{\nu}_e) \simeq 2.7 \times 10^{-8}$. The corresponding branching of $J/\psi$ to HNL is additionally suppressed by $U^2$ and by the phase-space factor $f_{PS}$:

$$\sum_\alpha \text{BR}(J/\psi \to N\bar{\nu}_\alpha) = U^2 f_{PS}(M_N/M_{J/\psi})\,\text{BR}(J/\psi \to \nu_e\bar{\nu}_e) \tag{D.1.2}$$

We estimate this fraction at $M_N = M_D$ (just above the $D$-meson threshold) taking for simplicity $f_{PS} = 1$. Clearly, at masses below $M_D$ the production from $D$-mesons dominates (as the $J/\psi$ production fraction $f(J/\psi) \simeq 0.01$, see [110, Appendix A], reproduced for completeness in Appendix 4.1.1). Above $D$-meson mass but below $M_{J/\psi}$ we should compare with the production from $B$ mesons. We compare the probability to produce HNL from $B$-meson and from $J/\psi$:

$$\frac{\text{HNLs from } J/\psi}{\text{HNLs from } B} = \frac{X_{c\bar{c}} \times f(J/\psi) \times \text{BR}_{J/\psi \to N\bar{\nu}}}{X_{b\bar{b}} \times f(B) \times \text{BR}_{B\to NX}} = \\ = 3 \times 10^{-4}\left(\frac{X_{c\bar{c}}}{10^{-3}}\right)\left(\frac{10^{-7}}{X_{b\bar{b}}}\right) \tag{D.1.3}$$

where we have adopted $f(B) \times BR(B \to N + X) \sim 10^{-2}$ (c.f. Fig. 3.4, right panel) and used $f(J/\psi) \sim 10^{-2}$. The numbers in (3.1.6) are normalized to SHiP. We see therefore that $J/\psi$ decays contribute subdominantly while $X_{b\bar{b}}/X_{c\bar{c}} \gtrsim 10^{-8}$.

## D.2 Production from $\Upsilon$

The heavy mass of $\Upsilon$ opens up a possibility to produce HNLs up to $M_N \simeq 10$GeV. Similarly to Eq. (D.1.1) we can find the branching ratio $\text{BR}(\Upsilon \to \nu\bar{\nu}) = 4 \times 10^{-4}\,\text{BR}(\Upsilon \to e^+e^-)$ [323]. Therefore

$$\text{BR}(\Upsilon \to N\bar{\nu}_\alpha) = U_\alpha^2 f_{PS}(M_N/M_\Upsilon)\frac{27G_F^2M_\Upsilon^4}{64\pi^2\alpha^2}\left(-1+\frac{4}{3}\sin^2\theta_W\right)^2 \text{BR}(\Upsilon \to e^+e^-) \tag{D.2.1}$$

Using the latest measurement $\text{BR}(\Upsilon \to e^+e^-) \simeq 2.4 \times 10^{-2}$ [222] one finds that $\text{BR}(\Upsilon \to \nu\bar{\nu}) \simeq 10^{-5}$. We do not know the fraction $f(\Upsilon)$ out of all $b\bar{b}$ pairs, but one can roughly estimate it being equal to the fraction $f(J/\psi) \sim 1\%$ (see Appendix 4.1.1 in [110]), so

$$N_{\Upsilon\to N\bar{\nu}} \simeq 10^{-10} N_\Upsilon \times \left(\frac{U^2}{10^{-5}}\right) \tag{D.2.2}$$

where we have normalized $U^2$ to the current experimental limit for $M_N > 5$ GeV (c.f. Fig. 3.1).

# Appendix E

# Vector-dominance model

Here we provide the $F_\pi(s)$ formula, given by the vector-dominance model [294]

$$F_\pi(s) = \frac{\mathrm{BW}_\rho^{\mathrm{GS}}(s)\frac{1+c_\omega \mathrm{BW}_\omega^{\mathrm{KS}}(s)}{1+c_\omega} + c_{\rho'}\mathrm{BW}_{\rho'}^{\mathrm{GS}}(s) + c_{\rho''}\mathrm{BW}_{\rho''}^{\mathrm{GS}}(s) + c_{\rho'''}\mathrm{BW}_{\rho'''}^{\mathrm{GS}}(s)}{1 + c_{\rho'} + c_{\rho''} + c_{\rho'''}}, \tag{E.0.1}$$

where $c_i = |c_i|e^{i\phi_i}$ are the complex amplitudes of the Breit–Wigner (BW) functions. They are different for $\omega$ and $\rho$ mesons. For $\omega$ it is the usual BW function

$$\mathrm{BW}_\omega^{\mathrm{KS}}(s) = \frac{m_\omega^2}{m_\omega^2 - s - i m_\omega \Gamma_\omega}, \tag{E.0.2}$$

while for $\rho$ mesons the Gounaris-Sakurai (GS) model [324] is taken,

$$\mathrm{BW}_{\rho_i}^{\mathrm{GS}}(s) = \frac{m_{\rho_i}^2(1 + d(m_{\rho_i})\Gamma_{\rho_i}/m_{\rho_i})}{m_{\rho_i}^2 - s + f(s, m_{\rho_i}, \Gamma_{\rho_i}) - i m_{\rho_i}\Gamma(s, m_{\rho_i}, \Gamma_{\rho_i})}, \tag{E.0.3}$$

where

$$\Gamma(s, m, \Gamma) = \Gamma\frac{s}{m^2}\left(\frac{\beta_\pi(s)}{\beta_\pi(m^2)}\right)^3, \tag{E.0.4}$$

$$f(s, m, \Gamma) = \frac{\Gamma m^2}{k^3(m^2)}\left[k^2(s)\left(h(s) - h(m^2)\right) + (m^2 - s)k^2(m^2)h'(m^2)\right] \tag{E.0.5}$$

$$\beta_\pi(s) = \sqrt{1 - \frac{4m_\pi^2}{s}}, \tag{E.0.6}$$

$$d(m) = \frac{3}{\pi}\frac{m_\pi^2}{k^2(m^2)}\ln\left(\frac{m^2 + 2k(m^2)}{2m_\pi}\right) + \frac{m}{2\pi k(m^2)} - \frac{m_\pi^2 m}{\pi k^3(m^2)}, \tag{E.0.7}$$

$$k(s) = \frac{1}{2}\sqrt{s}\beta_\pi(s), \tag{E.0.8}$$

$$h(s) = \frac{2}{\pi}\frac{k(s)}{\sqrt{s}}\ln\left(\frac{\sqrt{s} + 2k(s)}{2m_\pi}\right) \tag{E.0.9}$$

and $h'(s)$ is a derivative of $h(s)$.

# Appendix F

# Estimation of the upper bound width

In this Section we estimate the ratio between $U_{\max}$ and $U_{\text{top}}$ as defined in Section 5.1.3.1.

The decay probability (5.1.9) can be rewritten in the form

$$P_{\text{decay}} \approx \int dE_X f_{E_X} e^{-l_{\text{target-det}}\Gamma M_X/E_X} = \int dE_X e^{-g(E_X)}, \tag{F.0.1}$$

where for clarity we have assumed $f_{E_X}$ to be dimensionless, and $g(E_X) = l_{\text{target-det}}\Gamma_X M_X/E_X - \ln(f_{E_X})$. Using the steepest descent method, one arrives at

$$P_{\text{decay}} \approx \sqrt{\frac{2\pi}{-g''(E_X^{\text{peak}})}} e^{-g(E_X^{\text{peak}})} \tag{F.0.2}$$

$E_X^{\text{peak}}$ is determined by the extremum criterion $g'(E_X^{\text{peak}}) = 0$. For the exponential spectrum of the form $f_{E_X} = f_0 e^{-E_X\delta}$ the integral and the peak energy are

$$E_X^{\text{peak}} = \sqrt{\frac{l_{\text{target-det}}\Gamma_X M_X}{\delta}}, \quad P_{\text{decay}} \approx \sqrt{\pi} f_0 e^{-2E_X^{\text{peak}}\delta} \sqrt{\frac{E_X^{\text{peak}}}{\delta}}, \tag{F.0.3}$$

while for the power law spectrum $f_{E_X} = f_0 E_X^{-\alpha}$ they are

$$E_X^{\text{peak}} = \frac{l_{\text{target-det}}\Gamma_X M_X}{\alpha}, \quad P_{\text{decay}} \approx \sqrt{\frac{2\pi}{\alpha}} f_0 e^{-\alpha} (E_X^{\text{peak}})^{-\alpha} \tag{F.0.4}$$

Expressing then $\Gamma_X \propto U^2$ and $U^2 \equiv U^2_{\max}(M_X) \times R$, one immediately arrives

at (F.0.5).

$$U_{\text{top}}^{2,\text{SHiP}}(M_N) \approx U_{\text{max}}^{2,\text{SHiP}}(M_N) \frac{\ln^2\left(f_0\sqrt{\pi}(\delta^{-3}\langle p_B\rangle)^{\frac{1}{4}} N_{\text{prod}}(M_N, U_{\text{max}}^{\text{SHiP}}(M_N)\right)}{4\langle p_B\rangle\delta}, \quad \text{(F.0.5)}$$

$$U_{\text{top}}^{2,\text{MAT}}(M_N) \approx U_{\text{max}}^{2,\text{MAT}}(M_N) \frac{\alpha}{\langle p_B\rangle} \left(\sqrt{\frac{2\pi}{\alpha^3}} N_{\text{prod}}(M_N, U_{\text{max}}^{\text{MAT}}(M_N))\right)^{\frac{1}{\alpha-2}}. \quad \text{(F.0.6)}$$

# Bibliography


[1] S. F. Novaes, *Standard model: An Introduction*, in *Particles and fields. Proceedings, 10th Jorge Andre Swieca Summer School, Sao Paulo, Brazil, February 6-12, 1999*, pp. 5–102, 1999. [hep-ph/0001283].

[2] M. Herrero, *The Standard model*, *NATO Sci. Ser. C* **534** (1999) 1–59, [hep-ph/9812242].

[3] **ATLAS** Collaboration, G. Aad et al., *Combined search for the Standard Model Higgs boson using up to 4.9 $fb^{-1}$ of pp collision data at $\sqrt{s} = 7$ TeV with the ATLAS detector at the LHC*, *Phys.Lett.* **B710** (2012) 49–66, [arXiv:1202.1408].

[4] **ATLAS** Collaboration, G. Aad et al., *Observation of a new particle in the search for the Standard Model Higgs boson with the ATLAS detector at the LHC*, *Phys. Lett.* **B716** (2012) 1–29, [arXiv:1207.7214].

[5] **CMS** Collaboration, S. Chatrchyan et al., *Combined results of searches for the standard model Higgs boson in pp collisions at $\sqrt{s} = 7$ TeV*, *Phys. Lett.* **B710** (2012) 26–48, [arXiv:1202.1488].

[6] **CMS** Collaboration, S. Chatrchyan et al., *Observation of a new boson at a mass of 125 GeV with the CMS experiment at the LHC*, *Phys.Lett.* **B716** (2012) 30–61, [arXiv:1207.7235].

[7] **ATLAS, CMS** Collaboration, G. Aad et al., *Combined Measurement of the Higgs Boson Mass in pp Collisions at $\sqrt{s} = 7$ and 8 TeV with the ATLAS and CMS Experiments*, *Phys. Rev. Lett.* **114** (2015) 191803, [arXiv:1503.07589].

[8] **ATLAS** Collaboration, X. Zhuang, *Early Search for Supersymmetry at ATLAS*, *PoS* **KRUGER2010** (2011) 051, [arXiv:1104.2907].

[9] **ATLAS** Collaboration, G. Aad et al., *Search for massive supersymmetric particles decaying to many jets using the ATLAS detector in pp collisions at $\sqrt{s} = 8$ TeV*, *Phys. Rev.* **D91** (2015), no. 11 112016, [arXiv:1502.05686]. [Erratum: Phys. Rev. D93 (2016), no.3 039901].

[10] **ATLAS** Collaboration, G. Aad et al., *Search for new phenomena in final states with an energetic jet and large missing transverse momentum in pp collisions at $\sqrt{s} = 8$ TeV with the ATLAS detector*, *Eur. Phys. J.* **C75** (2015), no. 7 299, [arXiv:1502.01518]. [Erratum: Eur. Phys. J. C75 (2015), no.9 408].

[11] **ATLAS** Collaboration, G. Aad et al., *Search for direct pair production of a*

*chargino and a neutralino decaying to the* 125 *GeV Higgs boson in* $\sqrt{s} = 8$ *TeV pp collisions with the ATLAS detector*, *Eur. Phys. J.* **C75** (2015), no. 5 208, [arXiv:1501.07110].

[12] **ATLAS** Collaboration, G. Aad et al., *Search for squarks and gluinos in events with isolated leptons, jets and missing transverse momentum at* $\sqrt{s} = 8$ *TeV with the ATLAS detector*, *JHEP* **04** (2015) 116, [arXiv:1501.03555].

[13] **ATLAS** Collaboration, G. Aad et al., *Search for Scalar Charm Quark Pair Production in pp Collisions at* $\sqrt{s} = 8$ *TeV with the ATLAS Detector*, *Phys. Rev. Lett.* **114** (2015), no. 16 161801, [arXiv:1501.01325].

[14] **CMS** Collaboration, V. Khachatryan et al., *Searches for Supersymmetry using the* $M_{T2}$ *Variable in Hadronic Events Produced in pp Collisions at* 8 *TeV*, *JHEP* **05** (2015) 078, [arXiv:1502.04358].

[15] **CMS** Collaboration, V. Khachatryan et al., *Search for Physics Beyond the Standard Model in Events with Two Leptons, Jets, and Missing Transverse Momentum in pp Collisions at* $\sqrt{s} = 8$ *TeV*, *JHEP* **04** (2015) 124, [arXiv:1502.06031].

[16] **CMS** Collaboration, V. Khachatryan et al., *Search for Supersymmetry Using Razor Variables in Events with b-Tagged Jets in pp Collisions at* $\sqrt{s} = 8$ *TeV*, *Phys. Rev.* **D91** (2015) 052018, [arXiv:1502.00300].

[17] **CMS** Collaboration, V. Khachatryan et al., *Searches for supersymmetry based on events with b jets and four W bosons in pp collisions at* 8 *TeV*, *Phys. Lett.* **B745** (2015) 5–28, [arXiv:1412.4109].

[18] **ATLAS** Collaboration, G. Aad et al., *Search for dark matter in events with heavy quarks and missing transverse momentum in pp collisions with the ATLAS detector*, *Eur. Phys. J.* **C75** (2015), no. 2 92, [arXiv:1410.4031].

[19] **ATLAS** Collaboration, G. Aad et al., *Search for production of* $WW/WZ$ *resonances decaying to a lepton, neutrino and jets in pp collisions at* $\sqrt{s} = 8$ *TeV with the ATLAS detector*, *Eur. Phys. J.* **C75** (2015), no. 5 209, [arXiv:1503.04677]. [Erratum: Eur. Phys. J. C75 (2015), 370].

[20] **ATLAS** Collaboration, G. Aad et al., *Search for a Heavy Neutral Particle Decaying to* $e\mu$, $e\tau$, *or* $\mu\tau$ *in pp Collisions at* $\sqrt{s} = 8$ *TeV with the ATLAS Detector*, *Phys. Rev. Lett.* **115** (2015), no. 3 031801, [arXiv:1503.04430].

[21] **ATLAS** Collaboration, N. Bousson, *ATLAS Exotic Searches*, *EPJ Web Conf.* **28** (2012) 09012, [arXiv:1201.5256].

[22] J. Tam, *Summary of results on exotic searches from ATLAS*, Tech. Rep. ATL-PHYS-PROC-2014-212, CERN, Geneva, Oct, 2014.

[23] **ATLAS, CDF, CMS, D0** Collaboration, S. Rahatlou, *Exotic Searches at LHC and Tevatron*, [arXiv:1201.4810].

[24] P. Bargassa, *Beyond the Standard Model physics: Strong Susy production searches at ATLAS and CMS*, in *Proceedings, 49th Rencontres de Moriond on Electroweak Interactions and Unified Theories: La Thuile, Italy, March 15-22, 2014*, pp. 359–368, 2014.

[25] **ATLAS, CMS** Collaboration, T. R. T. Fernandez, *Exotic searches in the large hadron collider*, in *Proceedings, 49th Rencontres de Moriond on Electroweak Interactions and Unified Theories: La Thuile, Italy, March 15-22, 2014*, pp. 431–438, 2014.

[26] **ATLAS, CMS** Collaboration, M. J. Flowerdew, *Electroweak SUSY production searches at ATLAS and CMS*, in *Proceedings, 49th Rencontres de Moriond on Electroweak Interactions and Unified Theories: La Thuile, Italy, March 15-22, 2014*, pp. 375–382, 2014.

[27] **ATLAS, CMS** Collaboration, P. D. Thompson, *Beyond the Standard Model Higgs Searches at the LHC*, in *Proceedings, 49th Rencontres de Moriond on Electroweak Interactions and Unified Theories: La Thuile, Italy, March 15-22, 2014*, pp. 347–352, 2014.

[28] **CMS** Collaboration, "CMS Supersymmetry Physics Results." https://twiki.cern.ch/twiki/bin/view/CMSPublic/PhysicsResultsSUSY, 2015.

[29] **ATLAS** Collaboration, "ATLAS Exotics Public Results." https://twiki.cern.ch/twiki/bin/view/AtlasPublic/SupersymmetryPublicResults, 2015.

[30] **ATLAS** Collaboration, "ATLAS Supersymmetry Searches." https://twiki.cern.ch/twiki/bin/view/AtlasPublic/ExoticsPublicResults, 2015.

[31] **CMS** Collaboration, "CMS Exotica Public Physics Results." https://twiki.cern.ch/twiki/bin/view/AtlasPublic/ExoticsPublicResults, 2015.

[32] D. Buttazzo, G. Degrassi, P. P. Giardino, G. F. Giudice, F. Sala, A. Salvio, and A. Strumia, *Investigating the near-criticality of the Higgs boson*, *JHEP* **12** (2013) 089, [arXiv:1307.3536].

[33] G. Degrassi, S. Di Vita, J. Elias-Miro, J. R. Espinosa, G. F. Giudice, G. Isidori, and A. Strumia, *Higgs mass and vacuum stability in the Standard Model at NNLO*, *JHEP* **08** (2012) 098, [arXiv:1205.6497].

[34] F. Bezrukov, M. Yu. Kalmykov, B. A. Kniehl, and M. Shaposhnikov, *Higgs Boson Mass and New Physics*, *JHEP* **10** (2012) 140, [arXiv:1205.2893].

[35] F. Bezrukov, J. Rubio, and M. Shaposhnikov, *Living beyond the edge: Higgs inflation and vacuum metastability*, *Phys. Rev.* **D92** (2015), no. 8 083512, [arXiv:1412.3811].

[36] F. Bezrukov and M. Shaposhnikov, *Why should we care about the top quark Yukawa coupling?*, *J. Exp. Theor. Phys.* **120** (2015) 335–343, [arXiv:1411.1923].

[37] **Planck** Collaboration, P. A. R. Ade et al., *Planck 2015 results. XIII. Cosmological parameters*, *Astron. Astrophys.* **594** (2016) A13, [arXiv:1502.01589].

[38] P. J. E. Peebles, *Dark Matter*, *Proc. Nat. Acad. Sci.* **112** (2013) 2246, [arXiv:1305.6859].

[39] V. Lukovic, P. Cabella, and N. Vittorio, *Dark matter in cosmology*, *Int. J. Mod. Phys.* **A29** (2014) 1443001, [arXiv:1411.3556].

[40] G. Bertone and D. Hooper, *A History of Dark Matter*, *Submitted to: Rev. Mod. Phys.* (2016) [arXiv:1605.04909].

[41] G. D. Starkman, *Modifying Gravity: You Can't Always Get What You Want*, *Phil. Trans. Roy. Soc. Lond.* **A369** (2011) 5018–5041, [arXiv:1201.1697].

[42] J. Lesgourgues and S. Pastor, *Massive neutrinos and cosmology*, *Phys. Rept.* **429** (2006) 307–379, [astro-ph/0603494].

[43] **Particle Data Group** Collaboration, K. A. Olive et al., *Review of Particle Physics*, *Chin. Phys.* **C38** (2014) 090001.

[44] S. Tremaine and J. E. Gunn, *Dynamical Role of Light Neutral Leptons in Cosmology*, *Phys. Rev. Lett.* **42** (1979) 407–410.

[45] A. Boyarsky, O. Ruchayskiy, and D. Iakubovskyi, *A Lower bound on the mass of Dark Matter particles*, *JCAP* **0903** (2009) 005, [arXiv:0808.3902].

[46] S. D. M. White, C. S. Frenk, and M. Davis, *Clustering in a Neutrino Dominated Universe*, *Astrophys. J.* **274** (1983) L1–L5.

[47] C. D. Anderson, *The Positive Electron*, *Phys. Rev.* **43** (1933) 491–494.

[48] A. G. Cohen, A. De Rujula, and S. L. Glashow, *A Matter–Antimatter Universe?*, *Astrophys. J.* **495** (1998) 539–549, [astro-ph/9707087].

[49] **Planck** Collaboration, P. A. R. Ade et al., *Planck 2013 results. XVI. Cosmological parameters*, *Astron. Astrophys.* **571** (2014) A16, [arXiv:1303.5076].

[50] F. Iocco, G. Mangano, G. Miele, O. Pisanti, and P. D. Serpico, *Primordial Nucleosynthesis: from precision cosmology to fundamental physics*, *Phys. Rept.* **472** (2009) 1–76, [arXiv:0809.0631].

[51] M. Pospelov and J. Pradler, *Big Bang Nucleosynthesis as a Probe of New Physics*, *Ann. Rev. Nucl. Part. Sci.* **60** (2010) 539–568, [arXiv:1011.1054].

[52] G. Steigman, *Primordial Nucleosynthesis in the Precision Cosmology Era*, *Ann. Rev. Nucl. Part. Sci.* **57** (2007) 463–491, [arXiv:0712.1100].

[53] G. Steigman, *Observational tests of antimatter cosmologies*, *Ann. Rev. Astron. Astrophys.* **14** (1976) 339–372.

[54] F. W. Stecker, *On the Nature of the Baryon Asymmetry*, *Nucl. Phys.* **B252** (1985) 25–36.

[55] G. Steigman, *When Clusters Collide: Constraints On Antimatter On The Largest Scales*, *JCAP* **0810** (2008) 001, [arXiv:0808.1122].

[56] **AMS** Collaboration, J. Alcaraz et al., *Search for anti-helium in cosmic rays*, *Phys. Lett.* **B461** (1999) 387–396, [hep-ex/0002048].

[57] C. Bambi and A. D. Dolgov, *Antimatter in the Milky Way*, *Nucl. Phys.* **B784** (2007) 132–150, [astro-ph/0702350].

[58] A. D. Sakharov, *Violation of CP Invariance, C asymmetry, and Baryon Asymmetry of the Universe*, *Pisma Zh. Eksp. Teor. Fiz.* **5** (1967) 32–35.

[59] **Super-Kamiokande** Collaboration, H. Nishino et al., *Search for Proton Decay via $p \to e^+\pi^0$ and $p \to \mu^+\pi^0$ in a Large Water Cherenkov Detector*, *Phys. Rev. Lett.* **102** (2009) 141801, [arXiv:0903.0676].

[60] G. 't Hooft, *Symmetry Breaking Through Bell-Jackiw Anomalies*, *Phys. Rev. Lett.* **37** (1976) 8–11.

[61] V. A. Kuzmin, V. A. Rubakov, and M. E. Shaposhnikov, *On the Anomalous Electroweak Baryon Number Nonconservation in the Early Universe*, *Phys. Lett.* **B155** (1985) 36.

[62] K. Kajantie, M. Laine, K. Rummukainen, and M. E. Shaposhnikov, *The Electroweak phase transition: A Nonperturbative analysis*, *Nucl. Phys.* **B466** (1996) 189–258, [hep-lat/9510020].

[63] C. S. Wu, E. Ambler, R. W. Hayward, D. D. Hoppes, and R. P. Hudson, *Experimental Test of Parity Conservation in Beta Decay*, *Phys. Rev.* **105** (1957) 1413–1414.

[64] J. H. Christenson, J. W. Cronin, V. L. Fitch, and R. Turlay, *Evidence for the $2\pi$ Decay of the $K_2^0$ Meson*, *Phys. Rev. Lett.* **13** (1964) 138–140.

[65] **KTeV** Collaboration, A. Alavi-Harati et al., *Observation of direct CP violation in $K_{S,L} \to \pi\pi$ decays*, *Phys. Rev. Lett.* **83** (1999) 22–27, [hep-ex/9905060].

[66] **NA48** Collaboration, V. Fanti et al., *A New measurement of direct CP violation in two pion decays of the neutral kaon*, *Phys. Lett.* **B465** (1999) 335–348, [hep-ex/9909022].

[67] **BaBar** Collaboration, B. Aubert et al., *Measurement of CP violating asymmetries in $B^0$ decays to CP eigenstates*, *Phys. Rev. Lett.* **86** (2001) 2515–2522, [hep-ex/0102030].

[68] **Belle** Collaboration, K. Abe et al., *Observation of large CP violation in the neutral B meson system*, *Phys. Rev. Lett.* **87** (2001) 091802, [hep-ex/0107061].

[69] Y. Nir, *CP violation in and beyond the standard model*, in *Proceedings, 27th SLAC Summer Institute on Particle Physics: CP Violation in and Beyond the Standard*

*Model (SSI 99): Stanford, USA, July 7-16, 1999*, pp. 165–243, 1999. [hep-ph/9911321].

[70] M. E. Shaposhnikov, *Baryon Asymmetry of the Universe in Standard Electroweak Theory*, *Nucl. Phys.* **B287** (1987) 757–775.

[71] M. B. Gavela, P. Hernandez, J. Orloff, O. Pene, and C. Quimbay, *Standard model CP violation and baryon asymmetry. Part 2: Finite temperature*, *Nucl. Phys.* **B430** (1994) 382–426, [hep-ph/9406289].

[72] P. Huet and E. Sather, *Electroweak baryogenesis and standard model CP violation*, *Phys. Rev.* **D51** (1995) 379–394, [hep-ph/9404302].

[73] K. Kajantie, M. Laine, K. Rummukainen, and M. E. Shaposhnikov, *Is there a hot electroweak phase transition at $m_H$ larger or equal to $m_W$?*, *Phys. Rev. Lett.* **77** (1996) 2887–2890, [hep-ph/9605288].

[74] K. Rummukainen, M. Tsypin, K. Kajantie, M. Laine, and M. E. Shaposhnikov, *The Universality class of the electroweak theory*, *Nucl. Phys.* **B532** (1998) 283–314, [hep-lat/9805013].

[75] F. Csikor, Z. Fodor, and J. Heitger, *Endpoint of the hot electroweak phase transition*, *Phys. Rev. Lett.* **82** (1999) 21–24, [hep-ph/9809291].

[76] D. E. Morrissey and M. J. Ramsey-Musolf, *Electroweak baryogenesis*, *New J. Phys.* **14** (2012) 125003, [arXiv:1206.2942].

[77] M. Trodden, *Electroweak baryogenesis*, *Rev. Mod. Phys.* **71** (1999) 1463–1500, [hep-ph/9803479].

[78] A. G. Cohen, D. B. Kaplan, and A. E. Nelson, *Progress in electroweak baryogenesis*, *Ann. Rev. Nucl. Part. Sci.* **43** (1993) 27–70, [hep-ph/9302210].

[79] I. Affleck and M. Dine, *A New Mechanism for Baryogenesis*, *Nucl. Phys.* **B249** (1985) 361–380.

[80] M. Fukugita and T. Yanagida, *Resurrection of grand unified theory baryogenesis*, *Phys. Rev. Lett.* **89** (2002) 131602, [hep-ph/0203194].

[81] W. Buchmuller, P. Di Bari, and M. Plumacher, *Leptogenesis for pedestrians*, *Annals Phys.* **315** (2005) 305–351, [hep-ph/0401240].

[82] S. Davidson, E. Nardi, and Y. Nir, *Leptogenesis*, *Phys. Rept.* **466** (2008) 105–177, [arXiv:0802.2962].

[83] M. Shaposhnikov, *Baryogenesis*, *J. Phys. Conf. Ser.* **171** (2009) 012005.

[84] A. Pilaftsis, *The Little Review on Leptogenesis*, *J. Phys. Conf. Ser.* **171** (2009) 012017, [arXiv:0904.1182].

[85] M. Drewes, B. Garbrecht, P. Hernandez, M. Kekic, J. Lopez-Pavon, J. Racker, N. Rius, J. Salvado, and D. Teresi, *ARS Leptogenesis*, *Int. J. Mod. Phys.* **A33** (2018), no. 05n06 1842002, [arXiv:1711.02862].

[86] A. Pilaftsis and T. E. J. Underwood, *Electroweak-scale resonant leptogenesis*, *Phys. Rev.* **D72** (2005) 113001, [hep-ph/0506107].

[87] A. Pilaftsis and T. E. J. Underwood, *Resonant leptogenesis*, *Nucl. Phys.* **B692** (2004) 303–345, [hep-ph/0309342].

[88] E. K. Akhmedov, V. A. Rubakov, and A. Yu. Smirnov, *Baryogenesis via neutrino oscillations*, *Phys. Rev. Lett.* **81** (1998) 1359–1362, [hep-ph/9803255].

[89] T. Asaka and M. Shaposhnikov, *The nuMSM, dark matter and baryon asymmetry of the universe*, *Phys. Lett.* **B620** (2005) 17–26, [hep-ph/0505013].

[90] M. Shaposhnikov, *The nuMSM, leptonic asymmetries, and properties of singlet fermions*, *JHEP* **08** (2008) 008, [arXiv:0804.4542].

[91] S. Eijima, M. Shaposhnikov, and I. Timiryasov, *Freeze-out of baryon number in low-scale leptogenesis*, *JCAP* **1711** (2017), no. 11 030, [arXiv:1709.07834].

[92] S. Eijima and M. Shaposhnikov, *Fermion number violating effects in low scale leptogenesis*, *Phys. Lett.* **B771** (2017) 288–296, [arXiv:1703.06085].

[93] E. W. Kolb and M. S. Turner, *Grand Unified Theories and the Origin of the Baryon Asymmetry*, *Ann. Rev. Nucl. Part. Sci.* **33** (1983) 645–696.

[94] A. D. Dolgov, *NonGUT baryogenesis*, *Phys. Rept.* **222** (1992) 309–386.

[95] A. Riotto and M. Trodden, *Recent progress in baryogenesis*, *Ann. Rev. Nucl. Part. Sci.* **49** (1999) 35–75, [hep-ph/9901362].

[96] M. Dine and A. Kusenko, *The Origin of the matter - antimatter asymmetry*, *Rev. Mod. Phys.* **76** (2003) 1, [hep-ph/0303065].

[97] W. Buchmuller, *Baryogenesis: 40 Years Later*, in *Proceedings on 13th International Symposium on Particles, strings, and cosmology (PASCOS 2007): London, UK, July 2-7, 2007*, 2007. [arXiv:0710.5857].

[98] S. Weinberg, *A Model of Leptons*, *Phys. Rev. Lett.* **19** (1967) 1264–1266.

[99] J. N. Bahcall and M. H. Pinsonneault, *Standard solar models, with and without helium diffusion and the solar neutrino problem*, *Rev. Mod. Phys.* **64** (1992) 885–926.

[100] S. M. Bilenky, *Neutrino oscillations: brief history and present status*, in *Proceedings, 22nd International Baldin Seminar on High Energy Physics Problems, Relativistic Nuclear Physics and Quantum Chromodynamics, (ISHEPP 2014): Dubna, Russia, September 15-20, 2014*, 2014. [arXiv:1408.2864].

[101] P. F. de Salas, D. V. Forero, C. A. Ternes, M. Tortola, and J. W. F. Valle, *Status of neutrino oscillations 2018: first hint for normal mass ordering and improved CP sensitivity*, *Phys. Lett.* **B782** (2018) 633–640, [arXiv:1708.01186].

[102] B. Pontecorvo, *Mesonium and anti-mesonium*, *Sov. Phys. JETP* **6** (1957) 429.

[103] Z. Maki, M. Nakagawa, and S. Sakata, *Remarks on the unified model of elementary particles*, *Prog. Theor. Phys.* **28** (1962) 870–880.

[104] S. Weinberg, *Varieties of Baryon and Lepton Nonconservation*, *Phys. Rev.* **D22** (1980) 1694.

[105] A. Strumia and F. Vissani, *Neutrino masses and mixings and...*, [hep-ph/0606054].

[106] **LBNE** Collaboration, C. Adams et al., *The Long-Baseline Neutrino Experiment: Exploring Fundamental Symmetries of the Universe*, [arXiv:1307.7335].

[107] **SHiP** Collaboration, P. Mermod, *Hidden sector searches with SHiP and NA62*, in *2017 International Workshop on Neutrinos from Accelerators (NuFact17) Uppsala University Main Building, Uppsala, Sweden, September 25-30, 2017*, 2017. [arXiv:1712.01768].

[108] **NA62** Collaboration, E. Cortina Gil et al., *Search for heavy neutral lepton production in $K^+$ decays*, *Phys. Lett.* **B778** (2018) 137–145, [arXiv:1712.00297].

[109] M. Drewes, J. Hajer, J. Klaric, and G. Lanfranchi, *NA62 sensitivity to heavy neutral leptons in the low scale seesaw model*, [arXiv:1801.04207].

[110] S. Alekhin et al., *A facility to Search for Hidden Particles at the CERN SPS: the SHiP physics case*, *Rept. Prog. Phys.* **79** (2016), no. 12 124201, [arXiv:1504.04855].

[111] **SHiP** Collaboration, M. Anelli et al., *A facility to Search for Hidden Particles (SHiP) at the CERN SPS*, [arXiv:1504.04956].

[112] V. V. Gligorov, S. Knapen, M. Papucci, and D. J. Robinson, *Searching for Long-lived Particles: A Compact Detector for Exotics at LHCb*, *Phys. Rev.* **D97** (2018), no. 1 015023, [arXiv:1708.09395].

[113] D. Curtin and M. E. Peskin, *Analysis of Long Lived Particle Decays with the MATHUSLA Detector*, *Phys. Rev.* **D97** (2018), no. 1 015006, [arXiv:1705.06327].

[114] J. A. Evans, *Detecting Hidden Particles with MATHUSLA*, *Phys. Rev.* **D97** (2018), no. 5 055046, [arXiv:1708.08503].

[115] F. Kling and S. Trojanowski, *Heavy Neutral Leptons at FASER*, *Phys. Rev.* **D97** (2018), no. 9 095016, [arXiv:1801.08947].

[116] J. L. Feng, I. Galon, F. Kling, and S. Trojanowski, *Dark Higgs bosons at the ForwArd Search ExpeRiment*, *Phys. Rev.* **D97** (2018), no. 5 055034, [arXiv:1710.09387].

[117] P. Minkowski, *$\mu \to e\gamma$ at a Rate of One Out of $10^9$ Muon Decays?*, *Phys. Lett.* **B67** (1977) 421–428.

[118] P. Ramond, *The Family Group in Grand Unified Theories*, in *International Symposium on Fundamentals of Quantum Theory and Quantum Field Theory Palm Coast, Florida, February 25-March 2, 1979*, pp. 265–280, 1979. [hep-ph/9809459].

[119] R. N. Mohapatra and G. Senjanovic, *Neutrino Mass and Spontaneous Parity Violation*, *Phys. Rev. Lett.* **44** (1980) 912.

[120] T. Yanagida, *Horizontal Symmetry and Masses of Neutrinos*, *Prog. Theor. Phys.* **64** (1980) 1103.

[121] J. Orloff, S. Lavignac, and M. Cribier, eds., *Seesaw mechanism. Proceedings, International Conference, SEESAW25, Paris, France, June 10-11, 2004*, 2005.

[122] E. Ma, *Pathways to naturally small neutrino masses*, *Phys. Rev. Lett.* **81** (1998) 1171–1174, [hep-ph/9805219].

[123] G. Lazarides, Q. Shafi, and C. Wetterich, *Proton Lifetime and Fermion Masses in an $SO(10)$ Model*, *Nucl. Phys.* **B181** (1981) 287–300.

[124] R. N. Mohapatra and G. Senjanovic, *Neutrino Masses and Mixings in Gauge Models with Spontaneous Parity Violation*, *Phys. Rev.* **D23** (1981) 165.

[125] J. Schechter and J. W. F. Valle, *Neutrino Masses in $SU(2) \times U(1)$ Theories*, *Phys. Rev.* **D22** (1980) 2227.

[126] E. Ma and U. Sarkar, *Neutrino masses and leptogenesis with heavy Higgs triplets*, *Phys. Rev. Lett.* **80** (1998) 5716–5719, [hep-ph/9802445].

[127] R. Foot, H. Lew, X. G. He, and G. C. Joshi, *Seesaw Neutrino Masses Induced by a Triplet of Leptons*, *Z. Phys.* **C44** (1989) 441.

[128] T. Asaka, S. Eijima, and H. Ishida, *Mixing of Active and Sterile Neutrinos*, *JHEP* **04** (2011) 011, [arXiv:1101.1382].

[129] M. Shaposhnikov, *A Possible symmetry of the nuMSM*, *Nucl. Phys.* **B763** (2007) 49–59, [hep-ph/0605047].

[130] O. Ruchayskiy and A. Ivashko, *Experimental bounds on sterile neutrino mixing angles*, *JHEP* **06** (2012) 100, [arXiv:1112.3319].

[131] F. Maltoni, J. M. Niczyporuk, and S. Willenbrock, *Upper bound on the scale of Majorana neutrino mass generation*, *Phys. Rev. Lett.* **86** (2001) 212–215, [hep-ph/0006358].

[132] A. de Gouvea, *See-saw energy scale and the LSND anomaly*, *Phys. Rev.* **D72** (2005) 033005, [hep-ph/0501039].

[133] G. 't Hooft, *Naturalness, chiral symmetry, and spontaneous chiral symmetry breaking*, *NATO Sci.Ser.B* **59** (1980) 135.

[134] L. Canetti, M. Drewes, T. Frossard, and M. Shaposhnikov, *Dark Matter, Baryogenesis and Neutrino Oscillations from Right Handed Neutrinos*, *Phys. Rev.* **D87** (2013) 093006, [arXiv:1208.4607].

[135] S. Dodelson and L. M. Widrow, *Sterile-neutrinos as dark matter*, *Phys. Rev. Lett.* **72** (1994) 17–20, [hep-ph/9303287].

[136] A. D. Dolgov and S. H. Hansen, *Massive sterile neutrinos as warm dark matter*, *Astropart. Phys.* **16** (2002) 339–344, [hep-ph/0009083].

[137] K. Abazajian, G. M. Fuller, and M. Patel, *Sterile neutrino hot, warm, and cold dark matter*, *Phys. Rev.* **D64** (2001) 023501, [astro-ph/0101524].

[138] T. Asaka, M. Laine, and M. Shaposhnikov, *Lightest sterile neutrino abundance within the nuMSM*, *JHEP* **01** (2007) 091, [hep-ph/0612182]. [Erratum: JHEP02 (2015), 028].

[139] X.-D. Shi and G. M. Fuller, *A New dark matter candidate: Nonthermal sterile neutrinos*, *Phys. Rev. Lett.* **82** (1999) 2832–2835, [astro-ph/9810076].

[140] M. Laine and M. Shaposhnikov, *Sterile neutrino dark matter as a consequence of nuMSM-induced lepton asymmetry*, *JCAP* **0806** (2008) 031, [arXiv:0804.4543].

[141] M. Shaposhnikov and I. Tkachev, *The nuMSM, inflation, and dark matter*, *Phys. Lett.* **B639** (2006) 414–417, [hep-ph/0604236].

[142] A. Kusenko, *Sterile neutrinos, dark matter, and the pulsar velocities in models with a Higgs singlet*, *Phys. Rev. Lett.* **97** (2006) 241301, [hep-ph/0609081].

[143] K. Petraki and A. Kusenko, *Dark-matter sterile neutrinos in models with a gauge singlet in the Higgs sector*, *Phys. Rev.* **D77** (2008) 065014, [arXiv:0711.4646].

[144] A. Boyarsky, O. Ruchayskiy, and M. Shaposhnikov, *The Role of sterile neutrinos in cosmology and astrophysics*, *Ann. Rev. Nucl. Part. Sci.* **59** (2009) 191–214, [arXiv:0901.0011].

[145] A. Kusenko, *Sterile neutrinos: The Dark side of the light fermions*, *Phys. Rept.* **481** (2009) 1–28, [arXiv:0906.2968].

[146] A. Boyarsky, D. Iakubovskyi, and O. Ruchayskiy, *Next decade of sterile neutrino studies*, *Phys. Dark Univ.* **1** (2012) 136–154, [arXiv:1306.4954].

[147] A. Boyarsky, A. Neronov, O. Ruchayskiy, and M. Shaposhnikov, *Constraints on sterile neutrino as a dark matter candidate from the diffuse X-ray background*, *Mon. Not. Roy. Astron. Soc.* **370** (2006) 213–218, [astro-ph/0512509].

[148] A. Boyarsky, A. Neronov, O. Ruchayskiy, and M. Shaposhnikov, *The Masses of active neutrinos in the nuMSM from X-ray astronomy*, *JETP Lett.* **83** (2006) 133–135, [hep-ph/0601098].

[149] E. Bulbul, M. Markevitch, A. Foster, R. K. Smith, M. Loewenstein, and S. W. Randall, *Detection of An Unidentified Emission Line in the Stacked X-ray spectrum of Galaxy Clusters*, *Astrophys. J.* **789** (2014) 13, [arXiv:1402.2301].

[150] A. Boyarsky, O. Ruchayskiy, D. Iakubovskyi, and J. Franse, *Unidentified Line in X-Ray Spectra of the Andromeda Galaxy and Perseus Galaxy Cluster*, *Phys. Rev. Lett.* **113** (2014) 251301, [arXiv:1402.4119].

[151] A. Boyarsky, J. Franse, D. Iakubovskyi, and O. Ruchayskiy, *Checking the Dark Matter Origin of a* 3.53 *keV Line with the Milky Way Center*, *Phys. Rev. Lett.* **115** (2015) 161301, [arXiv:1408.2503].

[152] A. Boyarsky, A. Neronov, O. Ruchayskiy, M. Shaposhnikov, and I. Tkachev, *Where to find a dark matter sterile neutrino?*, *Phys. Rev. Lett.* **97** (2006) 261302, [astro-ph/0603660].

[153] A. Boyarsky, J. Nevalainen, and O. Ruchayskiy, *Constraints on the parameters of radiatively decaying dark matter from the dark matter halo of the Milky Way and Ursa Minor*, *Astron. Astrophys.* **471** (2007) 51–57, [astro-ph/0610961].

[154] A. Boyarsky, D. Iakubovskyi, O. Ruchayskiy, and V. Savchenko, *Constraints on decaying Dark Matter from XMM-Newton observations of M31*, *Mon. Not. Roy. Astron. Soc.* **387** (2008) 1361, [arXiv:0709.2301].

[155] A. Boyarsky, D. Malyshev, A. Neronov, and O. Ruchayskiy, *Constraining DM properties with SPI*, *Mon. Not. Roy. Astron. Soc.* **387** (2008) 1345, [arXiv:0710.4922].

[156] M. Loewenstein, A. Kusenko, and P. L. Biermann, *New Limits on Sterile Neutrinos from Suzaku Observations of the Ursa Minor Dwarf Spheroidal Galaxy*, *Astrophys. J.* **700** (2009) 426–435, [arXiv:0812.2710].

[157] D. Gorbunov, A. Khmelnitsky, and V. Rubakov, *Constraining sterile neutrino dark matter by phase-space density observations*, *JCAP* **0810** (2008) 041, [arXiv:0808.3910].

[158] T. Asaka, S. Blanchet, and M. Shaposhnikov, *The nuMSM, dark matter and neutrino masses*, *Phys. Lett.* **B631** (2005) 151–156, [hep-ph/0503065].

[159] F. L. Bezrukov and M. Shaposhnikov, *The Standard Model Higgs boson as the inflaton*, *Phys. Lett.* **B659** (2008) 703–706, [arXiv:0710.3755].

[160] **Planck** Collaboration, P. Ade et al., *Planck 2015 results. XIII. Cosmological parameters*, [arXiv:1502.01589].

[161] C. D. Froggatt and H. B. Nielsen, *Standard model criticality prediction: Top mass* $173 \pm 5$ *GeV and Higgs mass* $135 \pm 9$ *GeV*, *Phys. Lett.* **B368** (1996) 96–102, [hep-ph/9511371].

[162] G. Isidori, V. S. Rychkov, A. Strumia, and N. Tetradis, *Gravitational corrections to standard model vacuum decay*, *Phys. Rev.* **D77** (2008) 025034, [arXiv:0712.0242].

[163] J. Ellis, J. R. Espinosa, G. F. Giudice, A. Hoecker, and A. Riotto, *The Probable Fate of the Standard Model*, *Phys. Lett.* **B679** (2009) 369–375, [arXiv:0906.0954].

[164] J. Elias-Miro, J. R. Espinosa, G. F. Giudice, G. Isidori, A. Riotto, and A. Strumia, *Higgs mass implications on the stability of the electroweak vacuum*, *Phys. Lett.* **B709** (2012) 222–228, [arXiv:1112.3022].

[165] **CMS** Collaboration, C. Collaboration, *Combination of the CMS top-quark mass measurements from Run 1 of the LHC*, .

[166] **CMS** Collaboration, V. Khachatryan et al., "Combined mass and couplings of the Higgs boson at CMS." Talk at CERN https://indico.cern.ch/event/360238/, 2015.

[167] J. R. Espinosa, G. F. Giudice, and A. Riotto, *Cosmological implications of the Higgs mass measurement*, *JCAP* **0805** (2008) 002, [arXiv:0710.2484].

[168] **FCC-ee study Team** Collaboration, A. Blondel, E. Graverini, N. Serra, and M. Shaposhnikov, *Search for Heavy Right Handed Neutrinos at the FCC-ee*, *Nucl. Part. Phys. Proc.* **273-275** (2016) 1883–1890, [arXiv:1411.5230].

[169] F. Englert and R. Brout, *Broken Symmetry and the Mass of Gauge Vector Mesons*, *Phys. Rev. Lett.* **13** (1964) 321–323.

[170] P. W. Higgs, *Broken symmetries, massless particles and gauge fields*, *Phys. Lett.* **12** (1964) 132–133.

[171] P. W. Higgs, *Broken Symmetries and the Masses of Gauge Bosons*, *Phys. Rev. Lett.* **13** (1964) 508–509.

[172] G. S. Guralnik, C. R. Hagen, and T. W. B. Kibble, *Global Conservation Laws and Massless Particles*, *Phys. Rev. Lett.* **13** (1964) 585–587.

[173] V. Silveira and A. Zee, *Scalar Phantoms*, *Phys. Lett.* **B161** (1985) 136–140.

[174] M. Pospelov, A. Ritz, and M. B. Voloshin, *Secluded WIMP Dark Matter*, *Phys. Lett.* **B662** (2008) 53–61, [arXiv:0711.4866].

[175] D. Feldman, B. Kors, and P. Nath, *Extra-weakly Interacting Dark Matter*, *Phys. Rev.* **D75** (2007) 023503, [hep-ph/0610133].

[176] Z. Chacko, H.-S. Goh, and R. Harnik, *The Twin Higgs: Natural electroweak breaking from mirror symmetry*, *Phys. Rev. Lett.* **96** (2006) 231802, [hep-ph/0506256].

[177] G. Burdman, Z. Chacko, H.-S. Goh, and R. Harnik, *Folded supersymmetry and the LEP paradox*, *JHEP* **02** (2007) 009, [hep-ph/0609152].

[178] N. Craig and K. Howe, *Doubling down on naturalness with a supersymmetric twin Higgs*, *JHEP* **03** (2014) 140, [arXiv:1312.1341].

[179] N. Craig, S. Knapen, and P. Longhi, *Neutral Naturalness from Orbifold Higgs Models*, *Phys. Rev. Lett.* **114** (2015), no. 6 061803, [arXiv:1410.6808].

[180] G. Burdman, Z. Chacko, R. Harnik, L. de Lima, and C. B. Verhaaren, *Colorless Top Partners, a 125 GeV Higgs, and the Limits on Naturalness*, *Phys. Rev.* **D91** (2015), no. 5 055007, [arXiv:1411.3310].

[181] J. Shelton and K. M. Zurek, *Darkogenesis: A baryon asymmetry from the dark matter sector*, *Phys. Rev.* **D82** (2010) 123512, [arXiv:1008.1997].

[182] F. Bezrukov and D. Gorbunov, *Light inflaton Hunter's Guide*, *JHEP* **05** (2010) 010, [arXiv:0912.0390].

[183] F. Bezrukov and D. Gorbunov, *Light inflaton after LHC8 and WMAP9 results*, *JHEP* **07** (2013) 140, [arXiv:1303.4395].

[184] R. Kappl, M. Ratz, and M. W. Winkler, *Light dark matter in the singlet-extended MSSM*, *Phys. Lett.* **B695** (2011) 169–173, [arXiv:1010.0553].

[185] M. W. Winkler, *Light Dark Matter in Theory and Experiment*. PhD thesis, Tech. U., Munich, Dept. Phys., 2012.

[186] S. Tulin and H.-B. Yu, *Dark Matter Self-interactions and Small Scale Structure*, *Phys. Rept.* **730** (2018) 1–57, [arXiv:1705.02358].

[187] **XENON** Collaboration, E. Aprile et al., *First Dark Matter Search Results from the XENON1T Experiment*, *Phys. Rev. Lett.* **119** (2017), no. 18 181301, [arXiv:1705.06655].

[188] **PandaX-II** Collaboration, X. Cui et al., *Dark Matter Results From* 54-*Ton-Day Exposure of PandaX-II Experiment*, *Phys. Rev. Lett.* **119** (2017), no. 18 181302, [arXiv:1708.06917].

[189] T. Bringmann, J. Hasenkamp, and J. Kersten, *Tight bonds between sterile neutrinos and dark matter*, *JCAP* **1407** (2014) 042, [arXiv:1312.4947].

[190] M. Kaplinghat, S. Tulin, and H.-B. Yu, *Dark Matter Halos as Particle Colliders: Unified Solution to Small-Scale Structure Puzzles from Dwarfs to Clusters*, *Phys. Rev. Lett.* **116** (2016), no. 4 041302, [arXiv:1508.03339].

[191] M. Valli and H.-B. Yu, *Dark matter self-interactions from the internal dynamics of dwarf spheroidals*, [arXiv:1711.03502].

[192] N. Yoshida, V. Springel, S. D. M. White, and G. Tormen, *Weakly self-interacting dark matter and the structure of dark halos*, *Astrophys. J.* **544** (2000) L87–L90, [astro-ph/0006134].

[193] C. Firmani, E. D'Onghia, V. Avila-Reese, G. Chincarini, and X. Hernandez, *Evidence of self-interacting cold dark matter from galactic to galaxy cluster scales*, *Mon. Not. Roy. Astron. Soc.* **315** (2000) L29, [astro-ph/0002376].

[194] C. Firmani, E. D'Onghia, G. Chincarini, X. Hernandez, and V. Avila-Reese, *Constraints on dark matter physics from dwarf galaxies through galaxy cluster haloes*, *Mon. Not. Roy. Astron. Soc.* **321** (2001) 713, [astro-ph/0005001].

[195] P. Colin, V. Avila-Reese, O. Valenzuela, and C. Firmani, *Structure and subhalo population of halos in a selfinteracting dark matter cosmology*, *Astrophys. J.* **581** (2002) 777–793, [astro-ph/0205322].

[196] A. Loeb and N. Weiner, *Cores in Dwarf Galaxies from Dark Matter with a Yukawa Potential*, *Phys. Rev. Lett.* **106** (2011) 171302, [arXiv:1011.6374].

[197] L. G. van den Aarssen, T. Bringmann, and C. Pfrommer, *Is dark matter with long-range interactions a solution to all small-scale problems of Lambda CDM cosmology?*, *Phys. Rev. Lett.* **109** (2012) 231301, [arXiv:1205.5809].

[198] K. Bondarenko, A. Boyarsky, T. Bringmann, and A. Sokolenko, *Constraining self-interacting dark matter with scaling laws of observed halo surface densities*, *JCAP* **1804** (2018), no. 04 049, [arXiv:1712.06602].

[199] A. Sokolenko, K. Bondarenko, T. Brinckmann, J. Zavala, M. Vogelsberger, T. Bringmann, and A. Boyarsky, *Towards an improved model of self-interacting dark matter haloes*, [arXiv:1806.11539].

[200] K. Bondarenko, A. Boyarsky, V. Gorkavenko, A. Seleznov, and A. Sokolenko, *Phenomenology of GeV-scale Higgs-like scalar*, *to appear* (2018).

[201] R. S. Willey and H. L. Yu, *The Decays $K^{\pm} \to \pi^{\pm}\ell^{+}\ell^{-}$ and Limits on the Mass of the Neutral Higgs Boson*, *Phys. Rev.* **D26** (1982) 3287.

[202] R. S. Willey, *Limits on Light Higgs Bosons From the Decays $K^{\pm} \to \pi^{\pm}\ell^{-}\ell^{+}$*, *Phys. Lett.* **B173** (1986) 480–484.

[203] B. Grzadkowski and P. Krawczyk, *Higgs Particle Effects In Flavor Changing Transitions*, *Z. Phys.* **C18** (1983) 43–45.

[204] H. Leutwyler and M. A. Shifman, *Light Higgs Particle in Decays of $K$ and $\eta$ Mesons*, *Nucl. Phys.* **B343** (1990) 369–397.

[205] S. Dawson, *Higgs Boson Production in Semileptonic $K$ and $\pi$ Decays*, *Phys. Lett.* **B222** (1989) 143–148.

[206] H.-Y. Cheng and H.-L. Yu, *Are There Really No Experimental Limits on a Light Higgs Boson From Kaon Decay?*, *Phys. Rev.* **D40** (1989) 2980.

[207] J. F. Donoghue, J. Gasser, and H. Leutwyler, *The Decay of a Light Higgs Boson*, *Nucl. Phys.* **B343** (1990) 341–368.

[208] M. Spira, *QCD effects in Higgs physics*, *Fortsch. Phys.* **46** (1998) 203–284, [hep-ph/9705337].

[209] F. Sanfilippo, *Quark Masses from Lattice QCD*, *PoS* **LATTICE2014** (2015) 014, [arXiv:1505.02794].

[210] M. Drewes, *The Phenomenology of Right Handed Neutrinos*, *Int. J. Mod. Phys.* **E22** (2013) 1330019, [arXiv:1303.6912].

[211] **CMS** Collaboration, A. M. Sirunyan et al., *Search for heavy neutral leptons in events with three charged leptons in proton-proton collisions at $\sqrt{s} = 13$ TeV*, *Phys. Rev. Lett.* **120** (2018), no. 22 221801, [arXiv:1802.02965].

[212] **SHiP** Collaboration, *Sensitivity of the SHiP experiment towards heavy neutral leptons*, *to appear* (2018).

[213] Bondarenko, K. and Boyarsky, A. and Ovchynnikov, M. and Ruchayskiy, O., *Intensity frontier experiments in search for new physics: SHiP and MATHUSLA*, *to appear* (2018).

[214] A. D. Dolgov, S. H. Hansen, G. Raffelt, and D. V. Semikoz, *Heavy sterile neutrinos: Bounds from big bang nucleosynthesis and SN1987A*, *Nucl. Phys.* **B590** (2000) 562–574, [hep-ph/0008138].

[215] R. E. Shrock, *General Theory of Weak Leptonic and Semileptonic Decays. 1. Leptonic Pseudoscalar Meson Decays, with Associated Tests For, and Bounds on, Neutrino Masses and Lepton Mixing*, *Phys. Rev.* **D24** (1981) 1232.

[216] R. E. Shrock, *New Tests For, and Bounds On, Neutrino Masses and Lepton Mixing*, *Phys. Lett.* **B96** (1980) 159–164.

[217] L. M. Johnson, D. W. McKay, and T. Bolton, *Extending sensitivity for low mass neutral heavy lepton searches*, *Phys. Rev.* **D56** (1997) 2970–2981, [hep-ph/9703333].

[218] D. Gorbunov and M. Shaposhnikov, *How to find neutral leptons of the νMSM?*, *JHEP* **10** (2007) 015, [arXiv:0705.1729]. [Erratum: JHEP11 (2013), 101].

[219] A. Abada, A. M. Teixeira, A. Vicente, and C. Weiland, *Sterile neutrinos in leptonic and semileptonic decays*, *JHEP* **02** (2014) 091, [arXiv:1311.2830].

[220] G. Cvetic and C. S. Kim, *Rare decays of B mesons via on-shell sterile neutrinos*, *Phys. Rev.* **D94** (2016), no. 5 053001, [arXiv:1606.04140]. [Erratum: Phys. Rev. D95 (2017), no.3 039901].

[221] E. Graverini, E. van Herwijnen, and T. Ruf, *Mass dependence of branching ratios into HNL for FairShip*, 2016. http://cds.cern.ch/record/2133817/files/main.pdf?version=1.

[222] **Particle Data Group** Collaboration, C. Patrignani et al., *Review of Particle Physics*, *Chin. Phys.* **C40** (2016), no. 10 100001.

[223] **LHCb** Collaboration, R. Aaij et al., *Observation of $B_c^+ \to D^0 K^+$ decays*, *Phys. Rev. Lett.* **118** (2017), no. 11 111803, [arXiv:1701.01856].

[224] S. Ramazanov, *Semileptonic decays of charmed and beauty baryons with sterile neutrinos in the final state*, *Phys. Rev.* **D79** (2009) 077701, [arXiv:0810.0660].

[225] J. Mejia-Guisao, D. Milanes, N. Quintero, and J. D. Ruiz-Alvarez, *Exploring GeV-scale Majorana neutrinos in lepton-number-violating $\Lambda_b^0$ baryon decays*, [arXiv:1705.10606].

[226] H.-Y. Cheng and B. Tseng, *1/M corrections to baryonic form-factors in the quark model*, *Phys. Rev.* **D53** (1996) 1457, [hep-ph/9502391]. [Erratum: Phys. Rev. D55 (1997), 1697].

[227] S. Meinel, *$\Lambda_c \to \Lambda \ell^+ \nu_\ell$ form factors and decay rates from lattice QCD with physical quark masses*, *Phys. Rev. Lett.* **118** (2017), no. 8 082001, [arXiv:1611.09696].

[228] W. Detmold, C. Lehner, and S. Meinel, *$\Lambda_b \to p \ell^- \bar{\nu}_\ell$ and $\Lambda_b \to \Lambda_c \ell^- \bar{\nu}_\ell$ form factors from lattice QCD with relativistic heavy quarks*, *Phys. Rev.* **D92** (2015), no. 3 034503, [arXiv:1503.01421].

[229] G. Källén, *Elementary particle physics*. Addison-Wesley series in advanced physics. Addison-Wesley Pub. Co., 1964.

[230] C. Degrande, O. Mattelaer, R. Ruiz, and J. Turner, *Fully-Automated Precision Predictions for Heavy Neutrino Production Mechanisms at Hadron Colliders*, *Phys. Rev.* **D94** (2016), no. 5 053002, [arXiv:1602.06957].

[231] R. Ruiz, M. Spannowsky, and P. Waite, *Heavy neutrinos from gluon fusion*, *Phys. Rev.* **D96** (2017), no. 5 055042, [arXiv:1706.02298].

[232] A. Pilaftsis, *Radiatively induced neutrino masses and large Higgs neutrino*

*couplings in the standard model with Majorana fields*, *Z. Phys.* **C55** (1992) 275–282, [hep-ph/9901206].

[233] A. Datta, M. Guchait, and A. Pilaftsis, *Probing lepton number violation via majorana neutrinos at hadron supercolliders*, *Phys. Rev.* **D50** (1994) 3195–3203, [hep-ph/9311257].

[234] A. Buckley, J. Ferrando, S. Lloyd, K. Nordström, B. Page, M. Rüfenacht, M. Schönherr, and G. Watt, *LHAPDF6: parton density access in the LHC precision era*, *Eur. Phys. J.* **C75** (2015) 132, [arXiv:1412.7420].

[235] H.-L. Lai, M. Guzzi, J. Huston, Z. Li, P. M. Nadolsky, J. Pumplin, and C. P. Yuan, *New parton distributions for collider physics*, *Phys. Rev.* **D82** (2010) 074024, [arXiv:1007.2241].

[236] Ovchynnikov at el. to appear, 2018.

[237] V. Gribanov, S. Kovalenko, and I. Schmidt, *Sterile neutrinos in tau lepton decays*, *Nucl. Phys.* **B607** (2001) 355–368, [hep-ph/0102155].

[238] A. Atre, T. Han, S. Pascoli, and B. Zhang, *The Search for Heavy Majorana Neutrinos*, *JHEP* **05** (2009) 030, [arXiv:0901.3589].

[239] J. C. Helo, S. Kovalenko, and I. Schmidt, *Sterile neutrinos in lepton number and lepton flavor violating decays*, *Nucl. Phys.* **B853** (2011) 80–104, [arXiv:1005.1607].

[240] R. E. Shrock, *General Theory of Weak Processes Involving Neutrinos. 2. Pure Leptonic Decays*, *Phys. Rev.* **D24** (1981) 1275.

[241] M. L. Perl, *The Tau lepton*, *Rept. Prog. Phys.* **55** (1992) 653–722.

[242] E. Braaten, S. Narison, and A. Pich, *QCD analysis of the tau hadronic width*, *Nucl. Phys.* **B373** (1992) 581–612.

[243] S. G. Gorishnii, A. L. Kataev, and S. A. Larin, *The $O(\alpha_s^3)$-corrections to $\sigma_{tot}(e^+e^- \to hadrons)$ and $\Gamma(\tau^- \to \nu_\tau + hadrons)$ in QCD*, *Phys. Lett.* **B259** (1991) 144–150.

[244] **SHiP** Collaboration, A. Akmete et al., *The active muon shield in the SHiP experiment*, *JINST* **12** (2017), no. 05 P05011, [arXiv:1703.03612].

[245] **SHiP** Collaboration, M. De Serio, *Neutrino physics with the SHiP experiment at CERN*, *PoS* **EPS-HEP2017** (2017) 101.

[246] **SHiP Collaboration** Collaboration, H. Dijkstra and T. Ruf, *Heavy Flavour Cascade Production in a Beam Dump*, *CERN-SHiP-NOTE-2015-009* (Dec, 2015).

[247] J. P. Chou, D. Curtin, and H. J. Lubatti, *New Detectors to Explore the Lifetime Frontier*, *Phys. Lett.* **B767** (2017) 29–36, [arXiv:1606.06298].

[248] M. Cacciari, M. Greco, and P. Nason, *The $p_T$ spectrum in heavy flavor hadroproduction*, *JHEP* **05** (1998) 007, [hep-ph/9803400].

[249] M. Cacciari, S. Frixione, and P. Nason, *The $p_T$ spectrum in heavy flavor photoproduction*, *JHEP* **03** (2001) 006, [hep-ph/0102134].

[250] W. Bonivento et al., *Proposal to Search for Heavy Neutral Leptons at the SPS*, [arXiv:1310.1762].

[251] **NA62** Collaboration, B. Döbrich, *Searches for very weakly-coupled particles beyond the Standard Model with NA62*, in *Proceedings, 13th Patras Workshop on Axions, WIMPs and WISPs, (PATRAS 2017): Thessaloniki, Greece, 15 May 2017 - 19, 2017*, pp. 145–148, 2018. [arXiv:1711.08967].

[252] **SHiP** Collaboration, S. Collaboration, *A Facility to Search for Hidden Particles (SHiP) at the CERN SPS*, .

[253] **SHiP** Collaboration, A. Baranov, E. Burnaev, D. Derkach, A. Filatov, N. Klyuchnikov, O. Lantwin, F. Ratnikov, A. Ustyuzhanin, and A. Zaitsev, *Optimising the active muon shield for the SHiP experiment at CERN*, *J. Phys. Conf. Ser.* **934** (2017), no. 1 012050.

[254] **ATLAS** Collaboration, G. Aad et al., *Measurement of $D^{*\pm}$, $D^{\pm}$ and $D_s^{\pm}$ meson production cross sections in pp collisions at $\sqrt{s} = 7$ TeV with the ATLAS detector*, *Nucl. Phys.* **B907** (2016) 717–763, [arXiv:1512.02913].

[255] **CMS** Collaboration, V. Khachatryan et al., *Measurement of the total and differential inclusive $B^+$ hadron cross sections in pp collisions at $\sqrt{s} = 13$ TeV*, *Phys. Lett.* **B771** (2017) 435–456, [arXiv:1609.00873].

[256] **LHCb** Collaboration, R. Aaij et al., *Measurement of b-hadron production fractions in* 7 TeV *pp collisions*, *Phys. Rev.* **D85** (2012) 032008, [arXiv:1111.2357].

[257] **LHCb** Collaboration, R. Aaij et al., *Measurements of prompt charm production cross-sections in pp collisions at $\sqrt{s} = 13$ TeV*, *JHEP* **03** (2016) 159, [arXiv:1510.01707]. [Erratum: JHEP05 (2017), 074].

[258] **LHCb** Collaboration, D. Müller, *Charm production in pp collisions at* 5 *and* 13 *TeV at LHCb*, *PoS* **CHARM2016** (2016) 061.

[259] C.-Y. Wong and G. Wilk, *Tsallis Fits to $p_T$ Spectra for pp Collisions at LHC*, *Acta Phys. Polon.* **B43** (2012) 2047–2054, [arXiv:1210.3661].

[260] M. Cacciari, S. Frixione, N. Houdeau, M. L. Mangano, P. Nason, and G. Ridolfi, *Theoretical predictions for charm and bottom production at the LHC*, *JHEP* **10** (2012) 137, [arXiv:1205.6344].

[261] M. Cacciari, M. L. Mangano, and P. Nason, *Gluon PDF constraints from the ratio of forward heavy-quark production at the LHC at $\sqrt{s} = 7$ and* 13 *TeV*, *Eur. Phys. J.* **C75** (2015), no. 12 610, [arXiv:1507.06197].

[262] **LHCb** Collaboration, R. Aaij et al., *Search for rare $B^0_{(s)} \to \mu^+\mu^-\mu^+\mu^-$ decays*, *Phys. Rev. Lett.* **110** (2013) 211801, [arXiv:1303.1092].

[263] **CDF** Collaboration, F. Abe et al., *Observation of the $B_c$ meson in $p\bar{p}$ collisions at $\sqrt{s} = 1.8$ TeV*, *Phys. Rev. Lett.* **81** (1998) 2432–2437, [hep-ex/9805034].

[264] **CDF** Collaboration, F. Abe et al., *Observation of $B_c$ mesons in $p\bar{p}$ collisions at $\sqrt{s} = 1.8$ TeV*, *Phys. Rev.* **D58** (1998) 112004, [hep-ex/9804014].

[265] K.-m. Cheung, *$B_c$ meson production at the Tevatron revisited*, *Phys. Lett.* **B472** (2000) 408–411, [hep-ph/9908405].

[266] C.-H. Chang, C. Driouichi, P. Eerola, and X. G. Wu, *BCVEGPY: An Event generator for hadronic production of the $B_c$ meson*, *Comput. Phys. Commun.* **159** (2004) 192–224, [hep-ph/0309120].

[267] **SHiP** Collaboration, A. Akmete et al., *Sensitivity of the SHiP experiment towards Higgs-like scalar, to appear* (2018).

[268] M. Al-Turany, D. Bertini, R. Karabowicz, D. Kresan, P. Malzacher, T. Stockmanns, and F. Uhlig, *The fairroot framework*, *Journal of Physics: Conference Series* **396** (2012), no. 2 022001.

[269] T. Sjostrand, S. Mrenna, and P. Z. Skands, *A Brief Introduction to PYTHIA 8.1*, *Comput. Phys. Commun.* **178** (2008) 852–867, [arXiv:0710.3820].

[270] C. Andreopoulos et al., *The GENIE Neutrino Monte Carlo Generator*, *Nucl. Instrum. Meth.* **A614** (2010) 87–104, [arXiv:0905.2517].

[271] T. Sjostrand, S. Mrenna, and P. Z. Skands, *PYTHIA 6.4 Physics and Manual*, *JHEP* **05** (2006) 026, [hep-ph/0603175].

[272] **GEANT4** Collaboration, S. Agostinelli et al., *GEANT4: A Simulation toolkit*, *Nucl. Instrum. Meth.* **A506** (2003) 250–303.

[273] **SHiP collaboration** Collaboration, E. Van Herwijnen, H. Dijkstra, M. Ferro-Luzzi, and T. Ruf, *Simulation and pattern recognition for the SHiP Spectrometer Tracker*, *CERN-SHiP-NOTE-2015-002* (Mar, 2015).

[274] **SHiP Collaboration** Collaboration, B. Hosseini and W. M. Bonivento, *Particle Identification tools and performance in the SHiP Experiment*, *CERN-SHiP-NOTE-2017-002* (Jul, 2017).

[275] K. Bondarenko, A. Boyarsky, D. Gorbunov, and O. Ruchayskiy, *Phenomenology of GeV-scale Heavy Neutral Leptons*, [arXiv:1805.08567].

[276] **HERA-B** Collaboration, I. Abt et al., *Measurement of $D^0$, $D^+$, $D_s^+$ and $D^{*+}$ Production in Fixed Target 920-GeV Proton-Nucleus Collisions*, *Eur. Phys. J.* **C52** (2007) 531–542, [arXiv:0708.1443].

[277] C. Lourenco and H. K. Wohri, *Heavy flavour hadro-production from fixed-target to collider energies*, *Phys. Rept.* **433** (2006) 127–180, [hep-ph/0609101].

[278] B. W. Lee and S. Weinberg, *Cosmological Lower Bound on Heavy Neutrino Masses*, *Phys. Rev. Lett.* **39** (1977) 165–168.

[279] K. Bondarenko, I. Boiarska, A. Boyarsky, M. Ovchynnikov, and O. Ruchayskiy, *Light dark matter with scalar mediator at Intensity Frontier experiments, to appear* (2018).

[280] H.-Y. Cheng and C.-W. Chiang, *Revisiting Scalar and Pseudoscalar Couplings with Nucleons*, *JHEP* **07** (2012) 009, [arXiv:1202.1292].

[281] **MiniBooNE** Collaboration, R. Dharmapalan et al., *Low Mass WIMP Searches with a Neutrino Experiment: A Proposal for Further MiniBooNE Running*, [arXiv:1211.2258].

[282] **T2K** Collaboration, K. Abe et al., *Observation of Electron Neutrino Appearance in a Muon Neutrino Beam*, *Phys. Rev. Lett.* **112** (2014) 061802, [arXiv:1311.4750].

[283] R. D. Peccei and H. R. Quinn, *CP Conservation in the Presence of Instantons*, *Phys. Rev. Lett.* **38** (1977) 1440–1443.

[284] R. D. Peccei and H. R. Quinn, *Constraints Imposed by CP Conservation in the Presence of Instantons*, *Phys. Rev.* **D16** (1977) 1791–1797.

[285] F. Wilczek, *Problem of Strong p and t Invariance in the Presence of Instantons*, *Phys. Rev. Lett.* **40** (1978) 279–282.

[286] S. Weinberg, *A New Light Boson?*, *Phys. Rev. Lett.* **40** (1978) 223–226.

[287] J. Jaeckel and M. Spannowsky, *Probing MeV to* 90 *GeV axion-like particles with LEP and LHC*, *Phys. Lett.* **B753** (2016) 482–487, [arXiv:1509.00476].

[288] J. Redondo and A. Ringwald, *Light shining through walls*, *Contemp. Phys.* **52** (2011) 211–236, [arXiv:1011.3741].

[289] B. Döbrich, J. Jaeckel, F. Kahlhoefer, A. Ringwald, and K. Schmidt-Hoberg, *ALPtraum: ALP production in proton beam dump experiments*, *JHEP* **02** (2016) 018, [arXiv:1512.03069].

[290] M. Antonelli et al., *Flavor Physics in the Quark Sector*, *Phys. Rept.* **494** (2010) 197–414, [arXiv:0907.5386].

[291] F. J. Gilman and R. L. Singleton, *Analysis of Semileptonic Decays of Mesons Containing Heavy Quarks*, *Phys. Rev.* **D41** (1990) 142.

[292] E. Blucher et al., *Status of the Cabibbo angle*, in *3rd International Workshop on the CKM Unitarity Triangle (CKM 2005) San Diego, California, March 15-18, 2005*, 2005. [hep-ph/0512039].

[293] **FlaviaNet Working Group on Kaon Decays** Collaboration, M. Antonelli et al., *Precision tests of the Standard Model with leptonic and semileptonic kaon decays*, in *PHIPSI08, proceedings of the International Workshop on $e^+e^-$ Collisions from $\phi$ to $\psi$, Frascati (Rome) Italy, 7-10 April 2008*, 2008. [arXiv:0801.1817].

[294] **BaBar** Collaboration, J. P. Lees et al., *Precise Measurement of the $e^+e^- \to \pi^+\pi^-(\gamma)$ Cross Section with the Initial-State Radiation Method at BABAR*, *Phys. Rev.* **D86** (2012) 032013, [arXiv:1205.2228].

[295] L. M. Barkov et al., *Electromagnetic Pion Form-Factor in the Timelike Region*, *Nucl. Phys.* **B256** (1985) 365–384.

[296] **CMD-2** Collaboration, R. R. Akhmetshin et al., *High-statistics measurement of the pion form factor in the rho-meson energy range with the CMD-2 detector*, *Phys. Lett.* **B648** (2007) 28–38, [hep-ex/0610021].

[297] **KLOE** Collaboration, F. Ambrosino et al., *Measurement of $\sigma(e^+e^- \to \pi^+\pi^-)$ from threshold to 0.85 $GeV^2$ using Initial State Radiation with the KLOE detector*, *Phys. Lett.* **B700** (2011) 102–110, [arXiv:1006.5313].

[298] **KLOE** Collaboration, D. Babusci et al., *Precision measurement of $\sigma(e^+e^- \to \pi^+\pi^-\gamma)/\sigma(e^+e^- \to \mu^+\mu^-\gamma)$ and determination of the $\pi^+\pi^-$ contribution to the muon anomaly with the KLOE detector*, *Phys. Lett.* **B720** (2013) 336–343, [arXiv:1212.4524].

[299] **BESIII** Collaboration, M. Ablikim et al., *Measurement of the $e^+e^- \to \pi^+\pi^-$ cross section between 600 and 900 MeV using initial state radiation*, *Phys. Lett.* **B753** (2016) 629–638, [arXiv:1507.08188].

[300] J. L. Rosner, S. Stone, and R. S. Van de Water, *Leptonic Decays of Charged Pseudoscalar Mesons - 2015*, *Submitted to: Particle Data Book* (2015) [arXiv:1509.02220].

[301] **HPQCD** Collaboration, B. Colquhoun, C. T. H. Davies, R. J. Dowdall, J. Kettle, J. Koponen, G. P. Lepage, and A. T. Lytle, *B-meson decay constants: a more complete picture from full lattice QCD*, *Phys. Rev.* **D91** (2015), no. 11 114509, [arXiv:1503.05762].

[302] D. Ebert, R. N. Faustov, and V. O. Galkin, *Relativistic treatment of the decay constants of light and heavy mesons*, *Phys. Lett.* **B635** (2006) 93–99, [hep-ph/0602110].

[303] N. Dhiman and H. Dahiya, *Decay constants of pseudoscalar and vector B and D mesons in the light-cone quark model*, *Eur. Phys. J. Plus* **133** (2018), no. 4 134, [arXiv:1708.07274].

[304] D. Bečirević, G. Duplančić, B. Klajn, B. Melić, and F. Sanfilippo, *Lattice QCD and QCD sum rule determination of the decay constants of $\eta_c$, $J/\psi$ and $h_c$ states*, *Nucl. Phys.* **B883** (2014) 306–327, [arXiv:1312.2858].

[305] R. Escribano, S. Gonzàlez-Solís, P. Masjuan, and P. Sanchez-Puertas, *$\eta'$ transition form factor from space- and timelike experimental data*, *Phys. Rev.* **D94** (2016), no. 5 054033, [arXiv:1512.07520].

[306] S. Scherer, *Introduction to chiral perturbation theory*, *Adv. Nucl. Phys.* **27** (2003) 277, [hep-ph/0210398].

[307] T. Feldmann, *Quark structure of pseudoscalar mesons*, *Int. J. Mod. Phys.* **A15** (2000) 159–207, [hep-ph/9907491].

[308] H. Leutwyler, *On the 1/N expansion in chiral perturbation theory*, *Nucl. Phys. Proc. Suppl.* **64** (1998) 223–231, [hep-ph/9709408]. [,223(1997)].

[309] N. G. Deshpande and J. Trampetic, *Exclusive and semiinclusive B decays based on $b \to s\eta_c$ transition*, *Phys. Lett.* **B339** (1994) 270–274, [hep-ph/9406393].

[310] **CLEO** Collaboration, K. W. Edwards et al., *Study of B decays to charmonium states $B \to \eta_c K$ and $B \to \chi_{c0} K$*, *Phys. Rev. Lett.* **86** (2001) 30–34, [hep-ex/0007012].

[311] C. Bourrely, I. Caprini, and L. Lellouch, *Model-independent description of $B \to \pi l \nu$ decays and a determination of $|V_{ub}|$*, *Phys. Rev.* **D79** (2009) 013008, [arXiv:0807.2722]. [Erratum: Phys. Rev. D82 (2010), 099902].

[312] **HPQCD** Collaboration, H. Na, C. M. Bouchard, G. P. Lepage, C. Monahan, and J. Shigemitsu, *$B \to Dl\nu$ form factors at nonzero recoil and extraction of $|V_{cb}|$*, *Phys. Rev.* **D92** (2015), no. 5 054510, [arXiv:1505.03925]. [Erratum: Phys. Rev. D93 (2016), no.11 119906].

[313] S. Aoki et al., *Review of lattice results concerning low-energy particle physics*, *Eur. Phys. J.* **C77** (2017), no. 2 112, [arXiv:1607.00299].

[314] O. P. Yushchenko et al., *High statistic study of the $K^- \to \pi^0 \mu^- \nu$ decay*, *Phys. Lett.* **B581** (2004) 31–38, [hep-ex/0312004].

[315] **NA48** Collaboration, A. Lai et al., *Measurement of $K^0_{\mu 3}$ form factors*, *Phys. Lett.* **B647** (2007) 341–350, [hep-ex/0703002].

[316] **ETM** Collaboration, V. Lubicz, L. Riggio, G. Salerno, S. Simula, and C. Tarantino, *Scalar and vector form factors of $D \to \pi(K)\ell\nu$ decays with $N_f = 2 + 1 + 1$ twisted fermions*, *Phys. Rev.* **D96** (2017), no. 5 054514, [arXiv:1706.03017].

[317] G. Duplancic and B. Melic, *Form factors of $B, B_s \to \eta^{(\prime)}$ and $D$, $D_s \to \eta^{(\prime)}$ transitions from QCD light-cone sum rules*, *JHEP* **11** (2015) 138, [arXiv:1508.05287].

[318] C. J. Monahan, H. Na, C. M. Bouchard, G. P. Lepage, and J. Shigemitsu, *$B_s \to D_s \ell \nu$ Form Factors and the Fragmentation Fraction Ratio $f_s/f_d$*, *Phys. Rev.* **D95** (2017), no. 11 114506, [arXiv:1703.09728].

[319] D. Melikhov and B. Stech, *Weak form-factors for heavy meson decays: An Update*, *Phys. Rev.* **D62** (2000) 014006, [hep-ph/0001113].

[320] D. Ebert, R. N. Faustov, and V. O. Galkin, *New analysis of semileptonic B decays in the relativistic quark model*, *Phys. Rev.* **D75** (2007) 074008, [hep-ph/0611307].

[321] R. N. Faustov and V. O. Galkin, *Relativistic description of weak decays of $B_s$ mesons*, *AIP Conf. Proc.* **1701** (2016) 050020, [arXiv:1411.7232].

[322] N. Mathur, M. Padmanath, and R. Lewis, *Charmed-Bottom Mesons from Lattice QCD*, *PoS* **LATTICE2016** (2016) 100, [arXiv:1611.04085].

[323] L. N. Chang, O. Lebedev, and J. N. Ng, *On the invisible decays of the Upsilon and $J/\psi$ resonances*, *Phys. Lett.* **B441** (1998) 419–424, [hep-ph/9806487].

[324] G. J. Gounaris and J. J. Sakurai, *Finite width corrections to the vector meson dominance prediction for $\rho \to e^+e^-$*, *Phys. Rev. Lett.* **21** (1968) 244–247.

# Samenvatting

Het succes van het Standaardmodel heeft een hoogtepunt bereikt met de bevestiging van een van zijn belangrijkste voorspellingen - de ontdekking van het Higgsboson. De zoektocht naar nieuwe deeltjes is echter niet gestopt. De waargenomen en onverklaarde fenomenen in de deeltesfysica en kosmologie (zoals de neutrino massa's en oscillaties, donkere materie en baryon asymmetrie in het Universum) geven een indicatie dat er nieuwe deeltjes kunnen bestaan buiten het Standaardmodel. Desondanks zijn deze deeltjes tot nu toe niet waargenomen. Een mogelijke reden is dat deze deeltjes te zwaar zijn om gecreëerd te worden in deeltjesversnellers. Hierdoor is de bouw van grotere deeltjesversnellers die het *Energiefront* overschrijden het voornaamste aandachtspunt in de deeltjesfysica geworden.
Een andere mogelijkheid is dat de hypothetische deeltjes licht genoeg zijn (lichter dan het Higgsboson en het W-boson) om een interactie aan te gaan met deeltjes van het Standaardmodel op een wijze die vergelijkbaar, maar veel zwakker, is dan die van neutrino's. Om het mogelijke bestaan van hele lichte deeltjes te verkennen, besteedt de wetenschappelijke gemeenschap ook aandacht aan experimenten aan het *Intensiteitsfront*. Zulke experimenten richten zich op het opwekken van deeltjesbundels met hoge intensiteit en maken gebruik van grote detectoren in de zoektocht naar zeldzame interacties van hypothetische deeltjes die een zwakke interactie vertonen. Naast het uitvoeren van experimenten, zijn er in de afgelopen jaren ook een aantal nieuwe projecten voorgesteld die zoeken naar lichte deeltjes met een zwakke interactie in deeltjesversnellers over de hele wereld. Het CERN Management erkent het belang van de verkenning van het Intensiteitsfront en heeft in 2016 een studiegroep gecreëerd die zich toelegt op het analyseren van de potentie van zoektochten naar nieuwe deeltjes bij CERN buiten de LHC.
In dit proefschrift hebben wij de vooruitzichten van twee voorgestelde experimenten in CERN verkend, die beide voornamelijk gewijd zijn aan de zoektocht naar deeltjes buiten het Standaardmodel. Het eerste experiment is *SHiP* (Search for Hidden Particles), dat gebruik maakt van een stationair doel en de protonenbundel van het Super Proton Synchrotron (SPS). Het tweede experiment is *MATHUSLA* (MAssive Timing Hodoscope for Ultra Stable neutraL pArticles), een oppervlakte detector naast het ATLAS of CMS experiment. Beide experimenten zijn gevoelig voor vergelijkbare delen van de parameter ruimte. Daarom is het van belang om hun wetenschappelijke waarde af te wegen op een consistente en objectieve manier.

In dit proefschrift hebben wij ons geconcentreerd op enkele, goed-gemotiveerde uitbreidingen van het Standaardmodel, inclusief de 'heavy neutral leptons' (neutrino-achtige Majorana fermionen met een zwakke interactie en een massa van de orde van 1 GeV) en Higgs-achtige singulet scalars. Deze deeltjes kunnen direct verantwoordelijk zijn voor een aantal fenomenen buiten het Standaardmodel, of als poorten dienen die het Standaardmodel verbinden met oplossingen van de waargenomen fenomenen. Voor beide uitbreidingen hebben wij de fenomenologie van hun productie en detectie herzien, waarbij rekening is gehouden met de vereisten van de twee genoemde experimenten. Dit laatste aspect is niet gedaan in eerdere studies. Onze resultaten zijn geschikt voor gevoeligheidsanalyses van deeltjesfysica experimenten (van proton beam-dump tot de LHC) die gericht zijn op het zoeken naar deeltjes die als poorten dienen. Ze worden met name gebruikt door de SHiP samenwerking voor de officiële gevoeligheidsanalyses.

Wij hebben gebruik gemaakt van gedetailleerde Monte-Carlo simulaties van de productie en het verval van de genoemde deeltjes en dit aangevuld met onderzoek naar achtergrond deeltjes om het wetenschappelijke werkingsgebied in te schatten. We hebben de officiële software van het SHiP experiment - FairSHiP - uitgebreid. Hier hebben we onze bevindingen voor de productie en detectie van 'heavy neutral leptons' in SHiP geïmplementeerd. De resulterende gevoeligheidscurves zijn gebruikt in twee officiële artikelen van de SHiP samenwerking.

In de nieuwe aanpak zijn, o.a., het aantal productie en verval kanalen uitgebreid, wat ons in staat heeft gesteld het gevoeligheidsbereik van SHiP te verbeteren om zo een consistente vergelijking te maken met het bereik van MATHUSLA, waarbij indentieke benaderingen zijn gebruikt. We hebben bovendien een nieuwe en effectieve manier voorgesteld om de 4-dimensionale parameter ruimte van 'heavy neutral leptons' te scannen om zo gevoeligheidsgebieden te indentificeren voor arbitraire koppelingen. Dit op aandringen van meerdere onderzoeksgroepen; het is cruciaal om de vraag *Welke modellen van leptogenesis kunnen direct onderzocht worden in deeltjesfysica experimenten?* te kunnen beantwoorden.

Ten slotte hebben wij de extensie van SHiP - iSHiP - onderzocht. iSHiP is oorspronkelijk ontworpen om de eigenschappen van $\tau-$neutrinos te onderzoeken, maar is ook geschikt voor het detecteren van lichte donkere-materie deeltjes (leden van de 'donkere sector' die geproduceerd zijn via de scalar poort).

De volgende European Strategy for Particle Physics wordt in mei 2020 geformuleerd. De volgende generatie van Intensiteitsfront-experimenten is een van de agendapunten. Ongeacht welk Intensiteitsfront-experiment wordt goedgekeurd, zullen de resultaten van dit proefschrift gebruikt worden door veel theoriegroepen, experimentele samenwerkingen, de experts van de European Strategy for Particle Physics enzovoort. De SHiP samenwerking is bovendien bezig met het samenstellen van het *Comprehensive Design Report* - een officieel document dat het ontwerp van het experiment compleet vastlegt. De resultaten van dit proefschrift maken daar onderdeel vanuit.

# Summary

The recent success of the Standard Model has culminated in the confirmation of one of its most important predictions – the discovery of the Higgs boson. However the search for the new particles has not ended. The observed but unexplained phenomena in particle physics and cosmology (such as neutrino masses and oscillations, dark matter and baryon asymmetry of the Universe) indicate that new particles may exist beyond the Standard Model. Despite this, these particles have so far evaded our detection. One potential reason for this is because they could be too heavy to be created by accelerators, and hence constructing larger accelerators in order to cross the *Energy Frontier* is now seen as a primary focus for particle physics.

Alternatively, some of the hypothetical particles can be sufficiently light (lighter than the Higgs or $W$-boson), to interact with particles from the the Standard Model but even weaker than neutrinos do. In order to explore the possibility of super-light particles, the science community is also focussing their attention on experiments at the *Intensity Frontier*. Such experiments aim to create high-intensity particle beams and use large detectors to search for rare interactions of hypothetical 'feebly-interacting particles'. In addition to experiments that are already running, a number of new projects have been proposed in recent years in order to search for light and feebly interacting particles in accelerator facilities throughout the world. Recognizing the importance of exploring the Intensity Frontier, the CERN Management created, in 2016, a dedicated Study Group "Physics Beyond Colliders" that analyses the potential of non-LHC searches for new particles at CERN.

In this thesis we have explored the prospects of two proposed experiments at CERN, both with the primary aim to search for new particles beyond the Standard Model. The first is the – *Search for Hidden Particles* or *SHiP* –, which is a fixed-target experiment that uses the proton beam of the Super Proton Synchrotron (SPS). The second experiment is – MATHUSLA (*MAssive Timing Hodoscope for Ultra Stable neutraL pArticles*) – a surface detector proposed to sit alongside the ATLAS or CMS experiment. Both experiments are sensitive to similar regions of parameter space and therefore it is important to assess their scientific possibilities in a consistent and objective manner.

In this work we have concentrated on several well-motivated extensions of the Standard Model, such as *heavy neutral leptons* (neutrino-like Majorana fermions,

feebly interacting and with GeV-scale mass) and a *Higgs-like singlet scalar*. These particles can be directly responsible for some of the Beyond Standard Model phenomena or can serve as *portals* connecting the Standard Model to the particles that prove solutions for the observed phenomena.

For both extensions we have reviewed and revised the phenomenology of their production and detection, taking into account the direct requirements of the experiments in question, something that previous studies had not done. Our results are directly suitable for sensitivity studies of particle physics experiments (ranging from proton beam-dump to the LHC) aiming at searches for portal particles. In particular, they are being used by the SHiP collaboration for the official sensitivity studies.

We have used detailed Monte-Carlo simulations of both production and decay, complemented by background studies in order to estimate the experimental reach. We have extended the official software framework of the SHiP experiment – FairSHiP, implementing our new findings for the heavy neutral leptons to include the scalar production and detection of a singlet scalar in SHiP. The resulting sensitivity curves have been included into two official papers of the SHiP collaboration.

The new half-analytical approach allowed us to calculate more accurately the sensitivity reach of the SHiP experiment and compare it to that of MATHUSLA in a consistent manner under an identical set of assumptions. In addition, we have proposed a new and effective way to scan over the 4-dimensional parameter space of the heavy neutral leptons in order to identify sensitivity regions for arbitrary couplings. Such a feature was requested by many research groups and is crucial if we are to answer the question: *What models of leptogenesis can be directly probed at particle physics experiments?*

Finally, we have also examined the extension to SHiP known as iSHIP. While originally designed to study the properties of $\tau$-neutrinos, iSHIP is an extra detector that is suitable for detecting light dark matter particles – members of the "dark sector" produced via the scalar portal.

In May 2020 the next European Strategy for Particle Physics will be formulated. The question of the next-generation Intensity Frontier experiment will be a part of its scientific agenda. Regardless of which new Intensity Frontier experiment will be approved, the results of this project will be used by many theory groups as well as by experimental collaborations, by the experts of the European Strategy for Particle Physics, etc. In addition, the SHiP collaboration is currently preparing its *Comprehensive Design Report* — an official document that finalizes the design of the experiment. The results of this thesis are part of that effort.

# List of publications

[1] S. Alekhin *et. al.*, A facility to Search for Hidden Particles at the CERN SPS: the SHiP physics case, *Rept. Prog. Phys.* **79** (2016), no. 12 124201 [arXiv:1504.04855]. Contributing author. [Chapter 1]

[2] **SHiP** Collaboration, M. Anelli *et. al.*, A facility to Search for Hidden Particles (SHiP) at the CERN SPS, [arXiv:1504.04956]. Contributing author. [Chapter 4]

[3] **SHiP** Collaboration, A. Akmete *et. al.*, The active muon shield in the SHiP experiment, *JINST* **12** (2017), no. 05 P05011 [arXiv:1703.03612]. [Chapter 4]

[4] K. Bondarenko, A. Boyarsky, D. Gorbunov and O. Ruchayskiy, Phenomenology of GeV-scale Heavy Neutral Leptons, *Submitted to JHEP* (2018) [arXiv:1805.08567]. [Chapter 3]

[5] K. Bondarenko, A. Boyarsky, T. Bringmann and A. Sokolenko, Constraining self-interacting dark matter with scaling laws of observed halo surface densities, *JCAP* **1804** (2018), no. 04 049 [arXiv:1712.06602]. [Chapter 1]

[6] A. Sokolenko, K. Bondarenko, T. Brinckmann, J. Zavala Franco, M. Vogelsberger, T. Bringmann and A. Boyarsky, Towards an improved model of self-interacting dark matter haloes, *Submitted to JCAP* (2018) [arXiv:1806.11539]. [Chapter 1]

[7] **SHiP** Collaboration, A. Akmete *et. al.*, Sensitivity of the SHiP experiment towards heavy neutral leptons, *On review by the collaboration. To appear* (2018). Leading author. [Chapter 5]

[8] **SHiP** Collaboration, A. Akmete *et. al.*, Sensitivity of the SHiP experiment towards scalar portal, *On review by the collaboration. To appear* (2018). Leading author. [Chapter 5]

[9] K. Bondarenko, A. Boyarsky, V. Gorkavenko, A. Seleznov and A. Sokolenko, Phenomenology of GeV-scale Higgs-like scalar, *to appear* (2018). [Chapter 2]

[10] K. Bondarenko, A. Boyarsky, M. Ovchynnikov and O. Ruchayskiy, Intensity frontier experiments in search for new physics: SHiP and MATHUSLA, *to appear* (2018). [Chapter 5]

[11] K. Bondarenko, I. Boiarska, A. Boyarsky, M. Ovchynnikov and O. Ruchayskiy, Light dark matter with scalar mediator at Intensity Frontier experiments, *to appear* (2018). [Chapter 6]

# Curriculum vitæ

I was born in Kiev, Ukraine, on the 25th of May 1990. I have received the primary education at the school No. 63, and the secondary education at the Lyceum No. 171 in Kiev, with specialization in mathematics. In my last year at school, I have participated in the $38^{\text{th}}$ International Physics Olympiad and won a bronze medal.

After finishing high school, I entered the Physics Department of the Kiev Taras Shevchenko University in 2007. I have graduated in 2014. My Master thesis was titled "Calculation of production and decay rates of sterile neutrinos in the experiment on SPS". After the graduation, I started my Ph.D. studies at the Lorentz Insitute for Theoretical Physics in Leiden, under the supervision of Dr. Alexey Boyarsky.

During my Ph.D. studies, I was a teaching assistant for the courses "Classical mechanics B", "Particle physics and the early Universe", "Origin of the Standard Model", "Effective Field Theory". I have become a member of the SHiP collaboration and did a number of studies related to SHiP sensitivities for different models of new physics. I have visited a number of schools and conferences in the Netherlands, Italy, Switzerland, and Germany, where my work was presented.

After finishing my Ph.D. studies, I would like to continue my academic career and stay in the field of theoretical physics.

# Acknowledgements

First of all, I want to thank my supervisor Alexey Boyarsky for his scientific (and not only scientific) advice and help, for the constant encouragement during different stages of my Ph.D. studies, for developing my professional skills, and for building my current vision of physics.

I am grateful to my promotor Ana Achúcarro, and to my collaborators, Oleg Ruchayskiy, Anastasiia Sokolenko, Andrii Magalich, Maxim Ovchynnikov.

I would like to give special thanks to Stanislav Vilchynskyi, Dmytro Iakubovskyi, and to the Scientific and Educational Center of Bogolyubov Institute for Theoretical Physics in Kiev.

I want to express deep gratitude to my wife Olga, to my mother Tatiana and to my father Vladimir, and to my sister Taya. Thank you for the inspiration, for the understanding, and for providing the best conditions, which allowed me to concentrate on scientific work.

I thank Nashwan Sabti for help with the Dutch translation. Finally, I thank the secretaries of our institute, Marianne, Fran, and Manon, for the help in all sorts of practical things, and all the colleagues at the Lorentz Institute for providing the great atmosphere.